



EXPERIMENTAL INVESTIGATION
OF COMPRESSIBLE BOUNDARY LAYERS
UNDER THE INFLUENCE
OF PRESSURE GRADIENTS

THESIS
Raymond C. Wier
Captain, USAF
AFIT/GAE/ENY/96D-04

DISTRIBUTION STATEMENT A
Approved for public release
Distribution Unrestricted

DEPARTMENT OF THE AIR FORCE
AIR UNIVERSITY
AIR FORCE INSTITUTE OF TECHNOLOGY

Wright-Patterson Air Force Base, Ohio

DTIC QUALITY INSPECTED 1

19970214 006

EXPERIMENTAL INVESTIGATION
OF COMPRESSIBLE BOUNDARY LAYERS
UNDER THE INFLUENCE
OF PRESSURE GRADIENTS

THESIS
Raymond C. Wier
Captain, USAF
AFIT/GAE/ENY/96D-04

The views expressed in this thesis are those of the author and do not reflect the official policy or position
of the Department of Defense or the United States Government

EXPERIMENTAL INVESTIGATION
OF COMPRESSIBLE BOUNDARY LAYERS
UNDER THE INFLUENCE
OF PRESSURE GRADIENTS

THESIS

Presented to the Faculty of the School of Engineering
of the Air Force Institute of Technology
Air University
In Partial Fulfillment of the
Requirements for the Degree of
Master of Science in Aeronautical Engineering

Raymond C. Wier, B.S.

Captain, USAF

December 1996

Approved for public release; distribution unlimited

Acknowledgments

There are many people whom I would like to take this opportunity to thank. Foremost is my wife. Without her unlimited patience and understanding, I would have never completed this project. I have appreciated her tireless and loving support.

Second, I would like to thank my advisor, Dr. Rodney Bowersox, for his support and encouragement. His knowledge and good cheer kept me going when everything that could go wrong went wrong this summer. He has the uncanny ability to understand my concerns and lead me on the right path to solve them, without solving them himself. I would like to thank the lab technicians, especially Andy Pitts, for their vast knowledge of instrumentation and their practical knowledge. They solved many intractable problems for me. Thanks go to my reading committee, Major Thomas Buter and Dr. Philip Beran for their insight and advice. Thanks go to the shop who put up with my constant nagging about making parts.

Finally, I would like to thank my parents for their patience and support.

Raymond C. Wier

Table of Contents

Acknowledgments.....	ii
Table of Contents.....	iii
List of Figures.....	vi
List of Tables	ix
List of Symbols	xii
Abstract	xvi
1. Introduction	1-1
1.1 Motivation.....	1-1
1.2 Research Objectives.....	1-4
1.3 Overview of Current Study	1-5
2. Background.....	2-1
2.1 Governing Equations.....	2-1
2.1.1 The Compressible Navier-Stokes Equations.....	2-1
2.1.2 Reynolds-Averaged Navier-Stokes Equations (RANS)	2-2
2.1.3 Favré-Averaged Navier-Stokes Equations (FANS)	2-3
2.1.4 Comparison Between Favré-Averaged and Reynolds-Averaged N-S Equations	2-4
2.2 Literature Review	2-5
3. Facilities and Equipment.....	3-1
3.1 Mach 3.0 Wind Tunnel.....	3-1
3.1.1 High-Pressure Air Supply.....	3-1
3.1.2 Vacuum System	3-2
3.1.3 Plenum Chamber	3-2
3.1.4 Mach 3.0 Nozzle.....	3-2
3.1.5 Test Sections.....	3-3
3.2 Mach 1.7 Wind Tunnel.....	3-4
3.2.1 Plenum Chamber	3-4
3.2.2 Mach 1.7 Nozzle.....	3-5
3.3 Mach 5.0 Wind Tunnel.....	3-5
3.3.1 Air Supply.....	3-6
3.3.2 Pebble Bed Heaters	3-6
3.3.3 Plenum Chamber	3-6

3.3.4 Mach 5.0 Nozzle.....	3-7
3.3.5 Test Sections.....	3-7
3.4 Data Acquisition Equipment.....	3-8
3.5 Probes	3-8
3.5.1 Pressure Probes.....	3-8
3.5.2 Hot-Wire and Hot-Film Probes.....	3-9
3.6 Particle Image Velocimetry.....	3-10
3.7 Computer Equipment	3-11
4. Data Reduction Techniques.....	4-1
4.1 Mean Flow Data Reduction	4-1
4.1.1 Calculation of Mach Number, Velocity and Fluid Properties	4-1
4.1.1.1 Pressure and Temperature Methodology - ZPG Flow.....	4-2
4.1.1.2 Pressure and Temperature Methodology - FPG and CPG Flow.....	4-2
4.1.2 Calculation of Boundary Layer, Displacement and Momentum Thickness.....	4-3
4.1.3 Calculation of Van Driest Velocity Profile and Wall Shear Stress	4-4
4.2 Hot-Wire Data Reduction	4-5
4.2.1 Hot-Wire Theory.....	4-6
4.2.2 Separation of Turbulence Variables	4-8
4.2.3 Single Overheat Theory	4-9
4.2.4 Mach 2.8 Hot-Wire Probe Data	4-10
4.2.5 Mach 1.7 Hot-Wire Probe Data	4-10
4.2.6 Power Spectra Data Reduction	4-11
4.3 PIV Data Reduction.....	4-11
5. Mach 2.8 Results and Discussion	5-1
5.1 Flow Visualization	5-1
5.2 Mean Flow Results	5-3
5.2.1 Conventional Pressure Probe.....	5-3
5.2.2 Hot-Wire Mean Profiles.....	5-6
5.2.3 PIV Mean Profiles	5-9
5.2.4 Comparison Between Data Collection Methods.....	5-14
5.2.4.1 Mean Flow Comparison	5-14
5.2.4.2 Van Driest Correlation.....	5-16
5.3 Turbulence Results	5-19
5.3.1 Hot-Film Turbulence Results	5-20
5.3.1.1 Mass Flux Turbulence Intensity Profiles.....	5-20
5.3.1.2 Energy Spectra.....	5-23
5.3.2 PIV Turbulence Results	5-26
5.3.3 Comparison Between Data Collection Methods - Turbulence Quantities	5-28
5.3.4 Density Fluctuations	5-30
6. Mach 1.7 Results and Discussion	6-1
6.1 Mach 1.7 Conventional Pressure Data	6-1
6.2 Hot-Wire Results	6-3
6.2.1 Mean Flow Profiles.....	6-3
6.3 Turbulence Results	6-4
6.3.1 Mass Flux Turbulence Intensity Profiles	6-4
6.3.2 Energy Spectra	6-5

6.3.3 Separated Turbulence Results	6-6
7. Mach 5.0 Results and Discussion	7-1
8. Conclusions and Recommendations.....	8-1
8.1 Mach 2.8 Conclusions	8-1
8.2 Mach 1.7 Conclusions	8-2
8.3 Mach 5.0 Conclusions	8-3
8.4 Recommendations	8-3
Appendix A : Hot-Wire Calibration.....	A-1
A.1 Mach 2.8 Calibration	A-1
A.2 Mach 1.7 Calibration	A-3
Appendix B : Uncertainty Analysis	B-1
B.1 Elementary Uncertainties	B-1
B.2 Derived Uncertainties	B-3
B.2.1 Mean Flow Derived Uncertainties	B-3
B.2.2 Hot-Wire Derived Uncertainties	B-4
B.3 PIV Signal-to-Noise Uncertainty	B-4
Appendix C : Data Files.....	C-1
Bibliography	BIB-1
Vita.....	VITA

List of Figures

Figure 3-1: AFIT Mach 2.8 wind tunnel schematic	3-1
Figure 3-2: Pressure gradient contours & data collection locations	3-4
Figure 3-3: Optical glass floor schematic.....	3-4
Figure 3-4: Mach 5.0 wind tunnel schematic.....	3-6
Figure 3-5: PIV schematic.....	3-10
Figure 5-1: ZPG and CPG flow visualization images.....	5-1
Figure 5-2: ZPG and FPG flow visualization images	5-2
Figure 5-3: Pitot pressure profile	5-4
Figure 5-4: Cone-static pressure profile.....	5-4
Figure 5-5: Mach number profile.....	5-5
Figure 5-6: ZPG hot-film data.....	5-7
Figure 5-7: FPG hot-film data	5-7
Figure 5-8: CPG ($x = 68$ cm) hot-film data.....	5-9
Figure 5-9: CPG ($x = 70$ cm) hot-film data.....	5-9
Figure 5-10: ZPG velocity contour plot.....	5-12
Figure 5-11: FPG velocity contour plot.....	5-12
Figure 5-12: CPG velocity contour plot	5-12
Figure 5-13: ZPG velocity vectors	5-13
Figure 5-14: FPG velocity vectors.....	5-13
Figure 5-15: CPG velocity vectors	5-13
Figure 5-16: ZPG velocity comparison	5-15
Figure 5-17: FPG velocity comparison.....	5-15
Figure 5-18: CPG velocity comparison	5-16
Figure 5-19: ZPG Van Driest velocity profile	5-17

Figure 5-20: FPG Van Driest velocity profile	5-18
Figure 5-21: CPG ($x = 68$ cm) Van Driest velocity profile.....	5-18
Figure 5-22: CPG ($x = 70$ cm) Van Driest velocity profile.....	5-19
Figure 5-23: ZPG mass flux turbulence intensity	5-20
Figure 5-24: FPG mass flux turbulence intensity	5-21
Figure 5-25: CPG ($x = 68$ cm) mass flux turbulence intensity.....	5-22
Figure 5-26: CPG ($x = 70$ cm) mass flux turbulence intensity.....	5-23
Figure 5-27: ZPG power spectra data	5-24
Figure 5-28: FPG power spectra data.....	5-24
Figure 5-29: CPG power spectra data	5-25
Figure 5-30: ZPG u turbulence intensity contours (%)	5-27
Figure 5-31: FPG u turbulence intensity contours (%)	5-27
Figure 5-32: CPG u turbulence intensity contours (%).....	5-27
Figure 5-33: ZPG u turbulence intensity profiles	5-29
Figure 5-34: FPG u turbulence intensity profiles.....	5-29
Figure 5-35: CPG ($x = 68$ cm) u turbulence intensity profile	5-30
Figure 5-36: CPG ($x=70$ cm) u turbulence intensity profile	5-31
Figure 5-37: Density fluctuations	5-31
Figure 6-1: Mach 1.7 Pitot pressure profiles	6-1
Figure 6-2: Mach 1.7 Mach number profile.....	6-2
Figure 6-3: Mach 1.7 velocity profile.....	6-2
Figure 6-4: Mach 1.7 ZPG hot-film data	6-4
Figure 6-5: Mach 1.7 ZPG mass flux turbulence intensity	6-5
Figure 6-6: Mach 1.7 power spectra data.....	6-6
Figure 6-7: Mach 1.7 u turbulence intensity profiles.....	6-7
Figure 6-8: Mach 1.7 density fluctuation profiles.....	6-7

Figure 6-9: Mach 1.7 total temperature fluctuation profiles	6-8
Figure 7-1: Mach 5.0 Pitot pressure profiles	7-1
Figure 7-2: Mach 5.0 Mach number profile.....	7-2
Figure 7-3: Mach 5.0 velocity profile.....	7-2
Figure 7-4: Mach 5.0 CPG and FPG static pressure profiles	7-3
Figure A-1: Mach 2.8 hot-wire calibration curve (OHR = 2.03).....	A-2
Figure A-2: Mach 2.8 hot-wire calibration curve (OHR = 1.66).....	A-2
Figure A-3: Mach 1.7 hot-wire calibration curves.....	A-4

List of Tables

Table 1-1: Kolmogoroff scale calculations.....	1-1
Table 3-1: Pressure gradient test section curve coefficients.....	3-3
Table 4-1: Mach 2.8 probe and overheat ratio data.....	4-10
Table 4-2: Mach 1.7 probe and overheat ratio data.....	4-10
Table 5-1: Boundary layer thickness parameters.....	5-5
Table 5-2: Number of PIV images used to create the combined image	5-10
Table 6-1: Mach 1.7 boundary layer thickness.....	6-3
Table 7-1: Mach 5.0 boundary layer thickness.....	7-1
Table 8-1: Verification of Settles and Dodson criteria.....	8-2
Table A-1: Mach 2.8 sample raw calibration file (OHR = 2.03).....	A-1
Table A-2: Mach 2.8 sample raw calibration file (OHR = 1.66).....	A-1
Table A-3: Mach 2.8 calibration constants	A-3
Table A-4: Mach 1.7 sample raw calibration file (OHR = 1.95).....	A-3
Table A-5: Mach 1.7 sample raw calibration file (OHR = 1.66).....	A-4
Table A-6: Mach 1.7 calibration constants	A-5
Table B-1: Mach 2.8 ZPG reference conditions	B-2
Table B-2: Elementary uncertainties.....	B-3
Table B-3: Mean flow derived uncertainties	B-4
Table B-4: Boundary layer height uncertainty	B-4
Table B-5: Van Driest uncertainties	B-4
Table B-6: Hot-wire derived uncertainties	B-5
Table C-1: Mach 2.8 ZPG pressure data.....	C-1
Table C-2: Mach 2.8 FPG pressure data	C-2
Table C-3: Mach 2.8 ZPG hot-film data - traverse up	C-4

Table C-4: Mach 2.8 ZPG separated turbulence variables single overheat- traverse up	C-4
Table C-5: Mach 2.8 ZPG hot-film data - traverse down	C-5
Table C-6: Mach 2.8 ZPG separated turbulence variables single overheat - traverse down	C-5
Table C-7: Mach 2.8 FPG hot-film data - traverse up	C-6
Table C-8: Mach 2.8 FPG separated turbulence variables single overheat - traverse up.....	C-7
Table C-9: Mach 2.8 CPG ($x = 68$ cm) hot-film data - traverse up.....	C-8
Table C-10: Mach 2.8 CPG ($x=68$ cm) separated turbulence variables single overheat- traverse up	C-8
Table C-11: Mach 2.8 CPG ($x = 68$ cm) hot-film data - traverse down	C-9
Table C-12: Mach 2.8 CPG ($x=68$ cm) separated turbulence variables single overheat- traverse down..	C-9
Table C-13: Mach 2.8 CPG ($x = 70$ cm) hot-film data - traverse up.....	C-10
Table C-14: Mach 2.8 CPG ($x=70$ cm) separated turbulence variables single overheat- traverse up	C-10
Table C-15: Mach 2.8 CPG ($x = 70$ cm) hot-film data - traverse down	C-11
Table C-16: Mach 2.8 CPG ($x=70$ cm) separated turbulence variables single overheat- traverse down	C-11
Table C-17: Mach 2.8 discrete data turbulence intensity points	C-12
Table C-18: Mach 2.8 hot-film van Driest data	C-12
Table C-19: Mach 2.8 power spectra data.....	C-13
Table C-20: Mach 2.8 ZPG PIV data.....	C-17
Table C-21: Mach 2.8 FPG PIV data - 25 images.....	C-17
Table C-22: Mach 2.8 FPG PIV data - 93 images.....	C-18
Table C-23: Mach 2.8 CPG ($x = 68$ cm) PIV data	C-18
Table C-24: Mach 2.8 CPG ($x = 68$ cm) PIV data	C-19
Table C-25: PIV van Driest data	C-19
Table C-26: Mach 1.7 ZPG pressure data	C-20
Table C-27: Mach 1.7 FPG pressure data	C-22
Table C-28: Mach 1.7 ZPG hot-film data - traverse up	C-24
Table C-29: Mach 1.7 ZPG hot-film data - traverse down.....	C-25

Table C-30: Mach 1.7 ZPG separated turbulence variables - traverse down	C-26
Table C-31: Mach 1.7 ZPG separated turbulence variables - traverse down	C-26
Table C-32: Mach 1.7 discrete turbulence intensity data points	C-27
Table C-33: Mach 1.7 power spectra data.....	C-27
Table C-34: Mach 5.0 ZPG pressure data.....	C-30
Table C-35: Mach 5.0 FPG pressure data	C-31
Table C-36: Mach 5.0 CPG ($X_{ts} = 5.1$ cm) pressure data	C-33
Table C-37: Mach 5.0 CPG ($X_{ts} = 6.35$ cm) pressure data	C-34
Table C-38: Mach 5.0 wall static pressure data.....	C-34

List of Symbols

Symbol	Description
a, b	hot-wire calibration constants
A', B'	Constants in Crocco relationship and van Driest correlation
C _f	Coefficient of friction
CFD	Computational fluid dynamics
C _o	Constant used in Chapter 4
CPG	Combined pressure gradient
f	frequency, hot-wire sensitivity
FANS	Favré averaged Navier-Stokes equations
FPG	Favorable pressure gradient
g	hot-wire sensitivity
GLS	General least squares
h	Enthalpy
k	Constant in van Driest correlation, thermal conductivity
\bar{L}	Average vector length
LDV	Laser doppler velocimetry
M	Mach number
MOH	Multiple overheat ratios
N	Number of overheat ratios
Nu	Nusselt number
P	Stagnation or total pressure
p	Static pressure
PIV	Particle image velocity
Pr	Prandtl number

q	Heat flux vector
Q	Heat flux
r	Recovery factor
R	Resistance
RANS	Reynolds averages Navier-Stokes equations
Re	Reynolds number
RHS	Right hand side (of an equation)
SOH	Single overheat ratio
T	Characteristic time, temperature
t	time
TI	Turbulence intensity
u	axial velocity
u*	Van Driest friction velocity
u_{eff}	Van Driest effective velocity
u_{eff}⁺	Van Driest effective scaled velocity
V	Velocity vector
V_w	Wire voltage
x	coordinate tangent to the flow direction
y	coordinate normal to the wind tunnel ceiling
y⁺	Van Driest length scale
ZPG	Zero pressure gradient
α	Constant in single overheat ratio data reduction
β	Clauser's equilibrium factor, constant in single overheat ratio data reduction
δ	boundary layer thickness
δ*	Compressible displacement thickness
δ_i*	Incompressible displacement thickness

δ_{ij}	Kronecker delta
ΔL_{G-R}	Individual vector length
ϵ	Percent error
γ	Ratio of specific heats ($= 1.4$)
k	Constant in van Driest correlation
λ	Wavelength
μ	absolute viscosity
Π	Coles wake function
θ	Compressible momentum thickness
θ_i	Incompressible momentum thickness
ρ	density
τ	shear stress
TI	Turbulence intensity
ω	Constant in van Driest correlation

Subscripts

1,2	Wind tunnel station
bar	Average
c	Cone
e	Edge
l	Leads
M	Mach number
o	Reference or total
rms	Root mean square
s	Series
t	Total

ts	Test section
u	Velocity
w	Wall, wire
δ	Boundary layer height

Superscripts

$()''$	Favré fluctuating component
$()'$	Reynolds fluctuating component
$\overline{()}$	Time averaged variable
$\tilde{()}$	Favré averaged variable
$^\circ$	Degree
TF	Turbulent, Favré averaged
TR	Turbulent, Reynolds averaged

Abstract

This study examined the effect of mild pressure gradients on the mean and turbulent flow of high-speed boundary layers. Three Mach numbers (1.7, 3.0 and 5.0) were investigated. Three pressure gradients were examined; a zero pressure gradient (ZPG), a favorable pressure gradient (FPG), and a combined pressure gradient (CPG). The CPG consisted of an adverse pressure gradient followed by a favorable pressure gradient. Conventional pressure probes, hot-wire and particle image velocimetry (PIV) were used to examine the flow. Measurement included mean velocity, velocity turbulence intensity, mass flux turbulence intensity and energy spectra. Instantaneous (10 nsec) Mie scattering flow visualizations were acquired. Qualitatively, the flow visualizations indicated that the turbulent flow structures were strongly affected by the pressure gradients. For the Mach 2.8 case, the PIV contours and the hot-wire profiles both indicated that the boundary layer thickness increased by 40% and decreased by 100% relative to the ZPG for the favorable and adverse pressure gradients, respectively. Further, the PIV and hot-wire data indicated that the axial turbulence intensity levels increased by 22% for the CPG and decreased by 25% for the FPG. The energy spectra data indicated that once a pressure gradient was applied (favorable or adverse) the low frequency energy increased followed by a rapid decay. Lastly, it was found that nominally 20 to 30 PIV images were sufficient for mean flow boundary layer velocities, but 93 images (the maximum recorded in this study) were insufficient to adequately resolve Reynolds shear stresses.

EXPERIMENTAL INVESTIGATION OF COMPRESSIBLE BOUNDARY LAYERS UNDER THE INFLUENCE OF PRESSURE GRADIENTS

1. Introduction

1.1 Motivation

Current U.S. high-speed aerospace vehicles are designed to operate at such high velocities and Reynolds numbers that conventional wind tunnel testing rapidly becomes too expensive or time consuming. To reduce the cost of testing, computational fluid dynamics (CFD) play an ever increasing role in the design philosophy. CFD has demonstrated its reliability and accuracy for simple geometries such as flow over a flat plate, but results for more complex shapes are as yet unproven. For the exterior of the vehicle to the internal shape of the engine's inlet or nozzle, turbulent flow over curved surfaces dominates the design. The underlying physics of these types of flows are not understood (Bradshaw, 1974 & Spina et al., 1994); thus, accurate predictions are not possible.

Turbulence has proven to be the controlling factor in the understanding of high-speed high-Reynolds number flows. Turbulent flow is characterized by a wide range of temporal and size scales, with the smallest defined by Kolmogoroff scales for length, speed and time (Wilcox, 1994). To accurately resolve the smallest eddies in a turbulent flow, the programmer must space the CFD grid nodes at a resolution sufficient to capture these eddies. Detailed estimates of the Kolmogoroff scales for Mach 2.9 and Mach 5.0 flow, with corresponding CFD solution times, are listed in Table 1-1. The total number of grid points is based on a 6.35 cm x 6.35 cm x 75 cm volume and a 7.62 cm x 7.62 cm x 25.4 cm volume for the Mach 3.0 and Mach 5.0 tunnels, respectively. These volumes represent the total test section volume for each tunnel. The total number of calculations is based on the crude estimate of 10^7

calculations per grid point. The time to complete the solution is based on IBM's latest computational goal of 3 trillion calculations per second (Pressman, 1996).

Table 1-1: Kolmogoroff scale calculations

	Mach 3.0 tunnel	Mach 5.0 tunnel
Freestream Reynolds number (Re_δ , estimated)	1.9×10^6	1.21×10^6
Boundary layer thickness (δ) (m, estimated)	0.13	2.24×10^{-3}
Kolmogoroff length scale (m)	2.48×10^{-6}	1.09×10^{-8}
Total number of grid points	2.00×10^{14}	1.15×10^{21}
Total number of calculations	2.00×10^{21}	1.15×10^{28}
Time to complete the solution (years)	21,000	12,000

The time to complete the solution in Table 1-1 is only for the test section in question. Solution times over curved surfaces or entire vehicles, even with clustering, would naturally take longer. Hence, computational speed and memory are important limitations of modern CFD.

One successful method used to reduce the CFD solution time is by using approximate, time-averaged forms of the governing Navier-Stokes equations. The two most prevalent averaging techniques are Reynolds averaging and Favré averaging. Since the full Navier-Stokes equations are non-linear, the averaging techniques result in extra cross correlation fluctuation terms (see Sections 2.1.2 and 2.1.3). This leads to the closure problem wherein more unknowns than equations exist. The science and art of turbulence modeling is to define new variables to help solve this under-defined system.

The turbulence model evolution followed the classical approach of solution development. Simple flows were examined first and then extrapolated to more complex cases. For CFD this means the incompressible zero pressure gradient (ZPG) case was examined first. Once this case was satisfactorily understood, the existing models were extrapolated to flow with pressure gradients on an ad-hoc basis. Due to the quantity and quality of subsonic data with and without pressure gradients, this turned out to be a natural progression of model generality. However, for high-speed flow the situation is more complicated and not well understood. *This lack of understanding can be traced to the clear lack of accurate turbulence data* (Spina et al., 1994).

Morkovin's hypothesis provided the rationale for extrapolating incompressible models to compressible flows. Morkovin's hypothesis states that "the turbulence structure is unaffected by compressibility as long as the fluctuation Mach number is much less than unity" (Morkovin, 1964). While this hypothesis holds for most cases, Liou and Shih note that Morkovin's hypothesis does not apply for high-speed shear layers with shock or expansion wave interaction (Liou and Shih, 1991). Further, Spina et al. (Spina et al., 1994) indicate that the limitations of this hypothesis are more restrictive than originally believed. In any event, this hypothesis has led to the "ad-hoc" extrapolation of low-speed turbulence models, at all levels, to high-speed flow where the effects of compressibility are treated with correction factors (Wilcox, 1994).

Patel, Rodi and Scheuerer found that while some of these "extrapolation" models work well for flat plates, they fail for curved surfaces. They suggest refining the governing equations in the k-e model to adjusting equation constants based on empirical data (Patel, Rodi and Scheuerer, 1984). Degani and Smits found that a one-equation model provides better results than an algebraic model for compressible flow with regions of concave curvature (Degani and Smits, 1990). Again, they recommend empirical modifications to the equations to better match experimental data. These non-physical empirical corrections are prevalent in the literature (Bradshaw, 1973).

Shock waves will naturally occur in any high performance flight vehicle. As a result, they will interact with the boundary layer on the surfaces of the vehicle. The interaction between the shock wave and boundary layer is complex and difficult to model. However, its importance cannot be under-emphasized. If the shock interacts with a control surface for a missile, then the resulting adverse pressure gradient could cause the missile to miss its target due to lack of control authority. If a larger control surface were used to counteract the shock effects, a negative impact on missile speed and range would have to be accepted.

1.2 Research Objectives

As discussed in Section 1.1, the need for quality data is clear. Thus, addressing this need is the primary goal of this thesis. Data obtained from this thesis will assist in validation of current and future CFD codes as well as to aid the understanding of the physics of these flow conditions. An additional goal is to compare turbulence data obtained via hot-wire anemometry to turbulence data obtained by Laser Doppler Velocimetry (LDV). The final goal is to verify the applicability of PIV for compressible flow analysis.

Settles and Dodson established a set of criteria that data must adhere to in order to maximize the usefulness of the data (Settles and Dodson, 1994). Their criteria are:

1. Baseline applicability: All candidate studies for use must be experiments involving turbulent flow in either the supersonic or hypersonic Mach number range.
2. Simplicity: Experimental geometries must be sufficiently simple that they may be modeled by CFD methods.
3. Specific applicability: All candidate studies passing these criteria must be capable of providing some useful test of turbulence modeling.
4. Well-defined experimental boundary conditions: All incoming conditions must be carefully documented. This includes that state of the incoming boundary layer. For studies claiming “two-dimensional” flow, data indicating the extent of the spanwise flow variations should be provided.
5. Well-defined error bounds: The experimenter must provide an analysis of the accuracy and repeatability of the data, or error bounds on the data themselves. Further, error bounds on the data must be substantiated in a quantifiable manner.
6. Adequate documentation of the data: Data must be documented and tabulated in a machine-readable format.
7. Adequate spatial resolution of the data: Experiments must present data of sufficiently high resolution, compared with the scaled flow in question, such that the key features of the flow are clearly resolved.

The data in this research were acquired with the goal of meeting these criteria.

1.3 Overview of Current Study

PIV was used to make mean and fluctuating velocity measurement in the AFIT Mach 3.0 wind tunnel for three pressure gradients. The results of the PIV analysis were compared to LDV measurements. The pressure gradient models that were studied include the flat plate (ZPG) a favorable pressure gradient

(FPG) and a combined pressure gradient (CPG). These models have been the source of extensive study at AFIT (Dotter, 1994; Miller, 1994; Luker, 1995 & Hale, 1995).

Multiple overheat single hot-wire anemometry was used to investigate the mean and fluctuating mass flux in the boundary layer with the same three pressure gradients in Mach 2.8 flow. In addition, the ZPG was investigated under Mach 1.7 flow. Also, the power spectra of the boundary layer were investigated for three pressure gradients in Mach 2.8 flow. Power spectra data was acquired for the ZPG and FPG in Mach 1.7 flow. Finally, conventional pressure measurements (Pitot pressure and cone-static pressure) were made for the pressure gradient models in Mach 1.7, Mach 2.8 and Mach 5.0 flow.

1.4 Thesis Synopsis

An overview of the governing equations and a brief literature review are given in Chapter 2. The equipment used in this research effort is presented in Chapter 3. Chapter 4 documents the data analysis techniques. Chapters 5, 6 and 7 contain the results for Mach 2.8, Mach 1.7 and Mach 5.0 flow, respectively. Finally, chapter 8 contains the conclusion and recommendations drawn from this research.

2. Background

This section presents a discussion on the governing equations and a literature review.

2.1 Governing Equations

The Navier-Stokes equations are a set of coupled non-linear partial differential equations that govern all types of fluid flow, including turbulent flow. The nature of the Navier-Stokes equations makes them difficult to solve in closed form. As shown in Section 1.1, the solution time with current or near future computers for a simple grid would take far beyond the life span of any researcher. To combat these difficulties, scientists and engineers use an approximate form of the equations. The approximate forms create the problem of turbulence closure wherein the unknowns outnumber the equations.

This section assists the reader in development of the Reynolds and Favré time-averaged Navier-Stokes equations. The development highlights the closure problem as well as defines the cross-correlation terms that time averaging creates. In addition, the difference between compressible flows and incompressible flows becomes apparent.

2.1.1 The Compressible Navier-Stokes Equations

The Navier-Stokes equations in Cartesian form can be written as (Anderson, 1984):

$$\begin{aligned} \frac{D\rho}{Dt} + \rho \nabla \cdot \mathbf{V} &= 0 \\ \rho \frac{D\mathbf{V}}{Dt} &= \nabla \cdot \bar{\pi} + \rho \mathbf{f}_b \\ \rho \frac{Dh}{Dt} &= \frac{Dp}{Dt} + \frac{DQ}{Dt} - \nabla \cdot \mathbf{q} + \Phi \end{aligned} \tag{2.1}$$

where \mathbf{f}_b is the body force vector (normally neglected) acting on the fluid and

$$\begin{aligned} \frac{D}{Dt} &\equiv \frac{\partial}{\partial t} + \mathbf{V} \cdot \nabla \\ \pi_{ij} &= -p\delta_{ij} + \tau_{ij} \\ \tau_{ij} &= \mu \left\{ \left(\frac{\partial u_i}{\partial x_j} + \frac{\partial u_j}{\partial x_i} \right) - \frac{2}{3} \delta_{ij} \frac{\partial u_k}{\partial x_k} \right\} \end{aligned} \tag{2.2}$$

$$\Phi = \tau_{ij} \frac{\partial u_i}{\partial x_j}$$

2.1.2 Reynolds-Averaged Navier-Stokes Equations (RANS)

One method of simplifying the Navier-Stokes equations is known as Reynolds averaging. The Reynolds-averaged Navier-Stokes equations are derived by separating a variable into time invariant and time variant parts, as demonstrated for velocity below.

$$u(x, y, z, t) = \bar{u}(x, y, z, t) + u'(x, y, z, t) \quad (2.3)$$

\bar{u} is the time-averaged velocity. Note that the time-averaged velocity itself might also be a function of time. The time-averaged velocity is defined as (Wilcox, 1994)

$$\bar{u}(x, y, z, t) \equiv \frac{1}{T} \int_t^{t+T} u(x, y, z, t) dt \quad (2.4)$$

T is a characteristic time that must be larger than the period of the velocity fluctuations, but smaller than the period of the mean flow.

When the separated variables defined in Equation (2.3) are substituted into the Navier-Stokes equations and the rules of time averaging are applied, the RANS are created. The key rules of time averaging is that an average of a single fluctuating component is zero but an average of two or more fluctuating components are not equal to zero. Assuming zero body forces, the RANS equations are found to be (Wilcox, 1994)

$$\begin{aligned} \frac{\partial \bar{p}}{\partial t} + \frac{\partial (\bar{\rho} \bar{u}_j + m_j^{TR})}{\partial x_j} &= 0 \\ \frac{\partial (\bar{\rho} \bar{u}_i + \bar{\rho}' \bar{u}_i')}{\partial t} + \frac{\partial (\bar{\rho} \bar{u}_i \bar{u}_j)}{\partial x_j} &= -\frac{\partial \bar{p}}{\partial x_i} + \frac{\partial (\bar{\tau}_{ij} + \tau_{ij}^{TR})}{\partial x_j} \\ \frac{\partial (\bar{\rho} \bar{e}_o + \bar{\rho}' \bar{h}_o')}{\partial t} + \frac{\partial (\bar{\rho} \bar{h}_o \bar{u}_j)}{\partial x_j} &= \frac{\partial (\bar{u}_i \bar{\tau}_{ij} + \bar{u}_i' \bar{\tau}_{ij}' - \bar{q}_j - q_j^{TR})}{\partial x_j} \end{aligned} \quad (2.5)$$

where

$$\bar{m}_j^{TR} = \overline{\rho' u'}$$

$$\bar{\tau}_{ij} = \mu \left\{ \left(\frac{\partial \bar{u}_i}{\partial x_j} + \frac{\partial \bar{u}_j}{\partial x_i} \right) - \frac{2}{3} \delta_{ij} \frac{\partial \bar{u}_k}{\partial x_k} \right\}$$

$$\bar{\tau}_{ij}' = \mu \left\{ \left(\frac{\partial \bar{u}_i'}{\partial x_j} + \frac{\partial \bar{u}_j'}{\partial x_i} \right) - \frac{2}{3} \delta_{ij} \frac{\partial \bar{u}_k'}{\partial x_k} \right\}$$

$$\bar{\tau}_{ij}^{TR} = -\bar{\rho} \bar{u}_i' \bar{u}_j' - \bar{u}_i \bar{\rho}' \bar{u}_j' - \bar{u}_j \bar{\rho}' \bar{u}_i' - \bar{\rho}' \bar{u}_i' \bar{u}_j' \quad (2.6)$$

$$\bar{q}_i = -k \frac{\partial \bar{T}}{\partial x_i}$$

$$\bar{q}_i^{TR} = -\bar{\rho} \bar{u}_i' \bar{h}_o' - \bar{h}_o \bar{\rho}' \bar{u}_i' - \bar{u}_i \bar{\rho}' \bar{h}_o' - \bar{\rho}' \bar{u}_i' \bar{h}_o'$$

The subscript o in Equations (2.5) and (2.6) indicates stagnation quantities. The turbulence terms (noted by a superscript TR), \bar{m}_j^{TR} , $\bar{\tau}_{ij}^{TR}$ and \bar{q}_i^{TR} are known as the apparent mass flux, turbulent shear stress (Reynolds) and the turbulent heat flux, respectively. These are the “extra” terms discussed in the closure problem. For incompressible flow, the apparent mass flux and the final three terms of the turbulent Reynolds shear stress and turbulent heat flux are zero. The triple correlation in the RHS of the turbulent Reynolds shear stress and turbulent heat flux is usually assumed to be much smaller than the other terms. PIV and LDV directly measure the velocity and are more appropriate for Reynolds stress calculations.

2.1.3 Favré-Averaged Navier-Stokes Equations (FANS)

An alternate method of simplifying the Navier-Stokes equations is known as Favré averaging. The Favré-averaged Navier-Stokes equations are similar to the Reynolds averaged equations except the mass dependent terms (e.g., terms with ρ) are replaced by a mass averaged term, $\tilde{\phi}$, plus a fluctuation term, ϕ'' :

$$\phi = \tilde{\phi} + \phi'' \quad \phi'' \equiv \frac{\overline{\rho \phi}}{\rho} \quad (2.7)$$

Mass independent terms (such as ρ and p) are replaced by time variant and time invariant terms following the same approach as in Reynolds averaging. Note that the incompressible Favré -averaged equations reduce to the Reynolds-averaged equations. A key difference between Reynolds and Favré averaging becomes clear after inspection of Equations (2.3) and (2.7). This inspection shows that $\overline{\phi}' = 0$ but $\overline{\phi}'' \neq 0$. With Equation (2.7) and the time averaging rules, the FANS equations are found to be (Wilcox, 1994)

$$\begin{aligned} \frac{\partial \overline{\rho}}{\partial t} + \frac{\partial (\overline{\rho} \tilde{u}_j + m_j^{TF})}{\partial x_j} &= 0 \\ \frac{\partial (\overline{\rho} \tilde{u}_i)}{\partial t} + \frac{\partial (\overline{\rho} \tilde{u}_i \tilde{u}_j)}{\partial x_j} &= -\frac{\partial \overline{p}}{\partial x_i} + \frac{\partial (\overline{\tau}_{ij} + \tau_{ij}^{TF})}{\partial x_j} \\ \frac{\partial (\overline{\rho} \tilde{e}_o)}{\partial t} + \frac{\partial (\overline{\rho} \tilde{h}_o \tilde{u}_o)}{\partial x_j} &= \frac{\partial (\tilde{u}_i \overline{\tau}_{ij} + \overline{u_i'' \tau_{ij}'} - \overline{q_j} - q_j^{TF})}{\partial x_j} \end{aligned} \quad (2.8)$$

where

$$m_j^{TF} = 0$$

$$\overline{\tau}_{ij} = \mu \left\{ \left(\frac{\partial \tilde{u}_i}{\partial x_j} + \frac{\partial \tilde{u}_j}{\partial x_i} \right) - \frac{2}{3} \delta_{ij} \frac{\partial \tilde{u}_k}{\partial x_k} \right\} + \mu \left\{ \left(\frac{\partial \overline{u}_i''}{\partial x_j} + \frac{\partial \overline{u}_j''}{\partial x_i} \right) - \frac{2}{3} \delta_{ij} \frac{\partial \overline{u}_k''}{\partial x_k} \right\} \quad (2.9)$$

$$\tau_{ij}^{TF} = -\overline{\rho} \overline{u_i'' u_j''}$$

$$q_i^{TF} = -\overline{\rho} \overline{u_j'' h_o''}$$

Note that the apparent mass in the Favré averaged equation is identically zero.

Researchers have found that the FANS work well for compressible shear layers but fail when used to model shear layers in the vicinity of shocks or expansion waves (Wilcox, 1994).

2.1.4 Comparison Between Favré-Averaged and Reynolds-Averaged N-S Equations

An interesting relationship can be developed by equating the Reynolds averaged terms to the Favré averaged terms. The following example uses the u component of velocity. By the definition of Reynolds averaged and Favré averaged variables

$$u = \bar{u} + u' = \tilde{u} + u'' \quad (2.10)$$

Taking the time average and rearranging Equation (2.10) results in

$$\bar{u} - \tilde{u} = u'' = \frac{\overline{\rho u}}{\rho} = \frac{(\rho + \rho')(\bar{u} + u')}{\rho} \quad (2.11)$$

Expanding the RHS of Equation (2.11) and by use of the properties of time averaging

$$u'' = \frac{\overline{\rho' u'}}{\rho} \quad (2.12)$$

Thus, Equation (2.12) defines the relationship between Reynolds averaged variables and Favré averaged variables.

Through a similar set of identities, the relationship between the Reynolds shear stress and Favré shear stress can be determined.

$$\overline{\rho \bar{u}_i' \bar{u}_j'} = \overline{\rho \bar{u}_i'' \bar{u}_j''} - \overline{\rho \bar{u}_i''} \overline{\bar{u}_i''} \quad (2.13)$$

The last term on the RHS of Equation (2.13) is of fourth order. Usually, this term is much smaller than the other terms and is neglected. Thus,

$$\tau_{ij}^{TR} \approx \tau_{ij}^{TF} \quad (2.14)$$

Thus, hot-wire anemometry can be used to measure Reynolds stress as well as Favré stress.

2.2 Literature Review

Undoubtedly, many experiments have been conducted to measure mean flow quantities for supersonic and hypersonic flows; however, these experiments mainly concern ZPG flow (Robinson et al., 1983; Johnson and Rose, 1975; Fernando and Smits, 1990; Kistler, 1959 & Parrott et al., 1989) and rarely

measure turbulence quantities. Smith and Smits give as the reason for this lack of data as "... is that they are difficult to obtain. Reliable and accurate measurements of turbulence properties are difficult to make in any supersonic flow, and the difficulties are usually more extreme in the presence of flow distortions" (Smith and Smits, 1994). For many studies where turbulence quantities are measured, the quality of the data was found to be flawed and unusable (Bradshaw and Ferris, 1971). Settles and Dodson (Settles and Dodson, 1994) echo this concern. They surveyed over one hundred shock/boundary layer interaction studies and found only 19 that met their turbulence criteria. A brief summary of relevant research on this topic is presented below. The review presented here is not all inclusive. Instead papers relevant to the present thesis objectives (Section 1.2) are presented. A complete review can be found in Spina et al., 1994. In addition, a review of flow visualization research is given.

Bradshaw and Ferriss studied the turbulent kinetic energy equation for boundary layers in compressible flow with arbitrary pressure gradients (Bradshaw and Ferriss, 1971). They obtained correct trends for the ZPG case but were unable to find quality pressure gradient data to compare with their results.

Bradshaw conducted a series of calculations designed to show that bulk compression or dilation affects turbulent shear layers (Bradshaw, 1974). Bradshaw found bulk compression or dilation had a larger effect than was expected and should be accounted for in future studies. Fluctuating turbulence measurement were not made.

Adverse pressure gradients have been found to destabilize the boundary layer. In other words, the turbulent fluctuating properties increase (Dotter, 1994 & Hale, 1995). Adverse pressure gradients can be created by a shock interacting with the boundary layer or by concave curvature. Lewis and Gran (Lewis and Gran, 1972) created an adverse pressure gradient by shock wave boundary layer interaction. They found that turbulent results compare favorably with low-speed results. Fernando and Smits (Fernando and Smits, 1990) suggest that the turbulence quantities undergo a mild amplification while the mean flow structure remains unchanged. Both of these experiments are suspect because they do not include the effect of streamline curvature on the turbulence quantities.

Recall that adverse pressure gradients can be created by regions of concave curvature. Jayaram, Taylor and Smits found that the turbulence levels increased due to the combined effect of the pressure gradient, streamline curvature and bulk compression (Jayaram, Taylor and Smits, 1986). Interestingly, they found, for two of their three cases, that the weak shock wave had no effect on the turbulent quantities.

Few FPG studies have been made. The few that do exist suggest that the FPG acts to damp out the turbulent fluctuations. Bulk dilation and supersonic stream tube expansion provide the most likely explanations of this phenomena (Luker et al., 1997). Studies by Luker (Luker, 1995) and Miller (Miller, 1994) confirm the dampening effect of the pressure gradient.

Flow visualization provides an important diagnostic tool to understand the effect of the pressure gradient on the structure of the flow. Spina (Spina, 1988) discovered a wide range of temporal and spatial scales in a ZPG flow. Application of a FPG was found to increase the boundary layer thickness and assist the development of the elongated structures (Arnette et al., 1995).

Development of particle induced velocimetry is the latest technique available for researchers and scientists. This technique has been proven for a wide range of applications ranging from wake flow (Yao and Pachal, 1994) to supersonic flat plate flow (Glawe et al., 1996). However, its applicability to compressible flow with pressure gradients has yet to be established.

3. Facilities and Equipment

This chapter discusses the facilities and equipment used during the course of this research. Data were collected in both the AFIT Mach 3.0 blow-down, pressure-vacuum wind tunnel, the AFIT Mach 1.7 in-draft wind tunnel and the AFIT Mach 5.0 blow-down wind tunnel. In addition, this chapter describes wind tunnel configurations, the data collection system, probes, particle image velocimetry (PIV) and computer equipment.

3.1 Mach 3.0 Wind Tunnel

The AFIT Mach 3.0 wind tunnel is a blow-down, vacuum system. One end of the tunnel is connected to vacuum tanks, and the other to a continuous high-pressure air supply. This combination of high-pressure air (0.69 MPa) and vacuum provided the pressure differential for the tunnel to operate at its design conditions. A schematic of the AFIT Mach 3.0 wind tunnel is shown in Figure 3-1.

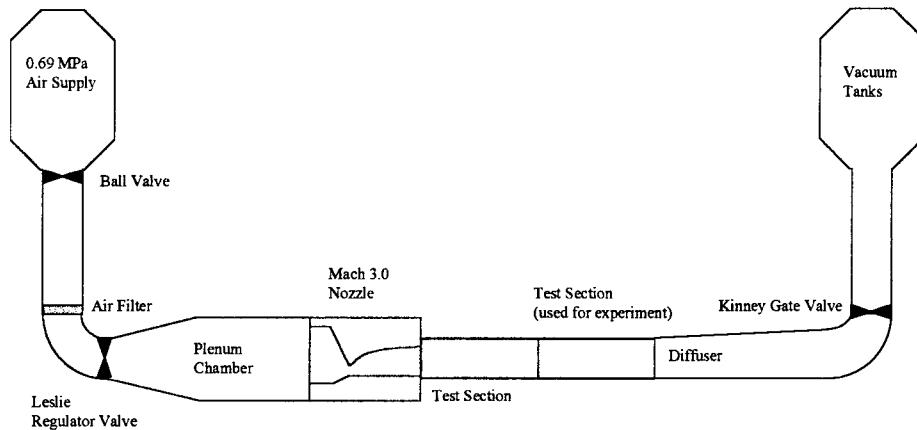


Figure 3-1: AFIT Mach 3.0 wind tunnel schematic

3.1.1 High-Pressure Air Supply

One Atlas Copco GAU 807 air compressor provided high pressure air nominally at 0.69 MPa with a flow rate of 0.5 kg/sec. Two Pioneer Air Systems, Inc. model R500A Refrigerant Air Dryers dried the air prior to the air entering the high-pressure air supply system. The air was filtered a second time by

a centrifugal moisture and particle separator in conjunction with several layers of Filtrite® particle air filters. This system supplied high pressure air to other laboratories in AFIT causing minor fluctuations in air pressure which had a negligible effect on tunnel operation.

3.1.2 Vacuum System

Three Stokes Penwalt model 212-11 MicroVac pumps were used to evacuate the 16.0 cubic meter vacuum tank system. With all three vacuum pumps in operation, the tanks could be evacuated to less than 5.0 mm of Hg in approximately six minutes. Wind tunnel operation began only when the pressure in the vacuum tanks reached 5.0 mm of Hg. This level of pressure allowed approximately 25 seconds of uninterrupted operation before the tunnel unstarted.

3.1.3 Plenum Chamber

The Plenum chamber's pressure (P_{t1}) and temperature (T_{t1}) were maintained at $2.19 \times 10^5 \pm 11.8 \times 10^3$ Pa and 295 ± 2 K, respectively during the testing period. An Endevco 0.69 MPa pressure transducer was used to measure the pressure and an Omega Engineering type K thermocouple was used to measure the temperature. The pressure and temperature were measured upstream of the nozzle but downstream of the flow straighteners.

3.1.4 Mach 3.0 Nozzle

A converging-diverging nozzle created the supersonic flow with a nominal Mach number of 2.9 with a measurement uncertainty of 1.8% (Huffman, Mach 2.9 lab manual). The distance from the throat to the exit was 27.0 cm and the nozzle exit cross section was 6.35 x 6.35 cm. The freestream turbulence was determined to be 0.8% with a standard deviation of 0.2% (Huffman, Mach 2.9 lab manual). At the measurement locations for the present experiments ($x_{ts} > 68$ cm), the Mach number was 2.8. This lower value in Mach number was the result of boundary layer growth.

3.1.5 Test Sections

The test sections of this tunnel were designed to be modular and completely interchangeable. Each test section was 32.8 cm long with inner dimensions of 6.35 cm square. The floor and ceiling sections were constructed out of aluminum alloy 1.91 cm thick. All the seams were fitted with rubber o-rings to tightly seal the sections together. The sections were also fitted with oversize holes to allow for individual section adjustment. This adjustment minimized the effects of expansions or shocks caused by non-aligned seams. The first section consisted of a flat plate ceiling and floor with either aluminum or Plexiglas walls. No measurements were made in this section.

The second test section consisted of a flat plate floor and three different ceilings; a flat plate, a favorable pressure gradient section and an adverse pressure gradient section. The pressure gradient sections matched a third-order polynomial defined by $y(x) = a_0 + a_1x + a_2x^2 + a_3x^3$. $y(x)$ represents the distance from a flat plate ceiling, and x is a scaled distance from the end of the test section. The coefficients for the pressure gradient polynomial are given in Table 3-1.

Table 3-1: Pressure gradient test section curve coefficients

Model	a_0	a_1	a_2	a_3
FPG	-0.2078	0.0897	-0.0095	-0.0360
CPG	1.1858	-0.5410	0.0748	-0.0028

These pressure gradient surfaces have been studied extensively in the Mach 3.0 wind tunnel (Hale, 1995; Luker 1995; Dotter, 1994; Miller, 1994). Figure 3-2 shows the pressure gradient contours and the data collection locations in the Mach 2.8 tunnel.

Data were collected at 71 cm from the throat for the flat plate surface, 71.5 cm from the throat for the FPG and 68 & 71 cm from the throat for the CPG. The walls for this section were either Plexiglas or optical glass as discussed by Hale and Luker (Hale, 1995; Luker, 1995). The optical glass was used when flow visualization data was collected. In addition, an optical glass floor was inserted for Particle Image Velocimetry (PIV) runs. A schematic of the optical glass floor is shown as Figure 3-3.

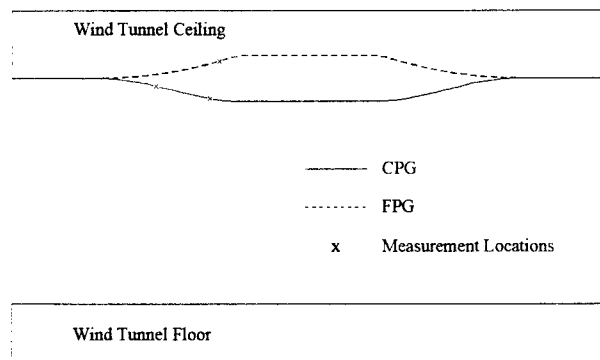


Figure 3-2: Pressure gradient contours & data collection locations

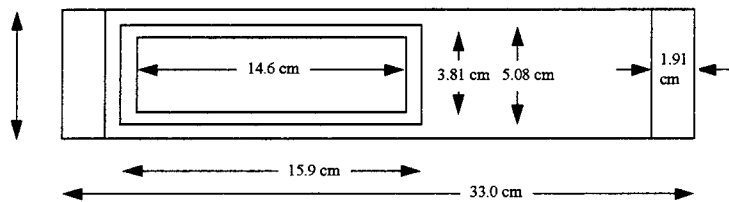


Figure 3-3: Optical glass floor schematic

3.2 Mach 1.7 Wind Tunnel

The AFIT Mach 1.7 wind tunnel is an in-draft, vacuum system. One end of the tunnel is connected to vacuum tanks, and the other end is open to the atmosphere. This combination of atmospheric air and vacuum provided the pressure differential for the tunnel to operate at its design conditions. The AFIT Mach 1.7 tunnel was identical to the AFIT Mach 2.8 tunnel with some exceptions. The exceptions are a different nozzle and a different source of high-pressure air. The same models and test sections were used in the Mach 1.7 tunnel as were used in the Mach 2.8 tunnel.

3.2.1 Plenum Chamber

The Plenum chamber's pressure (P_{tl}) and temperature (T_{tl}) were maintained at $9.47 \times 10^4 \pm 0.51 \times 10^3$ Pa and 295 ± 2 K, respectively during the testing period. An Endevco 0.104 MPa

pressure transducer was used to measure the pressure and an Omega Engineering type K thermocouple was used to measure the temperature. The pressure and temperature were measured upstream of the nozzle but downstream of the flow straighteners.

3.2.2 Mach 1.7 Nozzle

A converging-diverging nozzle created the supersonic flow with a nominal Mach number of 1.7. The distance from the throat to the exit was 27.0 cm and the nozzle exit cross section was 6.35 x 6.35 cm. The freestream turbulence was determined to be on the order of 1.0%.

3.3 Mach 5.0 Wind Tunnel

The AFIT Mach 5.0 wind tunnel is a blow-down wind tunnel system. One end of the tunnel is connected to ambient air, and the other end to the 17.9 MPa air tank. This combination of high-pressure air and ambient air provides the pressure differential for the tunnel to operate at its design conditions. A schematic of the AFIT Mach 5.0 wind tunnel is shown in Figure 3-4.

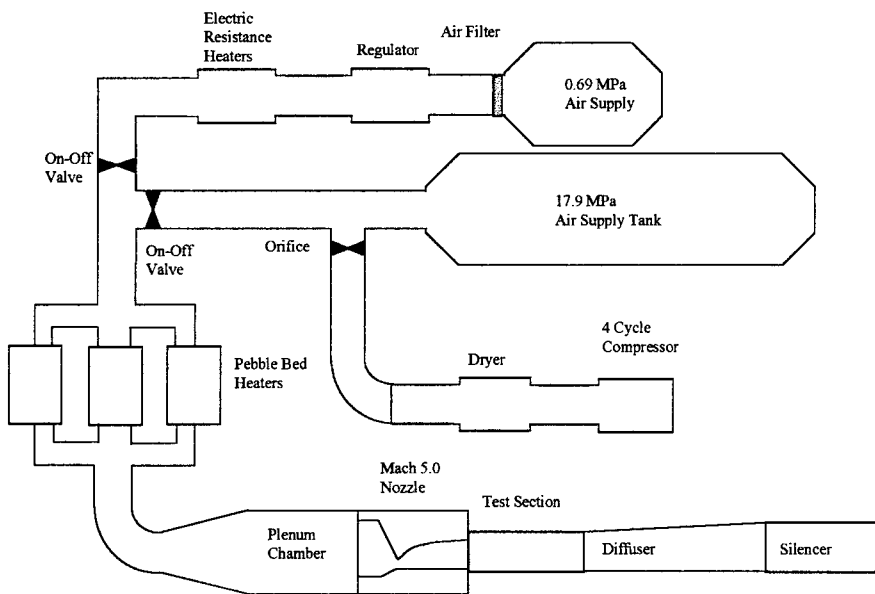


Figure 3-4: Mach 5.0 wind tunnel schematic

3.3.1 Air Supply

A 1.25 cubic meter tank supplied the high pressure air, at a mass flow rate of 1.25 kg/sec. A four cycle Eagle compressor Model HW40HH3 compressed the ambient source air and a Gas Driving Inc., dryer dried the air prior to it being inserted into the tank. The compressor and dryer system could charge the external tank at a rate of 0.69 MPa/hour. Two 20 second runs reduced the tank pressure to 1,800 psig. An Eagle brand regulator Model 03174506 throttled the air to 7.59 MPa before the nozzle throat.

3.3.2 Pebble Bed Heaters

Three pebble bed heaters were used to heat the high pressure air before it entered the nozzle throat. This raised the total temperature of the air to 375 K thereby reducing the possibility of oxygen liquefaction in the test section. The pebble bed heaters consisted of three cylinders 81 cm long with a diameter of 15 cm filled with ceramic pebbles. These ceramic pebbles were heated by 0.69 MPa lab air passing through two Reheat electric heaters, model HDA-2-12. The electric heaters could heat two of the three pebble beds at a rate of 19K/hour when the pebble beds temperature was 315K. Note this rate decreased as the temperature of the pebble beds increased. Each heater allowed 30 seconds of continuous tunnel operation before the heaters cooled to ambient conditions.

3.3.3 Plenum Chamber

The Plenum chamber's pressure and temperature were monitored during each test run. An Endevco 3.45 MPa pressure transducer measured the pressure and an Omega Engineering type K thermocouple measured the temperature upstream of the nozzle. The temperature was recorded by the data acquisition system.

3.3.4 Mach 5.0 Nozzle

A converging-diverging nozzle created the supersonic flow with a nominal Mach number of 5.0. The distance from the throat to the exit was 30.5 cm and the nozzle exit cross section was 7.62 x 7.62 cm.

3.3.5 Test Sections

The test sections of this tunnel were also designed to be modular and completely interchangeable. Each test section was 25.4 cm long with inner dimensions of 7.62 cm square. The ceiling sections were constructed out of aluminum alloy 2.54 cm thick. The walls and floor were constructed out of steel 1.25 cm thick. The walls had two circular optical quality glass inserts used for flow visualization. All the seams were fitted with rubber o-rings to tightly seal the sections together. The sections were also fitted with oversize holes to allow for individual section adjustment similar to the Mach 2.8 tunnel. This adjustment minimized the effects of expansions or shocks caused by non-aligned seams.

The test section ceilings consisted of a flat plate floor and three different ceilings; a flat plate, a favorable pressure gradient section and an adverse pressure gradient section. The pressure gradient sections matched the profiles used in the Mach 2.8 tunnel and are given in Section 3.1.5.

It was discovered that the ceramic pebbles in the pebble bed heater shed small particles during tunnel operation. These particles were carried by the high speed air through the tunnel. Due to the high-speed of these particles, they abraded the inner surface of the wind tunnel. Due to the risk of hot-wires breaking, only conventional pressure data were taken in the Mach 5.0 tunnel. Data were taken at $x_{ts} = 6.35$ cm for the FPG and ZPG configuration and at $x_{ts} = 6.35$ cm and 5.1 cm for the CPG configuration. In addition, wall static pressure data were taken along the surface of the FPG and CPG models. The CPG and FPG contours are the same shape as what was used in the Mach 2.8 tunnel except the contours begin at $x_{ts} = 1.90$ cm for the FPG and $x_{ts} = 3.81$ cm for the CPG.

3.4 Data Acquisition Equipment

A Nicolet Multipro was used to collect all the data used in this experiment. The Nicolet had four A/D converter boards each with four input / output BNC connectors. Inputs to the Nicolet consisted of voltage from the Endevco pressure conditioners or the bridge voltage from the IFA-100. The maximum sampling rate for each board was 1 MHz and the maximum number of discrete data points able to be collected per A/D board was of 262,144. The sampling rate decreased linearly with the number of active input / output channels. Thus, if four data inputs were collected, the maximum sampling rate per channel was 250 KHz (Nicolet Systems Operation, 1991).

3.5 Probes

Pressure probes and hot-film probes were used to measure the flow conditions for this experiment. Two types of pressure probes were used, a Pitot probe and two cone-static probes. A 10° axisymmetric cone-static probe was used in the Mach 2.8 and Mach 1.7 tunnel and a 20° axisymmetric cone was used in the Mach 5.0 tunnel. Two types of hot-film probes were used to measure flow velocity, fluctuations and power spectra, single hot-film probe and a single hot-wire probe.

3.5.1 Pressure Probes

Measurement of P_{t1} was obtained using the Pitot tube in the wind tunnel plenum. A 10° axisymmetric cone-static pressure probe collected p_c and a total pressure probe collected P_{t2} data at the downstream locations noted in Sections 3.1.5 and 3.2.5. The probes were aligned so they were normal to the wind tunnel ceiling. The wind tunnel ceilings were fitted with static pressure ports. The probes were connected to two $103.4 \times 10^3 \pm 5.6 \times 10^3$ Pa Endevco pressure transducers which were connected in turn to Endevco model 4225 signal conditioners. The signal conditioners filtered the high frequency noise and provided an output voltage for the data acquisition system. In addition, the signal conditioners were

calibrated for their transducer and recalibrated periodically. The local atmospheric pressure was recorded on a DPI 141 digital barometer. Pressure probes were sampled at 500 Hz by the Nicolet.

The probes were constructed out of stainless steel (0.3175 cm diameter stem) with the head of the probe extending approximately 1.9 cm from the stem. The axisymmetric cones each had four pressure taps 90° apart. The taps opened to a common settling chamber which corrected for any pressure differences between pressure taps.

It was discovered that the probes deflected approximately 2° during tunnel operation. Accordingly, the probes were pre-positioned so this deflection moved the probe to the desired measuring location during tunnel operation.

3.5.2 Hot-Wire and Hot-Film Probes

Two types of hot-film probes were used in this experiment, a single hot-film (TSI model 1218-20) and a single hot-wire (TSI model 1218-T1.5). Each probe had a thickness of 51.0 μm , sensing length of 1.0 mm, nominal resistance of 5.5 Ohms and a temperature coefficient of resistance of 0.24%. The hot-wire had a higher frequency response than the hot-film and was exclusively used for power spectra data.

A TSI 100 Intelligent Flow Analyzer constant temperature anemometer (CTA) was used for this study (IFA 100 instruction manual, 1987). The IFA 100 is composed of the Model 150 anemometer and the Model 157 Signal Conditioner. The IFA 100 was operated in the 1:1 bridge mode. The external resistance and overheat ratio were set by a series of external resistors. The bridge voltage output as measured by the TSI 100 was recorded by the Nicolet Multipro at a sampling frequency of 25 KHz for velocity and total temperature data and a frequency of 500 KHz for power spectra data.

All hot-films were calibrated before data acquisition occurred. The hot-film probes were calibrated by increasing P_{t2} while the probe was in the free-stream of the respective wind tunnel. The sampling frequency during calibration was 200 Hz. As with the pressure probes, the hot-film probes deflected 2° during tunnel operation and were pre-positioned to correct for this deflection.

3.6 Particle Image Velocimetry

A two laser PIV system was used for PIV measurement as well as flow visualization. A schematic of the WL/POPT PIV system is presented in Figure 3-5.

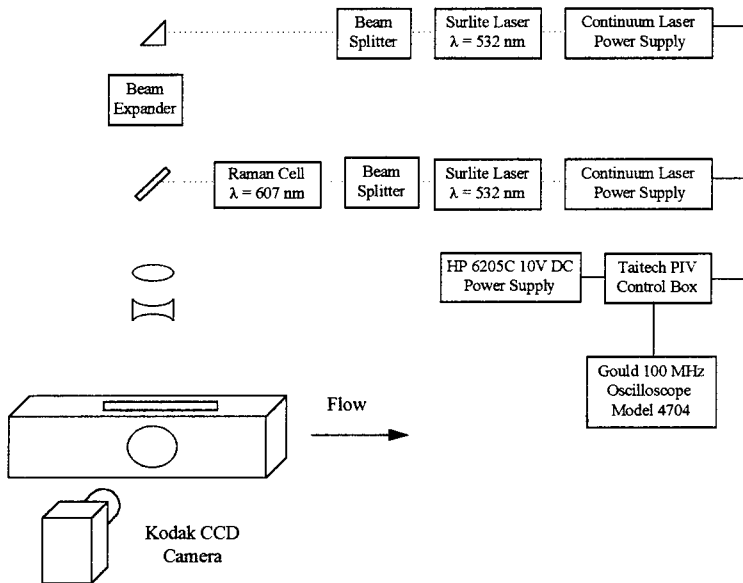


Figure 3-5: PIV schematic

Two Continuum power supplies Model SLI-10 were used to power the two Surlite Nd:YAG lasers. The Surlite lasers each produced two coherent laser beams with wavelengths (λ) of 532 and 1,064 nm. The beam splitter was used to eliminate the higher wavelength beam. One of the beams passed through a Princeton Optics Model RC1000 Raman cell that contained N₂ and H₂ at a pressure of 65.6 MPa. By Raman scattering off the N₂, the $\lambda = 532 \text{ nm}$ (green) beam was converted to $\lambda = 607 \text{ nm}$ (red). The beams were combined and a series of optics formed a laser sheet with a thickness < 1 mm. The laser sheet was manually aligned and focused on the ceiling of the test section.

Each laser was pulsed at 10 Hz with a 10 ns pulse width (Glawe et al, 1996). The time delay between the green and red pulse was adjusted by the Taitech Inc. PIV control box and monitored by the Gould Model 4074 oscilloscope. The nominal time delay was set to 300 ns and was recorded after each data run.

Images were recorded by a Kodak Model 460C CCD camera with a Nikon N90 lens. The lens settings were F4.2 with an exposure time of 0.125 seconds. A maximum of three images were taken per data run

3.7 Computer Equipment

Personal computers both at AFIT and at the authors residence were used for data reduction, traverse operation and IFA 100 operation. A Digital Equipment Corporation alpha station was also used for data reduction.

4. Data Reduction Techniques

This chapter presents the data reduction techniques used in this experiment. First, the mean flow data reduction techniques are discussed. They are followed by the hot-wire data reduction techniques and the PIV data reduction techniques.

4.1 Mean Flow Data Reduction

This section provides the background and methodology necessary to compute the mean flow properties.

4.1.1 Calculation of Mach Number, Velocity and Fluid Properties

Mean flow data were recorded for each pressure gradient model studied in this experiment. The mean flow data recorded included upstream Pitot pressure (P_{t1}), upstream total pressure (T_{t1}), downstream Pitot pressure (P_{t2}) and downstream cone-static pressure (p_c). P_{t2} and p_c were used to calculate the Mach number for the ZPG model in the Mach 2.8 wind tunnel via the following formula (Bowersox, 1992)

$$M = (-0.052976 + 4.684x - 18.678x^2 + 50.7006x^3 - 54.1577x^4)^{-1} \quad (4.1)$$

In equation (4.1), $x = p_c / P_{t2}$. Equation (4.1) is valid for Mach numbers between 1.5 to 4.4 and has a standard deviation of 0.06%. For the CPG and FPG models, iteration on the Rayleigh supersonic formula (Liepmann and Rosko, 1957) was used to calculate the Mach number.

With the Mach number and T_{t1} known, the local temperature was calculated using the following isentropic relationship. (Note, it was assumed that T_t was constant throughout the boundary layer.)

$$\frac{T_{t1}}{T} = 1 + \frac{\gamma - 1}{2} M^2 \quad (4.2)$$

The local velocity was calculated using the definitions of the Mach number and the speed of sound. The derived velocity is

$$\frac{u}{u_e} = \frac{M}{M_e} \sqrt{\frac{1 + \frac{\gamma - 1}{2} M^2}{1 + \frac{\gamma - 1}{2} M_e^2}} \quad (4.3)$$

where M_e was determined by selecting the largest Mach number from analysis of the pressure data and the output of Equation (4.1)

4.1.1.1 Pressure and Temperature Methodology - ZPG Flow

For the ZPG case it was assumed that the pressure gradient normal to the surface was zero. A modified Crocco-Busemann relation yields (Van Driest, 1951)

$$\frac{\rho_w}{\rho} = \frac{T_w}{T} = 1 + B' \left(\frac{u}{u_e} \right) - A'^2 \left(\frac{u}{u_e} \right)^2 \quad (4.4)$$

ρ_w was found from the perfect gas relation and measured p_w values. A' and B' are given by

$$B' = \frac{1 + \left(\frac{\gamma - 1}{2} \right) r M_e^2}{T_w / T_e} - 1 \quad A'^2 = \frac{\left(\frac{\gamma - 1}{2} \right) r M_e^2}{T_w / T_e} \quad (4.5)$$

r is the recovery factor and can be expressed as $\sqrt[3]{Pr}$. For air $Pr = 0.707$ and $r = 0.892$.

4.1.1.2 Pressure and Temperature Methodology - FPG and CPG Flow

For pressure gradient surfaces, the pressure gradient normal to the surface is not zero due to streamline curvature. This was verified by Luker and Hale (Luker, 1995 & Hale, 1995). Thus, a new method must be found to determine the local temperature and pressure. One method is to assume a linear variation in pressure between the boundary layer edge and the wall. Numerical studies of this flow proved this method (Fick, 1995). The wall pressure was measured by static ports and the following isentropic equation was used to compute the edge pressure.

$$\frac{p_e}{p_o} = \left(1 + \frac{\gamma - 1}{2} M^2 \right)^{\frac{-\gamma}{\gamma - 1}} \quad (4.6)$$

Assuming a linear variation in pressure and Equation (4.2), the perfect gas law was used to calculate the density.

4.1.2 Calculation of Boundary Layer, Displacement and Momentum Thickness

Different boundary layer thickness parameters were calculated based on the result of the conventional pressure data. One thickness was based on the Mach number (δ_M) and the other on the velocity (δ_u). The Mach number boundary layer thickness provides a measure of the temperature boundary layer thickness. The velocity boundary layer thickness was used to provide a more direct comparison to the LDV data (Hale, 1995 & Luker, 1995). The local Mach number or velocity was non-dimensionalized by the edge value and the location where the non-dimensional ratio was $> 99\%$ was selected as the appropriate thickness. Note, Luker and Hale (Luker, 1995 & Hale, 1995) selected 99.5% as their boundary layer criteria.

Numerical integration on the resulting velocity profiles and the known density profile were used to compute the momentum (θ) and displacement (δ^*) thickness. The compressible momentum and displacement thickness are defined as (White, 1991)

$$\theta \equiv \int_0^\infty \frac{\bar{\rho} \bar{u}}{\rho_e u_e} \left(1 - \frac{\bar{u}}{u_e} \right) dy \quad (4.7)$$

$$\delta^* \equiv \int_0^\infty \left(1 - \frac{\bar{\rho} \bar{u}}{\rho_e u_e} \right) dy \quad (4.8)$$

The incompressible momentum (θ_i) and displacement (δ_i^*) thickness were computed by setting the density ratio in Equations (4.7) and (4.8) to one. Due to the asymptotic nature of Equations (4.7) and (4.8), the differences in boundary layer thickness definitions between this study and Luker and Hale will be minimized in momentum and displacement thickness.

4.1.3 Calculation of Van Driest Velocity Profile and Wall Shear Stress

Van Driest developed the following skin friction coefficient (C_f) formula for flow over a flat plate (Van Driest, 1951)

$$\frac{0.242}{A' \sqrt{C_f (T_w/T_e)}} \left\{ \sin^{-1} \left(\frac{2A'^2 - B'}{\sqrt{4A'^2 + B'^2}} \right) + \sin^{-1} \left(\frac{B'}{\sqrt{4A'^2 + B'^2}} \right) \right\} = \kappa + \log(R_{ex} C_f) - \omega \log(T_w/T_e) \quad (4.9)$$

where $\kappa = 0.41$ and $\omega = 0.68$. Equation (4.9) does not have a closed form and must be solved by iteration to find C_f . With C_f and the known edge values, the wall shear stress can be calculated by the following

$$\tau_w = \frac{\rho_e u_e^2 C_f}{2} \quad (4.10)$$

Van Driest also proposed a velocity transformation in order to more easily compare compressible flows. The effective velocity (u_{eff}) is defined as

$$u_{eff} = \frac{u_e}{A'} \left\{ \sin^{-1} \left(\frac{2A'^2 (\bar{u}/u_e) - B'}{\sqrt{4A'^2 + B'^2}} \right) + \sin^{-1} \left(\frac{B'}{\sqrt{4A'^2 + B'^2}} \right) \right\} \quad (4.11)$$

The effective velocity is non-dimensionalized by the wall-friction velocity (u^*) given by

$$u^* \equiv \sqrt{\frac{\tau_w}{\rho_w}} \quad (4.12)$$

to obtain

$$u_{eff}^+ = \frac{u_{eff}}{u^*} \quad (4.13)$$

similarly, the y-coordinate is non-dimensionalized as

$$y^+ = \frac{yu^* \rho_w}{\mu_w} \quad (4.14)$$

A plot of y^+ versus u^+ is known as the law of the wall plot (White, 1991). The empirical relationship between y^+ and u^+ was first developed for incompressible flow and extended to compressible flow. White gives the empirical relationship as

$$u_{\text{eff}}^+ = \frac{\ln(y^+)}{\kappa} + C + \frac{2\Pi}{\kappa} \sin^2\left(\frac{\pi y}{2\delta}\right) \quad (4.15)$$

κ and C are constants given by, $\kappa = 0.41$ and $C = 5.0$. Π is known as Cole's wake parameter and is defined by (Coles, 1956)

$$\Pi \approx 0.8(\beta + 0.5)^{0.75} \quad (4.16)$$

β in Equation (4.16) is called Clauser's equilibrium parameter and is defined as (Clauser, 1954)

$$\beta = \frac{\delta^*}{\tau_w} \frac{dp_e}{dx} \quad (4.17)$$

Evans (Evans, 1985) extended Equation (4.15) for flows with zero or adverse pressure gradient by adding the following correction to Cole's wake parameter

$$u_{\text{eff}}^+ = \frac{\ln(y^+)}{\kappa} + C + (1 + 5TI) \frac{2\Pi}{\kappa} \sin^2\left(\frac{\pi y}{2\delta}\right) \quad (4.18)$$

were TI is the freestream turbulence intensity. For the Mach 2.8 tunnel, TI was approximately 0.015.

Equation (4.18) is valid for all regions of the boundary layer except the laminar sublayer. The laminar sublayer is the region in the boundary layer where the flow becomes laminar. This region exists below $y^+ = 10$ and in this region $u^+ = y^+$ (White, 1991).

4.2 Hot-Wire Data Reduction

Hot-wire data were collected at each measurement station. Hot-wires were used to collect power spectra data and hot-films were used to collect turbulence data. A series of eight overheat ranging from 1.5 to 2.0 were used for the MOH data and the highest overheat was used for single overheat (SOH) data. A nominal overheat of 1.8 was selected for the power spectra analysis. All of the MOH and SOH data reduction equations (except for the power spectra equations) have been incorporated into the FORTRAN code MSHEaR (Bowersox, 1994)

4.2.1 Hot-Wire Theory

For supersonic turbulent flow, it can be shown that the Nusselt number of a cylinder (the shape of a hot-wire) has the following non-dimensional functional relationship:

$$Nu = Nu(L/d, M, Pr, Re_e, \tau) \quad (4.19)$$

L/d is the wire aspect ratio, M is the Mach number, Pr is the Prandtl number, Re_e is the effective Reynolds number based on wire diameter, and τ is the temperature loading factor. Since single wires were used in this study, Re_e can be replaced by Re_x . The temperature loading factor can be written as $\tau = (T_w - T_e) / T_t$. T_w is the wire temperature, and T_e is the equilibrium temperature. The equilibrium temperature is defined as the temperature an unheated wire would reach if placed in the flow (Lomas, 1986). Equation (4.19) can be simplified by an application of a set of constraints. These constraints include a large wire aspect ratio (L/d much greater than one), a Mach number greater than 1.2, a constant Pr and a Re_x greater than 20. With these constraints, Equation (4.19) can be reduced to:

$$Nu = Nu(Re_x, \tau) \quad (4.20)$$

Bowersox and Schetz (Bowersox and Schetz, 1994) further reduced Equation (4.20) to the following

$$Nu = a\sqrt{Re_x} + b \quad (4.21)$$

The variables a and b in Equation (4.21) are calibration factors that depend on the overheat ratio. The Nusselt number can be related to the power supplied to the wire by the following (assuming $T_e = T_t$)

$$Nu = \frac{V_w^2 R_w}{\pi k_t L (T_w - T_t) (R_w + R_s + R_L)^2} \quad (4.22)$$

The power laws of viscosity and thermal conductivity were used

$$k_t = k_o \left(\frac{T_t}{T_o} \right)^{n_k} \quad \text{and} \quad \mu_t = \mu_o \left(\frac{T_t}{T_o} \right)^{n_\mu} \quad (4.23)$$

to simplify Equation (4.22). In Equation (4.23), $n_\mu = 0.77$, $n_k = 0.89$ (Bowersox, 1992), k_o , T_o and μ_o are constant reference values (White, 1991). Combining Equations (4.22) and (4.23), the hot-wire response can be found to equal

$$\frac{V_w^2}{C_o} = \left(\frac{T_t}{T_o} \right)^{n_k} \left(a \sqrt{Re_x} \left(\frac{T_o}{T_t} \right)^{\frac{n_\mu}{2}} + b \right) (T_w - T_t) \quad (4.24)$$

Re_x is the Reynolds number based on μ_o and C_o is a function of the resistance and properties of the wire.

It can be expressed as

$$C_o = \frac{(R_w + R_s + R_L)^2}{R_w} \pi L k_o \quad (4.25)$$

In order to extract the mean and fluctuation components of Equation (4.24), the voltages, Reynolds number and total temperature are replaced by their mean and fluctuating components. If the binomial theorem is used (keeping only first order terms) and noting that

$$\frac{\overline{V_w}^2}{C_o} = \left(\frac{\overline{T}_t}{T_o} \right)^{n_k} \left(a \sqrt{\overline{Re}_x} \left(\frac{T_o}{\overline{T}_t} \right)^{\frac{n_\mu}{2}} + b \right) (\overline{T}_w - \overline{T}_t) \quad (4.26)$$

then solving for $\frac{V'_w}{\overline{V}_w}$, yields the following hot-wire fluctuation equation

$$\frac{V'_w}{\overline{V}_w} = f \left(\frac{\overline{Re}'_x}{\overline{Re}_x} \right) + g \left(\frac{\overline{T}'_t}{\overline{T}_t} \right) \quad (4.27)$$

where f and g are hot-wire sensitivities and can be written as

$$f = 0.25 \left(1 + \frac{b}{a \sqrt{Re_x}} \right)^{-1} \quad \text{and} \quad g = \frac{\overline{T}_t}{2(\overline{T}_w - \overline{T}_t)} + \frac{n_k}{2} - f n_\mu \quad (4.28)$$

Equation (4.26) can be rewritten as

$$\sqrt{\overline{Re}_x} + x_i \overline{T}_t \sqrt{\overline{Re}_x} + y_i \overline{T}_t = z_i \quad (4.29)$$

In Equation (4.29), $x_i = -1/T_{wi}$, $y_i = -b_i/(a_i T_{wi})$ and $z_i = \overline{V}_{wi}^2 / (C_i a_i T_{wi}) - b_i/a_i$. The subscript i in Equation (4.29) is an index representing the number of overheat ratios. Since Equation (4.29) has two unknowns ($\sqrt{\overline{Re}_x}$ and \overline{T}_t), a minimum of two overheat ratios are necessary to solve this equation. If more overheats are available, then a least squares analysis can be used to solve Equation (4.29). The least squares analysis solves the following set of equations by the secant iteration method (Bowersox, 1992)

$$N\sqrt{Re_x} + \bar{T}_t \left(\sum_N y_i - \sum_N x_i z_i \right) + 2\bar{T}_t \sqrt{Re_x} \sum_N x_i + \\ \bar{T}_t^2 \sum_N x_i y_i + \bar{T}_t^2 \sqrt{Re_x} \sum_N x_i^2 = \sum_N z_i \quad (4.30)$$

$$\sqrt{Re_x} \left(\sum_N y_i - \sum_N x_i z_i \right) + \bar{T}_t \sum_N y_i^2 + 2\bar{T}_t \sqrt{Re_x} \sum_N x_i y_i + \\ \bar{T}_t Re_x \sum_N x_i^2 = \sum_N y_i z_i \quad (4.31)$$

N is the number of overheat ratios. To obtain the hot-wire fluctuation equation, Equation (4.27) is squared and averaged. The result of this process is

$$f_i^2 \overline{\left(\frac{Reo'_x}{Reo_x} \right)^2} + 2f_i g_i \overline{\left(\frac{Reo'_x}{Reo_x} \frac{T'_t}{T_t} \right)} + g_i^2 \overline{\left(\frac{T'_t}{T_t} \right)^2} = \overline{\left(\frac{V'_w}{V_w} \right)_i^2} \quad (4.32)$$

Unlike Equation (4.29), Equation (4.15) required three overheats to solve. If more overheat ratios are available, then a General Least Squares (GLS) method can be used to solve Equation (4.32). Application of the GLS method yields the following set of equations.

$$\begin{bmatrix} \sum_N f_i^4 & 2 \sum_N f_i^3 g_i & \sum_N f_i^3 g_i^2 \\ \sum_N f_i^3 g_i & 2 \sum_N f_i^2 g_i^2 & \sum_N f_i g_i^3 \\ \sum_N f_i^2 g_i^2 & 2 \sum_N f_i g_i^3 & \sum_N g_i^4 \end{bmatrix} \begin{bmatrix} \overline{\left(\frac{Reo'_x}{Reo_x} \right)^2} \\ \overline{\left(\frac{Reo'_x}{Reo_x} \frac{T'_t}{T_t} \right)} \\ \overline{\left(\frac{T'_t}{T_t} \right)^2} \end{bmatrix} = \begin{bmatrix} \sum_N f_i \overline{\left(\frac{V'_w}{V_w} \right)_i^2} \\ \sum_N f_i g_i \overline{\left(\frac{V'_w}{V_w} \right)_i^2} \\ \sum_N g_i \overline{\left(\frac{V'_w}{V_w} \right)_i^2} \end{bmatrix} \quad (4.33)$$

Solution of Equation (4.33) completes the MOH analysis

4.2.2 Separation of Turbulence Variables

Multiple overheat single hot-wire anemometry in supersonic flow can be used to determine the following conservative turbulence quantities.

$$\overline{(pu)'^2} \quad \overline{T_t'^2} \quad \overline{(pu)' T'}$$

Two assumptions must be made in order to separate the variables in Equation (4.34) into non-conservative

variables. The first assumption is that the fluid obeys the thermally perfect gas assumption. The second assumption is controversial, it is that the pressure fluctuations are small compared to the density and temperature fluctuations. This hypothesis has been demonstrated by Kistler and Bowersox (Kistler, 1959; Bowersox & Schetz 1994) Kistler postulated that p' is proportional to u'^2 , u'^2 is second order and is usually negligible compared to first order terms. Bowersox experimentally verified the $p' = 0$ assumption in a Mach 4.0 free mixing layer. With these two assumptions, the separated results can be calculated from the following set of equations.

$$\frac{\bar{u}'}{\bar{u}} = \frac{(\rho u)' }{\rho u} - \frac{p'}{\rho} \quad (4.35)$$

$$\frac{p'}{\rho} = \frac{1}{\alpha + \beta} \left(\beta \frac{(\rho u)' }{\rho u} - \frac{T'_t}{T_t} \right) \quad (4.36)$$

where $\alpha = (1 + 0.5(\gamma - 1)M^2)^{-1}$ and $\beta = (\gamma - 1)\alpha M^2$.

4.2.3 Single Overheat Theory

As the hot-wire's overheating is increased, the hot-wire becomes less sensitive to total temperature fluctuations. Thus, the SOH method can be used to obtain accurate results for flow where T'_t is small. If T'_t is assumed to be zero, Morkovin demonstrated that for $Pr = 1$ (Morkovin, 1961)

$$\frac{T'_t}{T_t} = -(\gamma - 1)M^2 \left(\frac{\bar{u}'}{\bar{u}} \right) \quad (4.37)$$

It can be shown that

$$\frac{\bar{u}'}{\bar{u}} = \frac{1}{1 - (\gamma - 1)M^2} \left(\frac{(\rho u)' }{\rho u} \right) \quad (4.38)$$

and

$$\frac{T'_t}{T_t} = 0 \quad (4.39)$$

4.2.4 Mach 2.8 Hot-Wire Probe Data

Eight overheat ratios were used to examine the flow for mean flow and turbulence results. They ranged from 1.52 to 2.03. In addition, the highest overheat was extracted for a SOH analysis (see Section 5.3). Power spectra data was obtained for a single overheat ratio only. The data in Table 4-1 contain the wire information and overheat ratios used in this experiment. Note that only one hot-wire and one hot-film was used to collect data for this experiment.

Table 4-1: Mach 2.8 probe and overheat ratio data

Probe	Purpose	OHR
1218-20 S/N 75014	ZPG, FPG, CPG mean flow and turbulence	2.03, 1.98, 1.87, 1.81, 1.74, 1.66, 1.58, 1.52
1218-T1.5 S/N 43456	FPG, CPG power spectra	1.85
1218-T1.5 S/N 43456	ZPG power spectra	1.88

4.2.5 Mach 1.7 Hot-Wire Probe Data

Table 4-2 presents the probe information for the probes used in this portion of the study. Note the same probe was used for the Mach 1.7 mean flow as the Mach 2.9 mean flow. A hot-film was used to evaluate the power spectra. The film had a frequency response of 140 KHz that is somewhat less than what was used for the Mach 2.9 power spectra data.

Table 4-2: Mach 1.7 probe and overheat ratio data

Probe	Purpose	OHR
1218-20 S/N 75014	ZPG mean flow and turbulence	1.98, 1.89, 1.82, 1.73, 1.66
1214-10 S/N K746	ZPG power spectra	1.77
1214-20 S/N 9446	FPG power spectra	2.01

4.2.6 Power Spectra Data Reduction

SOH hot-wire anemometry was used to evaluate the energy spectra in the boundary layer. The hot-wire response was sampled at 500 KHz for 0.52 seconds. The hot-wire output was divided into 511 blocks of 1,024 data points for ease of data reduction. A discrete Fourier transform (DFT) (Reid, 1983) was performed on each block to convert the hot-wire results from the time domain to the frequency domain. The classic DFT is modeled by the following equation

$$V(f) = \frac{1}{N} \sum_{n=1}^{N} V(t_n) e^{-j \frac{2\pi f t_n}{N}} \quad (4.40)$$

where N is the sample size of 1,024 points. The output of the DFT was $(|V(f)|/\sqrt{N})^2$ versus frequency.

To obtain the final result, the average of the 511 blocks was calculated.

4.3 PIV Data Reduction

A CCD camera was used to acquire and digitize the particles in the flow. A raw digitized image looked like red and green dots against a black background. The red and green dots were seed particles illuminated by the red or green laser. Due to the quality of the digitized image, software image enhancement was not required. With this image, the velocity field was calculated using a cross-correlation technique. The cross-correlation technique performs a Fourier transform on the intensity distribution of the red and green images over a small patch of the digitized image. In this experiment, a patch size of 128 x 128 pixels (approximately 2 mm x 2 mm) was used. The patches were overlapped by 64 pixels to more accurately map the flowfield. An intensity-weighted peak-searching routine developed by Innovative Scientific Solutions Inc., determined the locations of the red and green peaks to sub-pixel accuracy (Glawe et al, 1996). With the red and green peaks located, knowledge of the time delay between the red and green laser and knowledge of which laser fired first, the velocity vector could be drawn for that patch connecting the red and green peaks.

Filtering was performed on the calculated vector field to eliminate unnecessary and incorrect vectors by one of two methods. The software developed by Innovative Scientific Solutions Inc., was used to compare each vector's length and magnitude to its neighbors. If the difference in length or magnitude of any particular vector compared to its neighbor exceeded a specified input, the vector was deleted. Typically, this filtering process was repeated three times. In the event that this filter sequence did not remove a bad vector, a manual deletion of the vectors was performed. Manual deletion was required approximately every three images.

Calibration of the images was necessary due to large amounts of scatter in the laser time base. The average vector length in the freestream was calculated for each image by averaging all the vectors in the lower left hand corner of the image. This location represents undisturbed freestream flow for each pressure gradient model. The freestream velocity was divided by the average vector length to obtain each image's calibration factor. Each image's vector field was multiplied by the calibration factor. Thus, the velocity of each vector in the vector field can be found by the following

$$u = \Delta L_{G-R} * \frac{U_e}{\bar{L}} \quad (4.41)$$

ΔL_{G-R} is one vector length and \bar{L} is the average vector length.

This process effectively removed the scatter and adjusted the vector field such that the freestream vector's length matched the freestream velocity. After filtering and calibration, the calculated vector fields over the entire image were averaged together to obtain a composite vector field.

5. Mach 2.8 Results and Discussion

While measurements were obtained at three Mach numbers during the course of this study, the main test condition was Mach 2.8. This chapter presents the results from the Mach 2.8 phase of this experiment. Flow visualization is discussed first, followed by a discussion of the mean flow and turbulence results. Recall that the objectives of this study are to, quantify the effects of pressure gradients on the flow validate PIV as a flow diagnostic tool and compare turbulence data obtained via hot-wire anemometry to turbulence data obtained by LDV.

5.1 Flow Visualization

In order to better understand the flow, it is useful to have some type of flow visualization. Traditional visualization techniques include shadowgraphs and schlieren photographs; however, the Mie scattering images of PIV can also be used for flow visualization. Flow visualization images comparing the CPG to the ZPG and the FPG to the ZPG are presented as Figures 5-1 and 5-2, respectively. Two images were taken for each pressure gradient to illustrate data repeatability.

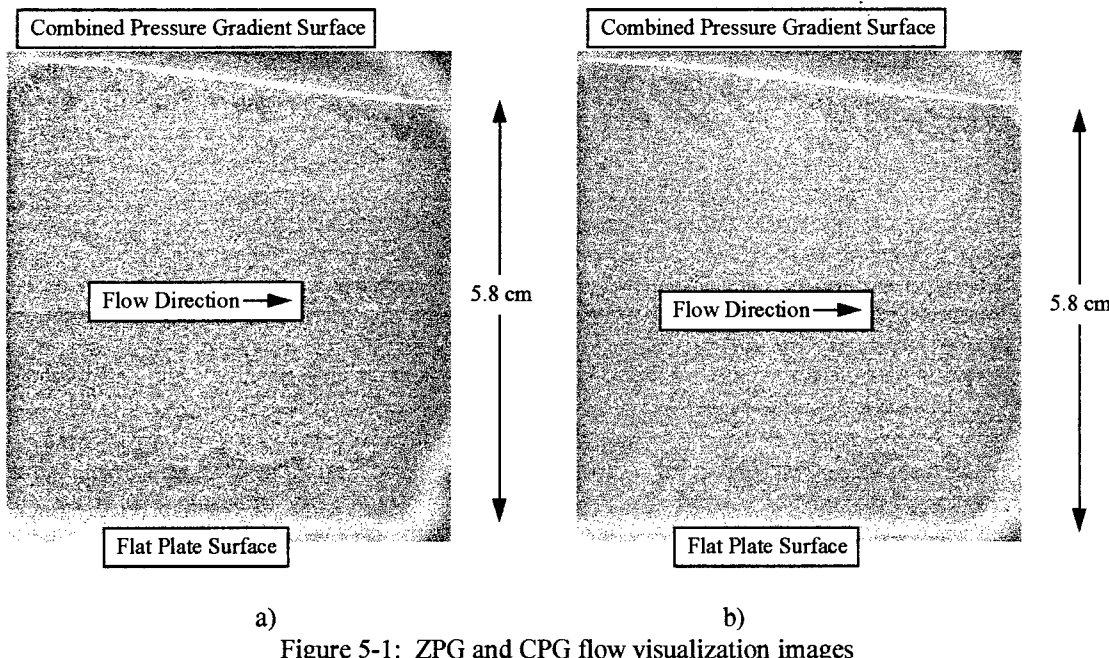


Figure 5-1: ZPG and CPG flow visualization images

Note in both figures, the ZPG boundary layer (along the tunnel floor) is uniform and the structures have an inclination of between 45° - 60° . This effect has been noted by Spina (Spina, 1988). The ZPG flow structures span $\sim \frac{1}{2}$ the boundary layer. Application of a CPG causes a decreases in the boundary layer thickness. Further, the CPG structures are inclined approximately 50° - 70° . Finally, the structures are smaller and span the entire boundary layer.

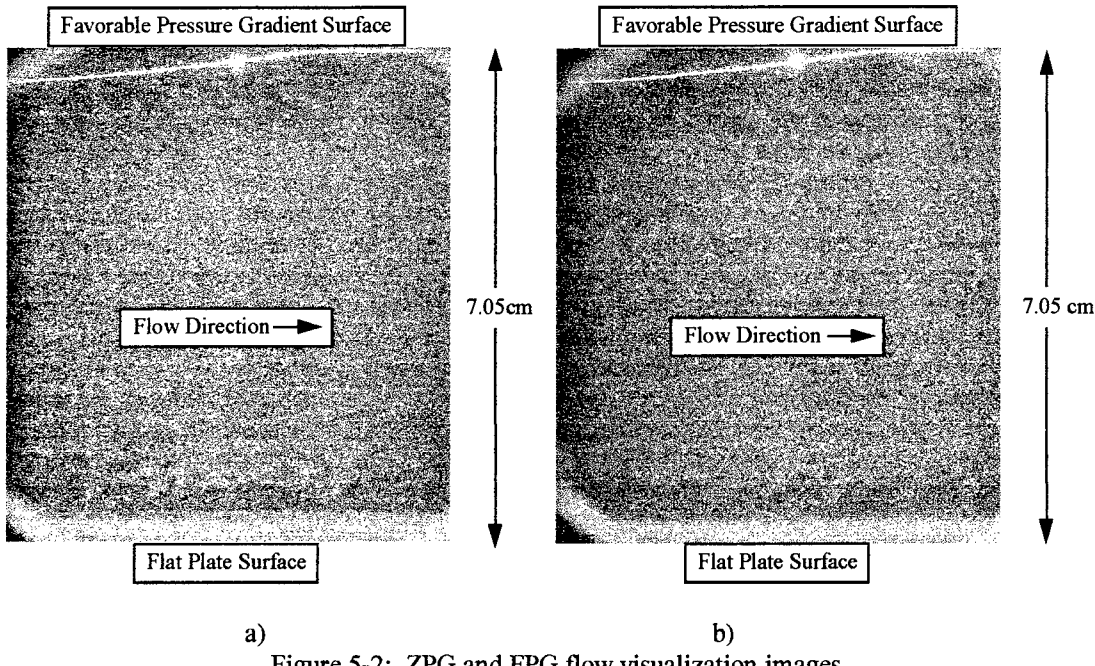


Figure 5-2: ZPG and FPG flow visualization images

Figure 5-2 shows the comparison between the FPG and ZPG surfaces. As compared to the ZPG, the FPG boundary layer grows in the streamwise direction, as expected. More small scale structures are evident on the boundary layer edge; however, no large scale structures are seen. This is consistent with the theory that a FPG promotes the disassociation of large scale structures into small scale structures (Luker et al., 1997). Thus, the FPG causes the boundary layer to grow while contributing to the conversion large scale structures to smaller scale structures.

Estimates of the boundary layer thickness can be ascertained from Figures 5-1 and 5-2. The estimated boundary layer thickness is 1.0 cm for the ZPG, 0.8 cm for the CPG and 1.1 cm for the FPG.

5.2 Mean Flow Results

Mean flow properties were required to map out the flow and make sure that the flow matched previous studies (Miller, 1994; Dotter, 1994; Luker, 1995 & Hale, 1995). Mean flow properties were evaluated by three different methods. First of all, conventional pressure probes (Pitot and cone-static) were used to compute the Mach number, static pressure (p) and velocity (u). Secondly, the hot-wire was used to calculate the mass flux and total temperature ratio. Finally, PIV was used to provide velocity information. Data were normalized by their edge values (or P_{t1} for pressure data) and plotted versus y/δ . Unless otherwise stated, δ is based on $u = 0.99 U_e$. Boundary layer thickness parameters are summarized in Table 5.1.

5.2.1 Conventional Pressure Probe

Pitot and cone-static measurements were taken along the tunnel centerline at positions 71.0 cm and 71.5 cm downstream of the nozzle for the ZPG and FPG, respectively. Pitot and cone-static data were not taken for the CPG. This data is available in Hale and Dotter (Hale, 1995 & Dotter, 1994). Figures 5-3 and 5-4 present the normalized Pitot and cone-static data.

The FPG flow is not as fully developed as the ZPG flow. This is demonstrated by the increasing trends in the Pitot and Cone-static pressure profiles. The data in Figures 5-3 and 5-4 in conjunction with Equation (4.1) and the supersonic Rayleigh Pitot formula was used to calculate the Mach number. The freestream Mach number was found to be 2.79 and 3.00 for the ZPG and FPG, respectively. The Mach number profile is shown in Figure 5-5.

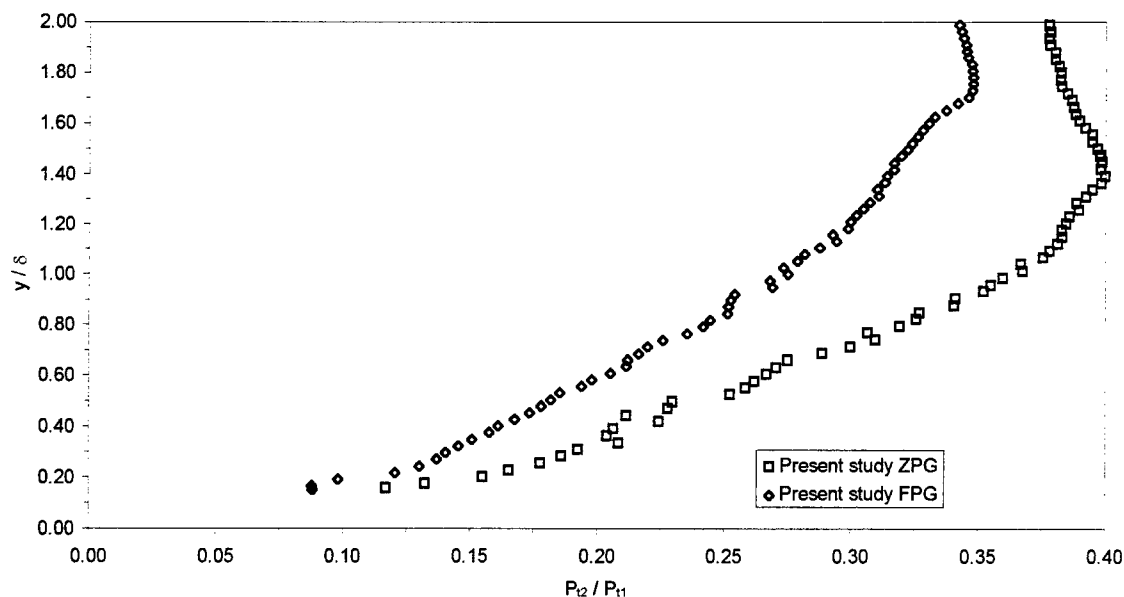


Figure 5-3: Pitot pressure profile

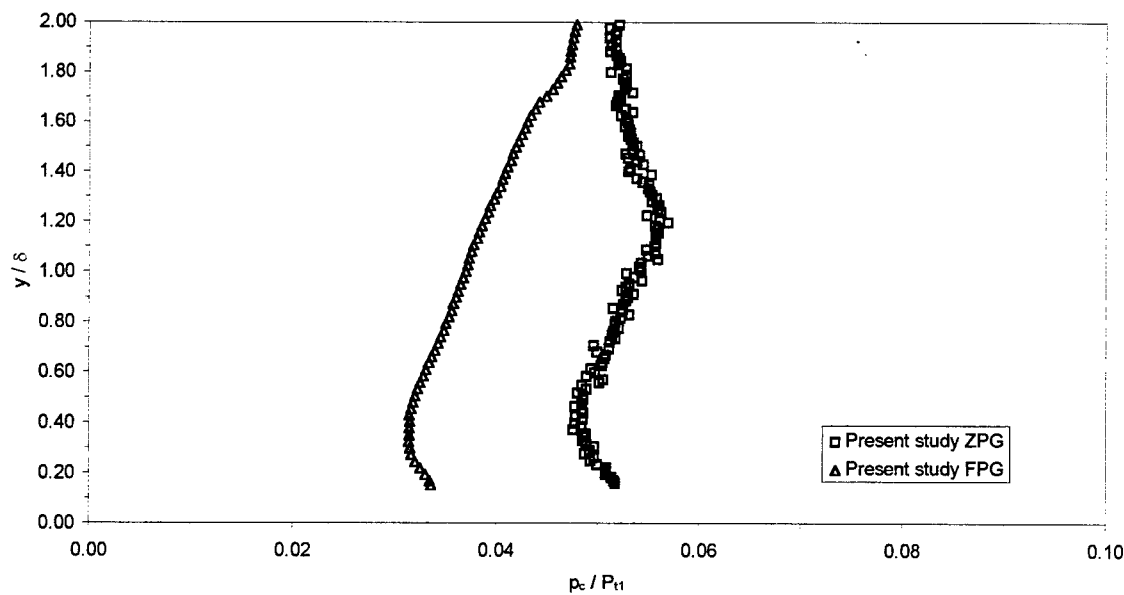


Figure 5-4: Cone-static pressure profile

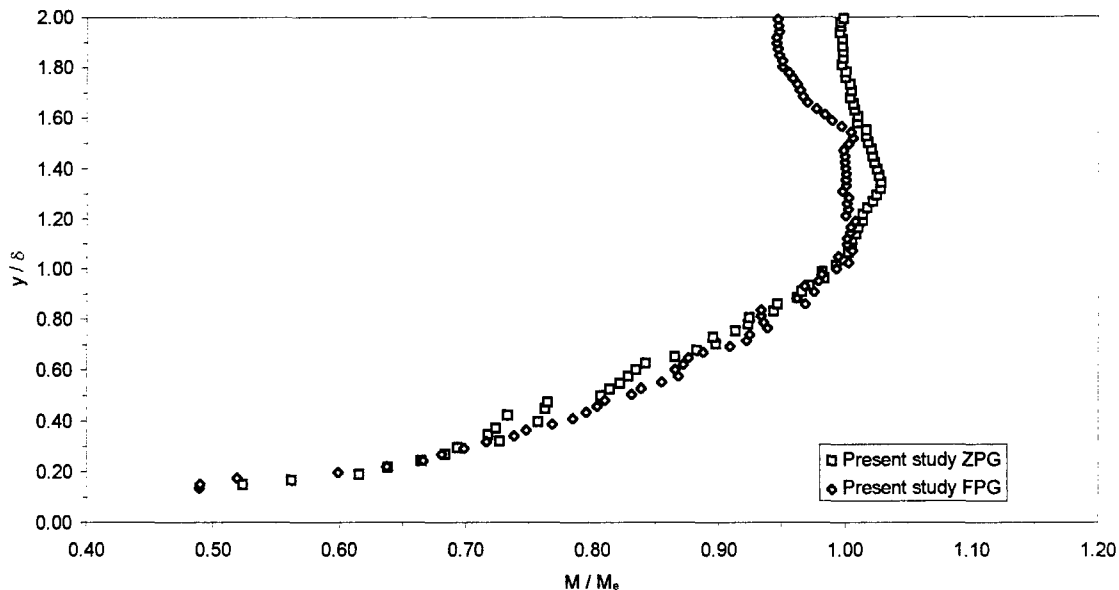


Figure 5-5: Mach number profile

These data in conjunction with the definitions of the boundary layer thickness parameters (Section 4.1.2) were used to compute δ_u and δ_M . Table 5.1 presents the results of these computations. Data from Luker and Hale (Luker, 1995 and Hale, 1995) are also presented to form a basis of comparison. The differences between the boundary layer parameters are within the 25% uncertainty expected by Luker (Luker, 1995).

Table 5-1: Boundary layer parameters

	ZPG		FPG		CPG	
	Luker	Present	Luker	Present	Hale ($x = 68$ cm)	Hale ($x=70$ cm)
δ_u (mm)	9.85	10.1	11.9	10.5	9.09	7.48
δ_M (mm)	10.8	10.6	13.1	11.6	10.04	8.44
M_e	2.79	2.82	2.91	3.00	2.72	2.51
U_e (m/sec)	602	604	606	616	596	575

5.2.2 Hot-Film Mean Profiles

Single wire data was acquired at the same locations as the mean flow data for the ZPG and FPG. For the CPG, data was collected the tunnel centerline at 68.0 cm and 70.0 cm downstream of the throat. For mean flow data, the hot-film was traversed towards the wall until the probe struck the wall. Then the probe was traversed back to its starting point. This allowed for accurate near wall data collection and for the wall's position to be accurately located. Due to the thickness of the boundary layer and limitations on run time, data collection was only possible during the initial probe motion (traverse up) for the FPG. For the ZPG and CPG, data was collected on the initial and final probe motion (traverse up & traverse down). A single hot-film was used for all mean flow measurements.

The mean flow data included the local Reynolds number and total temperature. The Reynolds number was converted to mass flux and non-dimensionalized by the freestream value. The total temperature was non-dimensionalized by T_{t1} . Figures 5-6 to 5-9 present the mass flux information for all pressure gradients. In addition, these figures present the total temperature profiles for each pressure gradient model during the traverse up motion.

The ZPG data is presented in Figure 5-6. There is excellent agreement between data collected during the traverse up and the traverse down movement. The single OHR data matches well with the multiple OHR data implying that the total temperature variations were small. This is confirmed by the total temperature profile which was reasonably constant across the boundary layer. The freestream mass flux was found to be approximately $400 \text{ kg/m}^2\text{-sec}$.

The FPG data is presented in Figure 5-7. Recall that data was only obtained during the traverse up movement. Again, the single OHR data matches the multiple OHR data well implying that the FPG has a stabilizing effect on total temperature ratio. This is confirmed by the accompanying total temperature profile. The freestream mass flux was found to be approximately $320 \text{ kg/m}^2\text{-sec}$.

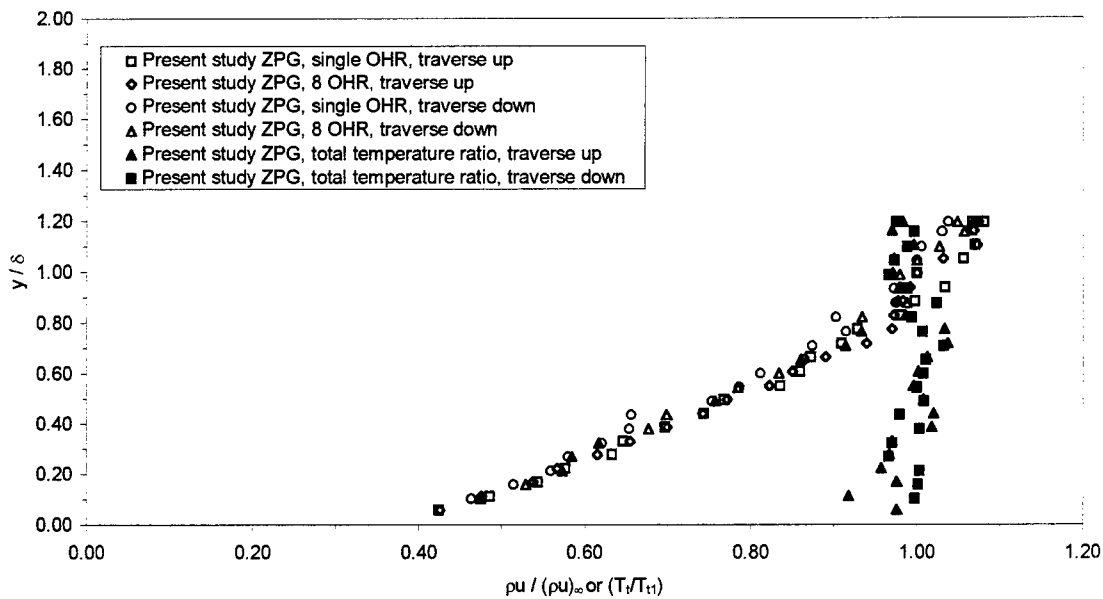


Figure 5-6: ZPG hot-film data

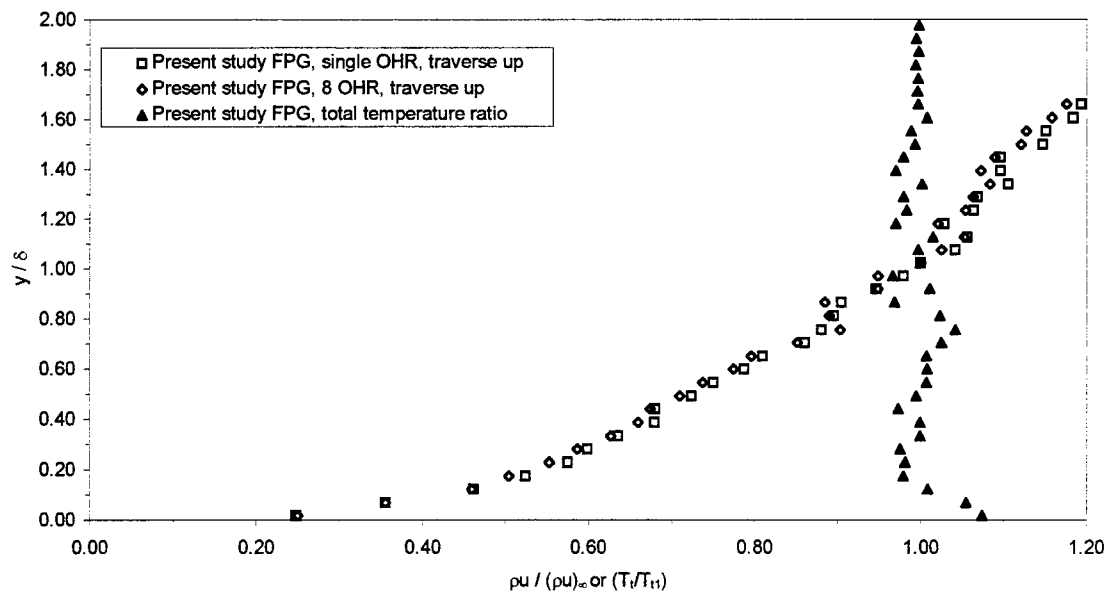


Figure 5-7: FPG hot-film data

Figures 5-8 and 5-9 present the CPG data at two different distances from the nozzle. Figure 5-8 shows data 68 cm downstream of the nozzle and Figure 5-9 shows data 70 cm downstream of the nozzle. The data in Figure 5-8 demonstrates the destabilizing effect of the CPG. The data scatter is slightly larger between the different data collection methods implying that the total temperature fluctuations were higher for the CPG than for the ZPG or FPG. Again, this is confirmed by the relatively large total temperature variations (~7%) noted in the total temperature profiles. The largest value of mass flux does not occur in the freestream as in the ZPG or FPG, but the largest value occurs near $y/\delta = 1.0$. This is the result of the compression wave formed by the CPG model. The freestream value of the mass flux is approximately 560 $\text{kg/m}^2\text{-sec}$.

The data in Figure 5-9 has similarities to the FPG as well as the upstream CPG data. The shape of the curve does not have the elbow present in Figure 5-8. As with the ZPG and FPG, the highest value of mass flux (420 $\text{kg/m}^2\text{-sec}$) occurs in the freestream. This indicates that this measurement location is downstream of the compression wave. Like in Figure 5-8, the scatter in the data is slightly larger throughout the boundary layer.

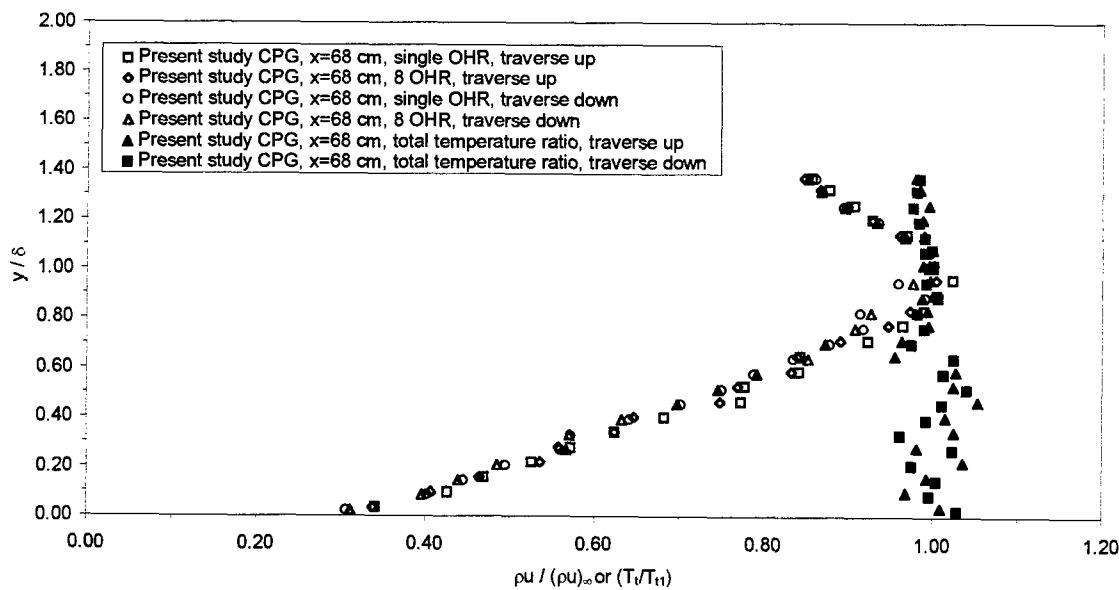


Figure 5-8: CPG ($x = 68$ cm) hot-film data

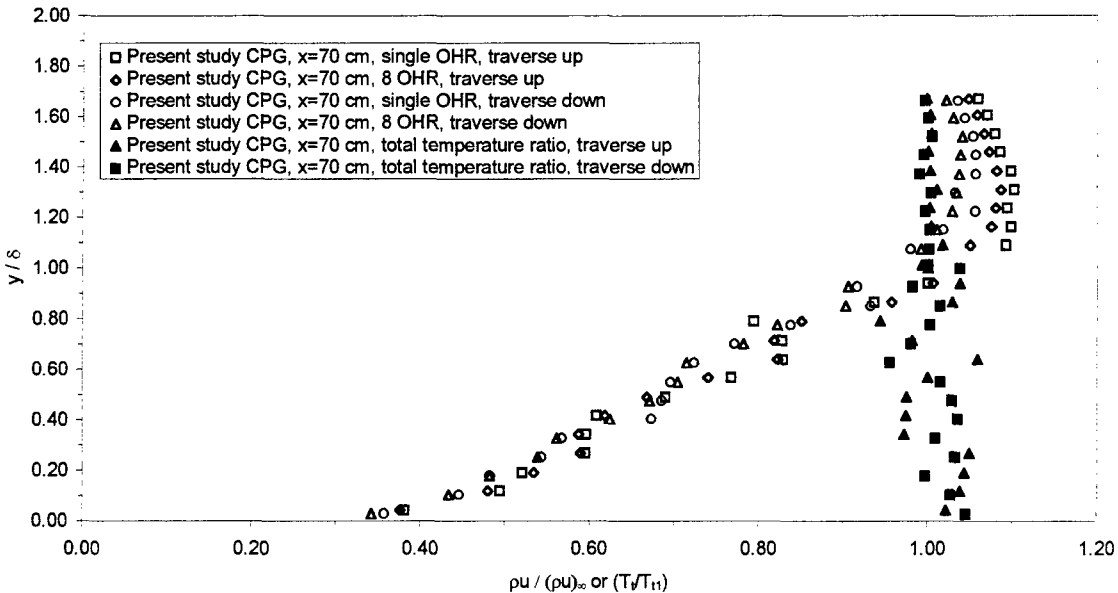


Figure 5-9: CPG ($x = 70$ cm) hot-film data

5.2.3 PIV Mean Profiles

A main advantage of PIV is that it can resolve data along an entire plane. Recall that one of the objectives of this study was to further evaluate PIV as a diagnostic tool for supersonic flow. The PIV portion of this analysis required a great deal of effort and time. PIV has only been used once at AFIT (Glawe et al., 1996) and rarely for supersonic flow. Thus, the procedures (seeding, camera use) were not well established. Several weeks were expended in trying various seeding techniques and camera types before acceptable results were obtained.

Recall that PIV takes images of the flow. The images were averaged together to obtain mean and turbulent statistics. The number of images used to create the combined image are listed in Table 5-2. For the present experimental set-up 1 to 3 images per run were attainable and each image required about 6 Mbytes of disk space (stored in a compressed TIFF file format).

Table 5-2: Number of PIV images used to create the combined image

Pressure gradient	Number of images
ZPG	25
CPG	30
FPG	25 or 93

The two different data set sizes for the FPG case allowed study of the effect of image sample size on flow field convergence. The results from the averaging are presented as Figures 5-10 to 5-12 for the ZPG, FPG and CPG, respectively. Locations where there was insufficient data to properly compute velocity or turbulence intensity are indicated by diamond shapes with locally high velocity gradients. The boundary layer thickness in Figures 5-10 to 5-12 is based on the location labeled ‘LDV and hot-film measurement location(s)’. The horizontal x axis does not correlate to any exact wind tunnel station. All profiles, unless otherwise stated, are extracted from the location labeled ‘LDV and hot-film measurement location(s)’.

The ZPG mean flow results are plotted in Figure 5-10. Note that PIV provides an entire plane of information. The velocity gradient shown in Figure 5-10 is uniform and relatively smooth throughout the boundary layer even with the relatively small number of images taken of this flowfield. The $u = 605$ m/sec ($u = 0.98 U_e$) contour does not grow across the image. Thus, the boundary layer is steady and does not grow significantly in the 2 cm PIV region. A 128×128 correlation block was used to compute the averages; however, the first data point was roughly 69 pixels from the wall (i.e., $y/\delta = 0.03$). The freestream velocity was calibrated to 600 m/sec.

The FPG mean flow results are plotted in Figure 5-11. This figure shows the effect of the favorable pressure gradient on the velocity profile. Both the boundary layer height and freestream velocity increased from their ZPG values. The boundary layer slightly grows from the $x = 1.0$ cm location to the $x = 3.0$ cm location, illustrating the effect of the FPG on the boundary layer structure. The acceleration due to the expansion is evident by a large area of velocity greater than 600 m/sec downstream of the LDV measurement location. Finally, the velocity gradient is evident in this figure.

The CPG results are plotted in Figure 5-12. This figure shows the effect of the combined pressure gradient on the velocity profile. The boundary layer height decreased from its ZPG and FPG value; however, the freestream velocity remained similar to the ZPG freestream velocity. Velocity gradients are clearly indicated in Figure 5-12. The boundary layer growth indicated in the aft hot-wire measurement location should be treated with caution as δ is based off the first measurement location. In addition, the expected compression wave is not apparent in this figure.

PIV derived velocity vectors are presented as Figures 5-13 to 5-15 for the ZPG, FPG and CPG, respectively. The vectors illustrate the grid size discussed in Chapter 4. Note the turning of the velocity vectors due to the pressure gradient in Figures 5-14 and 5-15. The wall boundary was sketched in after the vectors were drawn and do not exactly match the wall contour.

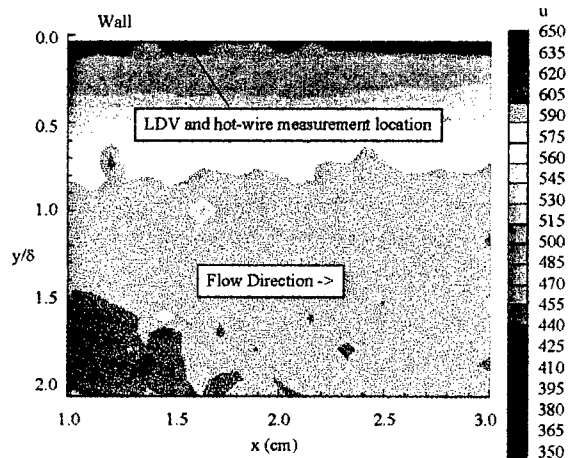


Figure 5-10: ZPG velocity contour plot

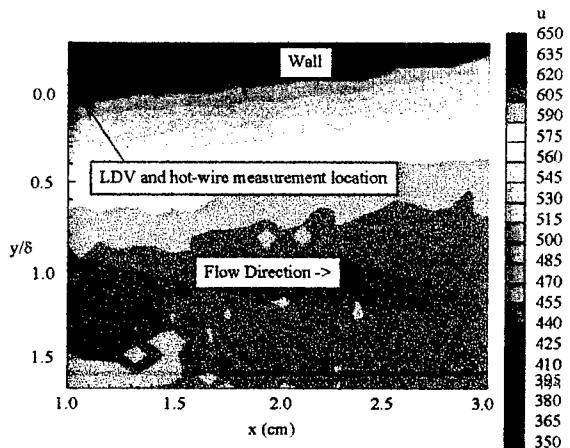


Figure 5-11: FPG velocity contour plot

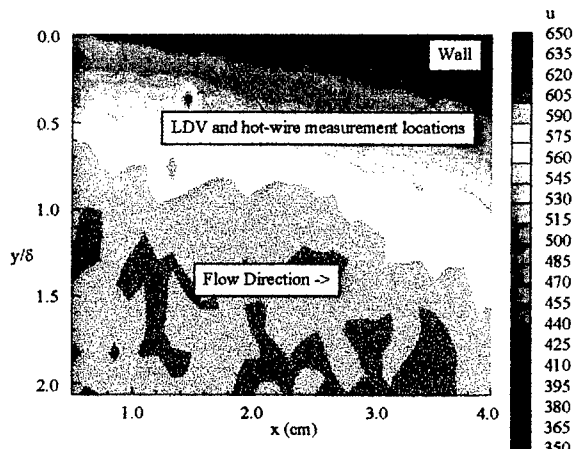


Figure 5-12: CPG velocity contour plot

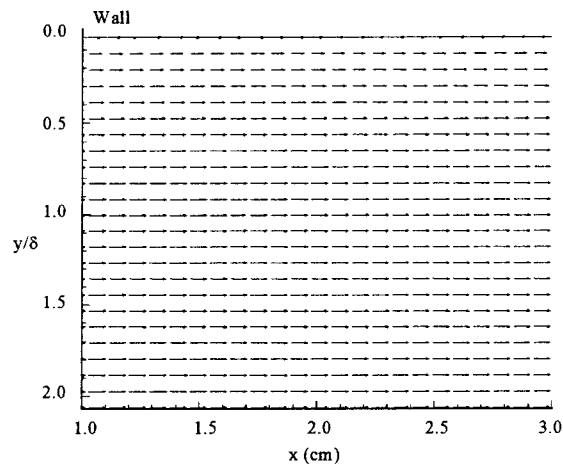


Figure 5-13: ZPG velocity vectors

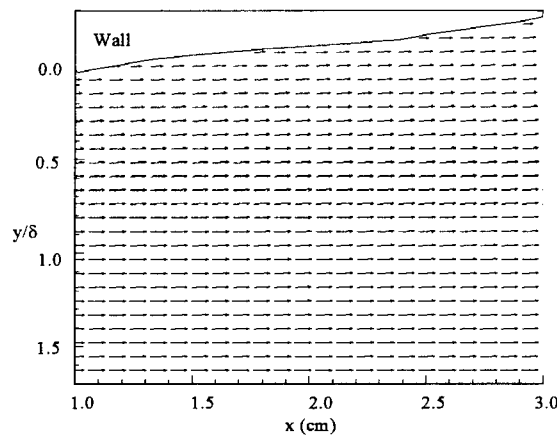


Figure 5-14: FPG velocity vectors

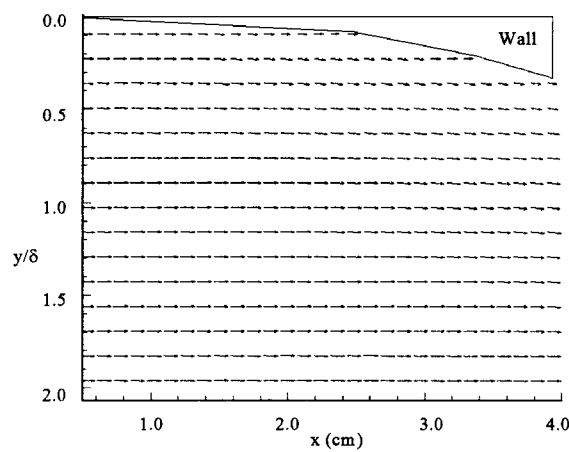


Figure 5-15: CPG velocity vectors

5.2.4 Comparison Between Data Collection Methods

This section compares the mean velocity for all of the data collection methods. In addition, the data are compared to the Van Driest profiles (Section 4.1.3).

5.2.4.1 Mean Flow Comparison

Since hot-wire anemometry and LDV only acquire data at one point and PIV provides data along an entire plane, a line (or profile) of data was extracted from the PIV images. This allows a better method to compare PIV results with the LDV results of Luker et al. (Luker et al., 1997). The PIV profile was extracted at the locations indicated in Figures 5-10 to 5-12, normal to the wall. The velocity comparisons between LDV, PIV and conventional pressure probes are presented as Figures 5-16 to 5-18 for the ZPG, FPG and CPG, respectively.

Figure 5-16 presents the ZPG velocity comparisons. There is excellent agreement between the LDV, PIV and conventional pressure velocity data above $y/\delta = 0.2$. Below this location in the boundary layer, PIV over-predicts the velocity ratio. This indicates that 25 images provides satisfactory mean flow data for the ZPG configuration.

Figure 5-17 presents the FPG data. Recall that the PIV FPG data was reduced with two different number of images to gauge the effect of number of images on mean flow quantities. The data for both image sample sizes predicts a fuller velocity profile than the LDV and pressure data; however the overall agreement is excellent. This indicates that velocity convergence has been reached with 25 images.

Figure 5-18 presents the CPG data. At both locations there is excellent agreement between the LDV and PIV data. This indicates that 30 images provides satisfactory mean flow data for the CPG configuration. Note that PIV resolved mean flow data closer to the wall.

From Figures 5-16 to 5-18, it was demonstrated that PIV can provide accurate mean flow data for as few as 25 images. Increasing the number of images does not assist in velocity convergence. This is an important finding since testing was time consuming and costly.

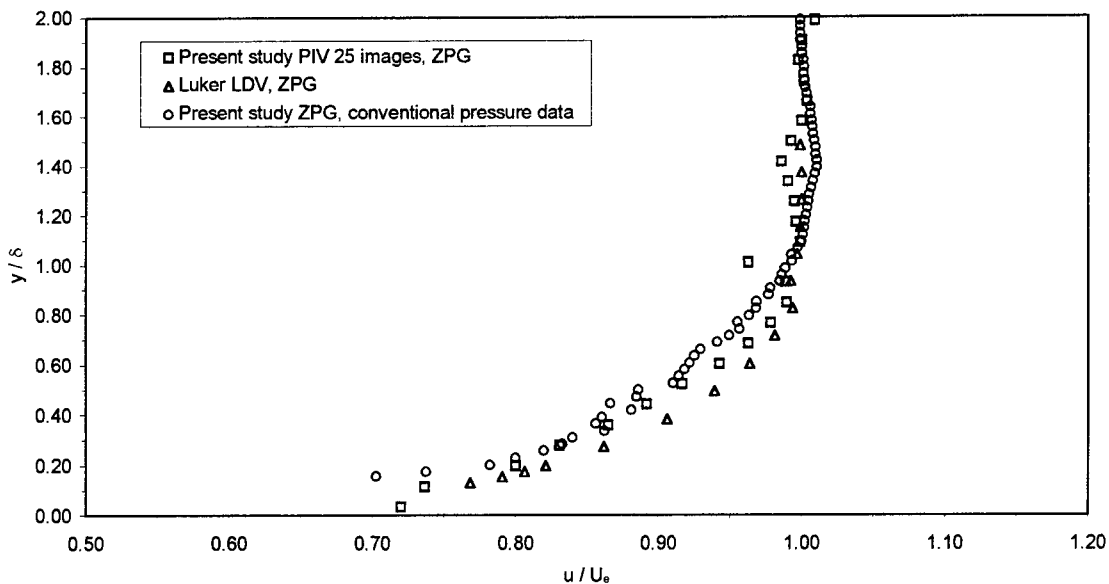


Figure 5-16: ZPG velocity comparison

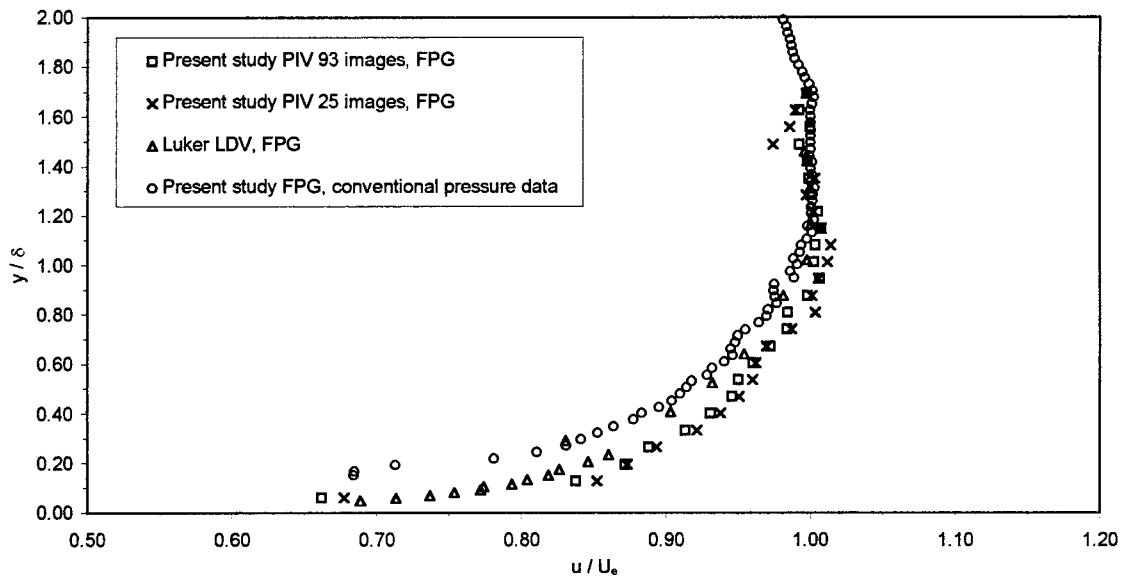


Figure 5-17: FPG velocity comparison

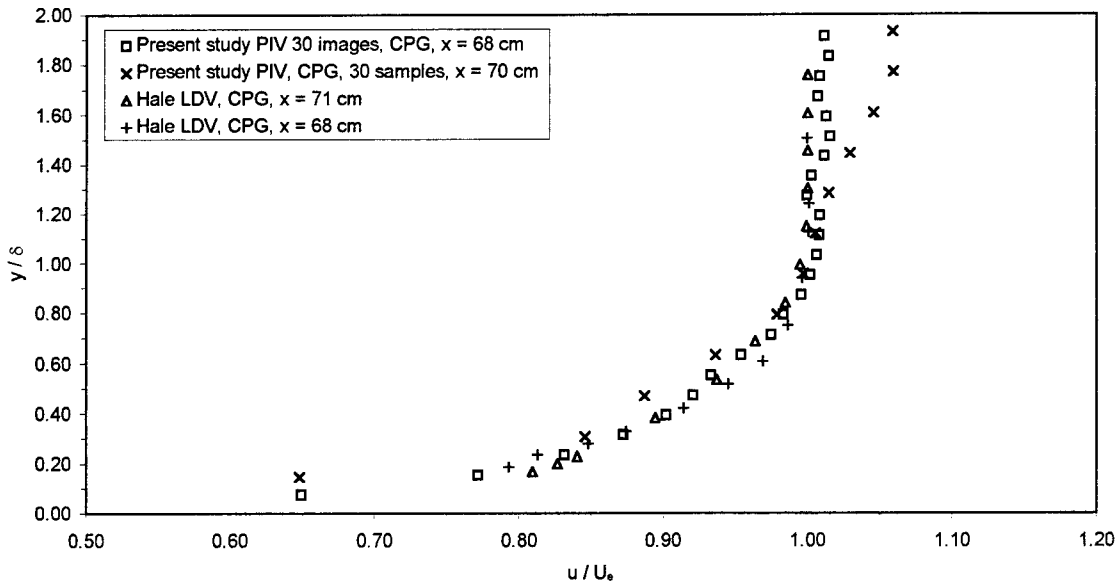


Figure 5-18: CPG velocity comparison

5.2.4.2 Van Driest Correlation

Another method used to validate PIV was to use the scaling laws proposed by Van Driest (Van Driest, 1951) to present the data. Evan's correction factor (Evans, 1985) was set equal to 1.5% for all pressure gradient cases. In addition, the hot-film data from this study was also scaled and plotted along with the LDV data by Luker et al. (Luker et al., 1997). This allows a comparison between the PIV data, LDV data and hot-film data. The profile for the ZPG is plotted in Figure 5-19 along with the theoretical flat plate values. For the flat plate, Clauser's parameter, β , equals 0.0. This value leads to a Coles wake parameter, Π , equal to 0.476. There is excellent agreement among the three data types and with the theory. The PIV lies closer to the theoretical values than either the LDV or hot-film data demonstrating the accuracy of the PIV method. In addition, PIV allows for data to be collected nearer to the wall ($y^+ \approx 31$) than LDV or the hot-film data. This is another illustration of the power of PIV. In addition to the ability to visualize a plane of data, near wall data can be collected even with the relatively large grid size (128 x 128 pixels) used in this study.

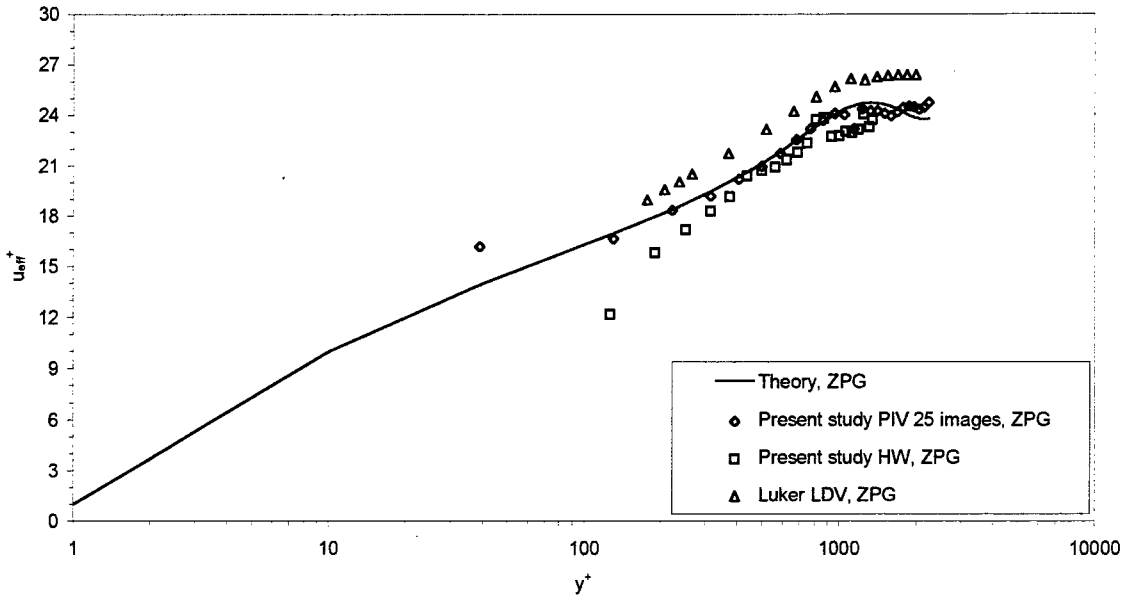


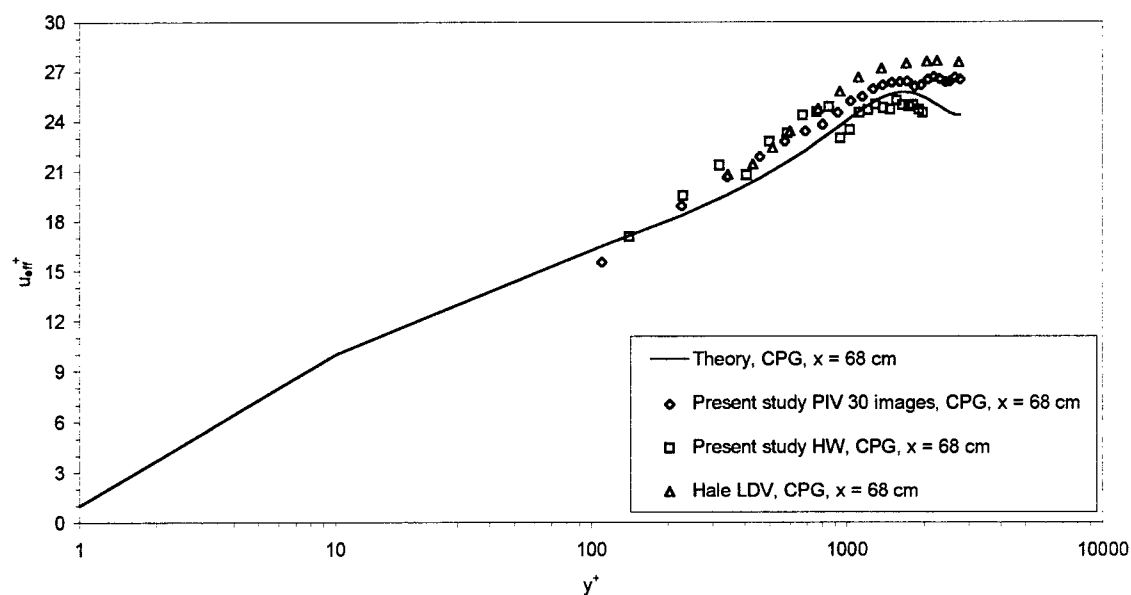
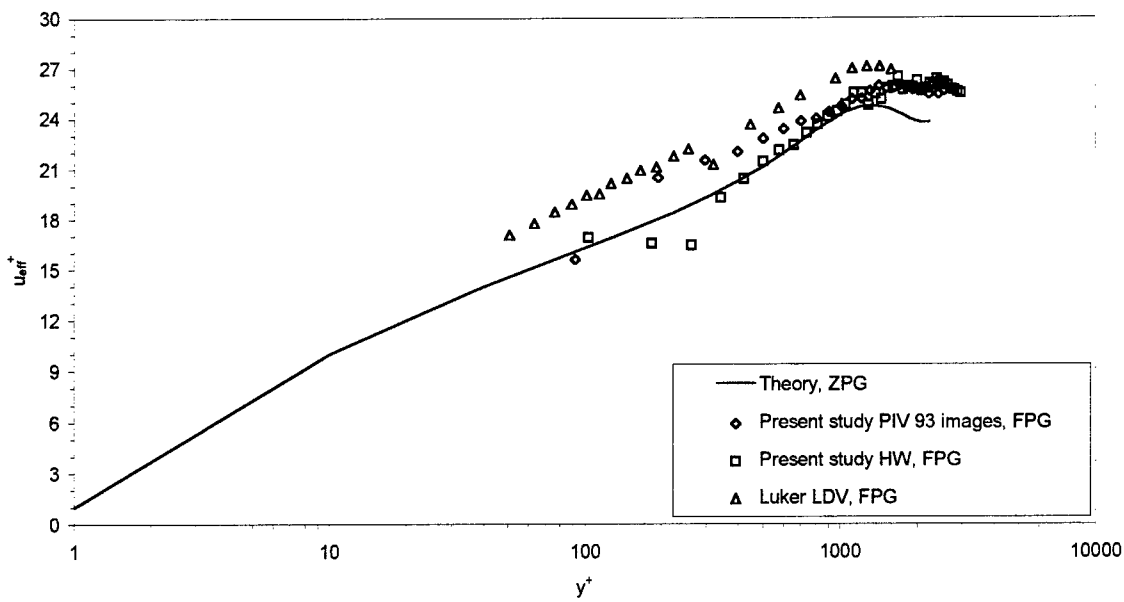
Figure 5-19: ZPG Van Driest velocity profile

For the FPG, β was found by Luker (Luker, 1995) to be -1.34, leading to an undefined Coles wake parameter. Thus, the FPG data was compared to the theoretical flat plate values. Figure 5-20 presents the FPG comparisons.

As with the ZPG, there is excellent agreement with the PIV and hot-film data to the theory. The PIV agreement is better than the LDV data found by Luker. However, in this case, LDV was able to resolve data closer to the wall. This is due to the effects of the wall slope and the 128 x 128 pixel patch size in the PIV data reduction.

For the CPG, β was found by Hale (Hale, 1995) to be 1.12 at $x = 68$ cm, leading to a Coles wake parameter equal of 1.15. Figure 5-21 presents the CPG comparisons for $x = 68$ cm. Again, note the excellent agreement between the PIV data and the theory. As with the FPG, PIV predicts the scaled velocity with more accuracy than the LDV predictions. The hot-film data also agrees well with the theory.

At $x = 71$ cm, β was found to be -0.94, leading to an undefined Coles wake parameter. Thus, the PIV data at $x = 70$ cm was compared to the theoretical flat plate values. The agreement between the



data types is good; however, the agreement between the data and the theory is not as good for this flow field condition. This is most likely due to inaccuracies in predicting the theory or due to the thinness of the boundary layer. Recall from Section 5.1 that the CPG reduced the boundary layer thickness by approximately 20%. Figure 5-22 presents the CPG comparisons for $x = 70$ cm.

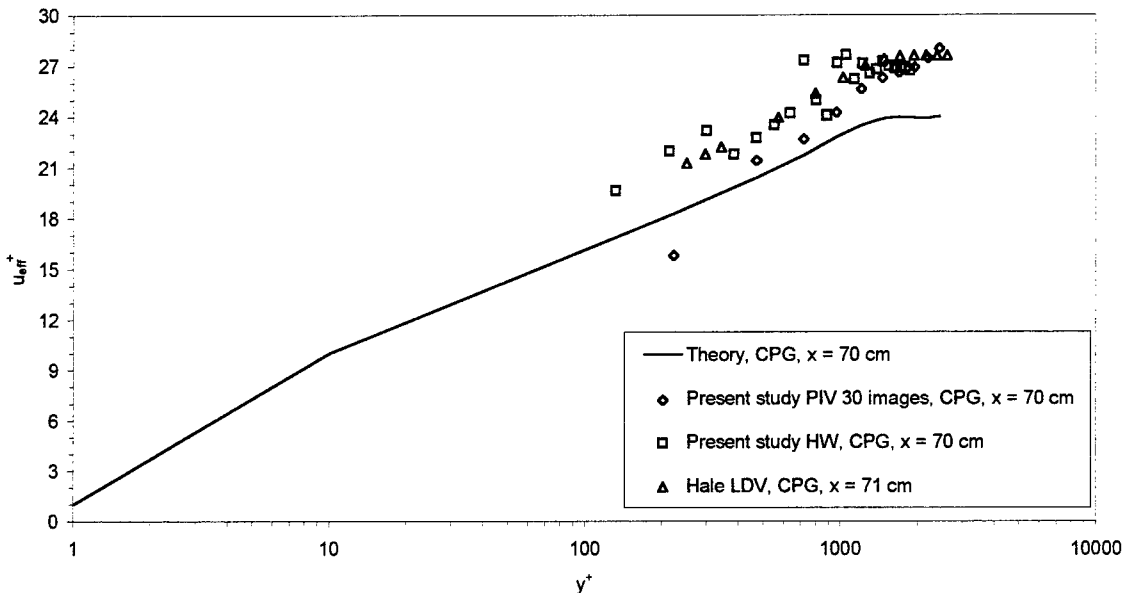


Figure 5-22: CPG ($x = 70$ cm) Van Driest velocity profile

As demonstrated in the previous four figures, use of Van Driest's scaling factors collapses the PIV data with the theory extremely well. This is a further indication of the accuracy and applicability of PIV for mean flow data reduction.

5.3 Turbulence Results

Hot-films and PIV were used to evaluate the fluctuating components of fluid properties. Hot-films were used to evaluate the mass flux, total temperature fluctuations and power spectra. Power spectra data was obtained by sampling the boundary layer at discrete locations in the boundary layer. A single hot-wire was used for all power spectra data. Finally, PIV was used to evaluate velocity fluctuations. This will assist in the validation of PIV as a flow diagnostic tool.

5.3.1 Hot-Film Turbulence Results

This section contains the hot-film turbulence results. Included in this section are the mass flux turbulence intensity profiles and the energy spectra results.

5.3.1.1 Turbulence Intensity Profiles

The fluctuating mass flux profiles are given in Figures 5-23 to 5-26 for the ZPG, FPG, and CPG (both locations), respectively.

Figure 5-23 presents the ZPG mass flux turbulence intensity (TI). There is excellent agreement between the multiple and single overheat methods as well as the two different traversing methods. The discrete points from the spectra data also show excellent agreement with the traverse data. The data indicates that the probe just barely reached the freestream. The maximum turbulence intensity occurs between $y/\delta = 0.3$ and $y/\delta = 0.5$ with a value of between 15% to 16%. Although this value is 5% higher than that found by Dotter (Dotter, 1994), it falls within the expected uncertainty bounds (see Appendix B).

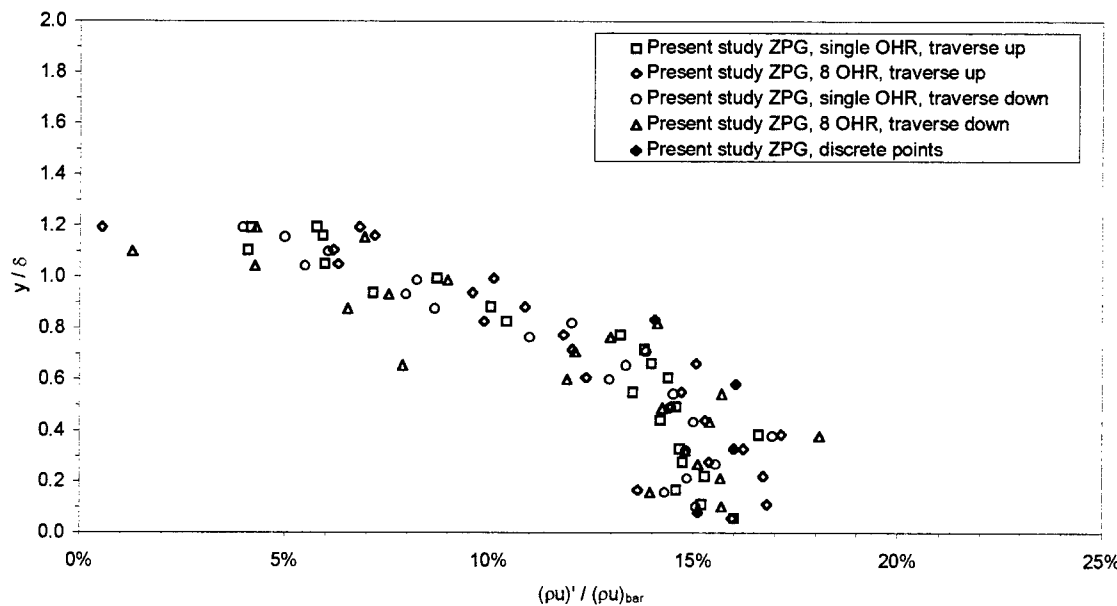


Figure 5-23: ZPG mass flux turbulence intensity

Figure 5-24 presents the FPG mass flux turbulence intensity. There is excellent agreement between the single overheat data, multiple overheat data and the discrete point data. The maximum turbulence intensity is 12% at a y/δ of 0.5. Thus, the FPG reduced the maximum turbulence intensity by 25% as compared to the ZPG. Note that traversing the probe into the wall provides near wall data.

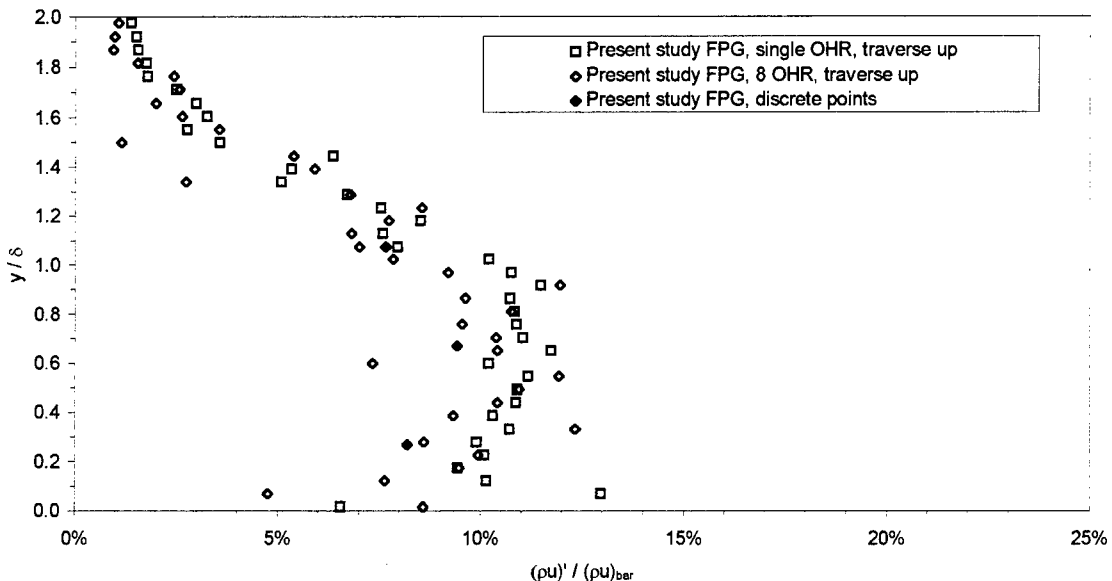


Figure 5-24: FPG mass flux turbulence intensity

Figure 5-25 presents the CPG mass flux turbulence intensity at $x = 68$ cm. Again, there is excellent agreement between the discrete data points, the traversed multiple overheat and single overheat data. The maximum turbulence intensity is 20% , a 25% increase over the ZPG value, at $y/\delta = 0.3$.

Figure 5-26 presents the CPG mass flux turbulence intensity at $x = 70$ cm. As with the ZPG and FPG, there is excellent agreement between the single and multiple overheat data. Discrete data points were not taken at this location. The maximum turbulence intensity is 22%. This level of turbulence intensity is higher than observed at the $x = 68$ cm location. This data contradicts the data by Hale (Hale, 1995) who found that the turbulence intensity was reduced at this location. This discrepancy could be explained by differing data collection and reduction methods. In addition, uncertainty in x location may play a part. Hale acquired data at $x = 71$ cm. Dotter (Dotter, 1994) collected data with a cross-wire at $x =$

71 cm. The magnitude of the peak turbulence intensity was roughly 20% which agrees well with the present study. As with the $x = 68$ cm data, the turbulence intensity increased as compared to the ZPG data in Figure 5-26.

The results in Figures 5-23 and 5-26 lead to the following conclusions. For the ZPG, the maximum mass flux turbulence intensity is between 15% to 16%. Application of a FPG damps out the turbulence as evidenced by the 25% reduction in the mass flux axial turbulence intensity. Application of the CPG has the opposite effect. The mass flux turbulence intensity increases by 22% as compared to the ZPG.

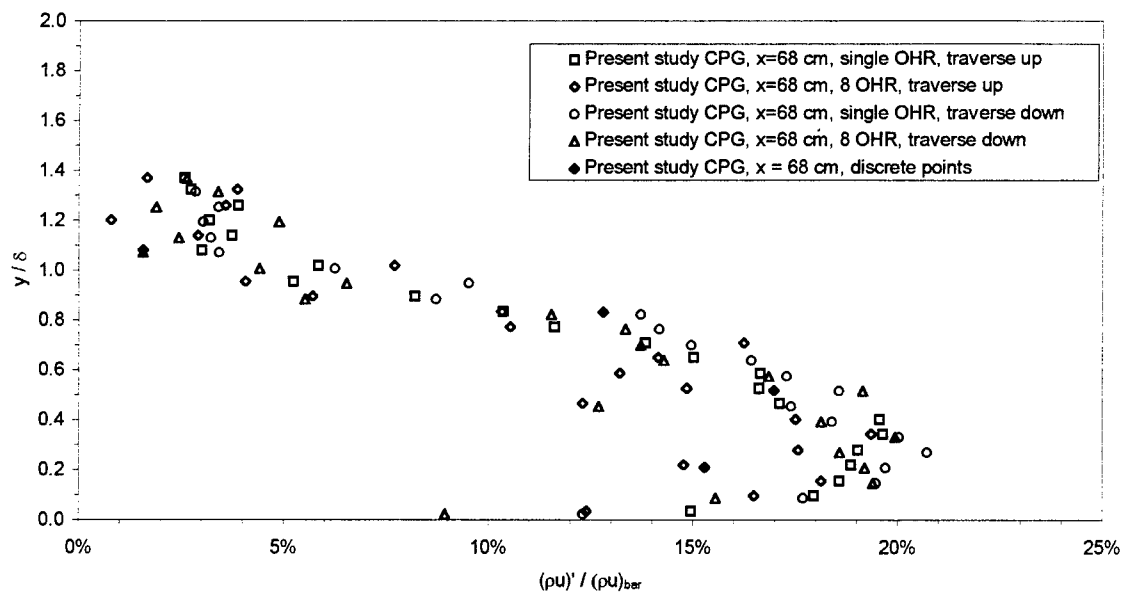


Figure 5-25: CPG ($x = 68$ cm) mass flux turbulence intensity

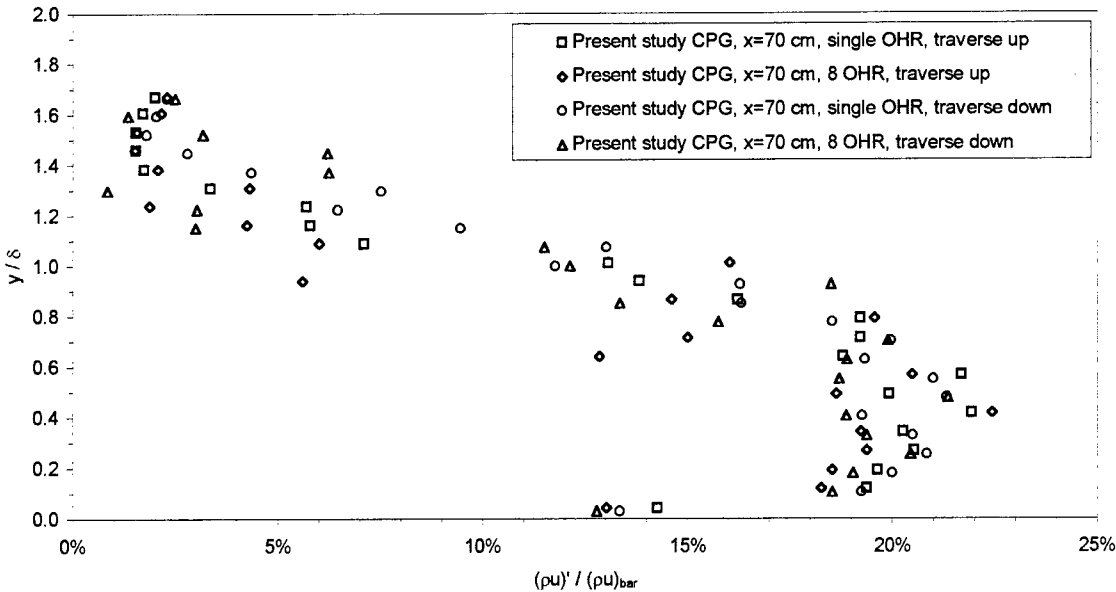


Figure 5-26: CPG ($x = 70$ cm) mass flux turbulence intensity

5.3.1.2 Energy Spectra

Hot-wires were used to interrogate the boundary layer to obtain energy spectra data. This will determine the effect of the pressure gradient on the power spectra. Figure 5-27 presents the power spectra data for the ZPG. The data in Figure 5-27 indicates that, for a ZPG, there is little variation in energy across the frequency spectrum. The roll-off frequency is approximately 40,000 Hz.

Figure 5-28 presents the power spectra for the FPG. The FPG data contains several key differences. First, the energy level is not constant across the frequency spectrum. The energy is more heavily weighted towards the lower frequency structures. This indicates that the higher frequency structures are feeding their energy in a FPG flow field to the low frequency structures their energy in a FPG flow field. This confirms the theory that application of a FPG causes disassociation of large scale structures into small scale structures. In addition, the roll-off frequency is lower, approximately 10,000 Hz. Finally, a cross-over between the inner region data and outer ration data occurs. This indicates that the large frequency structures contain less energy in the inner region, than they do in the outer region.

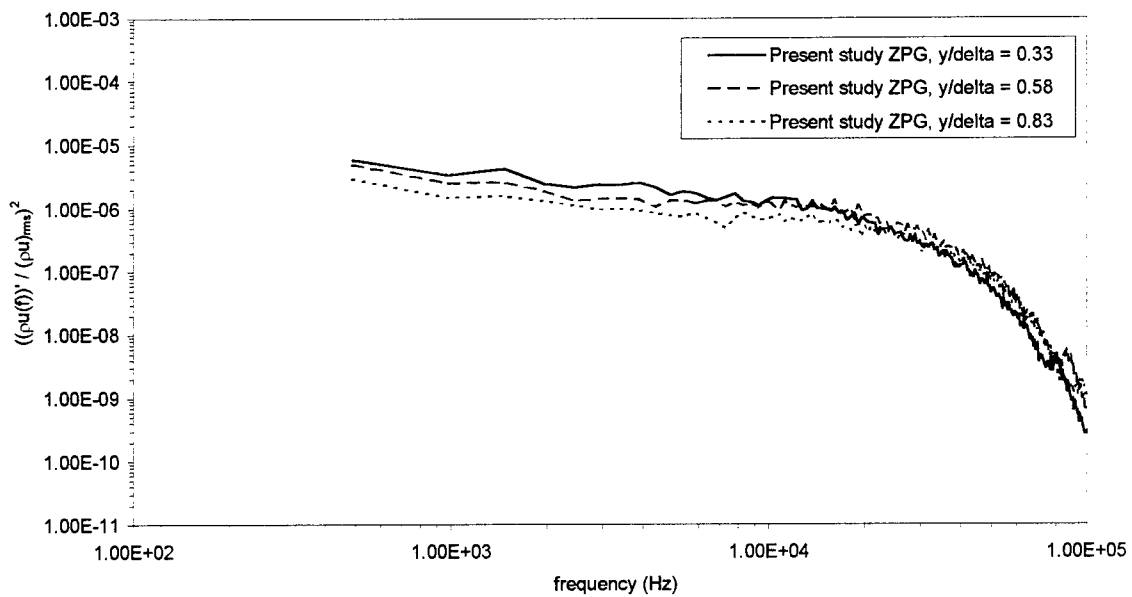


Figure 5-27: ZPG power spectra data

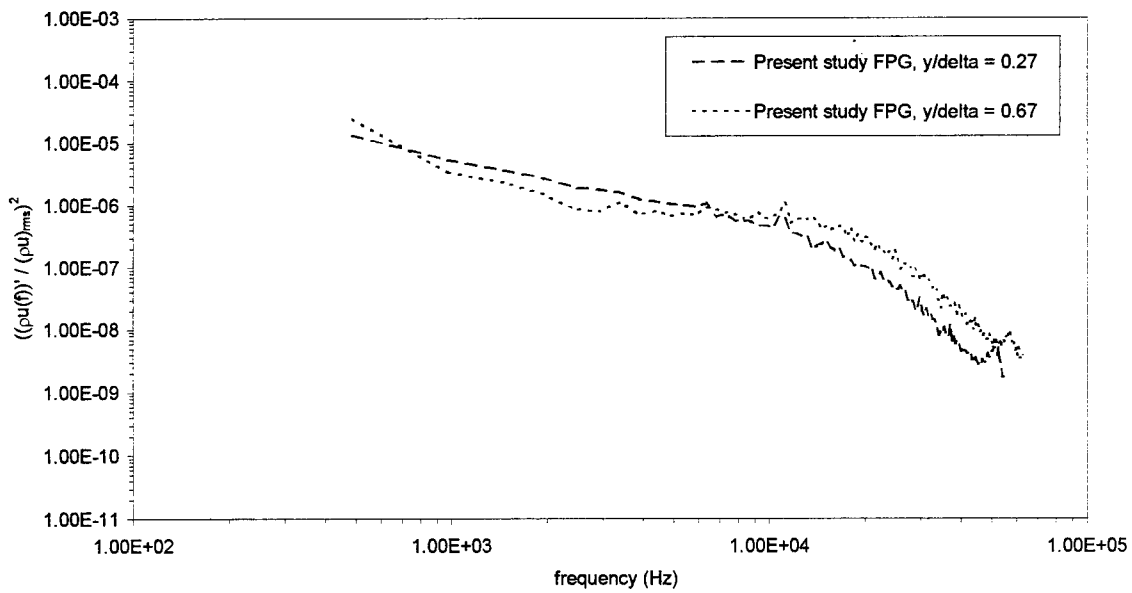


Figure 5-28: FPG power spectra data

Figure 5-29 presents the power spectra for the CPG. Data was taken at $x = 68$ cm only. The CPG power spectra data contains several key differences as compared to the ZPG flow. As with the FPG, the energy level is not constant across the frequency spectrum. The energy is more heavily weighted towards the lower frequency structures and the energy level is higher for the CPG than the FPG or ZPG. The roll-off frequency is approximately unchanged from the FPG conditions. Also the cross-over noted in the FPG data is repeated in Figure 5-29. These data confirm that the large scale structures contain most of the energy. This finding is consistent with the flow visualization results.

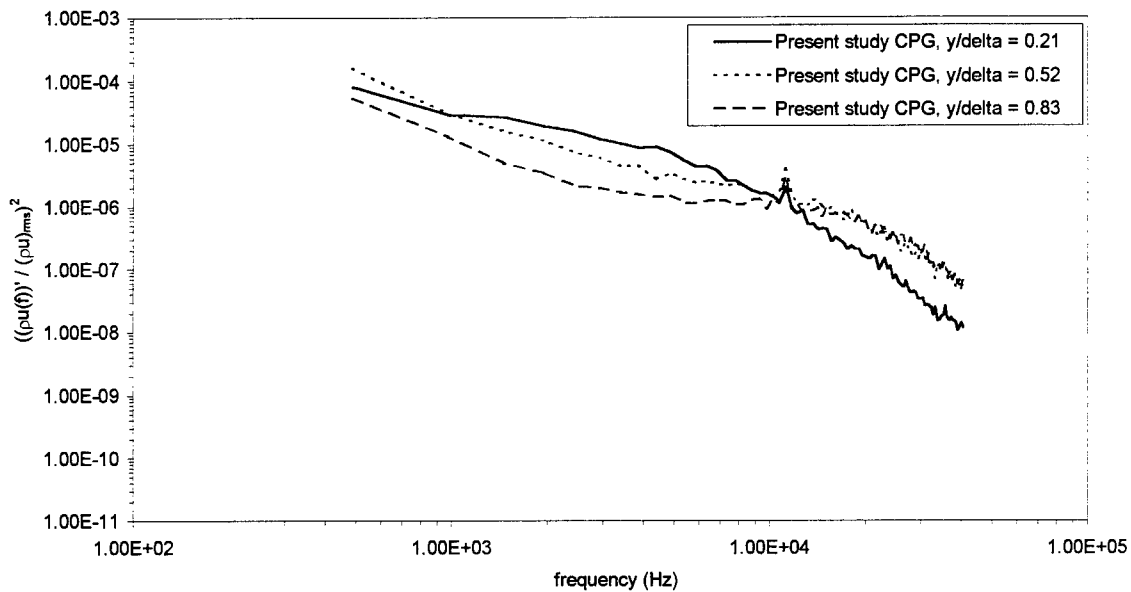


Figure 5-29: CPG power spectra data

The following statements sum up the effect of the pressure gradient on the power spectra. First, for the ZPG, the energy is evenly distributed among the frequency spectrum. Application of a pressure gradient shifts energy from the high frequency to the low frequency structures. The CPG results in a higher low frequency energy than the FPG. A cross-over in energy occurs between the inner region and outer regions of the boundary layer.

5.3.2 PIV Turbulence Results

PIV was used to compute the axial turbulence intensity (TI). Like LDV, PIV directly measures the velocity fluctuations, whereas hot-films measure mass flux TI. Figures 5-30 to 5-32 present PIV velocity TI contours for the ZPG, FPG and CPG, respectively. Note that the power of PIV allows an entire plane of data to be resolved.

In all figures, the TI in the freestream is between 3% and 4%, which is higher than that reported by Luker and Hale (Luker, 1995 & Hale, 1995). This suggests that PIV either is not sensitive to TI (low signal to noise ratio) or there were an insufficient number of samples taken. However, the boundary layer data is more reasonable as will be shown.

The ZPG contour plot of TI is presented in Figure 5-30. The maximum TI is near the wall with a magnitude of 15%. This shows close agreement with the mass flux TI obtained via hot-film techniques (Figure 5-26). Regions of TI in excess of 20% in the freestream or near the wall are due to either an insufficient number of samples or lack of seed. The TI gradient is resolved well throughout the boundary layer. As previously mentioned, the freestream TI is approximately 4%, twice as high as compared to Figure 5-26.

Figure 5-31 presents the FPG TI contour plot. The maximum TI in the boundary layer is approximately 13%, a 15% reduction from the ZPG results. Thus, the stabilizing effect of the FPG is observed in the PIV measurements. The PIV results presented in Figure 5-31 also indicate that the boundary layer is growing in the flow direction, again as previously demonstrated via hot-film techniques. The freestream TI is higher for the FPG, which is unexpected. Recall that in Figure 5-27 the freestream TI is approximately 1.5%.

Figure 5-32 shows the effect of the CPG on the TI. The highest TI is 26%, a 50% increase over the ZPG results. Again, PIV confirms the TI enhancement caused by the CPG. The freestream TI is approximately 5%, which is a 66% increase over the ZPG and confirms the destabilizing effect of the CPG on the flow.

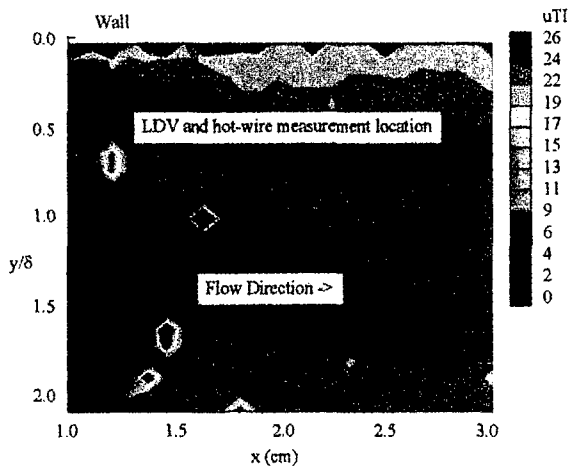


Figure 5-30: ZPG u turbulence intensity contours (%)

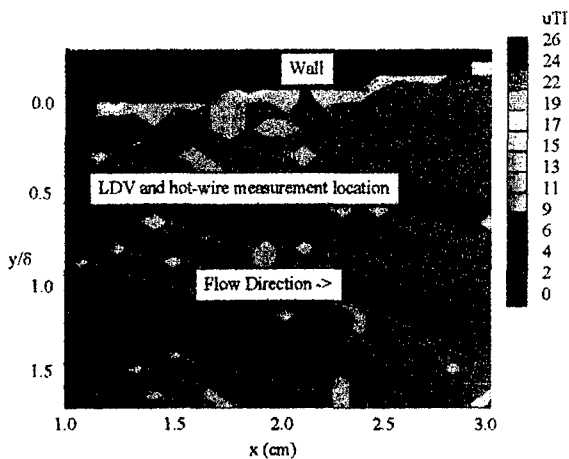


Figure 5-31: FPG u turbulence intensity contours (%)

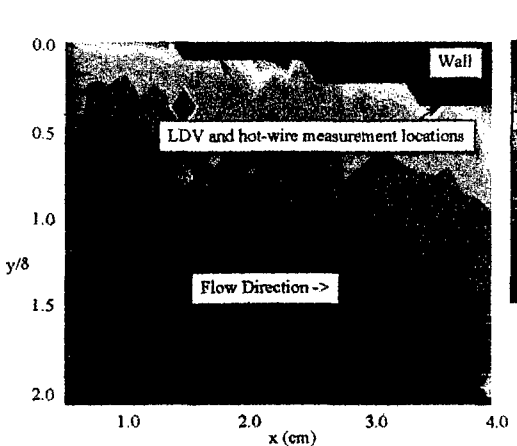


Figure 5-32: CPG u turbulence intensity contours (%)

5.3.3 Comparison Between Data Collection Methods - Turbulence Quantities

Data were extracted from the PIV contour plots and compared to the hot-film data and relevant data from the open literature (Luker, 1995, Hale, 1995 & Klebanoff, 1954). The data was extracted from the PIV in the same manner as described in Section 5.2.4. The line plot comparisons are presented as Figures 5-33 to 5-35 for the ZPG, FPG and CPG, respectively. In addition, the single overheat data was reduced as in Section 4.2.3 as another basis of comparison.

Figure 5-33 presents the ZPG turbulence intensity contours. In the boundary layer ($y/\delta < 1.0$) there is close agreement between the LDV and PIV data. Above $y/\delta = 1.0$, the LDV data drops to 1% while the PIV stabilizes at 3%. Klebanoff's data was for incompressible flow and appears to set a lower boundary for the TI. The hot-film data from the present experiment matches extremely well with the LDV data as well as the Klebanoff data.

Figure 5-34 contains the FPG turbulence intensity comparison. Note that the stabilizing effect of the FPG is apparent in all measurement techniques. In the boundary layer, the PIV compares favorably with the LDV and hot-film data. The divergence between the PIV and LDV data occurs above $y/\delta = 1.0$ with the LDV predicting a TI of 1% while the PIV predicts 3%. The hot-film data agrees with the LDV for near wall data and in the freestream; however, in the upper region of the boundary layer ($y/\delta > 0.2$) the PIV under predicts the turbulence intensity.

Figure 5-35 contains the CPG u turbulence intensity profile for $x = 68$ cm. The hot-film and LDV data match well; however, the PIV data consistently over predicts the TI by approximately 33% suggesting that an insufficient number of images was used to evaluate the flow.

Figure 5-36 contains the CPG u turbulence intensity profile for $x = 70$ cm. As with the $x = 68$ cm data, agreement between the hot-film and LDV data is excellent. Again, the PIV data consistently over predicts the TI by approximately 33%. Thus, PIV does not capture the TI accurately for this configuration.

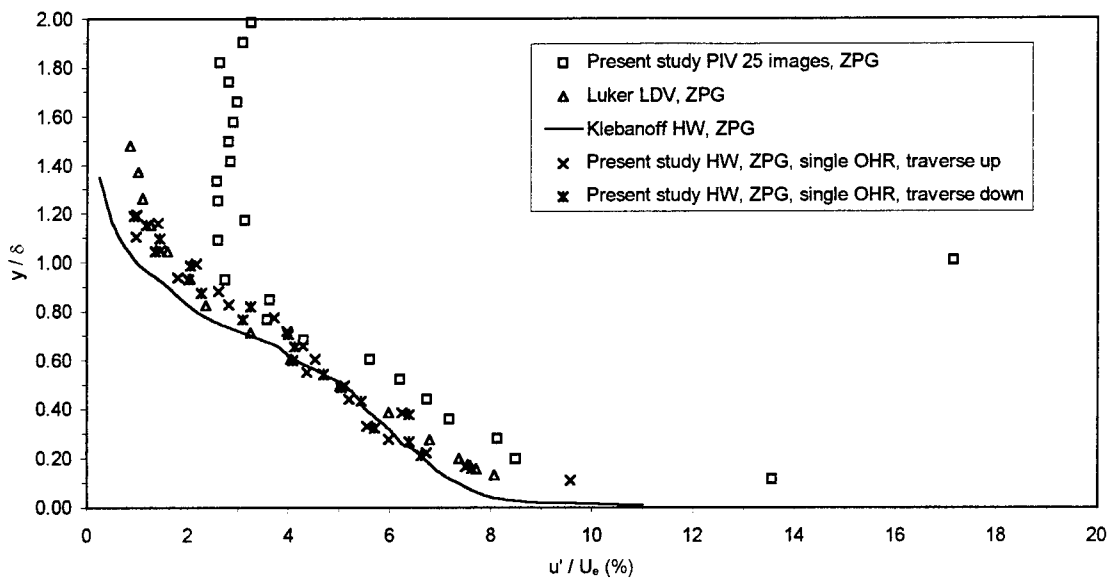


Figure 5-33: ZPG u turbulence intensity profiles

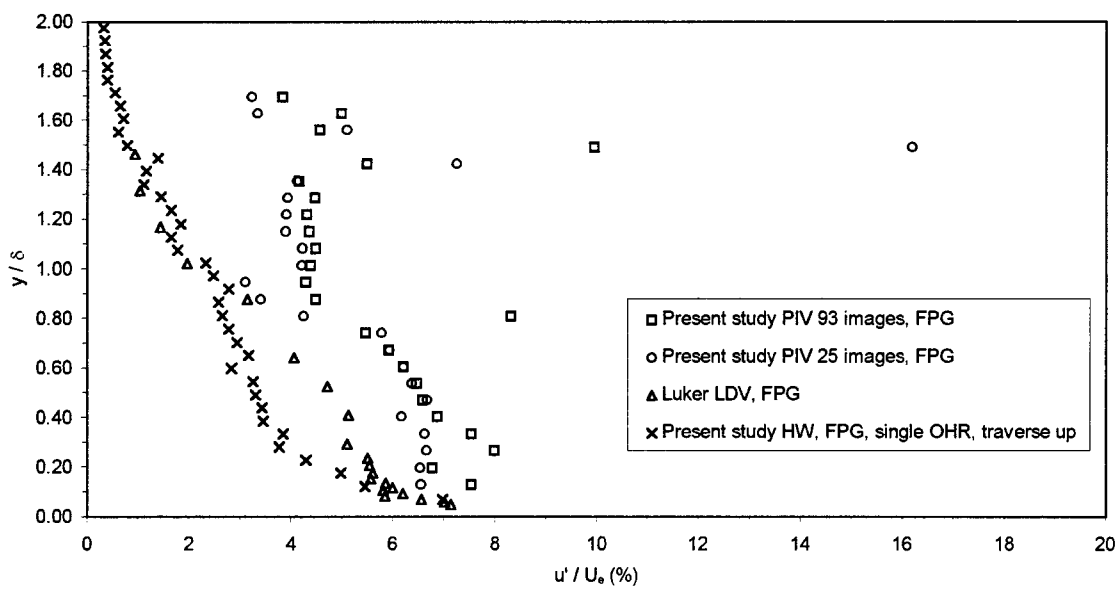


Figure 5-34: FPG u turbulence intensity profiles

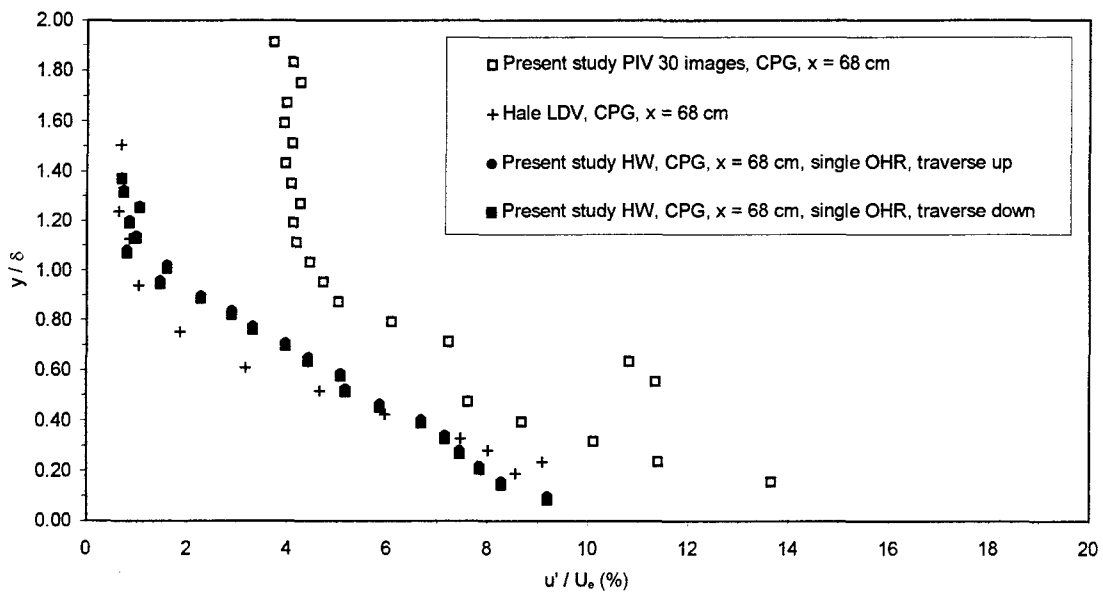


Figure 5-35: CPG ($x = 68$ cm) u turbulence intensity profile

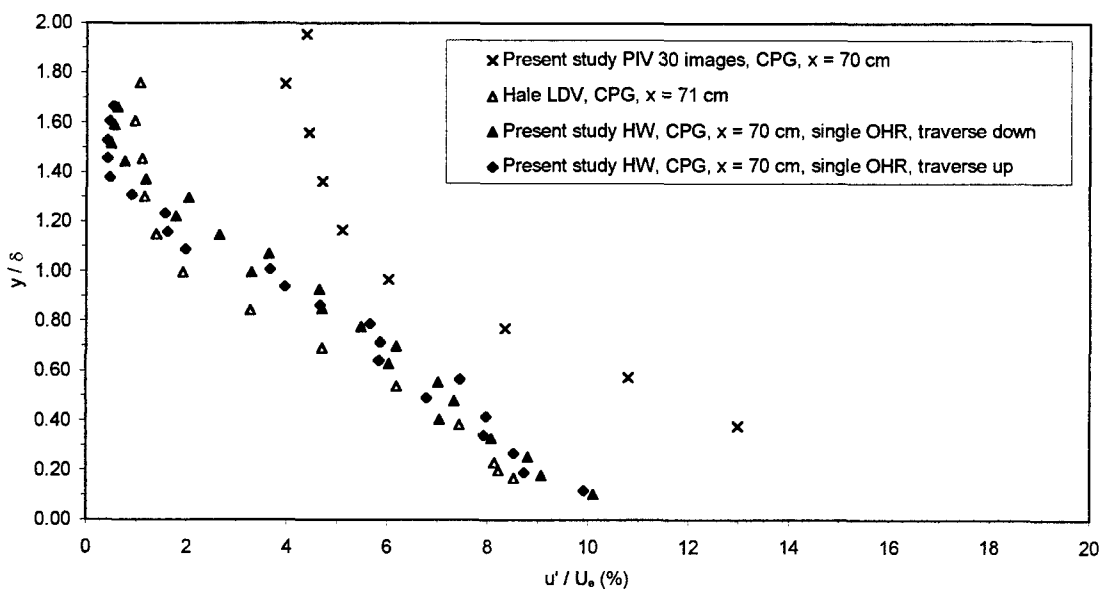


Figure 5-36: CPG ($x = 70$ cm) u turbulence intensity profile

The data in Figures 5-33 to 5-36 leads the conclusion that while PIV is accurate for mean flow quantities, it is inaccurate for turbulence quantities. Accuracy can be improved by increasing the number of images.

5.3.4 Density Fluctuations

Finally, the density fluctuations in the boundary layer were extracted from the hot-film data. Since PIV is only sensitive to the velocity, it cannot measure this fluctuation. The density fluctuation data is presented as Figure 5-37. The density fluctuation data exhibits the same FPG stabilizing trends and CPG destabilizing trends as indicated in Figures 5-26 to 5-29. The maximum density fluctuation is 10% for the ZPG, 7% for the FPG and 14% for the CPG. Finally, there is good agreement between the different traversing methods.

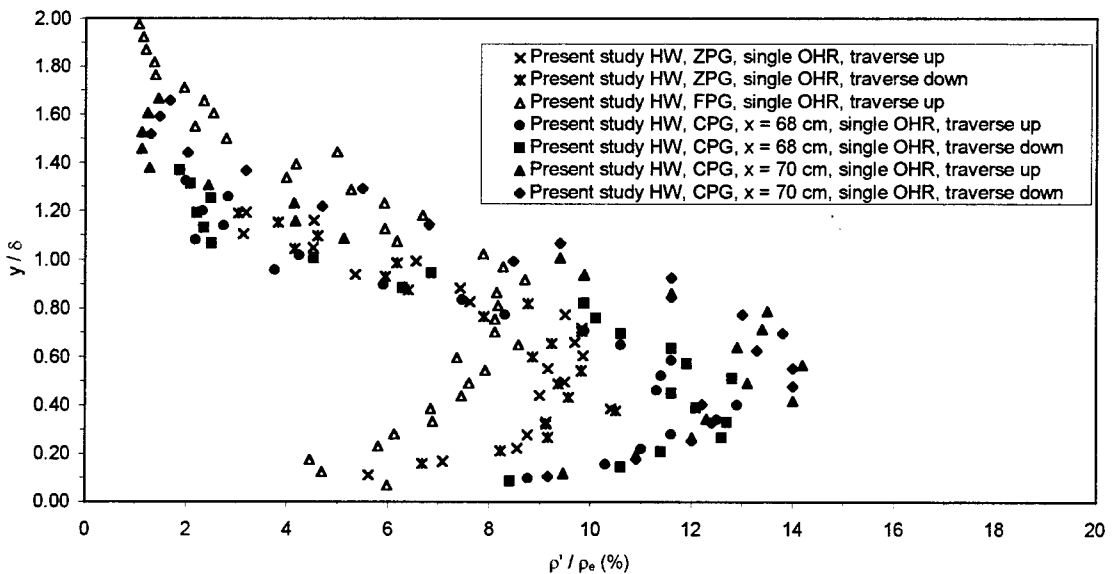


Figure 5-37: Density fluctuations

6. Mach 1.7 Results and Discussion

This chapter contains the results of the Mach 1.7 analysis. Since the main test condition for this study was Mach 2.8, only selected measurements were taken at Mach 1.7. Pressure and hot-wire data were acquired with the FPG model. Data were taken along the tunnel centerline at locations 2.5 and 11.5 cm downstream of the nozzle. The 2.5 cm location corresponded to ZPG flow and the 11.5 cm location was used as the FPG. The FPG location was the same as used in the Mach 2.8 configuration. The CPG model was not used because it “unstarted” the tunnel. Tunnel unstart is a condition where supersonic flow cannot be achieved due to flow blockage from either a model or a probe.

6.1 Mach 1.7 Conventional Pressure Data

Pitot pressure was taken at each measuring location. From the Pitot pressure, the methods of Sections 4.1.1.1 and 4.1.1.2 were used to compute the Mach number profile and velocity profile. Figures 6-1 to 6-3 present these results.

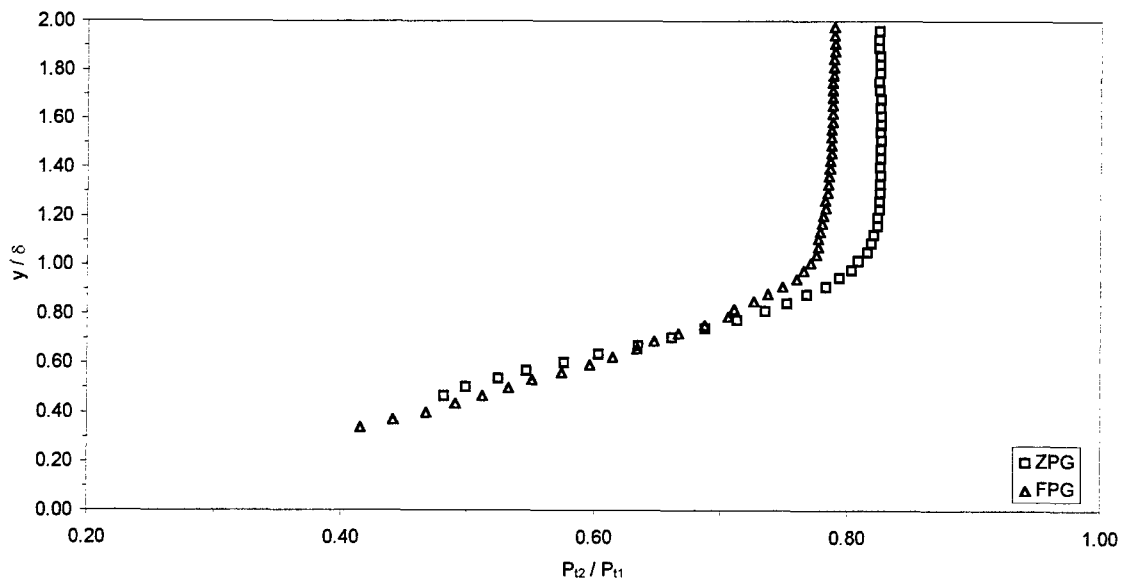


Figure 6-1: Mach 1.7 Pitot pressure profiles

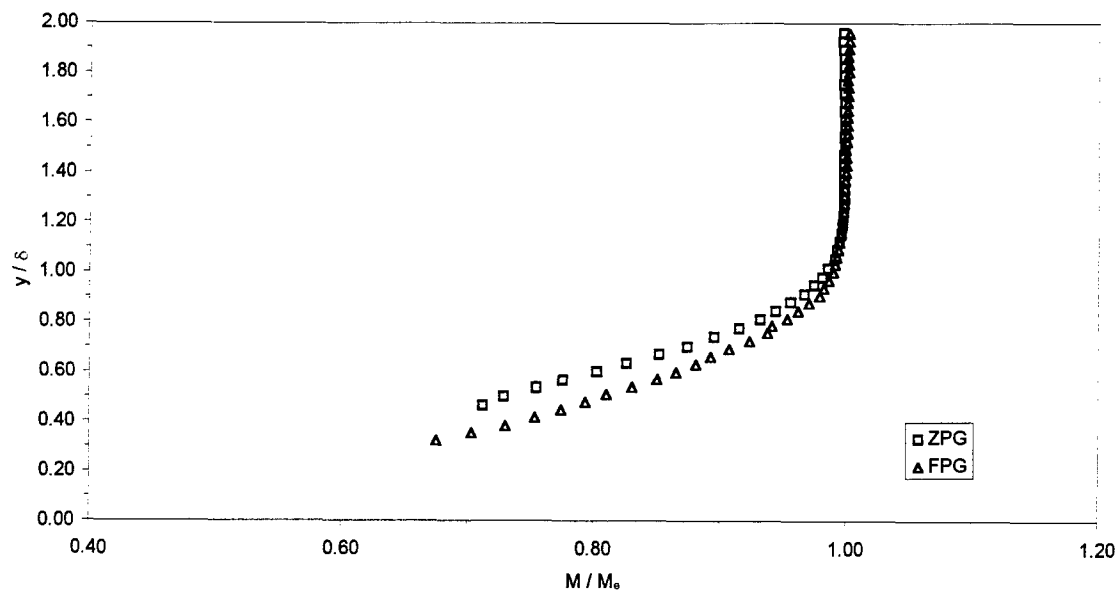


Figure 6-2: Mach 1.7 Mach number profile

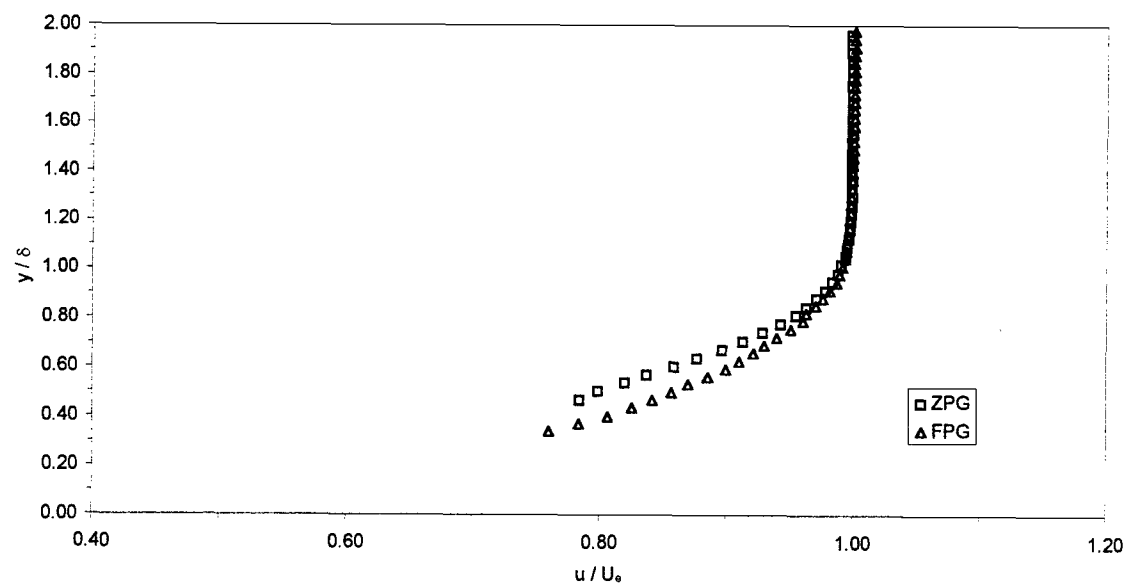


Figure 6-3: Mach 1.7 velocity profile

The data in these figures present the same trends as noted in the Mach 2.8 data. The data in these figures were used to calculate the boundary layer thickness. Table 6-1 presents the results of these calculations. Note that the values in Table 6-1 are lower than the boundary layer thickness in Mach 2.8 flow.

Table 6-1: Mach 1.7 boundary layer parameters

	ZPG	FPG
δ_u (mm)	3.91	4.70
δ_M (mm)	4.06	4.90
M_e	1.66	1.77
U_e (m/sec)	468	478

6.2 Hot-Wire Results

This section presents the Mach 1.7 hot-wire results. Since the boundary layer was not as thick as for the Mach 2.9 configuration, the averaging packet was reduced from 4,096 points to 2,048 points. This allowed a sufficient number of data points to be evaluated in the boundary layer.

6.2.1 Mean Flow Profiles

Figure 6-4 presents the Mach 1.7 ZPG mass flux ratio and total temperature ratio. Note the excellent agreement between the traverse up and traverse down data. The single overheat methodology aligns quite well with the multiple overheat data indicating that the total temperature is essentially constant through the boundary layer. This is confirmed by the total temperature profiles. Note that while the total temperature ratio is essentially constant for either the traverse up or traverse down profiles, there is a very slight difference between the traverse up and traverse down profiles. This difference is most likely due to a slight cooling of the flow straightener during the test run.

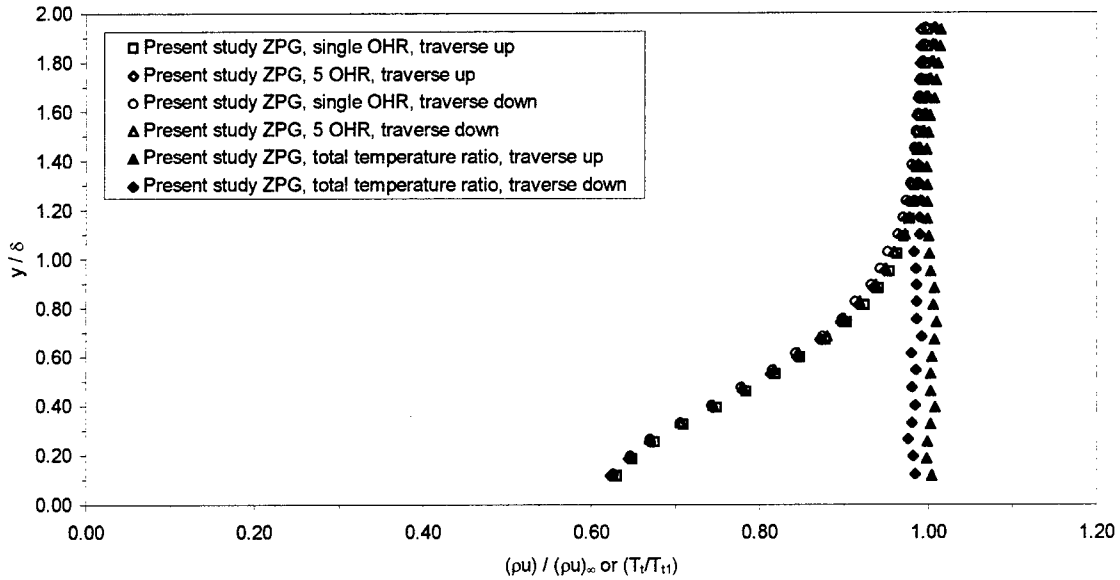


Figure 6-4: Mach 1.7 ZPG hot-film data

6.3 Turbulence Results

Hot-films were used to evaluate the fluctuation components of fluid properties. Hot-films were used to evaluate the mass flux, total temperature, and velocity fluctuations. Power spectra data were taken for both configurations, but turbulence information is only presented for the ZPG configuration.

6.3.1 Mass Flux Turbulence Intensity Profiles

The mass flux turbulence results are presented in Figure 6-5. There is excellent agreement between the traverse up and traverse down as well as the single versus multiple overheat data. The maximum TI decreased from 17% to 7% from Mach 2.9 to Mach 1.7, a 60% reduction. The freestream TI was found to be 1.5%.

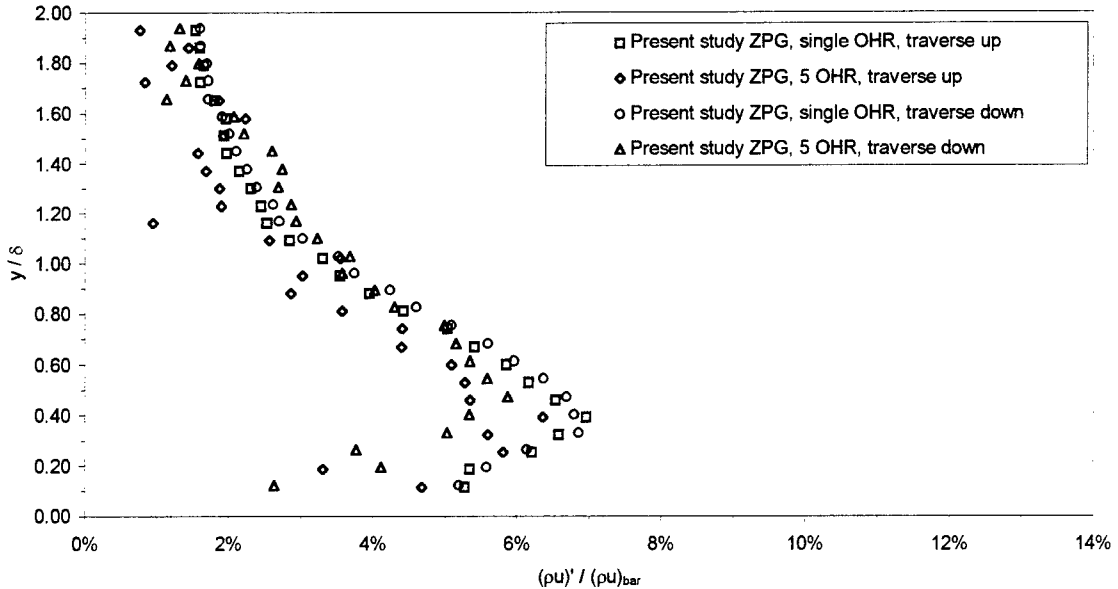


Figure 6-5: Mach 1.7 ZPG mass flux turbulence intensity

6.3.2 Energy spectra

Figure 6-6 presents the power spectra results. As with the Mach 2.8 results, the ZPG data indicates that the energy evenly spread throughout the frequency spectrum. In the outer region, the energy is more heavily weighted towards the larger scale structures. However, the Mach 1.7 FPG data exhibits opposite trends than the Mach 2.8 FPG data. In Figure 6-5, the FPG consistently maintains a higher level of energy than the ZPG. The data in Figures 5-11 and 5-12 indicate that the FPG has a lower level of energy than the ZPG. The fact that the Mach number is subsonic over a substantial portion of the boundary layer may be responsible for this opposite trend (Spina et al., 1994). Another possible explanation is compressibility. Since the Mach number is closer to one, the effects of compressibility may be lessened.

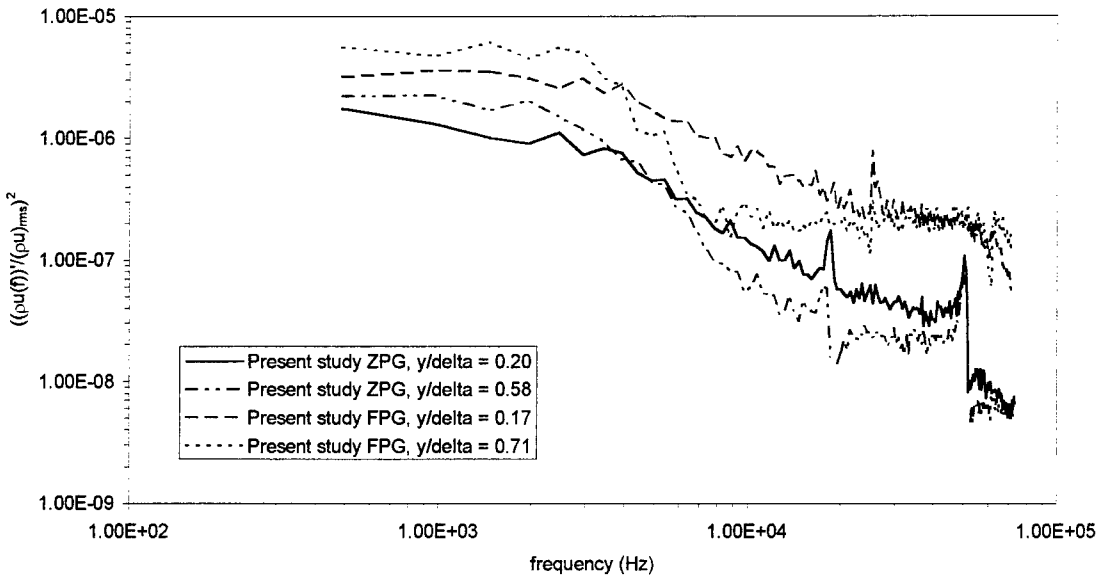


Figure 6-6: Mach 1.7 power spectra data

6.3.3 Separated Turbulence Results

Figures 6-7 to 6-9 present the separated turbulence intensity results for velocity, density and total temperature, respectively.

Figure 6-7 presents the Mach 1.7 u turbulence intensity profiles. There is excellent agreement between separated turbulence intensity profiles during the different traversing methods. The u TI is approximately 10% at $y/\delta = 0.2$ and 1% in the freestream. This is an increase of 20% from the Mach 2.8 ZPG condition.

Figure 6-8 presents the Mach 1.7 density fluctuation profiles. The density turbulence intensity is the lowest fluctuation as compared to the velocity and total temperature fluctuations with a value of 5% at $y/\delta = 0.2$. The freestream values is approximately 0.75%. This represents a 50% decrease from the Mach 2.8 ZPG value of density fluctuation. The agreement between the traverse up and traverse down data is not as good as it was for the u turbulence intensity. This could be due to the variation in total temperature between the traverse up and traverse down data noted in Figure 6-4.

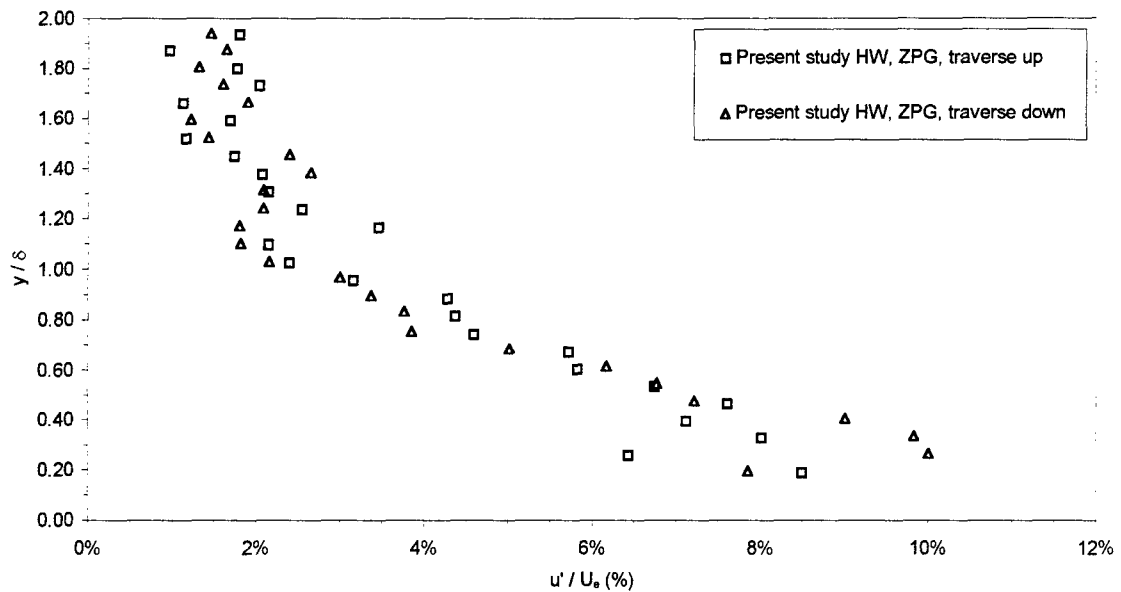


Figure 6-7: Mach 1.7 u turbulence intensity profiles

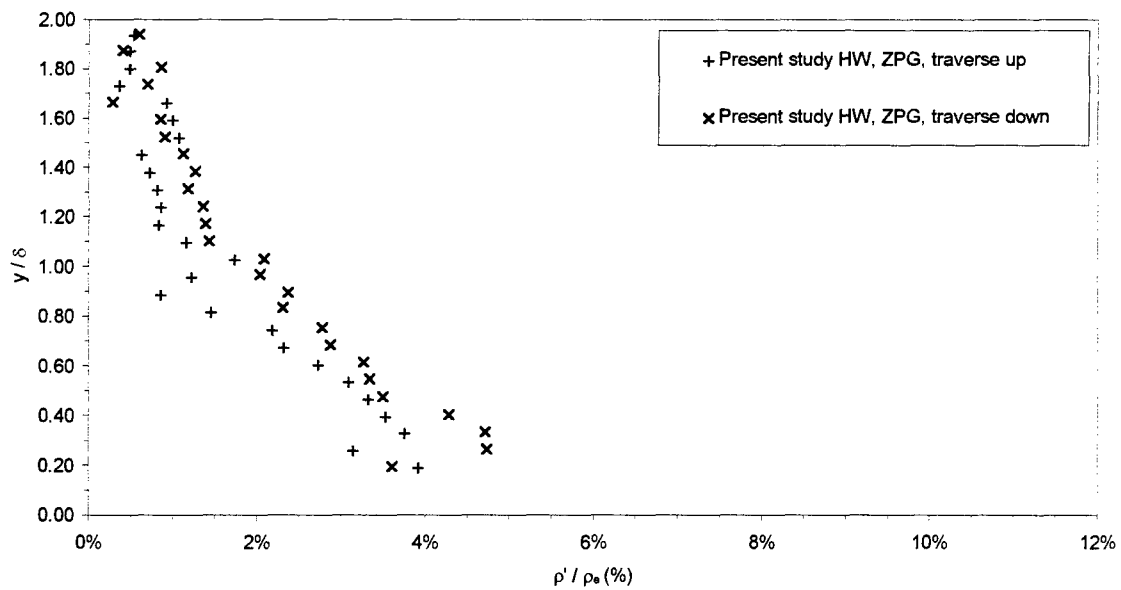


Figure 6-8: Mach 1.7 density fluctuation profiles

Figure 6-9 presents the Mach 1.7 total temperature fluctuation profiles. The temperature fluctuations lie between the density and velocity with a maximum value of 8%. The freestream value of total temperature fluctuation is approximately 2%. The scatter in the total temperature fluctuations is greater than the scatter in Figures 6-7 and 6-8. Again this is attributed to the change in total temperature between the traverse up and traverse down data.

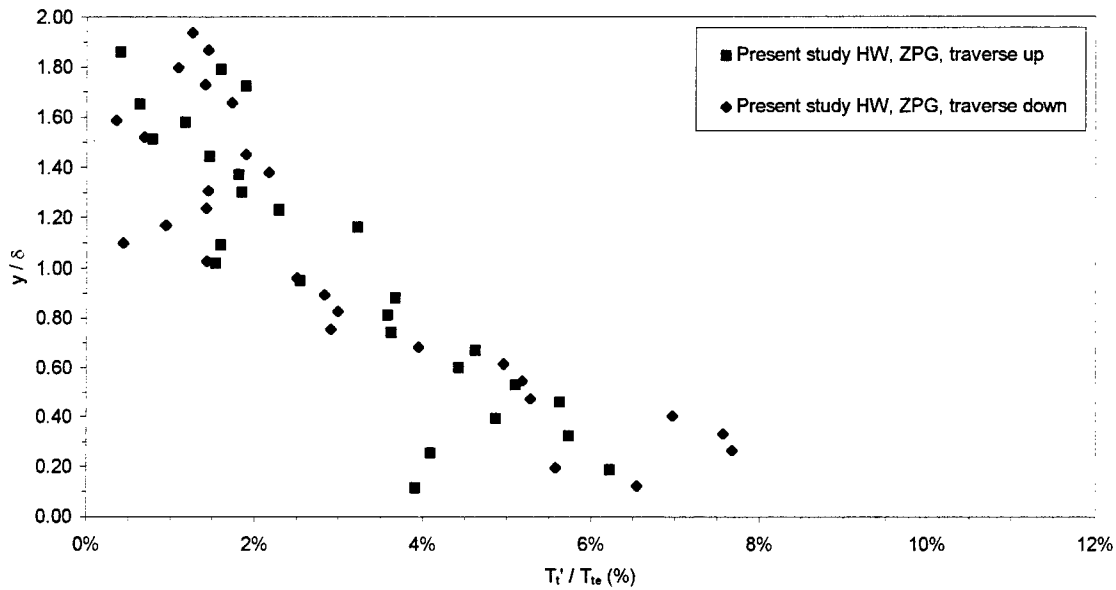


Figure 6-9: Mach 1.7 total temperature fluctuation profiles

Since FPG or CPG data was not taken, no conclusions on the effect of pressure gradients on the turbulent quantities can be made.

From the data in this chapter it can be noted that reducing the Mach number reduces the mass flux turbulence intensity by 20%. This was attributed to the 50% reduction in density turbulence intensity. Interestingly, the u turbulence intensity increases when the Mach number is decreased.

7. Mach 5.0 Results and Discussion

Pitot pressure was taken at each measuring location. From the Pitot pressure, Rayleigh supersonic Pitot formula was used to compute the Mach number profile and velocity profile. Figures 7-1 to 7-3 present these results.

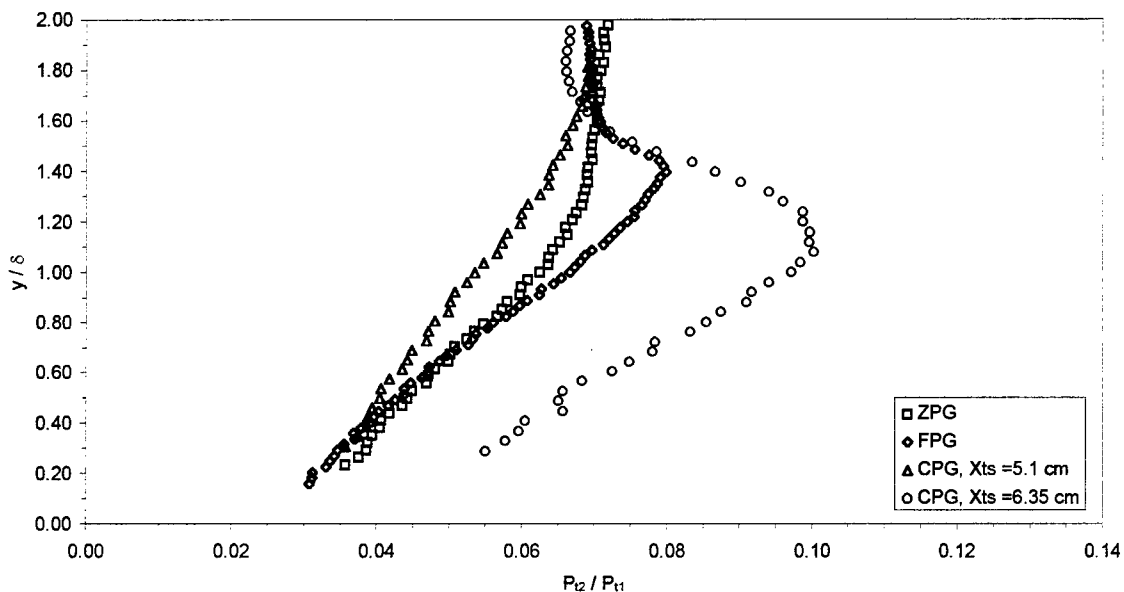


Figure 7-1: Mach 5.0 Pitot pressure profiles

The data in these figures present the same trends as noted in the Mach 2.8 data. Note the effect of the shock in the CPG Pitot pressure and Mach number profiles. The data in these figures were used to calculate the boundary layer thickness parameters. Table 7-1 presents the results of these calculations.

Table 7-1: Mach 5.0 boundary layer parameters

	ZPG	FPG	CPG ($x_{ts} = 5.1$ cm)	CPG ($x_{ts} = 6.35$ cm)
δ_u (mm)	8.46	10.8	6.17	5.51
δ_M (mm)	12.2	13.1	7.09	6.60
M_e	5.10	5.32	4.30	5.20
U_e (m/sec)	777	784	756	780

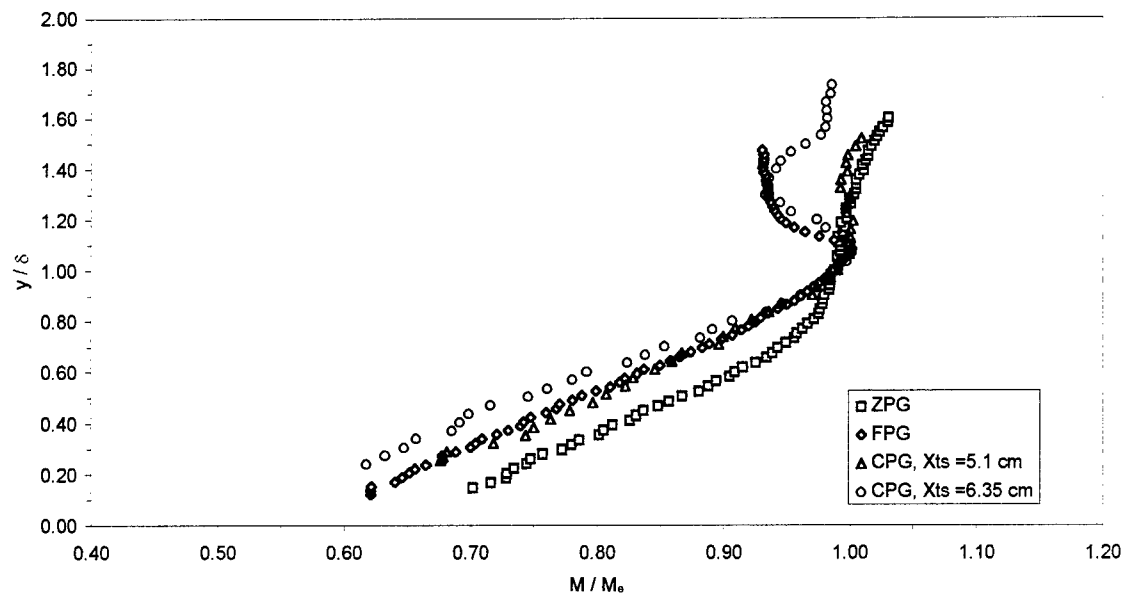


Figure 7-2: Mach 5.0 Mach number profile

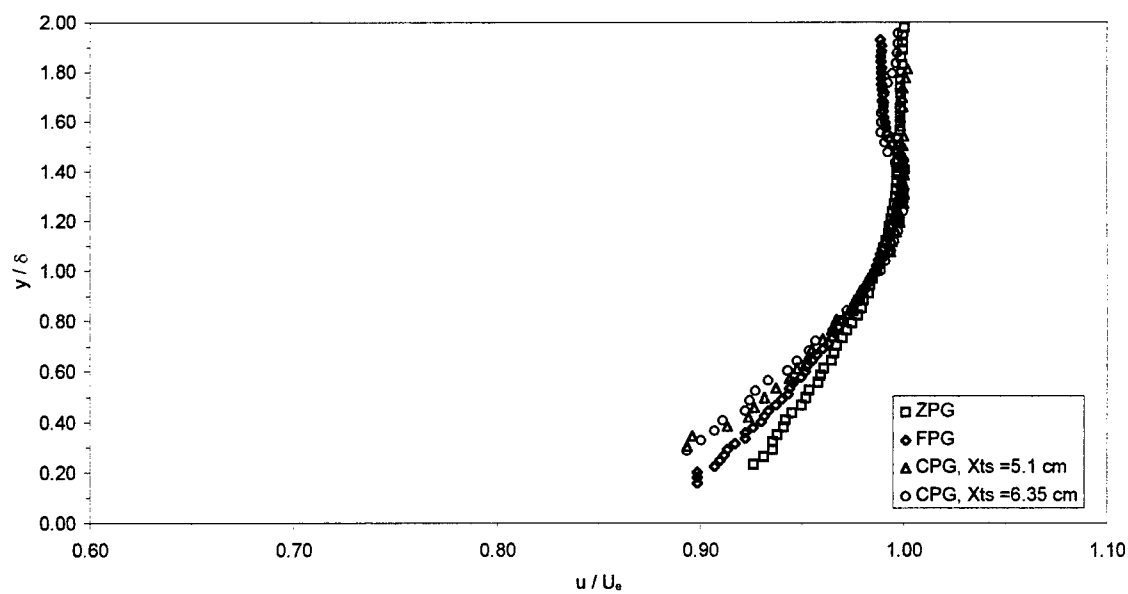


Figure 7-3: Mach 5.0 velocity profile

The surface static pressure profile is presented as Figure 7-4. The FPG data clearly shows the effect of the shock near the end of the FPG surface. The CPG data shows the effect of the compression followed by the expansion on the wall static pressure. Wall static pressure ports are marked with an x in Figure 7-4.

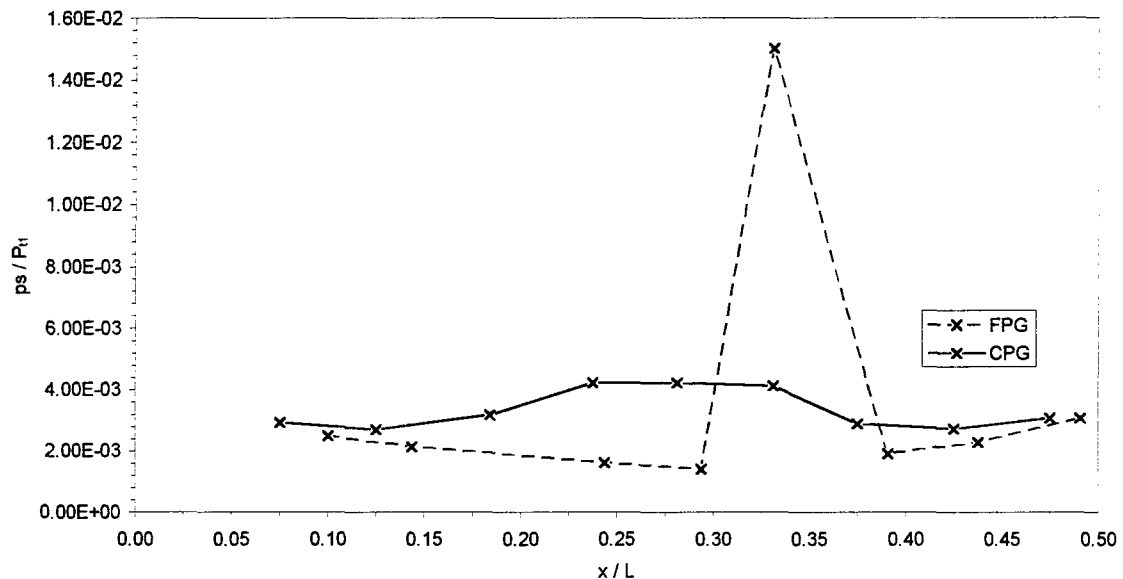


Figure 7-4: Mach 5.0 CPG and FPG static pressure profiles

8. Conclusions and Recommendations

Bradshaw (Bradshaw, 1977) has noted that pressure gradients distort turbulent flow properties of a supersonic boundary layer by an order of magnitude more than indicated by the additional production. Spina (Spina et al., 1994) restated this concept almost 20 years later. During this time, little quality research has been done on these types of flows (Settles and Dodson, 1994). The intentions of this study were to help fill this void of information. Recall that the main objective of this study was to obtain a better understanding of supersonic boundary layers under the influence of pressure gradients. The objective was met by using a variety of measurement techniques (PIV, hot-wire, conventional probes and Mie-scattering flow visualization) to provide empirical information. A second goal was the evaluation of PIV as a flow diagnostic tool. The measurements taken in this study included conventional pressure probe pressure profiles, hot-wire mass flux turbulence intensity and energy spectra data and PIV for mean and fluctuating velocities.

8.1 Mach 2.8 Conclusions

PIV was validated for mean flow quantities as demonstrated by the comparison between LDV and PIV data. Application of Van Driest's scaling laws (Van Driest, 1951), satisfactorily reduced the PIV derived velocity data to theoretical values. PIV was not validated for fluctuation quantities with the number of samples used in this study. PIV consistently overpredicted the freestream turbulence intensity and underpredicted the turbulence intensity in the boundary layer. A likely explanation for this effect is PIV's low signal-to-noise ratio. For a further discussion of this effect see Appendix B. An increase in the number of images could aid in solving this problem.

Multiple overheat hot-wire anemometry was used to investigate the effects of pressure gradients on mean flow and fluctuation turbulence quantities. Traversing the hot-film probe into the wall allowed for accurate, near wall measurements to be taken. The ZPG mass flux turbulence intensity showed excellent agreement between single overheat and multiple overheat data reduction methodologies. The

FPG was found to reduce the maximum mass flux turbulence intensity by 25%, from 17% to 12.5%. The CPG was found to increase the maximum mass flux turbulence intensity 20% ($x = 68$ cm) and 22% ($x = 70$ cm) from the 17% ZPG value.

Separating the mass flux components into velocity and density fluctuations was accomplished for a single overheat ratio. The separated turbulence intensities accurately matched the LDV data by Luker (Luker et al., 1997). These data also confirmed the effects of the pressure gradients on the turbulent quantities.

Power spectra measurements were taken for the three pressure gradient models with a hot-wire tuned to give a high frequency response. The ZPG spectra indicated that the energy was evenly distributed among the different frequencies. Once any pressure gradient is applied the energy is shifted to the lower frequencies. This confirms the hypothesis that a FPG causes the large scale structures to disassociate into smaller scale structures. For the CPG, this effect can be explained by the reduction of the boundary layer thickness and the corresponding reduction in structure sizes. At a sufficiently high frequency, the ZPG maintained a higher level of energy than the FPG or CPG.

Recall that Settles and Dodson (Settles and Dodson, 1994) established a set of criteria used to judge data. It was a goal of this study to satisfy these criteria. Table 8-1 lists the criteria and how they were satisfied for the Mach 2.8 data.

Table 8-1: Verification of Settles and Dodson criteria

Settles and Dodson criteria	How satisfied
Baseline applicability	Mach 2.8 flow
Simplicity	Simple model design
Specific applicability	Simple models and obtaining of turbulence data
Well defined experimental boundary conditions	See Luker (Luker, 1995)
Well defined error bounds	See appendix B
Adequate documentation of data	See appendix C
Adequate spatial resolution of the data	Near wall data acquired, PIV data

8.2 Mach 1.7 Conclusions

Multiple overheat hot-wire measurements were taken for the ZPG configuration. The u velocity turbulence intensity was found to be 10% and the maximum mass flux turbulence intensity was found to be 7%. Recall that for the Mach 2.8 tunnel, the ZPG u velocity turbulence intensity was 8% and the mass flux turbulence intensity was found to be 10%. Note that in the Mach 1.7 tunnel the velocity turbulence intensity is higher while the mass flux turbulence intensity is higher in the Mach 2.8 tunnel. This is due to the density fluctuations. The maximum density fluctuation is approximately 9% in the Mach 2.9 tunnel while it peaks at 5% in the Mach 1.7 tunnel.

Power spectra measurements were taken for the ZPG and FPG in the Mach 1.7 tunnel. The cross-over noted in the Mach 2.9 tunnel was found in the Mach 1.7 tunnel. However, the FPG always maintained a higher energy level across the frequencies measured. This is opposite of what was noted in the Mach 2.9 tunnel. This was a result of the reduced level of compressibility and the fact that the Mach number was subsonic for a substantial portion of the boundary layer for this flow.

8.3 Mach 5.0 Conclusions

Conventional pressure measurements were taken in Mach 5.0 flow for the three pressure gradients. The effects of the pressure gradient on boundary layer thickness noted in Mach 2.8 and Mach 1.7 flow were also noted in Mach 5.0 flow. Using the ZPG as a reference, the FPG caused the boundary layer thickness to increase while the CPG caused the boundary layer thickness to decrease.

8.4 Recommendations

Several recommendations can be made to improve on the study. First, more images should be taken for PIV analysis. More images will allow a better estimate of turbulence intensity to be made and allow a better understanding of data closure. Currently, it is not known how many images are required to achieve data closure.

Second, multiple overheat cross-wire anemometry should be accomplished for all pressure gradient models. This will allow measurements of v'_{rms} and the cross correlation terms found in the Reynolds averaged Navier-Stokes equations. In addition, more accurate measurements of the wall shear stress should be made. This will allow a more accurate estimate of the Van Driest velocity and length correlation.

Third, the boundary layer power spectrum should be investigated in Mach 5.0 flow with a hot-wire. The Mach 1.7 power spectra data should be repeated with a hot-wire, as opposed to the hot-film used in this study, to confirm the pressure gradient effect on the spectra.

Finally, hot-wire measurements should be taken in the Mach 5.0 tunnel. This will allow a better understanding of the effect of Mach number on the mean flow and turbulence quantities. In addition, the ceramic pebbles in the pebble bed heater should be replaced with stainless steel pebbles. This will eliminate the abrasion problem currently noted in the Mach 5.0 tunnel.

Appendix A : Hot-Wire Calibration

This appendix presents additional hot-wire calibration data, including calibration curves.

A.1 Mach 2.8 Calibration

Hot-wires were calibrated by placing them in the freestream and varying the total pressure in the plenum by adjusting the Kinney valve. With the Total temperature and Mach number as inputs, the MSHEaR code converted the plenum pressure and output bridge voltage to a Reynolds number and a Nusselt number. Recall that Equation (4.21) indicates that the Nusselt number is a linear function of the square root of the Reynolds number. Tables A-1 and A-2 present raw calibration data for two different overheat ratios. Figures A-1 and A-2 present the linear curvefit and the raw data.

Table A-1: Mach 2.8 sample raw calibration file (OHR = 2.03)

HW voltage (volt)	P _{t1} (psi)	P _{t2} / P _{t1}	Mach	T _{t1} (K)	ρu (kg/m ² s)	Re	Re ^{1/2}	curve fit	Nu data
4.161	13.6	0.456	2.61	294.26	75.85	212.69	14.584	1.516	1.54
4.434	17.4	0.456	2.61	294.26	96.84	271.54	16.478	1.744	1.75
4.656	21.1	0.456	2.61	294.26	117.17	328.57	18.126	1.942	1.93
4.891	25.2	0.456	2.61	294.26	140.24	393.26	19.831	2.147	2.13
5.103	29.3	0.456	2.61	294.26	162.57	455.88	21.351	2.330	2.31
5.28	32.7	0.456	2.61	294.26	181.45	508.82	22.557	2.475	2.48
5.418	35.9	0.456	2.61	294.26	199.35	559.02	23.644	2.606	2.61
5.555	39.3	0.456	2.61	294.26	218.29	612.13	24.741	2.738	2.74
5.666	42.2	0.456	2.61	294.26	234.59	657.83	25.648	2.847	2.85
5.774	45.3	0.456	2.61	294.26	251.83	706.17	26.574	2.958	2.96

Table A-2: Mach 2.8 sample raw calibration file (OHR = 1.66)

HW voltage (volt)	P _{t1} (psi)	P _{t2} / P _{t1}	Mach	T _{t1} (K)	ρu (kg/m ² s)	Re	Re ^{1/2}	curve fit	Nu data
3.324	11.3	0.456	2.61	294.26	62.52	175.33	13.241	1.297	1.35
3.457	14.2	0.456	2.61	294.26	78.87	221.18	14.872	1.469	1.46
3.615	17	0.456	2.61	294.26	94.62	265.33	16.289	1.618	1.6
3.777	20.2	0.456	2.61	294.26	112.2	314.62	17.738	1.771	1.75
3.915	22.7	0.456	2.61	294.26	126.01	353.34	18.797	1.882	1.88
4.044	25.8	0.456	2.61	294.26	143.64	402.8	20.070	2.016	2
4.198	29.6	0.456	2.61	294.26	164.74	461.96	21.493	2.166	2.16
4.322	33.1	0.456	2.61	294.26	184.12	516.31	22.722	2.296	2.29
4.465	37.4	0.456	2.61	294.26	208.04	583.39	24.153	2.447	2.44
4.574	40.6	0.456	2.61	294.26	225.76	633.07	25.161	2.553	2.56
4.662	43.3	0.456	2.61	294.26	240.52	674.46	25.970	2.638	2.66
4.721	45.6	0.456	2.61	294.26	253.38	710.53	26.656	2.710	2.73

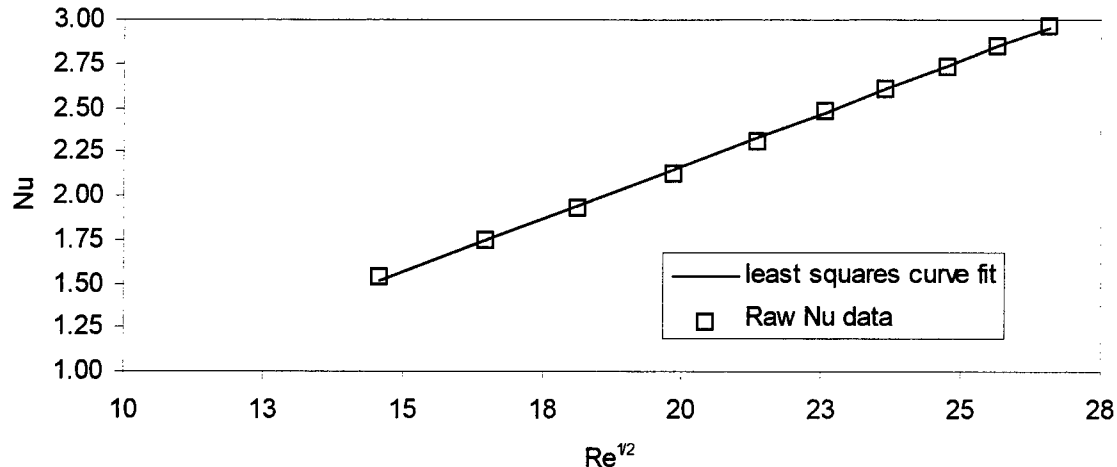


Figure A-1: Mach 2.8 hot-wire calibration curve (OHR = 2.03)

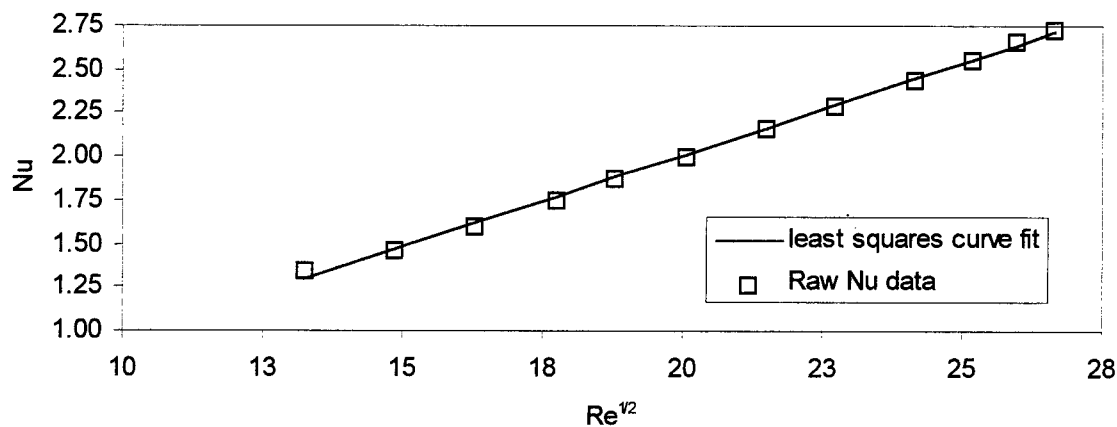


Figure A-2: Mach 2.8 hot-wire calibration curve (OHR = 1.66)

Note the excellent agreement between the data and the least-squares curve fit. The minimum correlation coefficient (squared) was always greater than 0.99. This indicates that the curve fit is extremely accurate in modeling the data.

With this curve, a given bridge voltage could be easily and accurately converted to a mass flux. Table A-3 presents the constants used in Equation (4.21) for all the overheat ratios used in the Mach 2.8 portion of the experiment.

Table A-3: Mach 2.8 calibration constants

OHR	a	b
2.03	0.120	-0.238
1.98	0.117	-0.192
1.87	0.112	-0.138
1.81	0.110	-0.113
1.74	0.107	-0.090
1.66	0.105	-0.098
1.58	0.102	-0.071
1.52	0.101	-0.087

The constant a is the slope and b is the y-intercept. Note that a is only weakly dependent on OHR. Further study is required to fully examine this relationship. It might be possible to specify the slope and keep it constant throughout the overheat ratios.

A.2 Mach 1.7 Calibration

Although the calibration theory was identical between the Mach 1.7 and Mach 2.9 calibration, application was different. The Mach 1.7 tunnel did not have an easy method to vary the plenum total pressure. Calibration cards were devised to solve this problem. A card with a series of holes punched in it was placed over the entrance to the tunnel. This card reduced the amount of flow that could enter the tunnel and thereby the plenum total pressure was reduced. A series of cards were created that established a different plenum pressure. Tables A-4 and A-5 present sample Mach 1.7 calibration data. Figure A-3 presents the least squares curvefit and the raw calibration data for all overheat ratios used in the Mach 1.7 phase of this study.

Table A-4: Mach 1.7 sample raw calibration file (OHR = 1.95)

HW voltage (volt)	P _{t1} (psi)	P _{t2} / P _{t1}	Mach	T _{t1} (K)	ρu (kg/m ² s)	Re	Re ^{1/2}	curve fit	Nu data
5.138	13.4	0.817	1.79	299.26	151.59	419.59	20.484	2.474	2.49
4.861	11	0.817	1.79	299.26	123.7	342.4	18.504	2.252	2.23
4.355	6.5	0.817	1.79	299.26	73.52	203.51	14.266	1.777	1.79
3.655	3	0.817	1.79	299.26	33.85	93.69	9.679	1.262	1.26

Table A-5: : Mach 1.7 sample raw calibration file (OHR = 1.66)

HW voltage	P _{t1}	P _{t2} / P _{t1}	Mach	T _{t1}	ρu	Re	Re ^{1/2}	curve	Nu
(volt)	(psi)			(K)	(kg/m ² s)			fit	data
4.352	13.5	0.817	1.79	299.26	151.71	419.94	20.492	2.320	2.33
4.106	10.8	0.817	1.79	299.26	122.15	338.11	18.388	2.110	2.07
3.782	6.6	0.817	1.79	299.26	73.95	204.7	14.307	1.702	1.76
3.138	3	0.817	1.79	299.26	33.35	92.31	9.608	1.233	1.21

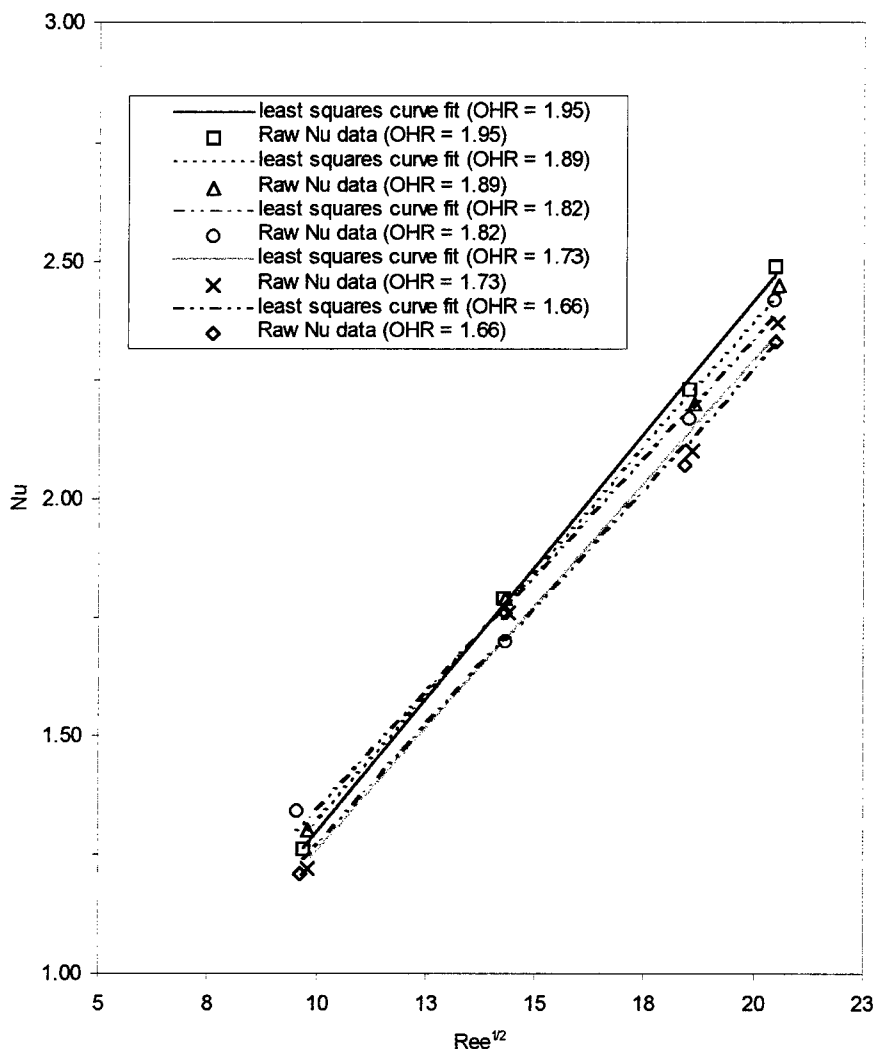


Figure A-3: Mach 1.7 hot-wire calibration curves

The different overheats were plotted on the same axis in Figure A-3 to illustrate the insensitivity of the overheat ratio on the slope. Table A-6 presents the calibration constants for all five overheat ratios.

Table A-6: Mach 1.7 calibration constants

OHR	a	b
1.95	0.112	0.177
1.89	0.105	0.272
1.82	0.098	0.362
1.73	0.104	0.220
1.66	0.100	0.274

Appendix B : Uncertainty Analysis

This section provides uncertainty estimates for the data presented in this thesis. This analysis augments the well-documented analysis by Luker (Luker, 1995) and Huffman (Dotter, 1995). Elementary uncertainties are presented first followed by the derived uncertainties.

Uncertainty analysis is necessary to determine the validity of the data. If the uncertainty is large or not presented it can call into question the appropriateness of the data and reflect on the reputation of the researcher. The absolute uncertainty, Δf is found by taking the partial derivative of f with respect to the dependent variable x_i :

$$\Delta f = \sum_{i=1}^N \frac{\partial f}{\partial x_i} \Bigg|_{f_o} \Delta x_i \quad (B.1)$$

where f_o is the mean value of f . Taking a partial derivative is necessary to isolate the individual dependency of x on f . The uncertainty defined in Equation (B.1) can be converted to a percentage value by the following

$$\epsilon_f = 100\% * \frac{\Delta f}{f_o} \quad (B.2)$$

Summing each of these uncertainties over each dependent variable gives the maximum possible uncertainty. This assumes that each uncertainty reaches its maximum value simultaneously. A more reasonable approach uses the Euclidean norm defined as

$$\epsilon_f = \|\epsilon_i\| = \sqrt{\sum_i \epsilon_i^2} \quad (B.3)$$

The Euclidean norm will be used to compute the uncertainties in this study.

B.1 Elementary Uncertainties

This section documents the elementary uncertainties. Uncertainties are based off the Mach 2.8 ZPG values given in Table B-1.

Table B-1: Mach 2.8 ZPG reference conditions

Variable	Value
T _{t1}	296 K
P _{t1}	3.15×10^5 Pa
P _{t2}	1.83×10^5 Pa
p _c	1.83×10^4 Pa
Mach	2.78
P _e	1.21×10^4 Pa
P _w	8.02×10^3 Pa
T _w	296 K
T _e	114 K
ρ _e	0.245 kg / m ³
ρ _w	0.095 kg / m ³
U _e	604 m/sec
V _w	5.0 Volts
a	0.11
b	-0.15
R _l	0.2 Ω
R _w	5.5 Ω
R _s	50.0 Ω
L	1.0 mm
d	5.1×10^{-5} m

Cone-static, Pitot and plenum pressure were measured by pressure transducers. The pressure transducers had two sources of uncertainty. They were a gain uncertainty of 0.5% and a gain stability uncertainty of 0.2%. The ambient pressure was measured by a RDS corporation DP141 ambient pressure meter. The least significant digit was 0.0001 in Hg leading to an uncertainty in ambient pressure of $3.43 \times 10^{-4}\%$. Since this uncertainty is two orders of magnitude less than the gain uncertainty and gain stability uncertainty, it will be neglected. Huffman (Huffman, 1995) found that the digital conversion uncertainty was ± 0.0041 atm for plenum pressure and ± 0.00046 atm for Pitot pressure. Combining the pressure source of uncertainty leads to a Euclidean pressure uncertainty of 0.54%.

Two sources of uncertainty were inherent in the temperature measurement. Luker (Luker, 1995) found that the assumption of constant total temperature variation leads to an uncertainty of up to 4%. Recall from Figure 5-10 the maximum scatter in total temperature is 5%. Temperature measurement

uncertainty was found to equal 0.75% (Temperature handbook, 1992). Combining these leads to a Euclidean uncertainty of 5.1%.

The position uncertainty of the probe was mainly due to probe deflection. It was found that the deflection was equal to 1.5° . Assuming that the tangent of this angle equals the uncertainty in x location leads to an x uncertainty of 2.6%

Huffman found that the y position uncertainty was 4.1% and the hot-wire voltage uncertainty was 1.0% (Huffman, 1995).

Table B-2 summarizes the elementary uncertainty data.

Table B-2: Elementary uncertainties

Elementary	Value
ϵ_{Pt1}	0.54%
ϵ_{Pt2}	0.54%
ϵ_{Pcs}	0.54%
ϵ_{Tt1}	5.1%
ϵ_x	2.6%
ϵ_y	4.1%
ϵ_{Vw}	1.0%

B.2 Derived Uncertainties

The uncertainties described in Section B-1 propagate into derived uncertainties. Derived uncertainties are uncertainties in quantities derived from the variables listed in Table B-2.

B.2.1 Mean Flow Derived Uncertainties

Recall from chapter 4, that the Mach number was calculated based on the cone-static pressure and Pitot pressure. Equation 4.1 was linearized and the uncertainties listed in Table B-2 were applied. With the Mach number uncertainty, the isentropic equations were linearized and used to compute the uncertainty in pressure and temperature. With the pressure and temperature uncertainty known, the density uncertainty could be found from the linearized equation of state. The uncertainty in the viscosity was calculated by linearizing Sutherland's law. Table B-3 presents the mean flow derived uncertainties.

Table B-3: Mean flow derived uncertainties

Uncertainty	Equation	Value
ϵ_{Me}	See equation 4.1	0.62%
ϵ_{Pw}	$\ \epsilon_{Pw} \ $	0.58%
ϵ_{Pe}	$\ \epsilon_{P12}, 4.25 \epsilon_{Me} \ $	2.69%
ϵ_{Te}	$\ \epsilon_{P12}, 1.214 \epsilon_{Me} \ $	0.93%
ϵ_{Tw}	$\ \epsilon_T \ $	5.1%
ϵ_{pw}	$\ \epsilon_{Tw}, \epsilon_{Pw} \ $	5.1%
ϵ_{pe}	$\ \epsilon_{Te}, \epsilon_{Pe} \ $	2.9%
ϵ_{Ue}	$\ \epsilon_{Me}, 0.5 \epsilon_{Te} \ $	0.78%
ϵ_μ	$\ \text{Sutherland's Law} \ $	2.0%

Uncertainty in the boundary layer was calculated graphically as in Luker (Luker, 1995). The boundary height uncertainties are listed in Table B-4.

Table B-4: Boundary layer height uncertainty

Uncertainty	Value
$\epsilon_{\delta M}$	21.7%
$\epsilon_{\delta u}$	5.1%

The uncertainty in the van Driest correlation was calculated as in Luker (Luker, 1995). The van Driest uncertainties are listed in Table B-5.

Table B-5: Van Driest uncertainties

Uncertainty	Equation	Value
$\epsilon_{u\text{eff}}$	$\ 0.5 \epsilon_{pe}, 0.5 \epsilon_{pw}, 2.0 \epsilon_u \ $	3.3%
ϵ_{tw}	See Luker (Luker, 1995)	7.0%
ϵ_{u^*}	$\ 0.5 \epsilon_{tw}, 0.5 \epsilon_{pw} \ $	4.3%
ϵ_y^+	$\ \epsilon_y, \epsilon_{u^*}, \epsilon_\mu, \epsilon_{pw} \ $	8.8%
$\epsilon_{u\text{eff}}^+$	$\ 0.5 \epsilon_{tw}, 0.5 \epsilon_{u\text{eff}} \ $	7.7%

B.2.2 Hot-Wire Derived Uncertainties

The uncertainty in the Nusselt number was determined from Equation 4.22. The Reynolds number uncertainty was found by linearizing King's law (Equation 4.21) The separation of variables

uncertainty was determined by the outline given in Huffman (Huffman, 1995). The results of the hot-wire derived uncertainty analyses are given in Table B-6.

Table B-6: Hot-wire derived uncertainties

Hot-wire	derived	Equation	Value
ε_{Nu}		$\parallel 2.0 \varepsilon_{Vw}, \varepsilon_{Te} \parallel$	5.4%
ε_{Re}		$\parallel \varepsilon_{Vw}, 2.0 \varepsilon_{Nu} \parallel$	6.5%
$\varepsilon_{(\rho u)}$		ε_{Re}	6.5%
$\varepsilon_{(\rho u)'}^y$		ε_{Re}	6.5%
$\varepsilon_{p'}$		$\parallel 0.46 \varepsilon_{Me}, 0.77 \varepsilon_{(\rho u)'}, \varepsilon_{Tr} \parallel$	7.2%
$\varepsilon_{u'}$		$\parallel \varepsilon_{p'}, \varepsilon_{(\rho u)'} \parallel$	9.7%

B.3 PIV Signal-to-Noise Ratio Uncertainty

The signal-to-noise ratio for the PIV system is a function of the temporal separation consistency of the seed particles, the camera alignment, the camera focus, the pixel resolution of the camera and the software data reduction algorithm. The uncertainty of these effects cannot be quantified at this time; however, by inspection of the PIV results, it can be shown that the combination of these effects accounts for a 3% increase in the axial turbulence intensity.

Appendix C : Data Files

This section contains the data necessary to reproduce all the figures in this thesis. The Mach 2.8 data is presented first (pressure followed by hot-wire and PIV) followed by the Mach 1.7 data (pressure and hot-wire) and the Mach 5.0 data (pressure only). All rms values have been non-dimensionalized by their respective freestream value.

Table C-1: Mach 2.8 ZPG pressure data

y(in)	P _{t1} (psia)	P _{t2} (psia)	PT2/PT1	P _s /PT2	Mach	M/Me	u/Ue	p _w /p	p/p _e
0.0625	31.8164	3.7234	0.1170	0.3015	1.4750	0.5231	0.7027	0.6882	0.5609
0.0699	31.7446	4.1989	0.1323	0.2674	1.5838	0.5616	0.7376	0.6589	0.5859
0.0801	31.7430	4.9182	0.1549	0.2283	1.7352	0.6153	0.7824	0.6194	0.6232
0.0910	31.7384	5.2463	0.1653	0.2140	1.8002	0.6384	0.8003	0.6030	0.6402
0.1021	31.7430	5.6387	0.1776	0.1991	1.8741	0.6646	0.8198	0.5848	0.6601
0.1128	31.8429	5.9274	0.1861	0.1894	1.9271	0.6834	0.8331	0.5721	0.6748
0.1234	31.6556	6.0913	0.1924	0.1843	1.9550	0.6932	0.8400	0.5655	0.6827
0.1337	31.7946	6.6252	0.2084	0.1694	2.0491	0.7266	0.8622	0.5437	0.7100
0.1445	31.7352	6.4666	0.2038	0.1736	2.0232	0.7174	0.8562	0.5496	0.7024
0.1554	31.8008	6.5669	0.2065	0.1709	2.0404	0.7235	0.8602	0.5457	0.7074
0.1666	31.7836	7.1332	0.2244	0.1574	2.1344	0.7569	0.8812	0.5247	0.7357
0.1768	31.7477	6.7134	0.2115	0.1672	2.0668	0.7329	0.8663	0.5397	0.7153
0.1873	31.7477	7.2332	0.2278	0.1552	2.1502	0.7625	0.8846	0.5213	0.7406
0.1980	31.6837	7.2684	0.2294	0.1544	2.1563	0.7647	0.8859	0.5199	0.7425
0.2090	31.8508	8.0338	0.2522	0.1397	2.2749	0.8067	0.9102	0.4949	0.7800
0.2195	31.6338	8.1745	0.2584	0.1373	2.2949	0.8138	0.9141	0.4908	0.7865
0.2300	31.7836	8.3197	0.2618	0.1349	2.3162	0.8214	0.9182	0.4865	0.7934
0.2407	31.7056	8.4487	0.2665	0.1329	2.3355	0.8282	0.9218	0.4827	0.7998
0.2517	31.6900	8.5679	0.2704	0.1310	2.3532	0.8345	0.9252	0.4792	0.8056
0.2626	31.7212	8.7184	0.2748	0.1288	2.3743	0.8419	0.9291	0.4750	0.8126
0.2732	31.7493	9.1628	0.2886	0.1225	2.4398	0.8652	0.9409	0.4624	0.8348
0.2837	31.7212	9.5033	0.2996	0.1181	2.4880	0.8823	0.9492	0.4534	0.8514
0.2947	31.7352	9.8194	0.3094	0.1143	2.5314	0.8977	0.9565	0.4455	0.8666
0.3058	31.7540	9.7267	0.3063	0.1154	2.5238	0.8950	0.9552	0.4468	0.8639
0.3165	31.7618	10.1273	0.3189	0.1108	2.5747	0.9130	0.9636	0.4377	0.8819
0.3271	31.7680	10.3382	0.3254	0.1086	2.6029	0.9230	0.9681	0.4327	0.8920
0.3376	31.6603	10.3509	0.3269	0.1085	2.6057	0.9240	0.9685	0.4323	0.8931
0.3487	31.7009	10.7962	0.3406	0.1040	2.6602	0.9433	0.9769	0.4229	0.9128
0.3598	31.7743	10.8290	0.3408	0.1037	2.6681	0.9461	0.9781	0.4216	0.9157
0.3704	31.8258	11.2041	0.3520	0.1002	2.7122	0.9618	0.9847	0.4142	0.9320
0.3809	31.7087	11.2488	0.3548	0.0998	2.7216	0.9651	0.9861	0.4127	0.9355
0.3916	31.6697	11.3907	0.3597	0.0986	2.7386	0.9711	0.9886	0.4099	0.9418
0.4026	31.7961	11.6797	0.3673	0.0961	2.7722	0.9830	0.9933	0.4045	0.9544
0.4134	31.6509	11.6012	0.3665	0.0968	2.7678	0.9815	0.9927	0.4052	0.9528
0.4240	31.6275	11.8733	0.3754	0.0945	2.8005	0.9931	0.9973	0.4000	0.9652
0.4344	31.8039	12.0154	0.3778	0.0934	2.8181	0.9993	0.9997	0.3972	0.9718
0.4455	31.7134	12.0840	0.3810	0.0929	2.8267	1.0024	1.0009	0.3959	0.9751
0.4562	31.7056	12.1360	0.3828	0.0925	2.8331	1.0047	1.0018	0.3949	0.9776
0.4670	31.7540	12.1487	0.3826	0.0924	2.8348	1.0053	1.0020	0.3946	0.9782
0.4775	31.7868	12.2189	0.3844	0.0919	2.8431	1.0082	1.0031	0.3933	0.9814
0.4882	31.7868	12.2594	0.3857	0.0916	2.8482	1.0100	1.0038	0.3926	0.9834
0.4991	31.6572	12.3343	0.3896	0.0910	2.8571	1.0131	1.0050	0.3912	0.9868
0.5101	31.7774	12.3456	0.3885	0.0909	2.8588	1.0137	1.0052	0.3909	0.9875

0.5209	31.6884	12.4275	0.3922	0.0903	2.8683	1.0171	1.0065	0.3895	0.9911
0.5313	31.7430	12.5343	0.3949	0.0896	2.8809	1.0216	1.0082	0.3876	0.9960
0.5422	31.6619	12.6078	0.3982	0.0890	2.8899	1.0248	1.0094	0.3862	0.9995
0.5531	31.7150	12.6781	0.3998	0.0885	2.8983	1.0278	1.0104	0.3850	1.0028
0.5641	31.8632	12.6832	0.3981	0.0885	2.8994	1.0282	1.0106	0.3848	1.0032
0.5747	31.7227	12.6436	0.3986	0.0888	2.8950	1.0266	1.0100	0.3854	1.0015
0.5851	31.7071	12.6118	0.3978	0.0890	2.8909	1.0251	1.0095	0.3861	0.9999
0.5960	31.6744	12.5701	0.3969	0.0893	2.8859	1.0234	1.0088	0.3868	0.9980
0.6071	31.7415	12.5273	0.3947	0.0896	2.8807	1.0215	1.0082	0.3876	0.9960
0.6181	31.6494	12.4968	0.3949	0.0898	2.8771	1.0202	1.0077	0.3881	0.9945
0.6286	31.7649	12.4535	0.3921	0.0901	2.8718	1.0184	1.0070	0.3889	0.9925
0.6392	31.8383	12.4083	0.3897	0.0905	2.8664	1.0164	1.0063	0.3898	0.9904
0.6500	31.9475	12.4074	0.3884	0.0905	2.8663	1.0164	1.0062	0.3898	0.9904
0.6608	31.6322	12.2533	0.3874	0.0916	2.8472	1.0096	1.0037	0.3927	0.9830
0.6717	31.6962	12.2557	0.3867	0.0916	2.8479	1.0099	1.0038	0.3926	0.9833
0.6819	31.6728	12.1899	0.3849	0.0921	2.8399	1.0070	1.0027	0.3938	0.9802
0.6927	31.8242	12.1768	0.3826	0.0922	2.8383	1.0065	1.0025	0.3941	0.9796
0.7037	31.6962	12.1156	0.3822	0.0927	2.8308	1.0038	1.0015	0.3952	0.9767
0.7147	31.7446	12.1409	0.3825	0.0925	2.8340	1.0049	1.0019	0.3947	0.9779
0.7251	31.7477	12.1180	0.3817	0.0926	2.8311	1.0039	1.0015	0.3952	0.9768
0.7357	31.6681	12.0417	0.3802	0.0932	2.8217	1.0006	1.0002	0.3966	0.9732
0.7466	31.6494	12.0302	0.3801	0.0933	2.8204	1.0001	1.0000	0.3969	0.9727
0.7576	31.6307	11.9588	0.3781	0.0939	2.8115	0.9970	0.9988	0.3982	0.9693
0.7683	31.6978	11.9728	0.3777	0.0938	2.8133	0.9976	0.9991	0.3980	0.9700
0.7787	31.6681	11.9801	0.3783	0.0937	2.8142	0.9979	0.9992	0.3978	0.9704
0.7894	31.6728	11.9625	0.3777	0.0938	2.8120	0.9972	0.9989	0.3982	0.9695
0.8002	31.7243	11.9639	0.3771	0.0938	2.8122	0.9972	0.9989	0.3981	0.9696
0.8113	31.5916	11.9185	0.3773	0.0942	2.8066	0.9952	0.9982	0.3990	0.9675
0.8220	31.6385	11.9393	0.3774	0.0940	2.8092	0.9962	0.9985	0.3986	0.9684
0.8287	31.6338	11.9347	0.3773	0.0941	2.8086	0.9960	0.9984	0.3987	0.9682
0.8349	31.7633	11.9855	0.3773	0.0937	2.8148	0.9982	0.9993	0.3977	0.9706
0.8457	31.7711	11.9857	0.3773	0.0937	2.8149	0.9982	0.9993	0.3977	0.9706
0.8565	31.6681	11.9546	0.3775	0.0939	2.8111	0.9968	0.9988	0.3983	0.9692
0.8674	31.6431	11.9445	0.3775	0.0940	2.8098	0.9964	0.9986	0.3985	0.9687

Table C-2: Mach 2.8 FPG pressure data

y(in)	P ₁₁ (psia)	P ₁₂ (psia)	P ₁₂ /P ₁₁	P _c (psia)	P _c / P ₁₁	Mach	P(Pa)	ρ (kg/m ³)	ρ/ρ _e	M/M _e	u/U _e
0.0625	31.5642	2.7763	0.0880	1.0600	3.36E-02	1.46674	4984	0.0844	0.4304	0.4889	0.6841
0.0695	31.5736	2.7742	0.0879	1.0572	3.35E-02	1.46736	5002	0.0847	0.4321	0.4891	0.6843
0.0799	31.5720	3.0985	0.0981	1.0420	3.30E-02	1.55645	5030	0.0884	0.4509	0.5188	0.7125
0.0906	31.5767	3.8072	0.1206	1.0267	3.25E-02	1.79615	5058	0.0985	0.5025	0.5987	0.7811
0.1015	31.5642	4.1069	0.1301	1.0118	3.21E-02	1.91195	5087	0.1043	0.5317	0.6373	0.8105
0.1124	31.5501	4.3158	0.1368	0.9989	3.17E-02	1.99732	5115	0.1089	0.5553	0.6658	0.8309
0.1232	31.5501	4.4317	0.1405	0.9937	3.15E-02	2.04183	5144	0.1117	0.5696	0.6806	0.8410
0.1338	31.5548	4.5862	0.1453	0.9902	3.14E-02	2.0939	5172	0.1149	0.5861	0.6980	0.8525
0.1448	31.5330	4.7565	0.1508	0.9912	3.14E-02	2.14761	5201	0.1184	0.6037	0.7159	0.8639
0.1558	31.5642	4.9763	0.1577	0.9919	3.14E-02	2.2123	5230	0.1225	0.6250	0.7374	0.8772
0.1667	31.5298	5.0779	0.1611	0.9937	3.15E-02	2.24252	5259	0.1249	0.6369	0.7475	0.8832
0.1773	31.5517	5.2868	0.1676	0.9935	3.15E-02	2.30479	5287	0.1291	0.6584	0.7683	0.8952
0.1880	31.5642	5.4781	0.1736	0.9991	3.17E-02	2.35252	5315	0.1326	0.6762	0.7842	0.9040
0.1990	31.5533	5.6155	0.1780	1.0045	3.18E-02	2.38425	5344	0.1352	0.6896	0.7947	0.9097
0.2100	31.5470	5.7387	0.1819	1.0111	3.20E-02	2.41033	5373	0.1375	0.7014	0.8034	0.9144
0.2207	31.5611	5.8452	0.1852	1.0181	3.23E-02	2.42947	5401	0.1395	0.7112	0.8098	0.9177
0.2312	31.5392	6.1150	0.1939	1.0267	3.26E-02	2.49267	5429	0.1442	0.7352	0.8309	0.9284
0.2421	31.5408	6.2417	0.1979	1.0354	3.28E-02	2.51458	5458	0.1464	0.7463	0.8382	0.9320
0.2531	31.5564	6.4709	0.2051	1.0438	3.31E-02	2.56395	5487	0.1504	0.7670	0.8546	0.9400
0.2641	31.5470	6.6711	0.2115	1.0530	3.34E-02	2.60334	5516	0.1538	0.7846	0.8678	0.9461
0.2749	31.5330	6.6851	0.2120	1.0607	3.36E-02	2.59559	5545	0.1541	0.7859	0.8652	0.9449

0.2854	31.5423	6.8195	0.2162	1.0703	3.39E-02	2.61472	5572	0.1562	0.7966	0.8716	0.9479
0.2963	31.5377	6.9329	0.2198	1.0808	3.43E-02	2.62802	5914	0.1668	0.8505	0.8760	0.9499
0.3074	31.5252	7.1153	0.2257	1.0886	3.45E-02	2.66311	5914	0.1694	0.8637	0.8877	0.9552
0.3183	31.5345	7.4182	0.2352	1.0984	3.48E-02	2.7259	5914	0.1741	0.8879	0.9086	0.9643
0.3289	31.5392	7.6224	0.2417	1.1056	3.51E-02	2.76532	5914	0.1771	0.9034	0.9218	0.9698
0.3396	31.5298	7.7102	0.2445	1.1155	3.54E-02	2.77207	5914	0.1777	0.9060	0.9240	0.9708
0.3506	31.5267	7.9233	0.2513	1.1230	3.56E-02	2.81412	5914	0.1810	0.9228	0.9380	0.9765
0.3723	31.5252	7.9605	0.2525	1.1377	3.61E-02	2.79831	5914	0.1797	0.9165	0.9328	0.9744
0.3829	31.5377	8.0095	0.2540	1.1433	3.63E-02	2.79964	5914	0.1798	0.9170	0.9332	0.9745
0.3938	31.5267	8.4824	0.2691	1.1515	3.65E-02	2.90437	5914	0.1882	0.9597	0.9681	0.9883
0.4047	31.5142	8.4452	0.2680	1.1574	3.67E-02	2.88447	5914	0.1866	0.9514	0.9615	0.9857
0.4157	31.5205	8.6681	0.2750	1.1658	3.70E-02	2.92461	5914	0.1898	0.9681	0.9749	0.9908
0.4264	31.5236	8.6150	0.2733	1.1717	3.72E-02	2.90193	5914	0.1880	0.9587	0.9673	0.9879
0.4368	31.5236	8.7864	0.2787	1.1759	3.73E-02	2.93638	5914	0.1908	0.9730	0.9788	0.9923
0.4479	31.5018	8.8622	0.2813	1.1829	3.76E-02	2.94384	5914	0.1914	0.9762	0.9813	0.9932
0.4590	31.5127	9.0559	0.2874	1.1895	3.77E-02	2.9784	5914	0.1943	0.9908	0.9928	0.9974
0.4698	31.4986	9.2628	0.2941	1.2014	3.81E-02	3.00698	5914	0.1967	1.0030	1.0023	1.0008
0.4804	31.5064	9.2139	0.2924	1.2070	3.83E-02	2.98276	5914	0.1946	0.9926	0.9943	0.9979
0.4911	31.5142	9.4104	0.2986	1.2157	3.86E-02	3.01616	5914	0.1975	1.0069	1.0054	1.0019
0.5022	31.5111	9.4396	0.2996	1.2253	3.89E-02	3.00424	5914	0.1964	1.0018	1.0014	1.0005
0.5131	31.5002	9.5108	0.3019	1.2347	3.92E-02	3.00413	5914	0.1964	1.0018	1.0014	1.0005
0.5238	31.4924	9.5902	0.3045	1.2410	3.94E-02	3.01189	5914	0.1971	1.0051	1.0040	1.0014
0.5343	31.4924	9.6703	0.3071	1.2518	3.97E-02	3.01159	5914	0.1971	1.0050	1.0039	1.0014
0.5451	31.4877	9.7810	0.3106	1.2607	4.00E-02	3.02307	5914	0.1980	1.0099	1.0077	1.0027
0.5562	31.5142	9.7735	0.3101	1.2717	4.04E-02	2.99956	5914	0.1961	0.9998	0.9999	0.9999
0.5672	31.4986	9.8583	0.3130	1.2792	4.06E-02	3.00609	5914	0.1966	1.0026	1.0020	1.0007
0.5778	31.5002	9.8892	0.3139	1.2857	4.08E-02	3.00187	5914	0.1962	1.0008	1.0006	1.0002
0.5885	31.4908	9.9681	0.3165	1.2934	4.11E-02	3.00714	5914	0.1967	1.0031	1.0024	1.0008
0.5993	31.4924	9.9765	0.3168	1.3030	4.14E-02	2.99205	5914	0.1954	0.9966	0.9973	0.9991
0.6103	31.5033	10.0662	0.3195	1.3089	4.15E-02	3.00114	5914	0.1962	1.0005	1.0004	1.0001
0.6211	31.5018	10.1421	0.3220	1.3197	4.19E-02	3.00059	5914	0.1961	1.0003	1.0002	1.0001
0.6316	31.4627	10.1887	0.3238	1.3272	4.22E-02	3.00084	5914	0.1962	1.0004	1.0003	1.0001
0.6423	31.4939	10.2676	0.3260	1.3375	4.25E-02	2.99924	5914	0.1960	0.9997	0.9997	0.9999
0.6531	31.4877	10.3294	0.3280	1.3459	4.27E-02	2.99796	5914	0.1959	0.9991	0.9993	0.9998
0.6642	31.4971	10.3989	0.3302	1.3553	4.30E-02	2.99865	5914	0.1960	0.9994	0.9996	0.9998
0.6749	31.5018	10.4776	0.3326	1.3670	4.34E-02	2.99539	5914	0.1957	0.9980	0.9985	0.9995
0.6853	31.4846	10.6162	0.3372	1.3794	4.38E-02	3.00636	5914	0.1966	1.0027	1.0021	1.0008
0.6961	31.4846	10.7541	0.3416	1.3906	4.42E-02	3.01747	5914	0.1976	1.0075	1.0058	1.0021
0.7071	31.4752	10.8871	0.3459	1.4107	4.48E-02	3.013	5914	0.1972	1.0056	1.0043	1.0015
0.7178	31.4596	10.9288	0.3474	1.4311	4.55E-02	2.99045	5914	0.1953	0.9959	0.9968	0.9989
0.7284	31.4861	10.9445	0.3476	1.4463	4.59E-02	2.96745	5914	0.1934	0.9861	0.9892	0.9961
0.7390	31.4752	10.9382	0.3475	1.4569	4.63E-02	2.95144	5914	0.1920	0.9794	0.9838	0.9941
0.7498	31.4659	10.9316	0.3474	1.4707	4.67E-02	2.9309	5914	0.1904	0.9707	0.9770	0.9916
0.7608	31.4799	10.9309	0.3472	1.4836	4.71E-02	2.91071	5914	0.1887	0.9623	0.9702	0.9891
0.7719	31.4674	10.8789	0.3457	1.4854	4.72E-02	2.89899	5914	0.1877	0.9574	0.9663	0.9876
0.7822	31.4643	10.8653	0.3453	1.4882	4.73E-02	2.89284	5914	0.1872	0.9549	0.9643	0.9868
0.7930	31.4721	10.8569	0.3450	1.4911	4.74E-02	2.88481	5914	0.1866	0.9516	0.9616	0.9858
0.8039	31.4580	10.8199	0.3439	1.4948	4.75E-02	2.87429	5914	0.1857	0.9473	0.9581	0.9844
0.8149	31.4721	10.8017	0.3432	1.4990	4.76E-02	2.86502	5914	0.1850	0.9435	0.9550	0.9832
0.8255	31.4534	10.7633	0.3422	1.5058	4.79E-02	2.8494	5914	0.1838	0.9371	0.9498	0.9812
0.8360	31.4705	10.7670	0.3421	1.5049	4.78E-02	2.84947	5914	0.1838	0.9371	0.9498	0.9812
0.8468	31.4799	10.7825	0.3425	1.5114	4.80E-02	2.842	5914	0.1832	0.9341	0.9473	0.9802
0.8578	31.4612	10.7789	0.3426	1.5159	4.82E-02	2.8377	5914	0.1828	0.9323	0.9459	0.9796
0.8687	31.4674	10.8021	0.3433	1.5206	4.83E-02	2.83525	5914	0.1826	0.9313	0.9451	0.9793
0.8790	31.4612	10.8164	0.3438	1.5231	4.84E-02	2.83509	5914	0.1826	0.9313	0.9450	0.9793
0.8897	31.4549	10.8419	0.3447	1.5220	4.84E-02	2.84156	5914	0.1831	0.9339	0.9472	0.9801
0.9007	31.4268	10.8576	0.3455	1.5271	4.86E-02	2.84001	5914	0.1830	0.9333	0.9467	0.9799
0.9116	31.4456	10.8965	0.3465	1.5330	4.87E-02	2.83755	5914	0.1828	0.9323	0.9459	0.9796
0.9224	31.4393	10.9241	0.3475	1.5365	4.89E-02	2.83978	5914	0.1830	0.9332	0.9466	0.9799

Table C-3: Mach 2.8 ZPG hot-film data - traverse up

y(in)	T _r /T ₁₁	Multiple overheat data				Single overheat data			
		Re ^k	(pu) _{rms}	(T _r) _{rms}	pu / (pu) _∞	Re ^k	(pu) _{rms}	pu / (pu) _∞	y/δ _u
0.0231	0.9760	13.1060	0.1594	0.0341	0.3977	12.9210	0.1600	0.3929	0.0582
0.0446	0.9180	14.1360	0.1680	0.1280	0.4442	13.8270	0.1519	0.4499	0.1123
0.0666	0.9760	14.7220	0.1363	0.0452	0.5018	14.6330	0.1458	0.5039	0.1678
0.0880	0.9570	15.2220	0.1671	0.1084	0.5294	15.0680	0.1527	0.5343	0.2217
0.1101	0.9670	15.8030	0.1537	0.0682	0.5747	15.7840	0.1473	0.5863	0.2773
0.1312	0.9700	16.2830	0.1622	0.0761	0.6115	15.9440	0.1467	0.5982	0.3305
0.1532	1.0180	16.5600	0.1714	0.0756	0.6531	16.5610	0.1659	0.6454	0.3859
0.1751	1.0200	17.0550	0.1528	0.0553	0.6938	17.1090	0.1419	0.6888	0.4411
0.1970	1.0080	17.4580	0.1444	0.0273	0.7211	17.3870	0.1458	0.7114	0.4962
0.2192	0.9960	18.0940	0.1470	0.0671	0.7680	18.1360	0.1351	0.7740	0.5521
0.2409	1.0020	18.3590	0.1236	0.0718	0.7941	18.3900	0.1437	0.7959	0.6068
0.2632	1.0120	18.7220	0.1506	0.0518	0.8312	18.5280	0.1397	0.8079	0.6630
0.2846	1.0370	19.0870	0.1203	0.0031	0.8782	18.9200	0.1379	0.8424	0.7169
0.3067	1.0330	19.4170	0.1182	0.0303	0.9066	19.1160	0.1321	0.8599	0.7725
0.3286	0.9860	19.7430	0.0987	0.0060	0.9085	19.6440	0.1042	0.9081	0.8277
0.3508	0.9770	19.9060	0.1087	0.0594	0.9183	19.8200	0.1004	0.9244	0.8836
0.3729	0.9790	19.9870	0.0959	0.0703	0.9266	20.1770	0.0715	0.9580	0.9393
0.3947	0.9710	20.1270	0.1010	0.0884	0.9344	19.8410	0.0872	0.9264	0.9942
0.4169	0.9720	20.4300	0.0629	0.0210	0.9639	20.3860	0.0596	0.9780	1.0501
0.4387	0.9960	20.6650	0.0618	0.0680	1.0022	20.5250	0.0410	0.9914	1.1050
0.4609	0.9700	20.8020	0.0719	0.0681	0.9982	20.4900	0.0592	0.9880	1.1610
0.4735	0.9830	20.7700	0.0052	0.0438	1.0032	20.6290	0.0417	1.0015	1.1927
0.4740	0.9750	20.7920	0.0682	0.0685	1.0000	20.4990	0.0578	0.9889	1.1940

Table C-4: Mach 2.8 ZPG separated turbulence variables single overheat- traverse up

y (inch)	Mach	(ρ) _{rms}	U _{rms}	ρ'U'	u''/u	ρbarubar	ρubar	y/δ _u
0.045	1.21	5.62E-02	9.57E-02	5.38E-03	-0.4150	39.9	68.2	0.112
0.067	1.54	7.08E-02	7.50E-02	5.31E-03	-0.2410	58.0	76.4	0.168
0.088	1.78	8.55E-02	6.72E-02	5.75E-03	-0.1230	71.0	81.0	0.222
0.110	1.91	8.75E-02	5.98E-02	5.23E-03	-0.1140	78.7	88.9	0.277
0.131	2.03	9.12E-02	5.55E-02	5.06E-03	-0.0611	85.1	90.7	0.330
0.153	2.04	1.04E-01	6.24E-02	6.46E-03	-0.1210	86.0	97.8	0.385
0.175	2.08	8.99E-02	5.20E-02	4.68E-03	-0.1560	88.1	104.0	0.441
0.197	2.16	9.48E-02	5.10E-02	4.83E-03	-0.1300	93.8	108.0	0.496
0.219	2.29	9.16E-02	4.35E-02	3.98E-03	-0.1240	103.0	117.0	0.552
0.241	2.34	9.85E-02	4.52E-02	4.45E-03	-0.1220	106.0	121.0	0.607
0.263	2.38	9.69E-02	4.28E-02	4.15E-03	-0.1150	108.0	122.0	0.662
0.285	2.49	9.83E-02	3.96E-02	3.89E-03	-0.0868	117.0	128.0	0.718
0.307	2.53	9.50E-02	3.71E-02	3.53E-03	-0.0876	119.0	130.0	0.773
0.329	2.60	7.61E-02	2.81E-02	2.14E-03	-0.0981	124.0	138.0	0.829
0.351	2.66	7.42E-02	2.62E-02	1.94E-03	-0.0737	130.0	140.0	0.884
0.373	2.71	5.34E-02	1.81E-02	9.68E-04	-0.0858	133.0	145.0	0.940
0.395	2.75	6.55E-02	2.17E-02	1.42E-03	-0.0287	136.0	140.0	0.995
0.417	2.78	4.51E-02	1.46E-02	6.57E-04	-0.0676	138.0	148.0	1.050
0.439	2.82	3.12E-02	9.80E-03	3.06E-04	-0.0575	142.0	150.0	1.106
0.461	2.83	4.52E-02	1.41E-02	6.35E-04	-0.0494	142.0	150.0	1.161
0.474	2.84	3.18E-02	9.86E-03	3.14E-04	-0.0583	143.0	152.0	1.194

Table C-5: Mach 2.8 ZPG hot-film data - traverse down

y(in)	T _t /T _{tl}	Multiple overheat data				Single overheat data			
		Re ^y	(pu) _{rms}	(T _t) _{rms}	pu / (pu) _c	Re ^y	(pu) _{rms}	pu / (pu) _c	y/δ _u
0.0407	0.9980	13.8700	0.1569	0.0648	0.4527	13.807	0.1506	0.4493	0.1025
0.0629	1.0020	14.6160	0.1394	0.0048	0.5040	14.548	0.1430	0.4989	0.1584
0.0844	1.0030	15.2100	0.1565	0.0686	0.5463	15.166	0.1484	0.5421	0.2126
0.1063	0.9660	15.5460	0.1510	0.0278	0.5568	15.445	0.1554	0.5623	0.2678
0.1281	0.9700	15.9580	0.1480	0.0389	0.5880	15.980	0.1481	0.6019	0.3227
0.1501	1.0030	16.5310	0.1808	0.1130	0.6454	16.398	0.1693	0.6338	0.3781
0.1722	0.9790	16.9310	0.1539	0.0745	0.6659	16.426	0.1500	0.6360	0.4338
0.1939	1.0090	17.4400	0.1423	0.0539	0.7213	17.604	0.1441	0.7305	0.4884
0.2163	1.0000	17.8130	0.1569	0.0639	0.7477	17.979	0.1451	0.7619	0.5448
0.2379	1.0080	18.3170	0.1190	0.0373	0.7951	18.276	0.1294	0.7873	0.5992
0.2598	1.0110	18.5820	0.0788	0.1201	0.8199	18.863	0.1334	0.8387	0.6544
0.2813	1.0320	19.0190	0.1210	0.0380	0.8708	18.955	0.1383	0.8469	0.7086
0.3036	1.0070	19.3840	0.1296	0.0797	0.8895	19.395	0.1099	0.8867	0.7647
0.3256	0.9940	19.4780	0.1410	0.0967	0.8906	19.267	0.1202	0.8750	0.8202
0.3478	1.0240	19.8270	0.0653	0.0442	0.9414	20.024	0.0866	0.9451	0.8761
0.3700	0.9880	19.9670	0.0755	0.0407	0.9323	19.998	0.0796	0.9426	0.9320
0.3917	0.9660	20.1350	0.0897	0.0513	0.9336	19.946	0.0823	0.9377	0.9866
0.4141	0.9730	20.2960	0.0427	0.0668	0.9533	20.283	0.0549	0.9697	1.0431
0.4358	0.9890	20.4620	0.0127	0.0578	0.9795	20.342	0.0605	0.9754	1.0977
0.4582	0.9970	20.6940	0.0695	0.0722	1.0076	20.589	0.0499	0.9992	1.1542
0.4733	0.9760	20.7680	0.0429	0.0281	1.0000	20.663	0.0397	1.0064	1.1922

Table C-6: Mach 2.8 ZPG separated turbulence variables single overheat - traverse down

y (inch)	Mach	(ρ) _{rms}	U _{rms}	p'U'	u''/u	pbarubar	pubar	y/δ _u
0.063	1.48	6.68E-02	7.62E-02	5.09E-03	-0.2660	55.4	75.5	0.158
0.084	1.76	8.22E-02	6.62E-02	5.44E-03	-0.1480	69.9	82.0	0.213
0.106	1.89	9.16E-02	6.38E-02	5.84E-03	-0.0913	77.3	85.1	0.267
0.128	2.00	9.11E-02	5.70E-02	5.19E-03	-0.0770	84.1	91.1	0.322
0.150	2.03	1.05E-01	6.38E-02	6.73E-03	-0.1100	85.3	95.9	0.378
0.172	2.10	9.56E-02	5.44E-02	5.20E-03	-0.0667	89.8	96.2	0.433
0.194	2.15	9.36E-02	5.05E-02	4.73E-03	-0.1580	93.1	111.0	0.489
0.216	2.29	9.82E-02	4.69E-02	4.60E-03	-0.1090	103.0	115.0	0.544
0.238	2.33	8.86E-02	4.08E-02	3.61E-03	-0.1180	105.0	119.0	0.599
0.260	2.37	9.23E-02	4.11E-02	3.79E-03	-0.1470	108.0	127.0	0.655
0.281	2.48	9.83E-02	4.00E-02	3.93E-03	-0.1010	115.0	128.0	0.708
0.304	2.53	7.89E-02	3.10E-02	2.44E-03	-0.1160	119.0	134.0	0.766
0.326	2.60	8.77E-02	3.25E-02	2.85E-03	-0.0602	124.0	132.0	0.821
0.348	2.66	6.39E-02	2.27E-02	1.45E-03	-0.1010	129.0	143.0	0.877
0.370	2.71	5.94E-02	2.02E-02	1.20E-03	-0.0662	133.0	143.0	0.932
0.392	2.74	6.17E-02	2.06E-02	1.27E-03	-0.0483	135.0	142.0	0.987
0.414	2.77	4.14E-02	1.35E-02	5.58E-04	-0.0593	138.0	147.0	1.043
0.436	2.82	4.60E-02	1.45E-02	6.67E-04	-0.0454	141.0	148.0	1.098
0.458	2.83	3.81E-02	1.18E-02	4.51E-04	-0.0553	143.0	151.0	1.154
0.473	2.84	3.03E-02	9.40E-03	2.85E-04	-0.0633	143.0	152.0	1.191

Table C-7: Mach 2.8 FPG hot-film data - traverse up

y(in)	T _t /T _{in}	Multiple overheat data				Single overheat data			
		Re ^y	(ρu) _{ms}	(T _t) _{ms}	ρu / (ρu) _x	Re ^y	(ρu) _{ms}	ρu / (ρu) _x	y/δ _u
0.0072	1.074	8.653	8.58E-02	5.18E-02	0.1974	8.835	6.55E-02	0.1963	0.0173
0.0287	1.055	10.392	4.76E-02	9.78E-02	0.2814	10.582	1.30E-01	0.2816	0.0692
0.0506	1.009	11.988	7.63E-02	6.93E-02	0.3635	12.066	1.01E-01	0.3661	0.1219
0.0726	0.979	12.682	9.46E-02	1.94E-02	0.3986	12.848	9.43E-02	0.4151	0.1749
0.0946	0.981	13.26	9.93E-02	1.45E-02	0.4365	13.461	1.01E-01	0.4556	0.2280
0.1163	0.975	13.696	8.60E-02	6.03E-02	0.4636	13.739	9.89E-02	0.4746	0.2802
0.1384	0.999	14.036	1.23E-01	6.97E-02	0.4950	14.151	1.07E-01	0.5035	0.3335
0.1602	0.999	14.402	9.32E-02	5.08E-02	0.5213	14.634	1.03E-01	0.5385	0.3860
0.1823	0.973	14.693	1.04E-01	3.26E-02	0.5331	14.647	1.09E-01	0.5394	0.4393
0.2041	0.995	14.954	1.09E-01	4.78E-02	0.5605	15.108	1.09E-01	0.5739	0.4918
0.2262	1.007	15.192	1.19E-01	4.56E-02	0.5828	15.378	1.12E-01	0.5946	0.5451
0.2483	1.008	15.562	7.33E-02	7.57E-02	0.6122	15.75	1.02E-01	0.6237	0.5983
0.2702	1.007	15.783	1.04E-01	5.01E-02	0.6292	15.969	1.17E-01	0.6412	0.6511
0.2924	1.025	16.226	1.04E-01	3.87E-02	0.6731	16.469	1.10E-01	0.6820	0.7046
0.3143	1.042	16.621	9.54E-02	5.31E-02	0.7140	16.66	1.09E-01	0.6979	0.7573
0.3366	1.023	16.603	1.08E-01	2.57E-02	0.7036	16.797	1.08E-01	0.7094	0.8111
0.3586	0.968	16.86	9.62E-02	7.35E-02	0.6995	16.882	1.07E-01	0.7166	0.8641
0.381	1.011	17.207	1.20E-01	5.74E-02	0.7497	17.27	1.15E-01	0.7499	0.9181
0.4029	0.966	17.467	9.20E-02	6.09E-02	0.7499	17.567	1.08E-01	0.7760	0.9708
0.4249	0.999	17.738	7.84E-02	6.48E-02	0.7904	17.75	1.02E-01	0.7922	1.0239
0.4463	0.997	17.966	7.01E-02	5.08E-02	0.8101	18.114	7.96E-02	0.8250	1.0754
0.4682	1.015	18.099	6.81E-02	7.54E-03	0.8319	18.24	7.58E-02	0.8366	1.1282
0.4904	0.97	18.093	7.73E-02	3.40E-02	0.8067	18.004	8.52E-02	0.8150	1.1817
0.5122	0.983	18.311	8.54E-02	6.53E-02	0.8333	18.309	7.55E-02	0.8429	1.2342
0.5345	0.979	18.407	6.79E-02	3.34E-02	0.8401	18.345	6.71E-02	0.8462	1.2880
0.5562	1.001	18.443	2.74E-02	4.67E-02	0.8561	18.661	5.08E-02	0.8756	1.3402
0.5784	0.97	18.556	5.90E-02	8.83E-03	0.8481	18.582	5.33E-02	0.8682	1.3937
0.6003	0.979	18.641	5.38E-02	1.03E-02	0.8612	18.586	6.36E-02	0.8686	1.4465
0.6224	0.993	18.816	1.14E-02	3.53E-02	0.8860	19.013	3.57E-02	0.9090	1.4998
0.6444	0.989	18.888	3.54E-02	1.89E-02	0.8905	19.044	2.76E-02	0.9119	1.5528
0.6662	1.008	19.031	2.64E-02	2.06E-02	0.9152	19.312	3.24E-02	0.9378	1.6053
0.6884	0.997	19.24	1.99E-02	1.70E-02	0.9291	19.39	3.00E-02	0.9454	1.6588
0.7101	0.996	19.41	2.57E-02	2.41E-02	0.9450	19.532	2.51E-02	0.9593	1.7111
0.7323	0.997	19.509	2.43E-02	3.22E-02	0.9551	19.707	1.78E-02	0.9765	1.7646
0.7539	0.994	19.518	1.55E-02	7.36E-03	0.9542	19.646	1.76E-02	0.9705	1.8166
0.776	0.998	19.548	9.34E-03	1.06E-02	0.9593	19.765	1.55E-02	0.9823	1.8699
0.7979	0.995	19.589	9.64E-03	2.10E-02	0.9618	19.772	1.50E-02	0.9830	1.9227
0.8198	0.998	19.63	1.06E-02	1.72E-02	0.9676	19.826	1.37E-02	0.9884	1.9754
0.8418	0.995	19.682	6.71E-03	1.20E-02	0.9707	19.861	1.42E-02	0.9919	2.0284
0.8635	0.994	19.742	9.18E-03	1.03E-02	0.9762	19.915	1.45E-02	0.9973	2.0807
0.8848	0.995	19.797	8.25E-03	1.31E-02	0.9821	19.942	1.47E-02	1.0000	2.1320
0.9059	0.994	19.832	7.37E-03	1.19E-02	0.9847	20.004	1.41E-02	1.0062	2.1829
0.928	0.996	19.872	9.22E-03	1.07E-02	0.9900	20.058	1.42E-02	1.0116	2.2361
0.9497	0.995	19.893	8.57E-03	1.05E-02	0.9919	20.09	1.38E-02	1.0149	2.2884
0.9717	0.993	19.921	7.29E-03	1.22E-02	0.9929	20.075	1.38E-02	1.0133	2.3414
0.9908	0.994	19.943	9.57E-03	1.02E-02	0.9962	20.109	1.46E-02	1.0168	2.3875
0.9939	0.998	19.959	1.25E-02	1.88E-03	1.0001	20.149	1.56E-02	1.0208	2.3949
0.9939	0.997	19.965	1.05E-02	8.53E-03	1.0000	20.178	1.42E-02	1.0238	2.3949

Table C-8: Mach 2.8 FPG separated turbulence variables single overheat - traverse up

y (inch)	Mach	(ρ) _{rms}	U _{rms}	ρ'U'	u''/u	ρbarubar	ρubar	v/δ _u
0.029	1.46	5.98E-02	6.97E-02	4.17E-03	0.0479	41.8	39.9	0.069
0.051	1.47	4.69E-02	5.45E-02	2.56E-03	-0.1970	41.7	51.9	0.122
0.073	1.49	4.45E-02	4.98E-02	2.22E-03	-0.2740	42.8	58.9	0.175
0.095	1.84	5.80E-02	4.29E-02	2.49E-03	-0.1650	54.0	64.6	0.228
0.116	2.01	6.12E-02	3.77E-02	2.31E-03	-0.1380	58.1	67.3	0.280
0.138	2.12	6.87E-02	3.84E-02	2.64E-03	-0.1470	60.9	71.4	0.333
0.160	2.22	6.84E-02	3.45E-02	2.36E-03	-0.1560	64.5	76.4	0.386
0.182	2.33	7.44E-02	3.43E-02	2.55E-03	-0.1120	68.0	76.5	0.439
0.204	2.40	7.59E-02	3.30E-02	2.51E-03	-0.1270	71.1	81.4	0.492
0.226	2.46	7.91E-02	3.26E-02	2.58E-03	-0.1200	74.2	84.3	0.545
0.248	2.54	7.36E-02	2.84E-02	2.09E-03	-0.1160	78.2	88.5	0.598
0.270	2.60	8.57E-02	3.17E-02	2.72E-03	-0.1040	81.5	90.9	0.651
0.292	2.62	8.10E-02	2.94E-02	2.38E-03	-0.1340	83.8	96.7	0.704
0.314	2.70	8.11E-02	2.77E-02	2.25E-03	-0.1100	88.1	99.0	0.757
0.337	2.77	8.17E-02	2.66E-02	2.17E-03	-0.0862	92.0	101.0	0.812
0.359	2.81	8.14E-02	2.58E-02	2.10E-03	-0.0707	94.5	102.0	0.865
0.381	2.80	8.70E-02	2.78E-02	2.42E-03	-0.1030	95.4	106.0	0.918
0.403	2.89	8.27E-02	2.48E-02	2.05E-03	-0.0918	100.0	110.0	0.971
0.425	2.91	7.88E-02	2.33E-02	1.84E-03	-0.0945	102.0	112.0	1.024
0.446	2.94	6.17E-02	1.78E-02	1.10E-03	-0.1110	104.0	117.0	1.075
0.468	3.00	5.93E-02	1.65E-02	9.77E-04	-0.0899	108.0	119.0	1.128
0.490	3.01	6.68E-02	1.84E-02	1.23E-03	-0.0507	110.0	116.0	1.181
0.512	3.00	5.91E-02	1.64E-02	9.68E-04	-0.0707	111.0	120.0	1.234
0.535	3.01	5.26E-02	1.45E-02	7.62E-04	-0.0583	113.0	120.0	1.289
0.556	3.00	3.98E-02	1.11E-02	4.40E-04	-0.0799	114.0	124.0	1.340
0.578	3.00	4.17E-02	1.16E-02	4.83E-04	-0.0607	116.0	123.0	1.393
0.600	2.99	4.98E-02	1.39E-02	6.91E-04	-0.0514	117.0	123.0	1.446
0.622	3.00	2.79E-02	7.76E-03	2.17E-04	-0.0793	119.0	129.0	1.499
0.644	3.00	2.16E-02	6.00E-03	1.29E-04	-0.0703	120.0	129.0	1.552
0.666	3.00	2.54E-02	7.06E-03	1.79E-04	-0.0838	122.0	133.0	1.605
0.688	3.01	2.35E-02	6.48E-03	1.52E-04	-0.0709	125.0	134.0	1.658
0.710	3.01	1.96E-02	5.43E-03	1.07E-04	-0.0635	127.0	136.0	1.711
0.732	2.96	1.38E-02	3.95E-03	5.46E-05	-0.0726	128.0	139.0	1.764
0.754	2.92	1.36E-02	3.98E-03	5.41E-05	-0.0640	129.0	138.0	1.817
0.776	2.90	1.19E-02	3.55E-03	4.23E-05	-0.0776	129.0	139.0	1.870
0.798	2.88	1.15E-02	3.48E-03	4.01E-05	-0.0801	128.0	139.0	1.923
0.820	2.86	1.05E-02	3.22E-03	3.39E-05	-0.0874	128.0	140.0	1.976

Table C-9: Mach 2.8 CPG ($x = 68$ cm) hot-film data - traverse up

y(in)	T_t/T_{t1}	Multiple overheat data				Single overheat data				y/δ_u
		$Re^{1/2}$	$(\rho u)_{rms}$	$(T_t)_{rms}$	$\rho u / (\rho u)_c$	$Re^{1/2}$	$(\rho u)_{rms}$	$\rho u / (\rho u)_c$	y/δ_u	
0.0126	1.0090	14.9490	0.1239	0.0115	0.3990	15.1240	0.1494	0.4046	0.0352	
0.0347	0.9680	16.6310	0.1648	0.0654	0.4803	16.9100	0.1796	0.5058	0.0970	
0.0562	0.9930	17.6210	0.1812	0.0173	0.5484	17.7430	0.1858	0.5568	0.1570	
0.0786	1.0350	18.6590	0.1477	0.0992	0.6320	18.7750	0.1886	0.6235	0.2196	
0.1001	0.9810	19.3830	0.1756	0.0663	0.6579	19.5860	0.1903	0.6785	0.2797	
0.1224	1.0250	20.2060	0.1935	0.0313	0.7362	20.4510	0.1964	0.7398	0.3420	
0.1441	1.0150	20.6300	0.1750	0.0434	0.7629	21.3920	0.1956	0.8094	0.4027	
0.1662	1.0530	21.9350	0.1230	0.0962	0.8837	22.7740	0.1711	0.9174	0.4644	
0.1883	1.0240	22.4460	0.1483	0.0732	0.9083	22.8300	0.1661	0.9219	0.5262	
0.2101	1.0270	23.3320	0.1320	0.0754	0.9832	23.7560	0.1664	0.9982	0.5871	
0.2325	0.9550	24.0080	0.1414	0.0889	0.9920	23.7770	0.1502	1.0000	0.6497	
0.2542	0.9630	24.6430	0.1623	0.1075	1.0509	24.8680	0.1384	1.0938	0.7103	
0.2767	0.9940	25.1460	0.1053	0.0592	1.1177	25.4250	0.1162	1.1434	0.7732	
0.2985	0.9930	25.4950	0.1032	0.0414	1.1479	25.7520	0.1036	1.1730	0.8341	
0.3210	1.0020	25.7990	0.0571	0.0632	1.1824	25.9480	0.0819	1.1909	0.8970	
0.3427	0.9970	25.8650	0.0406	0.0579	1.1847	26.1910	0.0523	1.2133	0.9576	
0.3649	0.9880	25.8990	0.0770	0.0575	1.1808	25.8960	0.0585	1.1861	1.0196	
0.3867	0.9990	25.7610	0.0156	0.0116	1.1771	25.8740	0.0299	1.1841	1.0805	
0.4081	0.9890	25.3720	0.0290	0.0265	1.1338	25.4850	0.0373	1.1488	1.1403	
0.4303	0.9880	24.9570	0.0078	0.0395	1.0960	24.9400	0.0318	1.1002	1.2024	
0.4513	0.9950	24.4940	0.0357	0.0030	1.0608	24.6580	0.0389	1.0754	1.2611	
0.4738	0.9840	24.1380	0.0385	0.0381	1.0226	24.2430	0.0273	1.0395	1.3239	
0.4908	0.9790	23.9080	0.0166	0.0080	1.0000	23.9570	0.0258	1.0152	1.3714	

Table C-10: Mach 2.8 CPG ($x=68$ cm) separated turbulence variables single overheat- traverse up

y (inch)	Mach	$(\rho)_{rms}$	U_{rms}	$\rho'U'$	u''/u	$p_{bar}u_{bar}$	ρ_{bar}	y/δ_u
0.035	1.54	8.76E-02	9.20E-02	8.06E-03	-0.0109	101.0	102.0	0.097
0.056	1.77	1.03E-01	8.27E-02	8.53E-03	0.0265	115.0	112.0	0.157
0.079	1.87	1.10E-01	7.84E-02	8.64E-03	-0.0283	122.0	126.0	0.220
0.100	1.97	1.16E-01	7.45E-02	8.63E-03	-0.0739	127.0	137.0	0.279
0.122	2.09	1.25E-01	7.15E-02	8.93E-03	-0.1130	132.0	149.0	0.341
0.144	2.20	1.29E-01	6.68E-02	8.60E-03	-0.1400	140.0	163.0	0.402
0.166	2.19	1.13E-01	5.85E-02	6.59E-03	-0.2030	147.0	185.0	0.464
0.188	2.35	1.14E-01	5.17E-02	5.91E-03	-0.1740	154.0	186.0	0.525
0.210	2.38	1.16E-01	5.08E-02	5.87E-03	-0.2290	155.0	201.0	0.587
0.233	2.44	1.06E-01	4.43E-02	4.69E-03	-0.2050	160.0	202.0	0.651
0.254	2.49	9.87E-02	3.97E-02	3.92E-03	-0.2410	167.0	221.0	0.710
0.277	2.50	8.30E-02	3.32E-02	2.76E-03	-0.2510	173.0	231.0	0.774
0.299	2.53	7.46E-02	2.90E-02	2.17E-03	-0.2560	176.0	237.0	0.835
0.321	2.54	5.90E-02	2.29E-02	1.35E-03	-0.2600	178.0	240.0	0.897
0.343	2.53	3.76E-02	1.47E-02	5.53E-04	-0.2620	181.0	245.0	0.958
0.365	2.57	4.24E-02	1.61E-02	6.82E-04	-0.2360	183.0	239.0	1.020
0.387	2.60	2.18E-02	8.06E-03	1.76E-04	-0.2200	186.0	239.0	1.081
0.408	2.61	2.73E-02	9.99E-03	2.73E-04	-0.1950	186.0	232.0	1.140
0.430	2.60	2.32E-02	8.61E-03	2.00E-04	-0.1520	188.0	222.0	1.202
0.451	2.58	2.83E-02	1.06E-02	3.00E-04	-0.1290	189.0	217.0	1.260
0.474	2.59	1.99E-02	7.40E-03	1.47E-04	-0.0935	190.0	210.0	1.324
0.491	2.59	1.88E-02	7.01E-03	1.32E-04	-0.0729	190.0	205.0	1.372

Table C-11: Mach 2.8 CPG ($x = 68$ cm) hot-film data - traverse down

Multiple overheat data						Single overheat data				
y(in)	T _r /T _{tl}	Re ^y	(ρu) _{ms}	(T _r) _{ms}	pu / (ρu) _c	Re ^y	(ρu) _{ms}	pu / (ρu) _c	y/δ _u	
0.0084	1.028	14.309	8.94E-02	8.16E-02	0.3655	14.35	1.23E-01	0.3610	0.0235	
0.0307	0.996	16.305	1.56E-01	6.69E-02	0.4646	16.454	1.77E-01	0.4746	0.0858	
0.0521	1.004	17.133	1.94E-01	7.23E-02	0.5158	17.318	1.95E-01	0.5258	0.1456	
0.0744	0.975	18.172	1.92E-01	5.09E-02	0.5690	18.247	1.97E-01	0.5837	0.2079	
0.0961	1.023	19.332	1.86E-01	4.69E-02	0.6652	19.417	2.07E-01	0.6610	0.2685	
0.1181	0.961	19.802	2.00E-01	5.54E-02	0.6694	19.615	2.00E-01	0.6745	0.3300	
0.1402	0.992	20.633	1.81E-01	2.66E-02	0.7424	20.781	1.84E-01	0.7571	0.3918	
0.162	1.011	21.534	1.27E-01	1.10E-01	0.8190	21.753	1.74E-01	0.8296	0.4527	
0.1844	1.04	22.052	1.91E-01	7.28E-02	0.8751	22.479	1.86E-01	0.8859	0.5153	
0.2059	1.012	22.931	1.69E-01	5.49E-02	0.9289	23.039	1.73E-01	0.9305	0.5753	
0.2284	1.025	23.688	1.43E-01	6.44E-02	1.0001	23.71	1.64E-01	0.9855	0.6382	
0.2501	0.974	24.373	1.37E-01	9.16E-02	1.0232	24.307	1.50E-01	1.0358	0.6988	
0.2725	0.989	24.746	1.33E-01	5.61E-02	1.0653	24.849	1.42E-01	1.0825	0.7614	
0.2945	0.981	25.068	1.15E-01	6.93E-02	1.0874	24.801	1.37E-01	1.0783	0.8229	
0.3167	1.006	25.663	5.50E-02	1.07E-01	1.1588	25.825	8.71E-02	1.1692	0.8849	
0.3389	0.992	25.634	6.53E-02	4.97E-02	1.1460	25.412	9.52E-02	1.1321	0.9470	
0.3606	0.995	25.925	4.40E-02	3.52E-02	1.1740	25.952	6.25E-02	1.1807	1.0076	
0.383	0.99	25.845	1.56E-02	4.80E-02	1.1630	25.912	3.42E-02	1.1771	1.0702	
0.4046	0.99	25.522	2.44E-02	1.02E-02	1.1344	25.502	3.20E-02	1.1401	1.1306	
0.4271	0.983	25.15	4.88E-02	4.94E-02	1.0960	25.097	3.04E-02	1.1042	1.1934	
0.4487	0.976	24.683	1.88E-02	3.69E-02	1.0511	24.537	3.41E-02	1.0555	1.2538	
0.471	0.98	24.25	3.38E-02	2.56E-02	1.0174	24.172	2.83E-02	1.0243	1.3161	
0.4899	0.984	24.009	2.62E-02	1.86E-03	1.0000	24.075	2.57E-02	1.0161	1.3689	

Table C-12: Mach 2.8 CPG ($x=68$ cm) separated turbulence variables single overheat- traverse down

y (inch)	Mach	(ρ) _{ms}	U _{ms}	ρ'U'	u''/u	ρbarubar	ρubar	y/δ _u
0.031	1.51	8.41E-02	9.27E-02	7.80E-03	0.0236	98.8	96.6	0.086
0.052	1.73	1.06E-01	8.84E-02	9.39E-03	0.0516	112.0	107.0	0.146
0.074	1.85	1.14E-01	8.34E-02	9.47E-03	0.0175	121.0	119.0	0.208
0.096	1.96	1.26E-01	8.16E-02	1.02E-02	-0.0630	126.0	134.0	0.269
0.118	2.08	1.27E-01	7.34E-02	9.32E-03	-0.0421	131.0	137.0	0.330
0.140	2.18	1.21E-01	6.33E-02	7.64E-03	-0.0944	139.0	154.0	0.391
0.162	2.24	1.16E-01	5.79E-02	6.71E-03	-0.1420	145.0	169.0	0.453
0.184	2.34	1.28E-01	5.80E-02	7.40E-03	-0.1510	153.0	180.0	0.514
0.206	2.36	1.19E-01	5.35E-02	6.38E-03	-0.1890	153.0	189.0	0.576
0.228	2.44	1.16E-01	4.85E-02	5.62E-03	-0.2020	160.0	200.0	0.637
0.250	2.48	1.06E-01	4.31E-02	4.59E-03	-0.2080	167.0	211.0	0.699
0.273	2.50	1.01E-01	4.04E-02	4.10E-03	-0.2180	172.0	220.0	0.763
0.294	2.54	9.87E-02	3.84E-02	3.79E-03	-0.1960	176.0	219.0	0.822
0.317	2.54	6.28E-02	2.43E-02	1.53E-03	-0.2560	177.0	238.0	0.886
0.339	2.53	6.85E-02	2.67E-02	1.83E-03	-0.2190	180.0	230.0	0.947
0.361	2.56	4.52E-02	1.73E-02	7.81E-04	-0.2430	182.0	240.0	1.009
0.383	2.59	2.49E-02	9.28E-03	2.31E-04	-0.2260	185.0	239.0	1.070
0.405	2.61	2.35E-02	8.58E-03	2.01E-04	-0.1960	186.0	232.0	1.132
0.427	2.59	2.21E-02	8.22E-03	1.82E-04	-0.1630	188.0	225.0	1.193
0.449	2.58	2.48E-02	9.31E-03	2.31E-04	-0.1220	189.0	215.0	1.255
0.471	2.59	2.07E-02	7.68E-03	1.59E-04	-0.0885	190.0	208.0	1.316
0.490	2.59	1.87E-02	6.97E-03	1.30E-04	-0.0819	190.0	207.0	1.369

Table C-13: Mach 2.8 CPG ($x = 70$ cm) hot-film data - traverse up

y(in)	T_f/T_{u1}	Multiple overheating data				Single overheating data				y/δ_u
		$Re^{\frac{1}{2}}$	$(\rho u)_{rms}$	$(T_f)_{rms}$	$\rho u / (\rho u)_c$	$Re^{\frac{1}{2}}$	$(\rho u)_{rms}$	$\rho u / (\rho u)_c$		
0.0127	1.0220	15.2550	0.1302	0.0377	0.3591	15.3110	0.1427	0.3567	0.0431	
0.0348	1.0370	17.1360	0.1826	0.0472	0.4577	17.4130	0.1937	0.4613	0.1182	
0.0565	1.0430	18.0530	0.1852	0.0634	0.5099	17.8690	0.1963	0.4858	0.1919	
0.0790	1.0490	18.9200	0.1937	0.0622	0.5623	19.1090	0.2052	0.5555	0.2683	
0.1007	0.9720	19.3670	0.1923	0.0759	0.5600	19.1260	0.2026	0.5565	0.3419	
0.1232	0.9740	19.8640	0.2242	0.0644	0.5898	19.3240	0.2193	0.5681	0.4184	
0.1448	0.9750	20.6440	0.1862	0.1485	0.6373	20.5790	0.1992	0.6443	0.4917	
0.1670	1.0000	21.5470	0.2048	0.0563	0.7065	21.7090	0.2168	0.7170	0.5671	
0.1889	1.0590	22.2840	0.1284	0.1227	0.7850	22.5540	0.1879	0.7739	0.6415	
0.2108	0.9820	22.7990	0.1499	0.1441	0.7809	22.5420	0.1921	0.7731	0.7158	
0.2330	0.9430	23.5590	0.1955	0.0973	0.8118	22.0720	0.1921	0.7412	0.7912	
0.2545	1.0280	24.2820	0.1461	0.0367	0.9134	23.9720	0.1622	0.8743	0.8642	
0.2770	1.0380	24.8180	0.0560	0.1064	0.9603	24.7690	0.1382	0.9334	0.9406	
0.2984	0.9930	25.1110	0.1602	0.1132	0.9548	24.7780	0.1306	0.9341	1.0133	
0.3208	1.0170	25.5180	0.0600	0.0721	1.0021	25.8960	0.0710	1.0203	1.0893	
0.3424	1.0030	25.9500	0.0425	0.0611	1.0266	25.9710	0.0578	1.0262	1.1627	
0.3645	1.0020	26.0150	0.0187	0.0640	1.0311	25.9150	0.0570	1.0218	1.2377	
0.3858	1.0100	26.0170	0.0431	0.0593	1.0366	26.0040	0.0334	1.0288	1.3101	
0.4075	1.0020	26.0270	0.0207	0.0360	1.0315	25.9530	0.0173	1.0248	1.3838	
0.4297	1.0000	25.9290	0.0152	0.0240	1.0229	25.8060	0.0153	1.0132	1.4591	
0.4512	1.0030	25.8370	0.0156	0.0133	1.0174	25.7280	0.0152	1.0071	1.5321	
0.4735	1.0020	25.7410	0.0215	0.0140	1.0092	25.6180	0.0170	0.9985	1.6079	
0.4918	0.9980	25.6580	0.0229	0.0194	1.0000	25.4950	0.0199	0.9889	1.6700	

Table C-14: Mach 2.8 CPG ($x=70$ cm) separated turbulence variables single overheating- traverse up

y (inch)	Mach	$(\rho)_{rms}$	U_{rms}	$\rho'U'$	u''/u	$\bar{\rho}u\bar{u}$	$\bar{\rho}u\bar{u}$	y/δ_u
0.035	1.54	9.46E-02	9.91E-02	9.37E-03	-0.0667	101.0	108.0	0.118
0.057	1.77	1.09E-01	8.72E-02	9.51E-03	0.0134	115.0	114.0	0.191
0.079	1.88	1.20E-01	8.52E-02	1.02E-02	-0.0610	122.0	130.0	0.268
0.101	1.97	1.23E-01	7.92E-02	9.78E-03	-0.0280	127.0	130.0	0.342
0.123	2.09	1.40E-01	7.97E-02	1.11E-02	-0.0055	132.0	133.0	0.417
0.145	2.20	1.31E-01	6.79E-02	8.92E-03	-0.0697	141.0	151.0	0.491
0.167	2.19	1.42E-01	7.45E-02	1.06E-02	-0.1200	148.0	168.0	0.566
0.189	2.35	1.29E-01	5.84E-02	7.57E-03	-0.1530	154.0	181.0	0.640
0.211	2.39	1.34E-01	5.85E-02	7.82E-03	-0.1420	155.0	181.0	0.715
0.233	2.45	1.35E-01	5.66E-02	7.67E-03	-0.0777	160.0	174.0	0.789
0.255	2.49	1.16E-01	4.66E-02	5.38E-03	-0.1830	167.0	205.0	0.864
0.277	2.50	9.87E-02	3.95E-02	3.90E-03	-0.2110	173.0	219.0	0.938
0.298	2.53	9.40E-02	3.66E-02	3.44E-03	-0.1960	176.0	219.0	1.009
0.321	2.54	5.12E-02	1.98E-02	1.02E-03	-0.2570	178.0	239.0	1.087
0.342	2.53	4.16E-02	1.62E-02	6.75E-04	-0.2500	181.0	241.0	1.158
0.364	2.57	4.13E-02	1.57E-02	6.47E-04	-0.2370	183.0	240.0	1.233
0.386	2.60	2.44E-02	9.04E-03	2.20E-04	-0.2290	186.0	241.0	1.307
0.407	2.61	1.26E-02	4.63E-03	5.85E-05	-0.2240	186.0	240.0	1.378
0.430	2.60	1.11E-02	4.14E-03	4.61E-05	-0.2080	188.0	238.0	1.456
0.451	2.58	1.11E-02	4.15E-03	4.59E-05	-0.2000	189.0	236.0	1.527
0.474	2.59	1.24E-02	4.61E-03	5.70E-05	-0.1880	190.0	234.0	1.605
0.492	2.59	1.45E-02	5.40E-03	7.83E-05	-0.1810	190.0	232.0	1.666

Table C-15: Mach 2.8 CPG (x = 70 cm) hot-film data - traverse down

Multiple overheat data						Single overheat data				
y(in)	T/T ₁₁	Re ^{1/2}	(ρu) _{rms}	(T ₁) _{rms}	pu / (ρu) _∞	Re ^{1/2}	(ρu) _{rms}	pu / (ρu) _∞	y/δ _u	
0.0085	1.0450	14.7050	0.1279	0.0459	0.3354	15.1180	0.1335	0.3442	0.0289	
0.0308	1.0260	16.6440	0.1852	0.0239	0.4243	16.8680	0.1924	0.4285	0.1046	
0.0524	0.9970	17.7130	0.1903	0.0657	0.4715	17.5570	0.1999	0.4642	0.1779	
0.0748	1.0320	18.5150	0.2043	0.0197	0.5273	18.6260	0.2083	0.5224	0.2540	
0.0965	1.0090	19.0500	0.1936	0.0741	0.5498	19.0410	0.2049	0.5460	0.3277	
0.1188	1.0350	19.9100	0.1887	0.0677	0.6105	20.7410	0.1925	0.6478	0.4034	
0.1408	1.0280	20.7000	0.2134	0.0606	0.6572	20.9290	0.2132	0.6596	0.4781	
0.1626	1.0150	21.2930	0.1870	0.1022	0.6897	21.0930	0.2098	0.6700	0.5521	
0.1848	0.9550	21.8960	0.1889	0.0606	0.7003	21.5020	0.1931	0.6962	0.6275	
0.2064	0.9800	22.7090	0.1987	0.0707	0.7660	22.2080	0.1995	0.7427	0.7009	
0.2288	1.0020	23.1020	0.1575	0.1007	0.8046	23.1370	0.1852	0.8062	0.7769	
0.2502	1.0140	24.1080	0.1333	0.0873	0.8835	24.4080	0.1631	0.8972	0.8496	
0.2726	0.9820	24.4180	0.1849	0.1180	0.8869	24.1910	0.1627	0.8813	0.9257	
0.2944	1.0370	25.1970	0.1213	0.0571	0.9795	25.2850	0.1176	0.9628	0.9997	
0.3164	1.0010	25.3840	0.1150	0.0324	0.9710	25.0190	0.1302	0.9426	1.0744	
0.3384	1.0020	25.6290	0.0299	0.1124	0.9901	25.5070	0.0945	0.9798	1.1491	
0.3601	0.9970	25.8900	0.0302	0.0778	1.0074	25.9810	0.0647	1.0165	1.2228	
0.3823	1.0030	25.9060	0.0083	0.0651	1.0125	25.6920	0.0752	0.9940	1.2982	
0.4038	0.9890	26.0530	0.0624	0.0403	1.0147	25.9840	0.0436	1.0168	1.3712	
0.4263	0.9940	26.0220	0.0620	0.0554	1.0158	25.9810	0.0279	1.0165	1.4476	
0.4477	1.0040	25.9770	0.0318	0.0403	1.0185	25.9450	0.0179	1.0137	1.5203	
0.4698	1.0000	25.8800	0.0134	0.0105	1.0082	25.8240	0.0202	1.0043	1.5953	
0.4900	0.9960	25.8070	0.0249	0.0185	1.0000	25.7210	0.0229	0.9963	1.6639	

Table C-16: Mach 2.8 CPG (x=70 cm) separated turbulence variables single overheat- traverse down

y (inch)	Mach	(ρ) _{rms}	U _{rms}	ρ'U'	u''/u	pbarubar	pubar	y/δ _u
0.031	1.51	9.16E-02	1.01E-01	9.23E-03	-0.0255	98.9	101.0	0.104
0.052	1.74	1.09E-01	9.06E-02	9.90E-03	0.0265	113.0	110.0	0.177
0.075	1.85	1.20E-01	8.80E-02	1.06E-02	-0.0225	121.0	124.0	0.253
0.097	1.96	1.24E-01	8.07E-02	1.00E-02	-0.0251	126.0	129.0	0.327
0.119	2.08	1.22E-01	7.05E-02	8.60E-03	-0.1420	132.0	153.0	0.403
0.141	2.19	1.40E-01	7.33E-02	1.03E-02	-0.1060	140.0	156.0	0.478
0.163	2.23	1.40E-01	7.01E-02	9.80E-03	-0.0849	145.0	159.0	0.552
0.185	2.35	1.33E-01	6.03E-02	8.01E-03	-0.0714	153.0	165.0	0.627
0.206	2.36	1.38E-01	6.17E-02	8.50E-03	-0.1270	154.0	176.0	0.698
0.229	2.44	1.30E-01	5.47E-02	7.14E-03	-0.1620	160.0	191.0	0.776
0.250	2.48	1.16E-01	4.70E-02	5.46E-03	-0.2140	167.0	212.0	0.847
0.273	2.50	1.16E-01	4.64E-02	5.40E-03	-0.1750	172.0	209.0	0.925
0.294	2.54	8.47E-02	3.29E-02	2.79E-03	-0.2270	176.0	228.0	0.996
0.316	2.54	9.39E-02	3.63E-02	3.41E-03	-0.2080	177.0	223.0	1.070
0.338	2.53	6.80E-02	2.65E-02	1.80E-03	-0.2250	180.0	232.0	1.145
0.360	2.56	4.68E-02	1.79E-02	8.37E-04	-0.2450	182.0	241.0	1.219
0.382	2.59	5.48E-02	2.04E-02	1.12E-03	-0.2130	185.0	235.0	1.294
0.404	2.61	3.19E-02	1.17E-02	3.73E-04	-0.2260	186.0	241.0	1.368
0.426	2.59	2.03E-02	7.56E-03	1.54E-04	-0.2190	188.0	241.0	1.443
0.448	2.58	1.30E-02	4.88E-03	6.33E-05	-0.2150	188.0	240.0	1.517
0.470	2.59	1.47E-02	5.47E-03	8.04E-05	-0.2020	190.0	238.0	1.592
0.490	2.59	1.67E-02	6.21E-03	1.04E-04	-0.1950	190.0	236.0	1.659

Table C-17: Mach 2.8 discrete data turbulence intensity points

y (in)	a	b	sqrt(Re)	f	V _{rms}	V _{bar}	T.I.	y/δ _u FPG
0.278	0.027806	-0.14622		18.064	0.352665	0.0607	1.83	9.405%
0.446	0.027806	-0.14622		20.152	0.338272	0.0517	1.996	7.657%
0.111	0.027806	-0.14622		15.622	0.376857	0.0506	1.64	8.187%
			fbar		0.355931			
y (in)	a	b	sqrt(Re)	f	V _{rms}	V _{bar}	T.I.	y/δ _u ZPG
0.03125	0.027897	-0.10393		17.33	0.318456	0.08133	1.69	15.112%
0.13125	0.027897	-0.10393		20.3	0.30619	0.09089	1.857	15.985%
0.23125	0.027897	-0.10393		21.27	0.303083	0.09676	1.991	16.035%
0.33125	0.027897	-0.10393		21.35	0.302842	0.09012	2.119	14.043%
			fbar		0.307643			
y (in)	a	b	sqrt(Re)	f	V _{rms}	V _{bar}	T.I.	y/δ _u CPG
0.075	0.02387	-0.12132		15.819	0.368353	0.0984	1.749	15.274%
0.185	0.02387	-0.12132		19.674	0.337084	0.1155	2.02	16.963%
0.298	0.02387	-0.12132		23.043	0.320749	0.0916	2.23	12.806%
			fbar		0.342062			

Table C-18: Mach 2.8 hot-film van Driest data

ZPG		FPG			CPG (x = 68 cm)			CPG (x = 70 cm)	
y+	ueff+	y+	ueff+		y+	ueff+		y+	
126.6	12.2		103.5	16.9	140.4	17.1		132.2	19.7
189.1	15.8		182.5	16.6	227.3	19.5		214.7	22.0
249.8	17.2		261.9	16.5	318.0	21.4		300.1	23.2
312.6	18.3		341.2	19.3	404.9	20.8		382.6	21.8
372.5	19.2		419.5	20.4	495.1	22.8		468.1	22.8
434.9	20.4		499.2	21.5	582.9	23.3		550.1	23.5
497.1	20.7		577.9	22.1	672.3	24.4		634.5	24.2
559.3	20.9		657.6	22.4	761.7	24.6		717.7	27.3
622.3	21.4		736.2	23.1	849.9	24.9		800.9	25.0
683.9	21.8		815.9	23.6	940.5	23.0		885.2	24.1
747.2	22.3		895.6	24.1	1028.3	23.5		966.9	27.2
808.0	23.7		974.6	24.4	1119.3	24.5		1052.4	27.6
870.7	23.8		1054.7	24.8	1207.5	24.7		1133.7	26.2
932.9	22.7		1133.7	25.5	1298.5	25.0		1218.8	27.1
995.9	22.8		1214.1	25.5	1386.3	24.8		1300.8	26.6
1058.7	23.0		1293.5	24.8	1476.1	24.7		1384.8	26.8
1120.5	23.0		1374.3	25.5	1564.3	25.3		1465.7	27.2
1183.6	23.1		1453.3	25.1	1650.9	25.0		1548.1	27.0
1245.5	24.1		1532.6	25.8	1740.7	24.9		1632.5	26.9
1308.5	23.3		1609.8	25.9	1825.6	25.0		1714.2	26.9
1344.3	23.7		1688.8	26.5	1916.6	24.7		1798.9	26.9
			1768.9	25.7	1985.4	24.6		1868.4	26.7
			1847.5	25.9					
			1928.0	25.9					
			2006.3	26.2					
			2086.3	25.7					
			2165.3	25.8					
			2245.0	26.1					
			2324.4	26.0					
			2403.0	26.3					
			2483.1	26.2					
			2561.4	26.2					
			2641.5	26.0					
			2719.4	25.8					
			2799.1	25.7					

Table C-19: Mach 2.8 power spectra data

frequency	ZPG, y/d = 0.33	ZPG, y/d = 0.58	ZPG, y/d = 0.83	FPG, y/d = 0.27	FPG, y/d = 0.67	CPG, y/d = 0.21	CPG, y/d = 0.52	CPG, y/d = 0.83
488.3	6.03E-06	4.97E-06	3E-06	1.34E-05	2.47E-05	8.09E-05	0.000158	5.4E-05
976.6	3.4E-06	2.51E-06	1.48E-06	5.31E-06	3.34E-06	2.97E-05	3.05E-05	1.29E-05
1465	4.3E-06	2.6E-06	1.58E-06	3.65E-06	2.33E-06	2.66E-05	1.62E-05	5.03E-06
1953	2.48E-06	1.92E-06	1.32E-06	2.7E-06	1.48E-06	1.94E-05	1.14E-05	3.48E-06
2441	2.15E-06	1.33E-06	1.13E-06	1.93E-06	8.64E-07	1.6E-05	7.43E-06	2.2E-06
2930	2.4E-06	1.42E-06	9.74E-07	1.77E-06	7.95E-07	1.2E-05	6.13E-06	1.99E-06
3418	2.35E-06	1.45E-06	9.83E-07	1.6E-06	1.13E-06	1.03E-05	4.47E-06	1.7E-06
3906	2.58E-06	1.39E-06	9.3E-07	1.24E-06	7.12E-07	8.64E-06	4.42E-06	1.55E-06
4395	2.15E-06	1.05E-06	8.45E-07	1.14E-06	8.12E-07	9.03E-06	2.73E-06	1.43E-06
4883	1.64E-06	1.32E-06	7.75E-07	1.04E-06	6.68E-07	7.24E-06	3.43E-06	1.48E-06
5371	1.89E-06	1.34E-06	7.44E-07	9.93E-07	7.28E-07	5.55E-06	2.79E-06	1.19E-06
5859	1.75E-06	1.19E-06	8.65E-07	9.39E-07	6.91E-07	4.39E-06	2.41E-06	1.11E-06
6348	1.48E-06	1.3E-06	7.08E-07	1.04E-06	9.13E-07	4.5E-06	2.53E-06	1.21E-06
6836	1.35E-06	1.31E-06	5.83E-07	6.5E-07	8.56E-07	3.84E-06	2.38E-06	1.29E-06
7324	1.51E-06	1.05E-06	4.8E-07	7.27E-07	7.67E-07	2.64E-06	2.15E-06	1.23E-06
7813	1.7E-06	1.25E-06	6.97E-07	5.56E-07	7.22E-07	2.61E-06	2.2E-06	1.09E-06
8301	1.33E-06	1.1E-06	8.63E-07	5.74E-07	6.07E-07	2.14E-06	2.25E-06	1.08E-06
8789	1.26E-06	1.2E-06	7.52E-07	5.41E-07	6.28E-07	1.82E-06	1.8E-06	1.26E-06
9277	1.12E-06	1.02E-06	6.71E-07	4.66E-07	7.76E-07	1.68E-06	1.66E-06	1.32E-06
9766	1.32E-06	1.29E-06	6.48E-07	4.73E-07	6.05E-07	1.63E-06	1.66E-06	9.34E-07
10250	1.48E-06	1.15E-06	7.2E-07	4.27E-07	6.5E-07	1.44E-06	1.49E-06	1.28E-06
10740	1.44E-06	9.29E-07	7.77E-07	6.43E-07	7.52E-07	1.21E-06	1.76E-06	1.1E-06
11230	1.44E-06	1.27E-06	6.16E-07	6.14E-07	1.09E-06	2.05E-06	4.01E-06	3.02E-06
11720	1.38E-06	1.13E-06	6.89E-07	3.52E-07	5.11E-07	9.51E-07	1.66E-06	9.29E-07
12210	1.38E-06	1.02E-06	6.26E-07	3.53E-07	5.94E-07	7.77E-07	1.09E-06	1.11E-06
12700	9.17E-07	1.09E-06	6.31E-07	3.16E-07	6.06E-07	8.87E-07	1.09E-06	8.37E-07
13180	9.81E-07	1.05E-06	7.23E-07	3.06E-07	5.89E-07	5.26E-07	1.06E-06	8.54E-07
13670	1.33E-06	1.06E-06	8.24E-07	1.91E-07	6.49E-07	5.35E-07	1.3E-06	8.51E-07
14160	9.98E-07	1.03E-06	6.05E-07	2.27E-07	5.4E-07	4.33E-07	1.21E-06	9.42E-07
14650	1.01E-06	1.12E-06	5.97E-07	2.38E-07	4.18E-07	4.61E-07	1.03E-06	6.93E-07
15140	9.69E-07	9.86E-07	6.3E-07	2.68E-07	4.62E-07	4.34E-07	8.97E-07	9.19E-07
15630	9.09E-07	9.31E-07	5.93E-07	2.11E-07	3.96E-07	2.78E-07	9.56E-07	7.6E-07
16110	1.03E-06	1.36E-06	6.73E-07	1.86E-07	4.42E-07	3.25E-07	8.16E-07	7.61E-07
16600	8.21E-07	9.59E-07	5.95E-07	1.94E-07	4.58E-07	2.94E-07	7.12E-07	7.8E-07
17090	8.92E-07	8.69E-07	5.06E-07	1.5E-07	4.38E-07	2.61E-07	6.15E-07	8.02E-07
17580	6.53E-07	8.73E-07	4.93E-07	1.37E-07	3.04E-07	2.1E-07	7.08E-07	7.16E-07
18070	7.35E-07	1E-06	4.49E-07	1.25E-07	4.39E-07	2.36E-07	9E-07	6.01E-07
18550	8.43E-07	6.61E-07	5.26E-07	1.05E-07	2.52E-07	2.08E-07	5.7E-07	6.04E-07
19040	5.47E-07	1.08E-06	5.23E-07	1.15E-07	3.3E-07	2.07E-07	6.35E-07	6.93E-07
19530	7.14E-07	9.26E-07	3.37E-07	1.03E-07	2.59E-07	1.65E-07	5.66E-07	5.49E-07
20020	6.63E-07	7.4E-07	5.11E-07	1.04E-07	3.14E-07	1.56E-07	6.02E-07	5.78E-07
20510	5.89E-07	7.87E-07	4.18E-07	9.44E-08	2.96E-07	1.47E-07	4.43E-07	4.09E-07
21000	5.88E-07	7.55E-07	5E-07	9.67E-08	2.25E-07	1.68E-07	4.09E-07	3.69E-07
21480	5.78E-07	7.39E-07	4.45E-07	6.5E-08	1.93E-07	1.61E-07	4.33E-07	4.99E-07
21970	3.74E-07	6.74E-07	4.03E-07	6.75E-08	2.38E-07	9.84E-08	3.25E-07	5.09E-07
22460	4.53E-07	5.74E-07	4.73E-07	8.21E-08	1.77E-07	1.18E-07	3.84E-07	4.74E-07
22950	4.66E-07	6.03E-07	4.49E-07	6.39E-08	1.72E-07	1.51E-07	4.59E-07	3.83E-07
23440	4.67E-07	5.93E-07	3.58E-07	6.48E-08	1.55E-07	1E-07	2.85E-07	4.03E-07
23930	4.66E-07	4.84E-07	4.47E-07	5.77E-08	1.73E-07	1.12E-07	3.45E-07	3.01E-07
24410	4.65E-07	5.05E-07	4.14E-07	4.77E-08	1.36E-07	7.09E-08	4E-07	3.85E-07
24900	3.92E-07	5.35E-07	3.68E-07	4.3E-08	1.85E-07	8.17E-08	3.12E-07	3.7E-07
25390	3.97E-07	5.81E-07	3.24E-07	4.46E-08	1.35E-07	6.32E-08	2.7E-07	2.48E-07
25880	4.14E-07	5.5E-07	3.83E-07	4.93E-08	9.23E-08	5.56E-08	1.9E-07	3.53E-07
26370	3.35E-07	5.23E-07	3.91E-07	4E-08	1.17E-07	5.26E-08	2.36E-07	3.39E-07
26860	3.05E-07	4.23E-07	3.66E-07	4.19E-08	1.1E-07	6.63E-08	2.6E-07	2.63E-07
27340	3E-07	5.35E-07	3.5E-07	2.93E-08	1E-07	4.72E-08	2.18E-07	2.55E-07

27830	3.79E-07	4.74E-07	3.22E-07	3.17E-08	9.76E-08	4.21E-08	1.79E-07	3.09E-07
28320	2.94E-07	4.93E-07	3.07E-07	2.81E-08	6.98E-08	4.52E-08	1.51E-07	2.19E-07
28810	3.83E-07	4.62E-07	3.35E-07	2.03E-08	9.15E-08	4.21E-08	1.74E-07	2.41E-07
29300	2.69E-07	4.98E-07	2.47E-07	2.21E-08	8.22E-08	3.52E-08	1.43E-07	2.27E-07
29790	2.93E-07	4.47E-07	3.36E-07	3.22E-08	6.25E-08	3.29E-08	1.77E-07	1.67E-07
30270	2.49E-07	4.52E-07	2.02E-07	1.93E-08	7.11E-08	3.54E-08	1.95E-07	1.89E-07
30760	2.37E-07	3.81E-07	2.63E-07	1.65E-08	7.45E-08	2.63E-08	1.55E-07	2.37E-07
31250	2.66E-07	3.11E-07	2.54E-07	2.17E-08	5.99E-08	2.73E-08	1.35E-07	1.89E-07
31740	2.36E-07	4.5E-07	2.63E-07	1.61E-08	6.29E-08	2.63E-08	1.74E-07	1.26E-07
32230	2.72E-07	3.67E-07	2.6E-07	1.78E-08	5.43E-08	2.46E-08	1.07E-07	1.28E-07
32710	2.79E-07	3.08E-07	2.16E-07	1.49E-08	4.63E-08	1.87E-08	1.08E-07	1.25E-07
33200	2.13E-07	3.65E-07	2.44E-07	1.42E-08	4.11E-08	2.53E-08	7.05E-08	1.08E-07
33690	2.35E-07	3.15E-07	2.07E-07	1.11E-08	4.27E-08	1.53E-08	1.07E-07	1.13E-07
34180	1.71E-07	2.91E-07	2.27E-07	8.26E-09	2.89E-08	1.58E-08	1.11E-07	1.14E-07
34670	1.85E-07	2.45E-07	2.05E-07	9.37E-09	2.2E-08	1.81E-08	8.83E-08	1.12E-07
35160	2.06E-07	2.72E-07	1.77E-07	8.97E-09	3.92E-08	1.88E-08	1.13E-07	1.22E-07
35640	1.74E-07	2.9E-07	1.63E-07	1.09E-08	3.19E-08	2.65E-08	1.28E-07	1.12E-07
36130	2.06E-07	2.32E-07	1.74E-07	7.76E-09	3.46E-08	1.8E-08	8.13E-08	9.41E-08
36620	1.76E-07	2.48E-07	1.9E-07	7.87E-09	2.96E-08	1.54E-08	6.24E-08	8.15E-08
37110	1.64E-07	2.35E-07	2.02E-07	1.21E-08	2.37E-08	1.72E-08	7.25E-08	9.45E-08
37600	1.5E-07	2.32E-07	1.81E-07	6.41E-09	2.48E-08	1.54E-08	7.55E-08	6.77E-08
38090	1.23E-07	2.37E-07	1.92E-07	7.73E-09	2.71E-08	1.51E-08	8.39E-08	7.91E-08
38570	1.13E-07	2.36E-07	1.26E-07	5.96E-09	2.4E-08	1.39E-08	5.19E-08	7.96E-08
39060	1.24E-07	2.09E-07	1.48E-07	6.53E-09	1.75E-08	1.07E-08	5.51E-08	5.87E-08
39550	1.12E-07	1.77E-07	1.48E-07	6.3E-09	2.41E-08	1.24E-08	5.54E-08	6.57E-08
40040	1.26E-07	1.8E-07	1.29E-07	4.47E-09	1.86E-08	1.43E-08	6.27E-08	4.84E-08
40530	1.24E-07	1.93E-07	1.37E-07	5.38E-09	1.62E-08	1.18E-08	5.47E-08	6.58E-08
41020	1.32E-07	2.04E-07	1.75E-07	4.68E-09	1.55E-08			
41500	1.36E-07	1.81E-07	1.2E-07	4.46E-09	1.77E-08			
41990	9.86E-08	2.01E-07	1.04E-07	4.18E-09	1.22E-08			
42480	1.03E-07	1.5E-07	1.22E-07	4.18E-09	1.18E-08			
42970	8.14E-08	1.48E-07	1.34E-07	4.38E-09	1.34E-08			
43460	8.6E-08	1.89E-07	8.89E-08	3.29E-09	1.32E-08			
43950	7.97E-08	1.49E-07	1.19E-07	3.29E-09	1E-08			
44430	1.04E-07	1.4E-07	1.12E-07	3.98E-09	1.53E-08			
44920	8.94E-08	1.24E-07	1.14E-07	3.08E-09	1.17E-08			
45410	8.3E-08	1.27E-07	1.23E-07	2.86E-09	1.18E-08			
45900	6.21E-08	1.21E-07	9.79E-08	2.92E-09	8.88E-09			
46390	7.39E-08	1.07E-07	1.01E-07	2.73E-09	9.3E-09			
46880	7.35E-08	1.51E-07	9.94E-08	3.31E-09	7.83E-09			
47360	6.43E-08	1.22E-07	8.81E-08	3.11E-09	8.27E-09			
47850	6.11E-08	1.08E-07	9.47E-08	3E-09	7.97E-09			
48340	9.19E-08	1.17E-07	8.56E-08	3.41E-09	7.19E-09			
48830	5.64E-08	1.06E-07	8.24E-08	4.15E-09	6.94E-09			
49320	5.82E-08	1.13E-07	9.32E-08	3.57E-09	8.44E-09			
49800	4.51E-08	8.52E-08	6.72E-08	4.44E-09	6.9E-09			
50290	5.23E-08	8.58E-08	8.57E-08	4.47E-09	6.09E-09			
50780	5.35E-08	8.15E-08	7.14E-08	5.1E-09	7.27E-09			
51270	4.9E-08	8.92E-08	6.62E-08	5.22E-09	5.52E-09			
51760	3.94E-08	8.62E-08	6.36E-08	5.18E-09	6.56E-09			
52250	3.84E-08	7.21E-08	6.62E-08	3.92E-09	5.61E-09			
52730	4.25E-08	8.16E-08	7.33E-08	5.18E-09	3.69E-09			
53220	3.85E-08	7.42E-08	4.91E-08	3.07E-09	6.66E-09			
53710	3.5E-08	7.73E-08	5.62E-08	2.91E-09	5.58E-09			
54200	2.5E-08	6.66E-08	5.24E-08	1.8E-09	6.98E-09			
54690	3.72E-08	4.4E-08	3.84E-08	1.74E-09	6.68E-09			
55180	2.74E-08	6.57E-08	5.63E-08		6.05E-09			
55660	3.16E-08	5.81E-08	4.61E-08		7.65E-09			
56150	2.41E-08	4.72E-08	4.7E-08		6.87E-09			
56640	3.14E-08	5.57E-08	4.74E-08		8.8E-09			

57130	2.31E-08	4.39E-08	4.02E-08		9.42E-09		
57620	2.4E-08	5.11E-08	3.24E-08		6.73E-09		
58110	2.13E-08	3.93E-08	3.02E-08		6.35E-09		
58590	1.95E-08	4.8E-08	3.93E-08		5.46E-09		
59080	2.22E-08	5.45E-08	3.41E-08		5.99E-09		
59570	2.17E-08	3.12E-08	3E-08		4.7E-09		
60060	2.07E-08	4.01E-08	3.11E-08		5.19E-09		
60550	1.72E-08	3.39E-08	3.08E-08		3.77E-09		
61040	2.04E-08	4.07E-08	3.21E-08		5.11E-09		
61520	1.33E-08	2.53E-08	2.88E-08		3.53E-09		
62010	1.34E-08	2.68E-08	2.97E-08		3.58E-09		
62500	1.48E-08	2.46E-08	1.84E-08		3.51E-09		
62990	1.21E-08	2.1E-08	1.81E-08		3.7E-09		
63480	1.91E-08	2.67E-08	1.98E-08				
63960	1.23E-08	2.09E-08	1.69E-08				
64450	1.38E-08	2.03E-08	1.59E-08				
64940	1.27E-08	2.33E-08	1.85E-08				
65430	1.06E-08	2.03E-08	1.89E-08				
65920	8.31E-09	2.01E-08	1.82E-08				
66410	9.8E-09	1.87E-08	1.9E-08				
66890	7.91E-09	1.99E-08	1.49E-08				
67380	8.61E-09	1.89E-08	1.72E-08				
67870	6.23E-09	1.47E-08	2.28E-08				
68360	7.97E-09	1.37E-08	1.28E-08				
68850	5.48E-09	1.63E-08	1.16E-08				
69340	7E-09	1.33E-08	1.18E-08				
69820	7.16E-09	1.67E-08	1.18E-08				
70310	3.68E-09	1.12E-08	1.44E-08				
70800	4.46E-09	1.29E-08	1.05E-08				
71290	4.65E-09	1.19E-08	9.02E-09				
71780	4.12E-09	8.68E-09	8.18E-09				
72270	4.53E-09	9.94E-09	9.49E-09				
72750	3.91E-09	1.03E-08	8.36E-09				
73240	3.67E-09	1.04E-08	6.92E-09				
73730	3.38E-09	7.88E-09	6.58E-09				
74220	2.95E-09	6.46E-09	6.92E-09				
74710	3.1E-09	8.36E-09	6.46E-09				
75200	3.67E-09	7.53E-09	6.26E-09				
75680	3.33E-09	6.5E-09	6.53E-09				
76170	3.37E-09	4.58E-09	6.24E-09				
76660	2.69E-09	4.7E-09	6.05E-09				
77150	4.5E-09	5.19E-09	6.55E-09				
77640	3.25E-09	3.79E-09	5.09E-09				
78130	2.69E-09	4.33E-09	4.91E-09				
78610	3.7E-09	4.16E-09	4.84E-09				
79100	3.93E-09	3.69E-09	5.35E-09				
79590	3.47E-09	3.52E-09	4.02E-09				
80080	4.93E-09	3.96E-09	3.72E-09				
80570	4.38E-09	4.04E-09	2.63E-09				
81050	3.41E-09	4E-09	2.16E-09				
81540	3.59E-09	3.51E-09	2.61E-09				
82030	3.09E-09	3.79E-09	1.8E-09				
82520	2.89E-09	3.57E-09	2.54E-09				
83010	2.16E-09	3.76E-09	1.63E-09				
83500	2.65E-09	3.7E-09	1.89E-09				
83980	2.45E-09	3.05E-09	2E-09				
84470	1.92E-09	4.63E-09	1.83E-09				
84960	2.09E-09	4.59E-09	1.92E-09				
85450	1.73E-09	5.15E-09	1.76E-09				
85940	1.59E-09	4.07E-09	1.76E-09				
86430	1.27E-09	5.71E-09	1.92E-09				

86910	1.78E-09	4.71E-09	1.22E-09					
87400	1.55E-09	4.72E-09	1.82E-09					
87890	1.59E-09	3.59E-09	1.6E-09					
88380	1.06E-09	3.9E-09	1.5E-09					
88870	1.05E-09	3.97E-09	1.65E-09					
89360	8.73E-10	4.65E-09	1.47E-09					
89840	9.35E-10	3.15E-09	1.4E-09					
90330	9.68E-10	3.26E-09	1.45E-09					
90820	6.27E-10	3.25E-09	1.31E-09					
91310	7.46E-10	2.35E-09	1.17E-09					
91800	8.73E-10	2.41E-09	1.45E-09					
92290	6.94E-10	2.43E-09	1.35E-09					
92770	6.72E-10	2.16E-09	1.46E-09					
93260	5.37E-10	1.62E-09	1.61E-09					
93750	6.19E-10	1.75E-09	1.11E-09					
94240	4.02E-10	1.74E-09	1.18E-09					
94730	5.52E-10	1.43E-09	1.33E-09					
95210	4.94E-10	1.36E-09	1.85E-09					
95700	4.13E-10	1.28E-09	1.44E-09					
96190	4.69E-10	1.2E-09	1.85E-09					
96680	3.42E-10	9.6E-10	1.82E-09					
97170	3.54E-10	9.88E-10	1.65E-09					
97660	2.96E-10	1.06E-09	1.56E-09					
98140	2.76E-10	9.01E-10	1.52E-09					
98630	2.75E-10	6.95E-10	1.29E-09					
99120	2.93E-10	6.61E-10	1.1E-09					
99610	2.87E-10	6.16E-10	1.2E-09					

Table C-20: Mach 2.8 ZPG PIV data

y (in)	u (m/s)	v (m/s)	uTI (%)	vTI (%)	shear	y/δ _u	y ⁺	u _{eff}	u ⁺
0.014	433.514	14.609	53.389	6.192	9.88E-05	0.035	38.971	465.194	16.210
0.046	443.560	20.154	13.568	4.647	-7.8E-05	0.116	130.522	477.645	16.644
0.078	481.606	15.508	8.489	3.475	-8.9E-05	0.197	222.074	526.193	18.336
0.111	500.204	12.904	8.129	4.180	-5.8E-05	0.279	313.625	550.838	19.194
0.143	520.826	11.498	7.187	4.334	-7.6E-06	0.360	405.177	578.987	20.175
0.175	536.771	13.568	6.738	3.931	0.000115	0.441	496.729	601.422	20.957
0.208	551.751	13.380	6.206	3.452	0.00013	0.523	588.280	623.094	21.712
0.240	567.558	11.181	5.609	2.797	0.000105	0.604	679.832	646.670	22.534
0.272	579.507	10.237	4.296	2.695	1.43E-05	0.685	771.383	665.027	23.173
0.304	589.037	10.259	3.582	2.410	4.6E-06	0.767	862.935	680.037	23.696
0.337	595.952	11.776	3.621	2.090	-1E-06	0.848	954.486	691.149	24.084
0.369	595.304	12.785	2.735	2.620	1.19E-06	0.929	1046.038	690.100	24.047
0.401	579.558	11.051	17.165	2.993	3.09E-06	1.011	1137.590	665.107	23.176
0.434	601.411	9.860	2.602	2.742	-1.3E-05	1.092	1229.141	700.061	24.394
0.466	599.442	11.992	3.121	2.641	-1.2E-05	1.173	1320.693	696.831	24.282
0.498	598.978	14.631	2.603	2.543	1.03E-06	1.255	1412.244	696.072	24.255
0.531	596.450	17.444	2.569	2.537	1.33E-05	1.336	1503.796	691.956	24.112
0.563	593.541	14.807	2.836	2.583	-1.1E-05	1.417	1595.347	687.252	23.948
0.595	597.547	14.877	2.805	3.034	-1.5E-05	1.499	1686.899	693.740	24.174
0.627	602.018	16.747	2.892	2.479	-1.2E-05	1.580	1778.450	701.061	24.429
0.660	604.290	18.742	2.960	2.890	-1.2E-05	1.661	1870.002	704.814	24.560
0.692	603.014	20.725	2.801	3.206	-3E-06	1.743	1961.553	702.703	24.486
0.724	600.511	21.776	2.624	3.080	4.45E-06	1.824	2053.105	698.584	24.343
0.757	602.101	21.328	3.075	2.600	2.13E-06	1.906	2144.656	701.197	24.434
0.789	607.687	17.228	3.251	2.397	9.06E-06	1.987	2236.208	710.470	24.757

Table C-21: Mach 2.8 FPG PIV data - 25 images

y (in)	u (m/s)	v (m/s)	uTI (%)	vTI (%)	shear	y/δ _u
2.042	411.144	31.607	-167.470	-159.012	-172.582	0.061
1.961	517.126	45.202	6.557	18.738	-0.00024	0.129
1.880	529.859	44.705	6.535	18.528	-4.7E-05	0.197
1.799	542.286	40.064	6.659	16.404	-3.7E-05	0.265
1.718	559.302	35.523	6.630	14.085	-6.2E-06	0.333
1.638	569.197	35.365	6.173	13.815	-5.8E-05	0.401
1.557	576.951	35.338	6.679	13.615	3.81E-05	0.469
1.476	582.564	29.688	6.371	11.413	0.000228	0.537
1.395	583.898	28.055	6.214	10.937	0.000188	0.605
1.314	588.501	37.541	5.938	13.820	0.000227	0.673
1.233	599.054	32.099	5.780	11.854	-2E-05	0.741
1.152	608.734	26.967	4.245	10.058	-0.00025	0.809
1.071	607.658	28.944	3.411	11.060	-0.00011	0.877
0.990	610.400	25.392	3.110	9.832	6.51E-05	0.945
0.909	613.976	20.376	4.210	8.805	0.000111	1.013
0.828	615.290	18.943	4.222	8.472	-6.2E-06	1.081
0.747	611.317	17.520	3.897	7.674	-5.4E-05	1.149
0.666	608.042	16.183	3.903	6.914	-3.2E-05	1.217
0.585	605.090	17.893	3.944	7.197	-1.4E-05	1.285
0.505	608.711	19.596	4.122	7.712	-2.8E-05	1.353
0.424	605.350	16.599	7.251	7.234	-0.00011	1.421
0.343	591.270	10.975	16.195	6.139	-8E-07	1.489
0.262	598.123	17.087	5.095	8.014	-5.9E-05	1.557
0.181	600.596	21.672	3.347	8.635	-7.8E-05	1.625
0.100	605.107	7.898	3.229	4.510	-0.00013	1.693

Table C-22: Mach 2.8 FPG PIV data - 93 images

y (in)	u (m/s)	v (m/s)	uTI (%)	vTI (%)	shear	y/δ _u	y ⁺	u _{eff}	u ⁺
0.025	401.798	30.281				0.061	91.59	425.05	15.62
0.054	508.438	40.714	7.547	16.927	6.44E-05	0.129	193.40	557.86	20.50
0.082	529.027	40.966	6.778	16.444	1.29E-04	0.197	295.20	585.60	21.52
0.110	539.129	37.625	7.992	15.021	8.79E-05	0.265	397.00	599.53	22.03
0.138	554.481	34.276	7.535	13.395	8.34E-05	0.333	498.80	621.14	22.82
0.167	564.971	33.749	6.868	13.062	1.39E-04	0.401	600.61	636.25	23.38
0.195	573.944	34.437	6.584	13.129	1.45E-04	0.469	702.41	649.40	23.86
0.223	576.676	32.273	6.466	12.142	1.68E-04	0.537	804.21	653.45	24.01
0.251	582.925	31.884	6.210	12.163	2.59E-04	0.605	906.01	662.80	24.35
0.279	590.046	33.639	5.922	12.505	-7.36E-05	0.673	1007.82	673.60	24.75
0.308	597.133	31.207	5.467	11.446	-3.22E-05	0.741	1109.62	684.51	25.15
0.336	597.509	29.104	8.321	10.793	-7.24E-05	0.809	1211.42	685.10	25.17
0.364	605.792	26.175	4.483	9.832	-5.13E-06	0.877	1313.22	698.08	25.65
0.392	610.852	23.638	4.294	8.949	-6.67E-07	0.945	1415.03	706.14	25.95
0.421	608.306	19.529	4.388	7.851	2.10E-06	1.013	1516.83	702.07	25.80
0.449	609.043	17.798	4.486	7.401	-1.75E-05	1.081	1618.63	703.25	25.84
0.477	611.238	17.073	4.364	7.075	-1.58E-05	1.149	1720.43	706.76	25.97
0.505	609.992	16.746	4.309	6.774	-3.54E-08	1.217	1822.24	704.76	25.90
0.533	606.995	17.616	4.475	6.981	-6.35E-06	1.285	1924.04	699.99	25.72
0.562	606.128	17.559	4.164	7.126	-1.34E-05	1.353	2025.84	698.61	25.67
0.590	605.532	15.035	5.499	6.606	-5.57E-06	1.421	2127.64	697.67	25.64
0.618	602.118	13.934	9.953	6.121	-4.52E-06	1.489	2229.45	692.29	25.44
0.646	606.671	15.681	4.563	6.729	3.53E-05	1.557	2331.25	699.48	25.70
0.675	602.161	13.846	4.990	6.138	7.94E-06	1.625	2433.05	692.36	25.44
0.703	605.395	10.005	3.831	4.653	6.01E-06	1.693	2534.85	697.45	25.63

Table C-23: Mach 2.8 CPG (x = 68 cm) PIV data

y (in)	u (m/s)	v (m/s)	uTI (%)	vTI (%)	shear	y/δ _u
3.176	386.885	-24.305				0.076
3.104	459.956	-31.319	13.657	15.259	-6.39E-05	0.156
3.031	495.582	-34.490	11.405	15.840	4.37E-04	0.236
2.959	519.896	-29.595	10.108	12.867	5.44E-04	0.316
2.886	537.433	-28.303	8.684	11.748	8.13E-04	0.395
2.814	548.670	-29.813	7.616	12.239	1.33E-03	0.475
2.741	556.021	-26.331	11.352	11.281	6.76E-04	0.555
2.669	568.590	-22.500	10.833	9.932	5.16E-04	0.635
2.596	580.834	-20.355	7.214	8.250	5.28E-04	0.715
2.523	585.771	-17.353	6.083	7.056	3.74E-04	0.795
2.451	593.433	-17.943	5.021	7.250	4.56E-04	0.874
2.378	596.967	-14.052	4.714	5.861	-8.94E-06	0.954
2.306	599.615	-12.494	4.444	6.224	-3.86E-04	1.034
2.233	600.659	-10.091	4.183	5.746	-3.12E-04	1.114
2.161	600.977	-8.592	4.124	5.480	-2.17E-04	1.194
2.088	595.692	-5.136	4.262	5.039	-1.58E-04	1.274
2.015	597.548	-3.509	4.090	4.432	-9.28E-05	1.353
1.943	602.682	-3.222	3.964	3.980	-1.55E-04	1.433
1.870	605.255	-5.606	4.097	4.340	-2.13E-04	1.513
1.798	603.632	-9.661	3.922	4.839	1.89E-04	1.593
1.725	600.125	-12.391	3.984	5.299	3.12E-04	1.673
1.653	600.807	-9.436	4.261	4.636	3.31E-04	1.753
1.580	604.552	-3.561	4.105	3.177	9.61E-05	1.832
1.508	602.623	-0.735	3.730	3.602	3.70E-05	1.912

Table C-24: Mach 2.8 CPG ($x = 68$ cm) PIV data

y (in)	u (m/s)	v (m/s)	uTI (%)	vTI (%)	shear	y/ δ_u
2.939	372.645	-34.276				0.178
2.818	486.216	-57.836	12.977	25.031	-1.37E-03	0.375
2.696	509.971	-60.384	10.802	25.028	-3.52E-03	0.573
2.575	538.253	-58.376	8.350	22.637	7.75E-04	0.770
2.453	562.558	-56.920	6.027	21.208	5.93E-04	0.967
2.332	573.278	-52.220	5.097	19.224	-4.25E-04	1.165
2.210	578.005	-42.729	4.696	15.464	1.68E-04	1.362
2.089	583.401	-32.907	4.432	11.949	1.47E-04	1.559
1.968	591.659	-25.485	3.951	9.527	1.15E-04	1.756
1.846	601.144	-16.466	4.377	6.759	9.98E-05	1.954
1.725	608.967	-10.690	5.712	4.687	-3.14E-05	2.151
1.603	608.813	-10.988	4.269	4.988	1.98E-04	2.348
1.482	608.541	-6.166	4.214	4.445	1.75E-04	2.546
1.360	609.529	-6.498	3.610	3.828	1.48E-04	2.743
1.239	611.187	-9.528	3.760	4.695	-4.94E-05	2.940
1.118	610.677	-11.504	4.475	5.098	-2.86E-05	3.137
0.996	607.883	-3.981	3.850	4.503	1.80E-05	3.335
0.875	599.867	-2.595	3.874	4.107	2.41E-05	3.532
0.753	603.164	-10.046	3.837	4.830	-3.23E-05	3.729
0.632	608.016	-8.008	3.693	4.610	2.99E-05	3.926
0.510	604.416	-7.928	3.611	4.503	5.31E-05	4.124
0.389	606.330	-5.445	4.472	3.429	5.69E-07	4.321
0.268	605.420	-7.244	4.457	4.279	-6.67E-05	4.518
0.146	600.821	-13.160	3.609	5.597	-2.06E-05	4.716
0.025	604.982	-9.446	4.007	5.286	-1.09E-04	4.913

Table C-25: PIV van Driest data

ZPG	y ⁺	ueff [*]	FPG		CPG ($x = 68$ cm)		CPG ($x = 70$ cm)	
			y ⁺	ueff [*]	y ⁺	ueff [*]	y ⁺	ueff [*]
39.0	16.2		91.6	15.6	110.0	15.5	222.9	15.8
130.5	16.6		193.4	20.5	225.3	18.9	469.7	21.4
222.1	18.3		295.2	21.5	340.7	20.6	716.5	22.7
313.6	19.2		397.0	22.0	456.0	21.9	963.3	24.3
405.2	20.2		498.8	22.8	571.4	22.8	1210.1	25.7
496.7	21.0		600.6	23.4	686.7	23.4	1456.9	26.3
588.3	21.7		702.4	23.9	802.1	23.8	1703.6	26.6
679.8	22.5		804.2	24.0	917.4	24.5	1950.4	26.9
771.4	23.2		906.0	24.4	1032.8	25.2	2197.2	27.4
862.9	23.7		1007.8	24.8	1148.1	25.5	2444.0	28.0
954.5	24.1		1109.6	25.2	1263.5	26.0	2690.8	28.5
1046.0	24.0		1211.4	25.2	1378.8	26.2	2937.6	28.5
1137.6	23.2		1313.2	25.7	1494.2	26.3	3184.3	28.5
1229.1	24.4		1415.0	25.9	1609.5	26.4	3431.1	28.6
1320.7	24.3		1516.8	25.8	1724.9	26.4	3677.9	28.7
1412.2	24.3		1618.6	25.8	1840.2	26.1	3924.7	28.7
1503.8	24.1		1720.4	26.0	1955.6	26.2	4171.5	28.5
1595.3	23.9		1822.2	25.9	2070.9	26.5	4418.3	28.0
1686.9	24.2		1924.0	25.7	2186.2	26.7	4665.1	28.2
1778.5	24.4		2025.8	25.7	2301.6	26.6	4911.8	28.5
1870.0	24.6		2127.6	25.6	2416.9	26.4	5158.6	28.2
1961.6	24.5		2229.4	25.4	2532.3	26.4	5405.4	28.4
2053.1	24.3		2331.2	25.7	2647.6	26.6	5652.2	28.3
2144.7	24.4		2433.0	25.4	2763.0	26.5	5899.0	28.0
2236.2	24.8		2534.9	25.6			6145.8	28.3

Table C-26: Mach 1.7 ZPG pressure data

y (in)	P ₁₁ (psia)	P ₁₂ (psia)	P ₁₂ / P ₁₁	p _c / P ₁₂	Mach	M/M _e	u/U _e	p _w / p	p / p _e
0.072	13.735	6.615	0.482	0.425	1.182	0.712	0.784	0.775	0.832
0.077	13.733	6.847	0.499	0.410	1.210	0.729	0.799	0.767	0.840
0.083	13.734	7.203	0.524	0.390	1.253	0.755	0.820	0.755	0.853
0.088	13.735	7.508	0.547	0.374	1.287	0.775	0.837	0.746	0.864
0.093	13.735	7.915	0.576	0.355	1.332	0.802	0.858	0.733	0.879
0.098	13.734	8.287	0.603	0.339	1.371	0.826	0.877	0.723	0.892
0.103	13.733	8.713	0.634	0.322	1.414	0.852	0.897	0.711	0.907
0.108	13.732	9.080	0.661	0.309	1.450	0.874	0.913	0.701	0.920
0.114	13.733	9.438	0.687	0.298	1.486	0.895	0.928	0.691	0.933
0.119	13.735	9.788	0.713	0.287	1.519	0.915	0.943	0.682	0.945
0.125	13.736	10.094	0.735	0.278	1.547	0.932	0.954	0.675	0.956
0.130	13.735	10.326	0.752	0.272	1.567	0.944	0.963	0.669	0.963
0.135	13.734	10.548	0.768	0.266	1.586	0.956	0.971	0.664	0.971
0.141	13.734	10.751	0.783	0.261	1.604	0.966	0.978	0.659	0.978
0.146	13.734	10.897	0.793	0.258	1.617	0.974	0.983	0.656	0.983
0.151	13.734	11.030	0.803	0.255	1.629	0.981	0.988	0.653	0.988
0.157	13.735	11.105	0.808	0.253	1.636	0.985	0.991	0.651	0.990
0.162	13.736	11.201	0.815	0.251	1.644	0.990	0.994	0.649	0.993
0.168	13.736	11.247	0.819	0.250	1.647	0.992	0.995	0.648	0.995
0.173	13.735	11.273	0.821	0.249	1.650	0.994	0.996	0.647	0.996
0.178	13.736	11.311	0.823	0.248	1.653	0.996	0.997	0.647	0.997
0.184	13.734	11.318	0.824	0.248	1.654	0.996	0.998	0.646	0.998
0.189	13.735	11.333	0.825	0.248	1.655	0.997	0.998	0.646	0.998
0.194	13.736	11.333	0.825	0.248	1.656	0.997	0.998	0.646	0.998
0.199	13.735	11.344	0.826	0.248	1.656	0.998	0.999	0.646	0.999
0.205	13.734	11.336	0.825	0.248	1.656	0.998	0.999	0.646	0.998
0.210	13.735	11.342	0.826	0.248	1.657	0.998	0.999	0.646	0.999
0.216	13.735	11.335	0.825	0.248	1.656	0.998	0.998	0.646	0.998
0.221	13.735	11.343	0.826	0.248	1.657	0.998	0.999	0.646	0.999
0.227	13.736	11.343	0.826	0.248	1.657	0.998	0.999	0.646	0.999
0.232	13.738	11.354	0.826	0.247	1.658	0.999	0.999	0.645	0.999
0.238	13.734	11.343	0.826	0.248	1.657	0.998	0.999	0.646	0.999
0.243	13.734	11.347	0.826	0.247	1.657	0.998	0.999	0.645	0.999
0.248	13.732	11.344	0.826	0.248	1.657	0.998	0.999	0.646	0.999
0.253	13.735	11.341	0.826	0.248	1.657	0.998	0.999	0.646	0.999
0.259	13.734	11.345	0.826	0.248	1.657	0.998	0.999	0.646	0.999
0.265	13.733	11.333	0.825	0.248	1.656	0.997	0.998	0.646	0.998
0.270	13.736	11.326	0.825	0.248	1.655	0.997	0.998	0.646	0.998
0.275	13.735	11.331	0.825	0.248	1.656	0.997	0.998	0.646	0.998
0.281	13.735	11.336	0.825	0.248	1.656	0.998	0.998	0.646	0.998
0.286	13.738	11.336	0.825	0.248	1.656	0.998	0.998	0.646	0.998
0.291	13.736	11.324	0.824	0.248	1.655	0.997	0.998	0.646	0.998
0.296	13.736	11.321	0.824	0.248	1.655	0.997	0.998	0.646	0.998
0.302	13.735	11.326	0.825	0.248	1.655	0.997	0.998	0.646	0.998
0.307	13.734	11.325	0.825	0.248	1.655	0.997	0.998	0.646	0.998
0.313	13.733	11.329	0.825	0.248	1.655	0.997	0.998	0.646	0.998
0.318	13.733	11.329	0.825	0.248	1.656	0.997	0.998	0.646	0.998
0.324	13.732	11.339	0.826	0.248	1.656	0.998	0.999	0.646	0.999
0.329	13.733	11.342	0.826	0.248	1.657	0.998	0.999	0.646	0.999
0.335	13.733	11.359	0.827	0.247	1.658	0.999	0.999	0.645	0.999
0.340	13.734	11.371	0.828	0.247	1.659	0.999	1.000	0.645	1.000
0.345	13.734	11.361	0.827	0.247	1.658	0.999	0.999	0.645	0.999
0.350	13.734	11.368	0.828	0.247	1.659	0.999	1.000	0.645	1.000
0.356	13.734	11.358	0.827	0.247	1.658	0.999	0.999	0.645	0.999
0.361	13.736	11.354	0.827	0.247	1.658	0.999	0.999	0.645	0.999
0.367	13.734	11.361	0.827	0.247	1.658	0.999	0.999	0.645	0.999
0.372	13.735	11.360	0.827	0.247	1.658	0.999	0.999	0.645	0.999

0.377	13.733	11.366	0.828	0.247	1.659	0.999	0.999	0.645	0.999
0.383	13.733	11.380	0.829	0.247	1.660	1.000	1.000	0.645	1.000
0.388	13.731	11.389	0.829	0.247	1.661	1.000	1.000	0.645	1.000
0.393	13.732	11.402	0.830	0.246	1.662	1.001	1.001	0.644	1.001
0.399	13.729	11.450	0.834	0.245	1.666	1.003	1.002	0.643	1.002
0.404	13.731	11.498	0.837	0.244	1.670	1.006	1.004	0.642	1.004
0.410	13.733	11.528	0.839	0.244	1.672	1.007	1.005	0.641	1.005
0.415	13.733	11.541	0.840	0.243	1.673	1.008	1.005	0.641	1.005
0.420	13.732	11.542	0.841	0.243	1.673	1.008	1.005	0.641	1.005
0.426	13.731	11.558	0.842	0.243	1.675	1.009	1.006	0.641	1.006
0.431	13.732	11.552	0.841	0.243	1.674	1.009	1.006	0.641	1.006
0.437	13.734	11.566	0.842	0.243	1.675	1.009	1.006	0.641	1.006
0.442	13.732	11.563	0.842	0.243	1.675	1.009	1.006	0.641	1.006
0.447	13.733	11.574	0.843	0.243	1.676	1.010	1.006	0.641	1.007
0.452	13.729	11.574	0.843	0.243	1.676	1.010	1.006	0.641	1.007
0.458	13.732	11.585	0.844	0.242	1.677	1.010	1.007	0.640	1.007
0.463	13.731	11.586	0.844	0.242	1.677	1.010	1.007	0.640	1.007
0.469	13.733	11.599	0.845	0.242	1.678	1.011	1.007	0.640	1.007
0.474	13.733	11.606	0.845	0.242	1.679	1.011	1.007	0.640	1.008
0.480	13.733	11.611	0.845	0.242	1.679	1.012	1.007	0.640	1.008
0.485	13.731	11.624	0.847	0.242	1.680	1.012	1.008	0.639	1.008
0.490	13.734	11.620	0.846	0.242	1.680	1.012	1.008	0.640	1.008
0.495	13.733	11.629	0.847	0.241	1.681	1.013	1.008	0.639	1.008
0.501	13.734	11.646	0.848	0.241	1.682	1.013	1.009	0.639	1.009
0.506	13.731	11.646	0.848	0.241	1.682	1.013	1.009	0.639	1.009
0.512	13.733	11.658	0.849	0.241	1.683	1.014	1.009	0.639	1.009
0.517	13.735	11.665	0.849	0.241	1.684	1.014	1.009	0.639	1.010

Table C-27: Mach 1.7 FPG pressure data

y (in)	P ₁₁ (psia)	P ₁₂ (psia)	P _{T2} / P _{T1}	p _c / P _{T2}	MACH	T (K)	P (Pa)	ρ (kg/m ³)	p / p _e	M/M _e	u/U _e
0.063	13.711	5.698	0.416	0.418	1.195	230.2	10372	0.157	0.476	0.675	0.760
0.068	13.712	6.052	0.441	0.394	1.244	225.9	10895	0.168	0.509	0.703	0.784
0.074	13.713	6.408	0.467	0.372	1.292	221.8	11397	0.179	0.543	0.730	0.806
0.080	13.714	6.725	0.490	0.354	1.333	218.3	11965	0.191	0.579	0.753	0.825
0.086	13.712	7.020	0.512	0.339	1.370	215.2	12490	0.202	0.613	0.774	0.842
0.092	13.714	7.303	0.533	0.326	1.404	212.3	13027	0.214	0.648	0.793	0.857
0.098	13.712	7.556	0.551	0.315	1.434	209.7	13546	0.225	0.682	0.810	0.870
0.104	13.712	7.874	0.574	0.303	1.470	206.6	14042	0.237	0.718	0.830	0.885
0.110	13.710	8.182	0.597	0.291	1.504	203.7	14570	0.249	0.755	0.850	0.899
0.115	13.711	8.424	0.614	0.283	1.531	201.5	15081	0.261	0.791	0.865	0.910
0.122	13.710	8.688	0.634	0.274	1.559	199.2	15629	0.273	0.829	0.881	0.921
0.127	13.713	8.875	0.647	0.268	1.579	197.5	16134	0.285	0.863	0.892	0.929
0.133	13.712	9.136	0.666	0.261	1.605	195.3	16674	0.298	0.902	0.907	0.940
0.140	13.713	9.422	0.687	0.253	1.634	192.9	17222	0.311	0.943	0.923	0.951
0.146	13.710	9.669	0.705	0.246	1.659	190.9	17758	0.324	0.983	0.937	0.960
0.151	13.708	9.740	0.711	0.245	1.665	190.3	18281	0.335	1.015	0.941	0.962
0.157	13.710	9.948	0.726	0.239	1.687	188.6	18783	0.347	1.052	0.953	0.970
0.163	13.708	10.101	0.737	0.236	1.702	187.4	19308	0.359	1.088	0.962	0.976
0.169	13.710	10.260	0.748	0.232	1.717	186.2	19830	0.371	1.125	0.970	0.981
0.175	13.710	10.414	0.760	0.229	1.732	185.0	20349	0.383	1.162	0.978	0.987
0.181	13.711	10.491	0.765	0.227	1.738	184.5	20883	0.394	1.196	0.982	0.989
0.187	13.712	10.567	0.771	0.225	1.745	183.9	21408	0.406	1.229	0.986	0.991
0.193	13.710	10.631	0.775	0.224	1.751	183.4	21954	0.417	1.264	0.989	0.993
0.199	13.709	10.646	0.777	0.224	1.754	183.2	22496	0.428	1.297	0.991	0.994
0.205	13.711	10.652	0.777	0.224	1.756	183.1	23015	0.438	1.328	0.992	0.995
0.210	13.709	10.670	0.778	0.223	1.757	183.0	23523	0.448	1.358	0.993	0.996
0.216	13.712	10.695	0.780	0.223	1.759	182.8	24045	0.458	1.389	0.994	0.996
0.222	13.708	10.707	0.781	0.222	1.761	182.7	24559	0.468	1.420	0.995	0.997
0.228	13.708	10.731	0.783	0.222	1.763	182.5	25104	0.479	1.453	0.996	0.997
0.234	13.710	10.726	0.782	0.222	1.763	182.5	25615	0.489	1.483	0.996	0.998
0.240	13.709	10.753	0.784	0.222	1.765	182.3	26149	0.500	1.515	0.997	0.998
0.246	13.709	10.753	0.784	0.222	1.765	182.3	26700	0.510	1.547	0.997	0.998
0.252	13.710	10.762	0.785	0.221	1.766	182.2	27236	0.521	1.579	0.998	0.999
0.258	13.711	10.769	0.785	0.221	1.767	182.2	27767	0.531	1.610	0.998	0.999
0.264	13.710	10.774	0.786	0.221	1.767	182.1	28289	0.541	1.641	0.999	0.999
0.270	13.712	10.787	0.787	0.221	1.768	182.1	28806	0.551	1.671	0.999	0.999
0.276	13.712	10.793	0.787	0.221	1.769	182.0	29331	0.562	1.702	0.999	1.000
0.282	13.711	10.791	0.787	0.221	1.769	182.0	29859	0.572	1.733	1.000	1.000
0.288	13.712	10.785	0.787	0.221	1.769	182.0	30381	0.582	1.763	0.999	1.000
0.294	13.711	10.799	0.788	0.221	1.770	181.9	30929	0.592	1.796	1.000	1.000
0.300	13.713	10.804	0.788	0.221	1.770	181.9	31469	0.603	1.827	1.000	1.000
0.306	13.712	10.803	0.788	0.221	1.770	181.9	32005	0.613	1.859	1.000	1.000
0.312	13.712	10.806	0.788	0.220	1.771	181.9	32551	0.624	1.890	1.000	1.000
0.318	13.708	10.805	0.788	0.220	1.771	181.9	33056	0.633	1.920	1.000	1.000
0.324	13.708	10.805	0.788	0.220	1.771	181.9	33569	0.643	1.949	1.000	1.000
0.329	13.709	10.810	0.789	0.220	1.771	181.8	34083	0.653	1.980	1.001	1.000
0.335	13.708	10.810	0.789	0.220	1.771	181.8	34625	0.663	2.011	1.001	1.000
0.341	13.709	10.807	0.788	0.220	1.771	181.9	35156	0.674	2.042	1.000	1.000
0.347	13.712	10.819	0.789	0.220	1.772	181.8	35684	0.684	2.074	1.001	1.001
0.353	13.712	10.822	0.789	0.220	1.772	181.8	36221	0.694	2.105	1.001	1.001
0.360	13.709	10.814	0.789	0.220	1.771	181.8	36766	0.705	2.136	1.001	1.001
0.366	13.711	10.817	0.789	0.220	1.772	181.8	37303	0.715	2.167	1.001	1.001
0.371	13.711	10.823	0.789	0.220	1.772	181.8	37828	0.725	2.198	1.001	1.001
0.377	13.709	10.824	0.790	0.220	1.772	181.7	38318	0.735	2.227	1.001	1.001
0.383	13.712	10.837	0.790	0.220	1.774	181.7	38849	0.745	2.259	1.002	1.001
0.389	13.712	10.832	0.790	0.220	1.773	181.7	39363	0.755	2.288	1.002	1.001

0.395	13.714	10.837	0.790	0.220	1.774	181.7	39902	0.765	2.320	1.002	1.001
0.401	13.712	10.835	0.790	0.220	1.773	181.7	40430	0.775	2.351	1.002	1.001
0.407	13.713	10.849	0.791	0.220	1.775	181.6	40952	0.786	2.383	1.003	1.002
0.413	13.711	10.845	0.791	0.220	1.774	181.6	41509	0.796	2.415	1.002	1.002
0.419	13.709	10.856	0.792	0.219	1.775	181.5	42040	0.807	2.446	1.003	1.002
0.425	13.712	10.848	0.791	0.220	1.775	181.6	42580	0.817	2.477	1.003	1.002
0.431	13.712	10.854	0.792	0.219	1.775	181.5	43084	0.827	2.507	1.003	1.002
0.437	13.712	10.846	0.791	0.220	1.774	181.6	43621	0.837	2.537	1.002	1.002
0.442	13.712	10.850	0.791	0.220	1.775	181.6	44126	0.847	2.567	1.003	1.002
0.448	13.711	10.853	0.792	0.219	1.775	181.5	44671	0.857	2.599	1.003	1.002
0.454	13.712	10.858	0.792	0.219	1.776	181.5	45202	0.868	2.631	1.003	1.002
0.460	13.711	10.863	0.792	0.219	1.776	181.5	45727	0.878	2.662	1.003	1.002
0.466	13.713	10.868	0.793	0.219	1.776	181.4	46273	0.889	2.694	1.004	1.002
0.473	13.709	10.878	0.793	0.219	1.777	181.4	46815	0.899	2.727	1.004	1.003
0.478	13.709	10.882	0.794	0.219	1.778	181.3	47334	0.910	2.758	1.004	1.003
0.484	13.711	10.889	0.794	0.219	1.778	181.3	47859	0.920	2.789	1.005	1.003
0.490	13.709	10.894	0.795	0.219	1.779	181.2	48376	0.930	2.819	1.005	1.003
0.496	13.710	10.894	0.795	0.219	1.779	181.2	48881	0.940	2.849	1.005	1.003
0.502	13.712	10.909	0.796	0.218	1.780	181.1	49426	0.951	2.882	1.006	1.004
0.508	13.710	10.914	0.796	0.218	1.781	181.1	49963	0.961	2.914	1.006	1.004
0.514	13.710	10.916	0.796	0.218	1.781	181.1	50494	0.972	2.946	1.006	1.004
0.520	13.710	10.917	0.796	0.218	1.781	181.1	51042	0.982	2.978	1.006	1.004
0.526	13.708	10.923	0.797	0.218	1.782	181.0	51570	0.993	3.009	1.007	1.004
0.532	13.712	10.943	0.798	0.218	1.783	180.9	52086	1.003	3.042	1.008	1.005
0.538	13.708	10.938	0.798	0.218	1.783	180.9	52608	1.013	3.072	1.007	1.004
0.543	13.709	10.944	0.798	0.218	1.783	180.9	53110	1.023	3.102	1.008	1.005

Table C-28: Mach 1.7 ZPG hot-film data - traverse up

y (in)	T_1 / T_{11}	Multiple overheat data				Single overheat data			y/δ_u
		$Re^{1/2}$	$(\rho u)_{rms}$	$(T_1)_{rms}$	$\rho u / \rho u_\infty$	$Re^{1/2}$	$(\rho u)_{rms}$	$\rho u / \rho u_\infty$	
0.0183	1.004	16.692	4.68E-02	3.91E-02	0.623	16.744	0.0527	0.6304	0.1169
0.0293	0.998	16.968	3.30E-02	6.23E-02	0.644	16.983	0.05342	0.6486	0.1871
0.0401	0.999	17.303	5.81E-02	4.09E-02	0.669	17.325	0.06199	0.6750	0.2561
0.0509	1.003	17.759	5.59E-02	5.74E-02	0.705	17.763	0.06576	0.7095	0.3250
0.0617	1.008	18.238	6.36E-02	4.87E-02	0.744	18.245	0.06964	0.7485	0.3940
0.0723	1.003	18.681	5.35E-02	5.63E-02	0.780	18.671	0.06529	0.7839	0.4617
0.0833	1.003	19.063	5.27E-02	5.10E-02	0.812	19.078	0.06156	0.8185	0.5319
0.0941	1.004	19.424	5.08E-02	4.43E-02	0.843	19.419	0.05845	0.8480	0.6009
0.105	1.007	19.743	4.40E-02	4.62E-02	0.871	19.759	0.05405	0.8779	0.6705
0.1163	1.009	20.016	4.40E-02	3.62E-02	0.896	20.037	0.05035	0.9028	0.7427
0.1273	1.006	20.251	3.57E-02	3.58E-02	0.917	20.272	0.04424	0.9241	0.8129
0.1381	1.007	20.446	2.86E-02	3.67E-02	0.935	20.455	0.03944	0.9409	0.8819
0.1489	1.003	20.598	3.01E-02	2.54E-02	0.948	20.6	0.03542	0.9543	0.9508
0.16	1.001	20.719	3.54E-02	1.54E-02	0.960	20.697	0.03305	0.9633	1.0217
0.1711	1	20.803	2.56E-02	1.60E-02	0.967	20.778	0.02836	0.9708	1.0926
0.1821	0.999	20.867	9.37E-03	3.23E-02	0.973	20.848	0.02521	0.9774	1.1628
0.1929	0.999	20.91	1.89E-02	2.29E-02	0.977	20.897	0.02443	0.9820	1.2318
0.2038	0.999	20.937	1.86E-02	1.85E-02	0.980	20.914	0.02295	0.9836	1.3014
0.215	0.998	20.97	1.67E-02	1.81E-02	0.983	20.943	0.02137	0.9863	1.3729
0.2261	0.998	20.988	1.56E-02	1.46E-02	0.985	20.951	0.01952	0.9870	1.4438
0.237	1	21	1.92E-02	7.79E-03	0.986	20.97	0.01922	0.9888	1.5134
0.2477	1.002	21.008	2.22E-02	1.17E-02	0.987	20.992	0.01946	0.9909	1.5817
0.2588	1.007	21.022	1.86E-02	6.26E-03	0.988	21.015	0.01786	0.9931	1.6526
0.2699	1.01	21.038	8.24E-03	1.89E-02	0.989	21.041	0.01601	0.9955	1.7235
0.2808	1.012	21.048	1.20E-02	1.60E-02	0.990	21.05	0.01633	0.9964	1.7931
0.2916	1.014	21.064	1.43E-02	4.03E-03	0.992	21.073	0.01584	0.9986	1.8621
0.3024	1.015	21.063	7.52E-03	1.62E-02	0.992	21.077	0.01526	0.9990	1.9310
0.3136	1.017	21.067	4.90E-03	1.71E-02	0.992	21.098	0.01508	1.0009	2.0026
0.3246	1.017	21.071	1.88E-02	1.31E-02	0.993	21.111	0.01553	1.0022	2.0728
0.3355	1.014	21.082	1.69E-02	9.18E-03	0.994	21.121	0.01561	1.0031	2.1424
0.3462	1.011	21.097	1.39E-02	1.51E-03	0.995	21.125	0.01531	1.0035	2.2107
0.3573	1.008	21.122	1.45E-02	5.32E-03	0.997	21.142	0.01553	1.0051	2.2816
0.3684	1.006	21.143	1.68E-02	1.28E-02	0.999	21.154	0.01544	1.0063	2.3525
0.3793	1.005	21.157	2.07E-02	1.51E-02	1.001	21.162	0.01691	1.0070	2.4221
0.3901	1.004	21.166	1.33E-02	7.34E-03	1.002	21.163	0.0148	1.0071	2.4911
0.4009	1.005	21.173	1.27E-02	5.21E-03	1.002	21.174	0.01465	1.0082	2.5600
0.4121	1.005	21.175	2.36E-02	2.28E-02	1.002	21.174	0.01635	1.0082	2.6315
0.423	1.004	21.172	1.97E-02	1.86E-02	1.002	21.165	0.01508	1.0073	2.7011
0.434	1.004	21.166	2.19E-02	2.05E-02	1.002	21.154	0.01599	1.0063	2.7714
0.4448	1.003	21.157	1.45E-02	8.83E-03	1.001	21.134	0.01452	1.0044	2.8404
0.4558	1.001	21.152	9.35E-03	1.29E-02	1.000	21.117	0.01491	1.0028	2.9106
0.4668	1	21.147	2.13E-02	2.26E-02	1.000	21.105	0.01507	1.0016	2.9808
0.4777	0.999	21.142	1.46E-02	4.61E-03	0.999	21.091	0.01468	1.0003	3.0504
0.4858	0.998	21.148	9.51E-03	8.65E-03	1.000	21.092	0.01363	1.0004	3.1022
0.4867	0.997	21.15	1.14E-02	1.20E-02	1.000	21.088	0.01492	1.0000	3.1079

Table C-29: Mach 1.7 ZPG hot-film data - traverse down

y (in)	T _t / T _{t1}	Re ^{1/2}	(ρu) _{rms}	(T _t) _{rms}	ρu / ρu _∞	Re ^{1/2}	(ρu) _{rms}	ρu / ρu _∞	y/δ _u
0.0194	0.984	16.687	2.63E-02	6.54E-02	0.6249	16.677	0.05189	0.6263	0.1239
0.0306	0.982	16.968	4.11E-02	5.58E-02	0.6453	16.94	0.05576	0.6462	0.1954
0.0414	0.976	17.321	3.77E-02	7.68E-02	0.6696	17.249	0.06129	0.6700	0.2644
0.052	0.981	17.754	5.02E-02	7.58E-02	0.7059	17.703	0.06851	0.7057	0.3321
0.0632	0.984	18.214	5.33E-02	6.97E-02	0.7445	18.16	0.06788	0.7426	0.4036
0.0745	0.981	18.659	5.87E-02	5.28E-02	0.7797	18.589	0.0668	0.7781	0.4757
0.0855	0.985	19.078	5.59E-02	5.18E-02	0.8174	19.027	0.06365	0.8152	0.5460
0.0962	0.98	19.434	5.35E-02	4.96E-02	0.8453	19.344	0.05954	0.8426	0.6143
0.1071	0.992	19.74	5.15E-02	3.95E-02	0.8792	19.7	0.05594	0.8739	0.6839
0.1184	0.986	20.015	4.98E-02	2.91E-02	0.9002	19.962	0.05084	0.8973	0.7561
0.1295	0.986	20.217	4.30E-02	2.99E-02	0.9185	20.138	0.04596	0.9132	0.8269
0.1403	0.986	20.426	4.02E-02	2.83E-02	0.9376	20.349	0.04231	0.9325	0.8959
0.1506	0.985	20.562	3.56E-02	2.50E-02	0.9495	20.464	0.03733	0.9430	0.9617
0.1611	0.983	20.679	3.67E-02	1.43E-02	0.9590	20.557	0.03516	0.9516	1.0287
0.1724	0.99	20.775	3.22E-02	4.30E-03	0.9725	20.689	0.03019	0.9639	1.1009
0.1834	0.99	20.833	2.92E-02	9.37E-03	0.9780	20.757	0.02689	0.9702	1.1711
0.194	0.991	20.876	2.85E-02	1.42E-02	0.9827	20.796	0.02601	0.9739	1.2388
0.2048	0.989	20.926	2.68E-02	1.45E-02	0.9861	20.846	0.02375	0.9786	1.3078
0.2162	0.988	20.953	2.74E-02	2.17E-02	0.9879	20.868	0.02244	0.9806	1.3806
0.2273	0.988	20.974	2.59E-02	1.89E-02	0.9899	20.897	0.02091	0.9834	1.4515
0.2382	0.993	20.983	2.20E-02	6.81E-03	0.9941	20.925	0.01995	0.9860	1.5211
0.2488	0.996	20.996	2.06E-02	3.47E-03	0.9973	20.948	0.019	0.9882	1.5888
0.2599	0.998	21.007	1.12E-02	1.72E-02	0.9997	20.965	0.01705	0.9898	1.6596
0.2711	1.001	21.018	1.39E-02	1.40E-02	1.0028	20.983	0.01707	0.9915	1.7312
0.2821	1.004	21.027	1.57E-02	1.09E-02	1.0056	21.003	0.0168	0.9934	1.8014
0.2928	1.006	21.036	1.17E-02	1.44E-02	1.0078	21.02	0.016	0.9950	1.8697
0.3035	1.007	21.041	1.31E-02	1.25E-02	1.0090	21.036	0.01586	0.9965	1.9381
0.3148	1.007	21.042	1.23E-02	1.05E-02	1.0091	21.041	0.01538	0.9970	2.0102
0.3259	1.008	21.048	1.11E-02	1.08E-02	1.0103	21.052	0.01429	0.9980	2.0811
0.3366	1.007	21.062	1.12E-02	1.28E-02	1.0110	21.06	0.01531	0.9988	2.1494
0.3472	1.004	21.085	1.09E-02	9.28E-03	1.0112	21.073	0.01474	1.0000	2.2171
0.3583	1.001	21.109	8.94E-03	1.29E-02	1.0115	21.087	0.01398	1.0013	2.2880
0.3695	1.001	21.13	1.59E-02	1.10E-02	1.0135	21.106	0.01515	1.0031	2.3595
0.3805	1	21.141	1.17E-02	5.32E-03	1.0139	21.11	0.014	1.0035	2.4298
0.3912	1	21.152	1.43E-02	6.80E-03	1.0149	21.12	0.01469	1.0045	2.4981
0.4019	1	21.176	3.56E-02	5.07E-02	1.0172	21.119	0.01383	1.0044	2.5664
0.4133	1.001	21.207	5.92E-02	8.20E-02	1.0209	21.13	0.01489	1.0054	2.6392
0.4244	1.006	21.44	1.20E-01	1.59E-01	1.0469	21.13	0.01473	1.0054	2.7101
0.4352	1.01	21.637	3.47E-02	4.66E-02	1.0691	21.117	0.01358	1.0042	2.7791
0.4458	1.009	21.612	3.57E-02	4.80E-02	1.0659	21.105	0.01352	1.0030	2.8467
0.4568	1.022	21.694	3.70E-02	7.04E-02	1.0832	21.101	0.01443	1.0027	2.9170
0.468	1.044	21.852	5.39E-02	1.00E-01	1.1147	21.09	0.01345	1.0016	2.9885

Table C-30: Mach 1.7 ZPG separated turbulence variables - traverse down

y (inch)	Mach	(ρ) _{rms}	U _{rms}	ρ'U'	u''/u	pbarubar	pubar	y/δ _u
0.029	0.97	3.92E-02	8.50E-02	-3.84E-03	-2.44E-01	78.6	104.0	0.188
0.040	1.03	3.14E-02	6.43E-02	-8.74E-04	-2.07E-01	85.7	108.0	0.257
0.051	1.08	3.75E-02	8.02E-02	-2.36E-03	-1.91E-01	92.3	114.0	0.326
0.062	1.13	3.52E-02	7.12E-02	-1.14E-03	-1.86E-01	98.4	121.0	0.396
0.072	1.18	3.32E-02	7.61E-02	-2.02E-03	-1.72E-01	105.0	126.0	0.463
0.083	1.26	3.09E-02	6.75E-02	-1.37E-03	-1.45E-01	113.0	132.0	0.534
0.094	1.34	2.72E-02	5.83E-02	-7.78E-04	-1.06E-01	122.0	137.0	0.603
0.105	1.43	2.31E-02	5.72E-02	-9.37E-04	-6.81E-02	132.0	142.0	0.673
0.116	1.50	2.18E-02	4.59E-02	-3.21E-04	-3.54E-02	141.0	146.0	0.744
0.127	1.56	1.45E-02	4.37E-02	-4.24E-04	-7.45E-03	148.0	149.0	0.814
0.138	1.60	8.52E-03	4.28E-02	-5.43E-04	6.78E-03	153.0	152.0	0.885
0.149	1.62	1.22E-02	3.16E-02	-1.19E-04	2.14E-02	157.0	154.0	0.955
0.160	1.64	1.73E-02	2.40E-02	1.89E-04	2.44E-02	159.0	155.0	1.026
0.171	1.65	1.15E-02	2.14E-02	3.11E-05	2.54E-02	160.0	156.0	1.096
0.182	1.65	8.27E-03	3.46E-02	-5.19E-04	2.45E-02	161.0	157.0	1.167
0.193	1.66	8.49E-03	2.55E-02	-1.83E-04	2.05E-02	161.0	158.0	1.237
0.204	1.66	8.15E-03	2.14E-02	-9.00E-05	1.82E-02	161.0	158.0	1.308
0.215	1.66	7.15E-03	2.07E-02	-9.97E-05	1.57E-02	161.0	159.0	1.378
0.226	1.66	6.20E-03	1.74E-02	-4.84E-05	1.48E-02	161.0	159.0	1.449
0.237	1.66	1.07E-02	1.16E-02	5.93E-05	1.21E-02	161.0	159.0	1.519
0.248	1.66	9.98E-03	1.69E-02	5.25E-05	8.11E-03	161.0	160.0	1.590
0.259	1.66	9.22E-03	1.13E-02	6.60E-05	3.69E-04	161.0	161.0	1.660
0.270	1.66	3.52E-03	2.04E-02	-1.68E-04	-6.38E-03	160.0	161.0	1.731
0.281	1.66	4.80E-03	1.77E-02	-9.62E-05	-8.22E-03	160.0	161.0	1.801
0.292	1.66	4.86E-03	9.66E-03	4.42E-05	-1.39E-02	160.0	162.0	1.872
0.302	1.66	5.31E-03	1.80E-02	-1.20E-04	-1.53E-02	160.0	162.0	1.936

Table C-31: Mach 1.7 ZPG separated turbulence variables - traverse down

y (inch)	Mach	(ρ) _{rms}	U _{rms}	ρ'U'	u''/u	pbarubar	pubar	y/δ _u
0.031	0.98	3.61E-02	7.85E-02	-2.89E-03	-2.18E-01	80.1	103.0	0.196
0.041	1.03	4.73E-02	1.00E-01	-5.43E-03	-1.77E-01	87.5	106.0	0.265
0.052	1.08	4.71E-02	9.83E-02	-4.68E-03	-1.62E-01	94.0	112.0	0.333
0.063	1.14	4.27E-02	9.01E-02	-3.55E-03	-1.51E-01	100.0	118.0	0.405
0.075	1.20	3.49E-02	7.21E-02	-1.48E-03	-1.37E-01	107.0	124.0	0.478
0.086	1.27	3.34E-02	6.77E-02	-1.29E-03	-1.13E-01	115.0	130.0	0.548
0.096	1.36	3.26E-02	6.17E-02	-1.00E-03	-6.61E-02	125.0	134.0	0.617
0.107	1.44	2.87E-02	5.01E-02	-3.43E-04	-3.69E-02	135.0	140.0	0.686
0.118	1.51	2.77E-02	3.85E-02	1.16E-04	4.19E-03	144.0	143.0	0.756
0.130	1.56	2.30E-02	3.76E-02	-4.82E-05	2.95E-02	150.0	146.0	0.833
0.140	1.60	2.36E-02	3.37E-02	-3.87E-05	4.37E-02	156.0	149.0	0.897
0.151	1.63	2.04E-02	2.99E-02	-1.95E-05	5.13E-02	159.0	151.0	0.968
0.161	1.64	2.08E-02	2.15E-02	2.26E-04	5.52E-02	161.0	152.0	1.032
0.172	1.65	1.43E-02	1.81E-02	2.52E-04	4.14E-02	161.0	155.0	1.103
0.183	1.65	1.38E-02	1.80E-02	1.69E-04	3.90E-02	162.0	156.0	1.173
0.194	1.66	1.35E-02	2.08E-02	1.00E-04	3.47E-02	162.0	156.0	1.244
0.205	1.66	1.18E-02	2.08E-02	7.29E-05	3.23E-02	162.0	157.0	1.314
0.216	1.66	1.26E-02	2.65E-02	-5.63E-05	3.18E-02	162.0	157.0	1.385
0.227	1.66	1.12E-02	2.40E-02	-1.69E-05	2.93E-02	162.0	157.0	1.455
0.238	1.66	8.99E-03	1.43E-02	9.86E-05	2.20E-02	162.0	158.0	1.526
0.249	1.66	8.48E-03	1.22E-02	1.02E-04	1.69E-02	161.0	159.0	1.596
0.260	1.66	2.76E-03	1.90E-02	-1.22E-04	1.27E-02	161.0	159.0	1.667
0.271	1.66	6.90E-03	1.60E-02	-5.42E-05	6.97E-03	161.0	160.0	1.737
0.282	1.66	8.59E-03	1.31E-02	-4.17E-07	2.94E-03	161.0	160.0	1.808
0.293	1.66	4.04E-03	1.64E-02	-7.38E-05	-9.32E-04	160.0	161.0	1.878
0.303	1.66	5.88E-03	1.46E-02	-3.87E-05	-2.85E-03	160.0	161.0	1.942

Table C-32: Mach 1.7 discrete turbulence intensity data points

y (in)	a	b	sqr(Re)	f	Vrms	Vbar	T.I.	y / δ_u FPG
0.03125	0.1861	0.2613	13.681	0.226731	0.1254	5.475	10.102%	0.118
0.08125	0.1861	0.2613	15.499	0.229233	0.1359	5.787	10.244%	0.307
0.13125	0.1861	0.2613	16.695	0.230606	0.1303	5.997	9.422%	0.495
0.18125	0.1861	0.2613	17.556	0.231486	0.091	6.138	6.405%	0.684
0.23125	0.1861	0.2613	17.841	0.23176	0.04982	6.184	3.476%	0.873
0.28125	0.1861	0.2613	17.941	0.231855	0.03855	6.2	2.682%	1.061
0.33125	0.1861	0.2613	18.000	0.23191	0.0363	6.206	2.522%	1.250
		fbar		0.230512				
y (in)	a	b	sqr(Re)	f	Vrms	Vbar	T.I.	y / δ_u ZPG
0.03125	0.0402	0.2185	17.33	0.190311	0.06042	3.134	10.130%	0.203
0.08125	0.0402	0.2185	20.3	0.1972	0.05398	3.332	8.215%	0.528
0.13125	0.0402	0.2185	21.27	0.199118	0.01321	3.394	1.955%	0.852
0.18125	0.0402	0.2185	21.35	0.19927	0.008352	3.399	1.233%	1.177
		fbar		0.196475				

Table C-33: Mach 1.7 power spectra data

frequency	ZPG, y/d = 0.20	ZPG, y/d = 0.58	ZPG, y/d = 0.85	FPG, y/d = 0.17	FPG, y/d = 0.44	FPG, y/d = 0.71
488	1.75E-06	2.2E-06	9.86E-08	3.65E-08	4.98E-08	5.42E-08
977	1.31E-06	2.22E-06	5.78E-08	4.15E-08	5.67E-08	4.7E-08
1465	1.01E-06	1.68E-06	3.56E-08	4.13E-08	4.95E-08	6.03E-08
1953	9.05E-07	2.03E-06	3.78E-08	3.83E-08	4.14E-08	4.64E-08
2441	1.11E-06	1.5E-06	2.62E-08	3.09E-08	2.85E-08	5.44E-08
2930	7.3E-07	1.18E-06	2.73E-08	3.75E-08	3.99E-08	5E-08
3418	8.27E-07	9.47E-07	1.45E-08	2.85E-08	2.78E-08	3.26E-08
3906	7.58E-07	6.76E-07	2.08E-08	3.18E-08	2.65E-08	2.81E-08
4395	5.22E-07	6.39E-07	1.48E-08	2.39E-08	1.9E-08	1.43E-08
4883	4.49E-07	4.38E-07	1.06E-08	2.03E-08	1.31E-08	1.25E-08
5371	4.6E-07	4.1E-07	1.03E-08	1.75E-08	1.37E-08	1.28E-08
5859	3.14E-07	2.77E-07	5.85E-09	1.58E-08	9.22E-09	7.15E-09
6348	3.22E-07	2.44E-07	4.51E-09	1.5E-08	8.61E-09	4.62E-09
6836	2.46E-07	1.75E-07	3.72E-09	1.16E-08	5.51E-09	3.89E-09
7324	2.23E-07	1.22E-07	3.14E-09	1.08E-08	6.31E-09	2.86E-09
7813	1.8E-07	9.79E-08	3.44E-09	1.08E-08	4.81E-09	2.54E-09
8301	1.65E-07	9.27E-08	2.48E-09	8.24E-09	4.69E-09	3.27E-09
8789	2.12E-07	8.12E-08	1.49E-09	7.78E-09	4.25E-09	2.14E-09
9277	1.55E-07	7.95E-08	1.87E-09	8.85E-09	3.76E-09	2.73E-09
9766	1.52E-07	5.47E-08	1.94E-09	6.91E-09	4.53E-09	3.02E-09
10250	1.38E-07	5.98E-08	1.68E-09	8.03E-09	4.82E-09	2.32E-09
10740	1.28E-07	7.47E-08	8.38E-10	8.09E-09	4.43E-09	2.66E-09
11230	1.18E-07	5.36E-08	2.1E-09	7.5E-09	3.43E-09	2.14E-09
11720	9.77E-08	5.17E-08	1.7E-09	6.19E-09	4.33E-09	2.56E-09
12210	1.31E-07	5.1E-08	1.18E-09	6.02E-09	4.55E-09	1.93E-09
12700	9.98E-08	3.57E-08	1.17E-09	4.54E-09	4.5E-09	2.15E-09
13180	9.89E-08	3.86E-08	1.96E-09	5.01E-09	3.39E-09	1.88E-09
13670	1.2E-07	5.05E-08	1.62E-09	5.16E-09	4.61E-09	2.08E-09
14160	8.58E-08	3.79E-08	1.11E-09	5.19E-09	4.34E-09	1.77E-09
14650	9.78E-08	3.11E-08	1.19E-09	4.61E-09	3.68E-09	1.76E-09
15140	7.63E-08	4.53E-08	9.48E-10	4.27E-09	3.78E-09	1.96E-09
15630	7.57E-08	3.96E-08	1.04E-09	4.41E-09	3.4E-09	1.8E-09
16110	6.92E-08	3.8E-08	1.17E-09	4.24E-09	3.32E-09	2.02E-09
16600	7.8E-08	3.64E-08	1.2E-09	5.46E-09	4.04E-09	1.98E-09
17090	8.55E-08	4.85E-08	4.21E-10	3.54E-09	3.18E-09	1.91E-09
17580	8.28E-08	6.08E-08	9.99E-10	4E-09	3.98E-09	2.22E-09
18070	1.41E-07	5.81E-08		3.18E-09	3.63E-09	2.31E-09

18550	1.75E-07	1.59E-08		3.65E-09	3.95E-09	1.66E-09
19040	6.79E-08			4.31E-09	3.8E-09	1.88E-09
19530	5.79E-08	1.39E-08		2.72E-09	3.61E-09	1.89E-09
20020	5.72E-08	1.7E-08	6.61E-10	3.27E-09	3.58E-09	1.89E-09
20510	5.22E-08	2.17E-08	3.27E-10	2.73E-09	3.19E-09	2.11E-09
21000	4.91E-08	1.81E-08	6.65E-10	3.08E-09	3.13E-09	1.6E-09
21480	5.45E-08	2.65E-08	3.85E-10	3.79E-09	3.1E-09	1.92E-09
21970	4.41E-08	2.33E-08	4.78E-10	2.52E-09	2.92E-09	1.81E-09
22460	5.67E-08	2.26E-08	5.78E-10	2.72E-09	2.96E-09	1.91E-09
22950	4.79E-08	2.18E-08	7.91E-10	2.32E-09	2.75E-09	1.4E-09
23440	6.36E-08	2.41E-08	6.78E-10	2.75E-09	2.63E-09	1.76E-09
23930	4.59E-08	2.83E-08	5.33E-10	2.25E-09	2.53E-09	1.48E-09
24410	5.46E-08	2.56E-08	6.79E-10	2.4E-09	2.11E-09	1.53E-09
24900	6.16E-08	2.5E-08	7.49E-10	2.53E-09	2.23E-09	1.12E-09
25390	4.34E-08	2.29E-08	7.17E-10	9.15E-09	9.83E-09	3.96E-09
25880	6.24E-08	2.52E-08	3.97E-10	4.15E-09	5.07E-09	2.33E-09
26370	5.09E-08	2.49E-08	7.22E-10	4.46E-09	4.02E-09	1.72E-09
26860	4.43E-08	2.31E-08	6.91E-10	3.41E-09	4.16E-09	1.86E-09
27340	4.52E-08	2.38E-08	8.62E-10	2.52E-09	3.41E-09	1.95E-09
27830	4.86E-08	2.31E-08	5.16E-10	2.4E-09	3.27E-09	2.05E-09
28320	4.37E-08	1.92E-08	4.65E-10	3.09E-09	3.76E-09	2.12E-09
28810	3.91E-08	2.07E-08	6.25E-10	2.28E-09	4.17E-09	1.87E-09
29300	4.24E-08	2.28E-08	5.41E-10	2.45E-09	3.12E-09	1.96E-09
29790	4.53E-08	2.73E-08	5.73E-10	3.13E-09	3.03E-09	1.71E-09
30270	4.49E-08	2.06E-08	3.66E-10	2.49E-09	3.36E-09	2.07E-09
30760	5E-08	2.37E-08	6.03E-10	2.23E-09	2.74E-09	1.62E-09
31250	4.46E-08	1.89E-08	5.69E-10	2.2E-09	2.71E-09	1.8E-09
31740	3.95E-08	1.96E-08	5.54E-10	2.95E-09	2.69E-09	1.68E-09
32230	4.55E-08	1.65E-08	4.91E-10	2.44E-09	3.81E-09	1.89E-09
32710	3.95E-08	2.49E-08	5.26E-10	2.41E-09	3.12E-09	2.13E-09
33200	3.35E-08	1.69E-08	5.62E-10	2.57E-09	2.99E-09	2.01E-09
33690	3.68E-08	2.41E-08	4.34E-10	2.71E-09	3.08E-09	2.03E-09
34180	4.06E-08	2.36E-08	3.77E-10	2.42E-09	2.86E-09	1.85E-09
34670	3.92E-08	2.61E-08	4.56E-10	2.62E-09	3.35E-09	2.03E-09
35160	4E-08	2.34E-08	5.05E-10	2.26E-09	3.04E-09	1.66E-09
35640	3.91E-08	2.16E-08	4.05E-10	2.42E-09	2.87E-09	2.15E-09
36130	3.62E-08	2.38E-08	3.57E-10	1.99E-09	3.12E-09	1.69E-09
36620	4.92E-08	2.02E-08	4.87E-10	2.85E-09	3.66E-09	2.25E-09
37110	2.83E-08	2.69E-08	5.94E-10	1.87E-09	2.88E-09	1.74E-09
37600	3.73E-08	1.95E-08	3.48E-10	2.23E-09	2.83E-09	2.32E-09
38090	3.32E-08	1.64E-08	4.96E-10	1.88E-09	3.42E-09	2.38E-09
38570	2.83E-08	2.22E-08	5.01E-10	2.55E-09	2.62E-09	1.48E-09
39060	3.77E-08	1.97E-08	5.43E-10	2.56E-09	2.72E-09	1.92E-09
39550	3.21E-08	2.32E-08	4.51E-10	2.09E-09	2.87E-09	2.08E-09
40040	3.21E-08	2.51E-08	5.46E-10	2.39E-09	2.75E-09	1.66E-09
40530	3.05E-08	2.05E-08	5.51E-10	1.93E-09	2.41E-09	1.92E-09
41020	4.55E-08	2.35E-08	4.33E-10	2.26E-09	3.07E-09	2.4E-09
41500	4.06E-08	2.37E-08	5.02E-10	2.18E-09	3.43E-09	1.52E-09
41990	4.1E-08	2.13E-08	4.96E-10	1.96E-09	2.07E-09	2.16E-09
42480	3.7E-08	2.33E-08	6.89E-10	2.15E-09	2.72E-09	1.98E-09
42970	3.35E-08	2.07E-08	5.05E-10	1.72E-09	2.2E-09	1.71E-09
43460	4E-08	2.13E-08	5.77E-10	2.37E-09	2.37E-09	1.9E-09
43950	3.72E-08	2.22E-08	4.52E-10	2.43E-09	2.61E-09	2.04E-09
44430	3.66E-08	2.25E-08	7.44E-10	2.11E-09	3.27E-09	1.91E-09
44920	4.51E-08	2.64E-08	5.07E-10	1.93E-09	2.44E-09	1.87E-09
45410	3.29E-08	2.47E-08	6.93E-10	2.15E-09	2.8E-09	2.02E-09
45900	4.04E-08	2.07E-08	6.73E-10	1.83E-09	3.37E-09	1.89E-09
46390	4.25E-08	2.62E-08	7.61E-10	2.21E-09	2.88E-09	2.56E-09
46880	4.84E-08	2.55E-08	1.07E-09	1.98E-09	3.24E-09	1.79E-09
47360	3.46E-08	3.17E-08	1.17E-09	1.96E-09	2.72E-09	2.39E-09

47850	5.45E-08	3.1E-08	1.39E-09	2.34E-09	2.33E-09	2.37E-09
48340	4.74E-08	3.51E-08	1.63E-09	1.99E-09	2.57E-09	2E-09
48830	5.97E-08	4.74E-08	1.23E-09	2.03E-09	2.48E-09	1.82E-09
49320	6.66E-08	5.88E-08	3.28E-09	2.07E-09	2.79E-09	2.34E-09
49800	8.04E-08	7.23E-08	3.75E-09	2.07E-09	2.99E-09	1.61E-09
50290	1.08E-07	7.39E-08	7.27E-09	1.96E-09	3.18E-09	1.76E-09
50780	7.93E-08	5.84E-08	1.42E-08	2.31E-09	2.67E-09	2E-09
51270	2.96E-08			2.06E-09	2.2E-09	2.07E-09
51760	8.08E-09		4.14E-09	1.76E-09	2.65E-09	2.41E-09
52250	1E-08			2.06E-09	2.32E-09	1.64E-09
52730	8.7E-09	4.67E-09		1.81E-09	2.16E-09	1.82E-09
53220	9.96E-09	6.26E-09	5.95E-10	1.52E-09	2.29E-09	1.72E-09
53710	1.13E-08	4.61E-09	5.15E-10	1.95E-09	2.01E-09	1.59E-09
54200	1.01E-08	6.15E-09	2.33E-10	1.45E-09	2.79E-09	1.54E-09
54690	1.27E-08	6.63E-09	2.53E-10	2.12E-09	2.72E-09	1.52E-09
55180	1.26E-08	6.34E-09	2.68E-10	1.94E-09	2.4E-09	1.45E-09
55660	1.07E-08	7.04E-09	1.89E-10	1.77E-09	2.7E-09	2.21E-09
56150	8.7E-09	5.51E-09	2.2E-10	1.79E-09	2.45E-09	1.55E-09
56640	1.27E-08	6.54E-09	2.57E-10	1.89E-09	1.81E-09	1.9E-09
57130	8.53E-09	5.13E-09	1.94E-10	1.3E-09	1.86E-09	1.48E-09
57620	1.22E-08	6.52E-09	2.14E-10	1.4E-09	2.33E-09	1.55E-09
58110	1.22E-08	6.08E-09	2.36E-10	1.33E-09	2.31E-09	1.81E-09
58590	1.03E-08	6.91E-09	2.32E-10	1.3E-09	1.78E-09	1.29E-09
59080	7.24E-09	5.63E-09	1.93E-10	1.34E-09	1.88E-09	1.27E-09
59570	8.54E-09	6.7E-09	1.86E-10	1.48E-09	1.59E-09	1.16E-09
60060	9.68E-09	6.31E-09	1.51E-10	1.18E-09	1.53E-09	8.08E-10
60550	8.55E-09	5.75E-09	1.85E-10	1.14E-09	1.03E-09	7.36E-10
61040	9.86E-09	4.8E-09	1.74E-10	1.7E-09	1.35E-09	7.6E-10
61520	7.9E-09	7.4E-09	2.36E-10	2.33E-09	2.5E-09	1.14E-09
62010	8.36E-09	7.04E-09	2.2E-10	2.3E-09	3.67E-09	2.41E-09
62500	8.26E-09	7.08E-09	2.06E-10	2E-09	2.94E-09	2.17E-09
62990	8.58E-09	6.81E-09	1.77E-10	1.88E-09	2.56E-09	2.39E-09
63480	8.36E-09	5.74E-09	2.31E-10	1.79E-09	2.26E-09	1.79E-09
63960	8E-09	7.95E-09	1.41E-10	1.41E-09	2.57E-09	2.07E-09
64450	7.35E-09	5.94E-09	2.25E-10	1.42E-09	2.35E-09	1.94E-09
64940	8.61E-09	5.51E-09	1.36E-10	1.38E-09	2.27E-09	1.99E-09
65430	7.86E-09	7.24E-09	1.23E-10	1.28E-09	1.61E-09	1.66E-09
65920	8.02E-09	7.68E-09	1.8E-10	1.3E-09	1.68E-09	1.7E-09
66410	7.52E-09	5.35E-09	1.41E-10	1.18E-09	1.88E-09	1.68E-09
66890	5.95E-09	5.17E-09	2.47E-10	9.81E-10	1.98E-09	2.18E-09
67380	6.93E-09	5.43E-09	1.58E-10	9.42E-10	1.68E-09	1.63E-09
67870	6.16E-09	5.51E-09	1.75E-10	8.56E-10	1.27E-09	1.64E-09
68360	6.29E-09	5.28E-09	1.8E-10	8.47E-10	1.63E-09	1.45E-09
68850	6.46E-09	7.08E-09	1.61E-10	8.81E-10	1.76E-09	1.59E-09
69340	5.41E-09	4.76E-09	1.69E-10	7.83E-10	1.49E-09	1.42E-09
69820	5.55E-09	5.73E-09	2.1E-10	7.95E-10	1.53E-09	1.23E-09
70310	6.53E-09	4.98E-09	1.73E-10	8.33E-10	1.72E-09	1.39E-09
70800	5.03E-09	6.07E-09	1.78E-10	6.41E-10	1.64E-09	1.47E-09
71290	6E-09	4.85E-09	1.82E-10	6.27E-10	1.18E-09	1.15E-09
71780	6.6E-09	7E-09	1.51E-10	5.97E-10	1.21E-09	
72270	5.93E-09	5.17E-09	1.97E-10	5.95E-10	1.08E-09	
72750	7.42E-09	4.91E-09	1.74E-10	5.15E-10	9.98E-10	
73240	6.62E-09	5.1E-09	2.14E-10	3.73E-10	1.08E-09	

Table C-34: Mach 5.0 ZPG pressure data

y (in)	P _{t1} (psia)	P _{t2} (psia)	P _{t2} / P _{t1}	ps / P _{t2}	Mach	M / M _e	u / U _e	p _w / p	p / p _e
0.0717	440	15.6941	0.0356	0.0594	3.5782	0.7016	0.9260	0.2873	0.5612
0.0807	439	16.4591	0.0375	0.0567	3.6515	0.7160	0.9312	0.2798	0.5764
0.0897	440	17.0137	0.0386	0.0548	3.7121	0.7279	0.9353	0.2737	0.5891
0.0985	440	17.0168	0.0387	0.0548	3.7157	0.7286	0.9356	0.2734	0.5898
0.1074	439	17.3033	0.0394	0.0539	3.7458	0.7345	0.9375	0.2704	0.5962
0.1165	440	17.7787	0.0404	0.0525	3.7958	0.7443	0.9408	0.2657	0.6069
0.1253	440	17.8884	0.0406	0.0521	3.8109	0.7472	0.9417	0.2643	0.6101
0.1345	440	18.4004	0.0418	0.0507	3.8618	0.7572	0.9449	0.2596	0.6211
0.1433	440	19.1654	0.0435	0.0487	3.9377	0.7721	0.9495	0.2529	0.6377
0.1524	441	19.5067	0.0442	0.0478	3.9783	0.7801	0.9518	0.2494	0.6466
0.1614	441	19.7657	0.0448	0.0472	4.0070	0.7857	0.9535	0.2469	0.6530
0.1705	441	20.6800	0.0469	0.0451	4.0880	0.8016	0.9580	0.2402	0.6711
0.1795	440	20.7227	0.0471	0.0450	4.1063	0.8051	0.9589	0.2388	0.6752
0.1885	440	21.1250	0.0481	0.0441	4.1422	0.8122	0.9608	0.2359	0.6834
0.1976	440	21.9204	0.0498	0.0425	4.2109	0.8257	0.9644	0.2306	0.6991
0.2066	440	22.0667	0.0501	0.0423	4.2369	0.8308	0.9657	0.2287	0.7051
0.2157	440	22.3654	0.0508	0.0417	4.2652	0.8363	0.9671	0.2266	0.7116
0.2248	440	23.0755	0.0524	0.0404	4.3231	0.8477	0.9698	0.2224	0.7251
0.2337	439	23.5174	0.0535	0.0397	4.3685	0.8566	0.9720	0.2192	0.7357
0.2429	441	24.1452	0.0547	0.0386	4.4231	0.8673	0.9745	0.2154	0.7486
0.2518	441	24.9436	0.0565	0.0374	4.4902	0.8804	0.9774	0.2109	0.7645
0.2610	441	25.2575	0.0573	0.0369	4.5299	0.8882	0.9791	0.2083	0.7740
0.2701	441	25.5410	0.0579	0.0365	4.5596	0.8940	0.9804	0.2064	0.7812
0.2792	440	26.2968	0.0597	0.0355	4.6149	0.9049	0.9826	0.2029	0.7946
0.2882	439	26.3303	0.0599	0.0354	4.6346	0.9087	0.9834	0.2017	0.7993
0.2970	440	26.7600	0.0608	0.0349	4.6666	0.9150	0.9847	0.1998	0.8071
0.3060	440	27.5036	0.0625	0.0339	4.7201	0.9255	0.9868	0.1966	0.8202
0.3153	439	27.9730	0.0637	0.0333	4.7647	0.9343	0.9885	0.1940	0.8312
0.3243	441	28.0918	0.0637	0.0332	4.7871	0.9386	0.9893	0.1927	0.8368
0.3334	440	28.2869	0.0642	0.0330	4.8058	0.9423	0.9900	0.1916	0.8414
0.3426	442	28.8141	0.0652	0.0324	4.8411	0.9492	0.9913	0.1897	0.8502
0.3516	440	29.1859	0.0663	0.0320	4.8738	0.9557	0.9924	0.1878	0.8584
0.3607	442	29.1463	0.0660	0.0320	4.8839	0.9576	0.9928	0.1873	0.8609
0.3698	441	29.5455	0.0669	0.0316	4.9087	0.9625	0.9937	0.1860	0.8671
0.3789	441	29.7772	0.0675	0.0313	4.9301	0.9667	0.9944	0.1848	0.8725
0.3879	441	30.0819	0.0682	0.0310	4.9539	0.9714	0.9952	0.1835	0.8785
0.3969	442	30.2648	0.0685	0.0308	4.9724	0.9750	0.9958	0.1826	0.8831
0.4061	441	30.2678	0.0687	0.0308	4.9798	0.9764	0.9961	0.1822	0.8850
0.4153	440	30.3654	0.0691	0.0307	4.9876	0.9780	0.9963	0.1818	0.8870
0.4242	440	30.3654	0.0690	0.0307	4.9907	0.9786	0.9964	0.1816	0.8878
0.4333	440	30.4354	0.0691	0.0306	4.9955	0.9795	0.9966	0.1814	0.8890
0.4424	442	30.7951	0.0697	0.0303	5.0153	0.9834	0.9973	0.1804	0.8940
0.4515	442	30.7067	0.0695	0.0304	5.0188	0.9841	0.9974	0.1802	0.8949
0.4606	442	30.7372	0.0696	0.0303	5.0217	0.9846	0.9975	0.1800	0.8956
0.4696	440	30.7067	0.0697	0.0304	5.0213	0.9846	0.9975	0.1801	0.8955
0.4787	442	30.9048	0.0700	0.0302	5.0374	0.9877	0.9980	0.1792	0.8996
0.4877	441	31.0876	0.0705	0.0300	5.0525	0.9907	0.9985	0.1785	0.9034
0.4966	442	31.0998	0.0704	0.0300	5.0536	0.9909	0.9985	0.1784	0.9037
0.5057	442	31.0236	0.0702	0.0301	5.0474	0.9897	0.9983	0.1787	0.9021
0.5148	442	31.1791	0.0705	0.0299	5.0601	0.9922	0.9987	0.1781	0.9054
0.5237	441	31.1943	0.0707	0.0299	5.0614	0.9924	0.9988	0.1780	0.9057
0.5328	442	31.0815	0.0704	0.0300	5.0521	0.9906	0.9985	0.1785	0.9033
0.5419	442	31.0511	0.0703	0.0300	5.0496	0.9901	0.9984	0.1786	0.9027
0.5509	442	31.2918	0.0708	0.0298	5.0693	0.9940	0.9990	0.1776	0.9077
0.5599	442	31.4320	0.0711	0.0297	5.0808	0.9962	0.9994	0.1771	0.9107
0.5690	442	31.1974	0.0706	0.0299	5.0617	0.9925	0.9988	0.1780	0.9058
0.5782	441	31.4930	0.0714	0.0296	5.0859	0.9972	0.9996	0.1768	0.9119

0.5872	442	31.4991	0.0713	0.0296	5.0864	0.9973	0.9996	0.1768	0.9121
0.5961	443	31.4808	0.0711	0.0296	5.0849	0.9970	0.9995	0.1769	0.9117
0.6052	442	31.7246	0.0718	0.0294	5.1047	1.0009	1.0001	0.1759	0.9168
0.6143	441	31.6606	0.0717	0.0295	5.0996	0.9999	1.0000	0.1761	0.9155
0.6233	442	31.8831	0.0722	0.0293	5.1177	1.0035	1.0006	0.1752	0.9201
0.6323	442	31.9654	0.0724	0.0292	5.1244	1.0048	1.0008	0.1749	0.9218
0.6413	441	31.9745	0.0724	0.0292	5.1252	1.0049	1.0008	0.1749	0.9220
0.6503	440	31.9836	0.0727	0.0292	5.1259	1.0051	1.0008	0.1748	0.9222
0.6594	442	32.1086	0.0726	0.0290	5.1360	1.0071	1.0011	0.1744	0.9248
0.6684	441	32.3463	0.0733	0.0288	5.1550	1.0108	1.0017	0.1734	0.9297
0.6776	441	32.3006	0.0733	0.0289	5.1517	1.0101	1.0016	0.1736	0.9288
0.6866	443	32.4591	0.0733	0.0287	5.1644	1.0126	1.0020	0.1730	0.9321
0.6955	442	32.5993	0.0737	0.0286	5.1756	1.0148	1.0023	0.1725	0.9350
0.7045	443	32.5871	0.0736	0.0286	5.1747	1.0147	1.0023	0.1725	0.9347
0.7135	442	32.7151	0.0741	0.0285	5.1850	1.0167	1.0026	0.1720	0.9374
0.7225	442	32.9132	0.0745	0.0283	5.2008	1.0198	1.0031	0.1713	0.9415
0.7318	442	33.0534	0.0748	0.0282	5.2120	1.0220	1.0034	0.1707	0.9444
0.7407	442	33.1570	0.0751	0.0281	5.2203	1.0236	1.0037	0.1704	0.9465
0.7497	442	33.3246	0.0754	0.0280	5.2335	1.0262	1.0041	0.1697	0.9499
0.7590	442	33.6050	0.0761	0.0278	5.2555	1.0305	1.0047	0.1687	0.9556
0.7679	442	33.6172	0.0761	0.0277	5.2569	1.0308	1.0048	0.1687	0.9560

Table C-35: Mach 5.0 FPG pressure data

y (in)	P ₁₁ (psia)	P ₁₂ (psia)	P ₁₂ / P ₁₁	ps / P ₁₂	Mach	P (Pa)	T (K)	p	ρ / ρ _e	M / M _e	u / U _e
0.063	506	15.56647	0.031	0.069	3.304	5278	113.1110	0.1626	0.5483	0.6210	0.8983
0.071	505	15.70056	0.031	0.069	3.303	5260	113.1185	0.1620	0.5464	0.6209	0.8983
0.080	505	15.72799	0.031	0.069	3.305	5243	113.0546	0.1616	0.5449	0.6212	0.8984
0.089	505	16.69409	0.033	0.065	3.405	5225	108.4737	0.1678	0.5659	0.6400	0.9067
0.097	506	16.96533	0.034	0.064	3.436	5206	107.0935	0.1694	0.5712	0.6459	0.9092
0.106	504	17.22742	0.034	0.063	3.463	5189	105.9113	0.1707	0.5756	0.6510	0.9113
0.115	505	17.47733	0.035	0.062	3.489	5171	104.8120	0.1719	0.5797	0.6558	0.9133
0.123	506	17.9558	0.036	0.060	3.535	5153	102.8689	0.1745	0.5886	0.6645	0.9168
0.132	507	18.7299	0.037	0.058	3.608	5136	99.9156	0.1791	0.6039	0.6781	0.9220
0.141	505	18.58666	0.037	0.058	3.604	5118	100.0602	0.1782	0.6009	0.6775	0.9217
0.149	506	19.16875	0.038	0.056	3.660	5100	97.8518	0.1816	0.6124	0.6880	0.9257
0.158	505	19.83009	0.039	0.055	3.722	5082	95.4583	0.1855	0.6256	0.6997	0.9299
0.167	506	20.03733	0.040	0.054	3.744	5064	94.6432	0.1864	0.6287	0.7038	0.9313
0.175	505	20.34209	0.040	0.053	3.773	5046	93.5926	0.1879	0.6335	0.7091	0.9331
0.184	506	21.02171	0.042	0.051	3.833	5029	91.4118	0.1917	0.6464	0.7205	0.9370
0.193	506	21.55809	0.043	0.050	3.883	5011	89.6608	0.1947	0.6566	0.7298	0.9400
0.201	506	22.12799	0.044	0.049	3.934	4993	87.9140	0.1979	0.6673	0.7394	0.9430
0.210	506	22.20418	0.044	0.049	3.946	4975	87.5005	0.1981	0.6681	0.7417	0.9438
0.219	505	22.55466	0.045	0.048	3.975	4957	86.5342	0.1996	0.6731	0.7472	0.9454
0.228	506	23.39275	0.046	0.046	4.042	4939	84.3584	0.2040	0.6879	0.7598	0.9492
0.236	505	23.80418	0.047	0.045	4.083	4921	83.0748	0.2064	0.6961	0.7674	0.9514
0.245	506	23.92304	0.047	0.045	4.098	4904	82.5927	0.2069	0.6977	0.7703	0.9522
0.254	507	24.64228	0.049	0.044	4.151	4886	80.9621	0.2103	0.7091	0.7803	0.9550
0.262	507	25.11161	0.050	0.043	4.193	4868	79.7012	0.2128	0.7177	0.7882	0.9572
0.271	508	25.84304	0.051	0.042	4.250	4850	78.0450	0.2165	0.7302	0.7989	0.9600
0.280	506	26.58666	0.053	0.041	4.310	4833	76.3538	0.2205	0.7437	0.8101	0.9629
0.288	507	27.00114	0.053	0.040	4.350	4815	75.2542	0.2229	0.7517	0.8176	0.9647
0.297	507	27.20837	0.054	0.040	4.372	4797	74.6426	0.2239	0.7551	0.8218	0.9658
0.306	506	27.93066	0.055	0.039	4.421	4779	73.3382	0.2271	0.7656	0.8310	0.9680
0.314	504	28.24456	0.056	0.038	4.452	4761	72.5187	0.2288	0.7714	0.8369	0.9693
0.323	506	29.2838	0.058	0.037	4.519	4743	70.8038	0.2334	0.7871	0.8495	0.9722
0.332	506	29.75314	0.059	0.036	4.564	4725	69.6807	0.2363	0.7968	0.8579	0.9741
0.340	507	30.24076	0.060	0.036	4.604	4708	68.7135	0.2387	0.8050	0.8654	0.9757

0.349	508	30.85942	0.061	0.035	4.648	4690	67.6477	0.2416	0.8145	0.8738	0.9775
0.358	506	31.56952	0.062	0.034	4.699	4672	66.4726	0.2449	0.8258	0.8832	0.9795
0.367	507	31.77066	0.063	0.034	4.726	4654	65.8599	0.2462	0.8303	0.8883	0.9805
0.375	507	32.66361	0.064	0.033	4.778	4636	64.6783	0.2497	0.8422	0.8981	0.9825
0.384	508	33.20609	0.065	0.033	4.822	4618	63.7106	0.2526	0.8516	0.9064	0.9841
0.393	507	33.73333	0.067	0.032	4.862	4600	62.8444	0.2551	0.8601	0.9140	0.9855
0.402	507	34.05333	0.067	0.032	4.891	4600	62.2387	0.2575	0.8684	0.9193	0.9865
0.410	507	34.52266	0.068	0.031	4.922	4600	61.5899	0.2602	0.8776	0.9252	0.9876
0.419	506	34.74513	0.069	0.031	4.943	4600	61.1594	0.2621	0.8838	0.9291	0.9883
0.428	508	35.30894	0.070	0.031	4.975	4600	60.5076	0.2649	0.8933	0.9351	0.9894
0.436	505	35.97332	0.071	0.030	5.015	4600	59.7030	0.2685	0.9053	0.9427	0.9907
0.445	507	36.48533	0.072	0.030	5.052	4600	58.9819	0.2718	0.9164	0.9495	0.9919
0.454	508	36.92418	0.073	0.029	5.084	4600	58.3593	0.2747	0.9262	0.9556	0.9929
0.462	508	37.31733	0.074	0.029	5.112	4600	57.8169	0.2772	0.9348	0.9609	0.9938
0.471	507	37.70438	0.074	0.029	5.139	4600	57.3163	0.2797	0.9430	0.9659	0.9946
0.480	506	38.12495	0.075	0.029	5.166	4600	56.8122	0.2821	0.9514	0.9710	0.9955
0.488	508	38.37485	0.076	0.028	5.186	4600	56.4342	0.2840	0.9578	0.9748	0.9961
0.497	508	38.84418	0.076	0.028	5.212	4600	55.9565	0.2864	0.9659	0.9798	0.9969
0.506	509	39.11542	0.077	0.028	5.233	4600	55.5784	0.2884	0.9725	0.9837	0.9975
0.514	507	39.19771	0.077	0.028	5.245	4600	55.3727	0.2895	0.9761	0.9858	0.9978
0.523	509	39.73409	0.078	0.027	5.269	4600	54.9367	0.2918	0.9839	0.9905	0.9986
0.532	508	39.89561	0.079	0.027	5.285	4600	54.6532	0.2933	0.9890	0.9935	0.9990
0.540	508	40.15162	0.079	0.027	5.301	4600	54.3753	0.2948	0.9940	0.9965	0.9995
0.549	508	40.59961	0.080	0.027	5.324	4600	53.9806	0.2969	1.0013	1.0008	1.0001
0.558	508	40.42285	0.080	0.027	5.327	4600	53.9298	0.2972	1.0022	1.0013	1.0002
0.567	509	40.13332	0.079	0.027	5.317	4600	54.1056	0.2962	0.9990	0.9994	0.9999
0.575	508	39.34399	0.077	0.028	5.253	4600	55.2259	0.2902	0.9787	0.9874	0.9981
0.584	509	38.44119	0.075	0.028	5.189	4600	56.3746	0.2843	0.9588	0.9754	0.9962
0.593	509	37.60685	0.074	0.029	5.130	4600	57.4809	0.2789	0.9403	0.9642	0.9944
0.601	510	36.96685	0.073	0.030	5.084	4600	58.3488	0.2747	0.9263	0.9557	0.9930
0.610	510	36.49752	0.072	0.030	5.051	4600	59.0012	0.2717	0.9161	0.9493	0.9919
0.619	510	36.18666	0.071	0.030	5.028	4600	59.4423	0.2697	0.9093	0.9451	0.9911
0.627	510	36.02818	0.071	0.030	5.017	4600	59.6713	0.2686	0.9058	0.9430	0.9908
0.636	509	35.83619	0.070	0.031	5.001	4600	59.9738	0.2673	0.9012	0.9401	0.9903
0.645	509	35.72038	0.070	0.031	4.992	4600	60.1531	0.2665	0.8985	0.9384	0.9900
0.653	509	35.63809	0.070	0.031	4.985	4600	60.2916	0.2659	0.8965	0.9371	0.9897
0.662	510	35.50704	0.070	0.031	4.975	4600	60.5120	0.2649	0.8932	0.9351	0.9894
0.671	511	35.55558	0.070	0.031	4.978	4600	60.4402	0.2652	0.8943	0.9357	0.9895
0.680	510	35.53447	0.070	0.031	4.975	4600	60.5025	0.2649	0.8934	0.9352	0.9894
0.688	508	35.46742	0.070	0.031	4.969	4600	60.6241	0.2644	0.8916	0.9340	0.9892
0.697	511	35.44608	0.069	0.031	4.966	4600	60.6795	0.2642	0.8907	0.9335	0.9891
0.706	511	35.46742	0.069	0.031	4.967	4600	60.6734	0.2642	0.8908	0.9336	0.9891
0.714	510	35.36075	0.069	0.031	4.958	4600	60.8538	0.2634	0.8882	0.9319	0.9888
0.723	509	35.31199	0.069	0.031	4.953	4600	60.9496	0.2630	0.8868	0.9310	0.9887
0.732	510	35.34856	0.069	0.031	4.954	4600	60.9208	0.2631	0.8872	0.9313	0.9887
0.740	510	35.40951	0.069	0.031	4.958	4600	60.8573	0.2634	0.8881	0.9319	0.9888
0.749	512	35.41256	0.069	0.031	4.957	4600	60.8779	0.2633	0.8878	0.9317	0.9888
0.758	511	35.32113	0.069	0.031	4.949	4600	61.0368	0.2626	0.8855	0.9302	0.9885

Table C-36: Mach 5.0 CPG ($X_{ts} = 5.1$ cm) pressure data

y (in)	P ₁₁ (psia)	P ₁₂ (psia)	P ₁₂ / P ₁₁	ps / P ₁₂	Mach	P (Pa)	T (K)	ρ	ρ / ρ_e	M / M _e	u / U _e
0.0717	440	15.6941	0.0356	0.0891	2.90673	12695	133.8382	0.3305	0.5379	0.6760	0.8934
0.0807	439	16.4591	0.0375	0.0860	2.92825	12740	132.6001	0.3348	0.5448	0.6810	0.8958
0.0897	440	17.0137	0.0386	0.0777	3.0879	12785	123.8379	0.3597	0.5855	0.7181	0.9129
0.0985	440	17.0168	0.0387	0.0727	3.19624	12830	118.2969	0.3779	0.6150	0.7433	0.9236
0.1074	439	17.3033	0.0394	0.0720	3.22421	12875	116.9171	0.3837	0.6244	0.7498	0.9262
0.1165	440	17.7787	0.0404	0.0694	3.28023	12921	114.2139	0.3942	0.6415	0.7628	0.9313
0.1253	440	17.8884	0.0406	0.0666	3.34619	12965	111.1318	0.4065	0.6616	0.7782	0.9371
0.1345	440	18.4004	0.0418	0.0634	3.42552	13011	107.5642	0.4215	0.6859	0.7966	0.9438
0.1433	440	19.1654	0.0435	0.0621	3.47127	13056	105.5736	0.4309	0.7013	0.8073	0.9476
0.1524	441	19.5067	0.0442	0.0597	3.53557	13102	102.8556	0.4438	0.7223	0.8222	0.9526
0.1614	441	19.7657	0.0448	0.0592	3.56141	13147	101.7890	0.4500	0.7324	0.8282	0.9546
0.1705	441	20.6800	0.0469	0.0563	3.63631	13193	98.7776	0.4654	0.7574	0.8457	0.9601
0.1795	440	20.7227	0.0471	0.0547	3.69534	13238	96.4861	0.4781	0.7780	0.8594	0.9643
0.1885	440	21.1250	0.0481	0.0541	3.72719	13284	95.2787	0.4858	0.7906	0.8668	0.9665
0.1976	440	21.9204	0.0498	0.0506	3.85439	13329	90.6512	0.5123	0.8338	0.8964	0.9749
0.2066	440	22.0667	0.0501	0.0505	3.86806	13375	90.1718	0.5168	0.8411	0.8995	0.9758
0.2157	440	22.3654	0.0508	0.0491	3.90957	13421	88.7367	0.5270	0.8576	0.9092	0.9784
0.2248	440	23.0755	0.0524	0.0476	3.96353	13467	86.9163	0.5399	0.8786	0.9218	0.9817
0.2337	439	23.5174	0.0535	0.0461	4.02285	13512	84.9725	0.5540	0.9017	0.9355	0.9852
0.2429	441	24.1452	0.0547	0.0454	4.06453	13558	83.6416	0.5648	0.9192	0.9452	0.9875
0.2518	441	24.9436	0.0565	0.0433	4.17042	13603	80.3844	0.5896	0.9596	0.9699	0.9934
0.2610	441	25.2575	0.0573	0.0432	4.18511	13649	79.9462	0.5949	0.9681	0.9733	0.9941
0.2701	441	25.5410	0.0579	0.0421	4.22355	13695	78.8147	0.6054	0.9854	0.9822	0.9961
0.2792	440	26.2968	0.0597	0.0415	4.25788	13741	77.8226	0.6152	1.0013	0.9902	0.9979
0.2882	439	26.3303	0.0599	0.0420	4.25704	13787	77.8466	0.6171	1.0043	0.9900	0.9978
0.2970	440	26.7600	0.0608	0.0412	4.29793	13831	76.6865	0.6284	1.0227	0.9995	0.9999
0.3060	440	27.5036	0.0625	0.0411	4.30498	13876	76.4888	0.6321	1.0288	1.0012	1.0002
0.3153	439	27.9730	0.0637	0.0412	4.30122	13923	76.5941	0.6334	1.0308	1.0003	1.0001
0.3243	441	28.0918	0.0637	0.0412	4.30247	13968	76.5591	0.6357	1.0346	1.0006	1.0001
0.3334	440	28.2869	0.0642	0.0410	4.30987	14014	76.3521	0.6395	1.0408	1.0023	1.0005
0.3426	442	28.8141	0.0652	0.0414	4.28803	14061	76.9652	0.6366	1.0360	0.9972	0.9994
0.3516	440	29.1859	0.0663	0.0414	4.29028	14106	76.9017	0.6391	1.0402	0.9977	0.9995
0.3607	442	29.1463	0.0660	0.0412	4.29856	14152	76.6688	0.6432	1.0467	0.9997	0.9999
0.3698	441	29.5455	0.0669	0.0418	4.26748	14198	77.5481	0.6379	1.0382	0.9924	0.9984
0.3789	441	29.7772	0.0675	0.0418	4.26925	14244	77.4977	0.6404	1.0422	0.9928	0.9985
0.3879	441	30.0819	0.0682	0.0414	4.28896	14289	76.9389	0.6471	1.0531	0.9974	0.9995
0.3969	442	30.2648	0.0685	0.0414	4.28701	14335	76.9940	0.6487	1.0557	0.9970	0.9994
0.4061	441	30.2678	0.0687	0.0413	4.29231	14381	76.8445	0.6521	1.0612	0.9982	0.9996
0.4153	440	30.3654	0.0691	0.0408	4.3187	14427	76.1062	0.6605	1.0750	1.0043	1.0009
0.4242	440	30.3654	0.0690	0.0405	4.33843	13513	75.5605	0.6231	1.0141	1.0089	1.0019

Table C-37: Mach 5.0 CPG ($X_{ts} = 6.35$ cm) pressure data

y (in)	P_{t1} (psia)	P_{t2} (psia)	P_{t2} / P_{t1}	ps / P_{t2}	Mach	P (Pa)	T (K)	ρ	ρ / ρ_e	M / M_e	u / U_e
0.0625	507	27.8481	0.0550	0.0738	3.210	11599.7	117.62	0.3436	1.0582	0.6173	0.8932
0.0712	506	29.1769	0.0577	0.0695	3.287	11243.4	113.87	0.3440	1.0595	0.6322	0.9001
0.0797	507	30.2070	0.0595	0.0662	3.366	10891.2	110.23	0.3443	1.0603	0.6473	0.9067
0.0883	507	30.6184	0.0604	0.0644	3.415	10539.0	108.04	0.3399	1.0467	0.6567	0.9107
0.0968	505	33.1693	0.0656	0.0586	3.563	10185.6	101.72	0.3489	1.0745	0.6852	0.9220
0.1052	506	32.9346	0.0650	0.0583	3.595	9839.2	100.41	0.3414	1.0515	0.6914	0.9244
0.1138	504	33.0931	0.0656	0.0572	3.630	9485.7	99.03	0.3338	1.0279	0.6981	0.9268
0.1224	505	34.5224	0.0683	0.0540	3.722	9132.3	95.49	0.3332	1.0262	0.7157	0.9331
0.1310	505	36.5582	0.0724	0.0502	3.876	8780.1	89.91	0.3403	1.0479	0.7453	0.9429
0.1396	505	37.7894	0.0748	0.0479	3.953	8425.0	87.26	0.3364	1.0361	0.7602	0.9475
0.1482	506	39.4687	0.0780	0.0452	4.058	8070.3	83.85	0.3354	1.0328	0.7804	0.9534
0.1568	505	39.6028	0.0784	0.0443	4.117	7715.3	82.02	0.3278	1.0094	0.7916	0.9565
0.1654	506	42.0744	0.0832	0.0411	4.284	7361.8	77.09	0.3328	1.0248	0.8238	0.9650
0.1739	506	43.1654	0.0853	0.0394	4.356	7009.6	75.07	0.3253	1.0019	0.8377	0.9684
0.1825	506	44.1955	0.0874	0.0379	4.437	6657.4	72.91	0.3181	0.9798	0.8533	0.9721
0.1911	505	45.9114	0.0909	0.0359	4.584	6301.1	69.19	0.3173	0.9773	0.8816	0.9784
0.1997	505	46.2740	0.0916	0.0350	4.635	5947.7	67.96	0.3049	0.9391	0.8914	0.9804
0.2083	506	47.5815	0.0940	0.0335	4.716	5595.5	66.08	0.2950	0.9086	0.9069	0.9836
0.2170	504	48.9681	0.0971	0.0319	4.855	5237.5	62.99	0.2897	0.8922	0.9337	0.9887
0.2256	506	49.7849	0.0984	0.0309	4.920	4882.5	61.63	0.2760	0.8501	0.9461	0.9910
0.2342	507	50.7571	0.1001	0.0297	4.998	4529.0	60.04	0.2628	0.8094	0.9611	0.9936
0.2429	507	50.4675	0.0996	0.0294	5.053	4168.2	58.96	0.2463	0.7586	0.9717	0.9954
0.2515	506	50.4614	0.0996	0.0288	5.103	3814.7	57.98	0.2292	0.7060	0.9814	0.9970
0.2601	505	49.8763	0.0987	0.0286	5.138	3458.4	57.32	0.2102	0.6475	0.9882	0.9981
0.2688	507	50.0378	0.0987	0.0280	5.185	3100.5	56.46	0.1913	0.5893	0.9971	0.9995
0.2775	506	48.5628	0.0960	0.0283	5.196	2745.4	56.25	0.1701	0.5237	0.9993	0.9999
0.2860	506	47.5479	0.0940	0.0283	5.201	2393.2	56.17	0.1485	0.4572	1.0001	1.0000
0.2944	504	45.4664	0.0902	0.0290	5.171	2045.5	56.70	0.1257	0.3871	0.9945	0.9991

Table C-38: Mach 5.0 wall static pressure data

CPG - X_{ts}	X_{ts} / L	ps (psia)	P_{t1}	P_{t1} / ps
0.750	0.0750	1.4	477	341
1.250	0.1250	1.295	477	368
1.840	0.1840	1.526	477	313
2.375	0.2375	2.048	485	237
2.813	0.2813	2.058	485	236
3.313	0.3313	2.001	485	242
3.750	0.3750	1.451	500	345
4.250	0.4250	1.361	500	367
4.750	0.4750	1.546	500	323
FPG - X_{ts}	X_{ts} / L	ps (psia)	P_{t1}	P_{t1} / ps
1.000	0.1000	1.224	493	402
1.438	0.1438	1.061	493	464
2.438	0.2438	0.789	486	616
2.938	0.2938	0.69	486	704
3.313	0.3313	7.295	486	67
3.906	0.3906	0.92	479	521
4.375	0.4375	1.092	479	439
4.906	0.4906	1.471	479	326

Bibliography

1. Anderson, D., et al. *Computational Fluid Mechanics and Heat Transfer, Series in Computational Methods in Mechanics and Thermal Sciences*, New York: Hemisphere Publishing Corporation, 1984.
2. Arnette, S. A., Samimy, M., and Elliot, G. S., "Structure of Supersonic Turbulent Boundary Layer After Expansion Regions," *AIAA Journal*, Vol. 33, No. 3, March 1995, pp. 430-438.
3. Bowersox, R. D. W. *Compressible Turbulence Measurements in a High-Speed High Reynolds Number Mixing Layer*. PhD dissertation, Virginia Polytechnic Institute and State University, Blacksburg, Virginia, September 1992.
4. Bowersox, R. D. W., "MSHEaR User's Manual," School of Engineering, Air Force Institute of Technology (AU), Wright-Patterson AFB OH, Winter Quarter 1994.
5. Bowersox, R. D. W., Schetz, J. A. et al., "Technique for Direct Measurement of Skin Friction in High Enthalpy Impulsive Scramjet Flowfields," *AIAA Journal*, Vol. 33, No. 7, July 1995, pp. 1286-1291.
6. Bradshaw, P., "The Effect of Mean Compression or Dilatation of the Turbulence Structure of Supersonic Boundary Layers," *Journal of Fluid Mechanics*, Vol. 63, Pt. 3, 1974, pp. 449-464.
7. Bradshaw, P., "The Effect of Streamline Curvature on Turbulent Flow," AGARDograph 169, 1973.
8. Bradshaw, P., and Ferriss, D. H., "Calculation of Boundary-Layer Development Using the Turbulent Energy Equation: Compressible Flow on Adiabatic Walls," *Journal of Fluid Mechanics*, Vol 46, 1971, pp. 83-110.
9. Clauser, F. H., "Turbulent Boundary Layers in the Adverse Pressure Gradients," *Journal of the Aeronautical Sciences*, Vol. 21., Feb. 1954, pp. 91-108.
10. Coles, D. E., "The Wall of the Wake in the Turbulent Boundary Layer," *Journal of Fluid Mechanics*, Vol. 1, 1956, pp. 191-226.
11. Degani, David, and Smits, Alexander J., "Effect of Short Regions of Surface Curvature on Compressible Turbulent Boundary Layers," *AIAA Journal*, Vol. 28, No. 1, January 1990, pp. 113-119.
12. Dotter, J. W., *Compressible Turbulence Measurements in a Supersonic Flow with Adverse Pressure Gradients*. MS Thesis. School of Engineering, Air Force Institute of Technology (AU), Wright-Patterson AFB OH, December 1994.
13. Evans, R. L., "Freestream Turbulence Effects on Turbulent Boundary Layers in an Adverse Pressure Gradient," *AIAA Journal*, Vol., 23, No. 11, November 1985, pp. 1814-1816.
14. Fernando, Emerick M., and Smits, Alexander J., "A Supersonic Turbulent Boundary Layer in an Adverse Pressure Gradient," *Journal of Fluid Mechanics*, Vol. 211, 1990, pp. 285 - 307.
15. Glawe D. D, Goss, L. P., Gogineni, S. P., Bowersox, R. D. W., Terry, W. F., and Dasgupta, S., "Digital Two-Color PIV Measurements in a Mach 2.8 Boundary Layer," AIAA paper 96-2799, 1996.

16. Hale, C. S. *Experimental Investigation of a Supersonic Boundary Layer Flow With Adverse Pressure Gradients*. MS Thesis. School of Engineering, Air Force Institute of Technology (AU), Wright-Patterson AFB OH, December 1995.
17. Hoffman, P. H., Muck, K. C., and Bradshaw, P., "The Effect of Concave Curvature on Turbulent Boundary Layers," *Journal of Fluid Mechanics*, Vol. 161, pp. 374-403.
18. Huffman, R., *AFIT Mach 2.9 Lab Manual*, undated.
19. Huffman, R. E., *Mach 2.9 Investigation Into the Flow Structure in the Vicinity of a Wrap-Around Fin*. MS Thesis. School of Engineering, Air Force Institute of Technology (AU), Wright-Patterson AFB OH, December 1995.
20. "Instruction Manual--IFA 100 System/Intelligent Flow Analyzer," TSI Incorporated, St. Paul, MN, 1987.
21. Jayaram, M., Taylor, M. W., and Smits, A. J., "The Response of a Compressible Turbulent Boundary Layer to Short Regions of Concave Surface Curvature," *Journal of Fluid Mechanics*, Vol. 175, 1985, pp. 343-362.
22. Johnson, Dennis A., and Rose, William C., "Laser Velocimeter and Hot-Wire Anemometer Comparison in a Supersonic Boundary Layer," *AIAA Journal*, Vol. 13, No. 4, April 1975, pp. 512-515.
23. Kistler, Alan J., "Fluctuation Measurements in a Supersonic Turbulent Boundary Layer," *The Physics of Fluids*, Volume 2, Number 3, May - June 1959, pp. 290-296.
24. Klebanoff, P. S., "Characteristics of Turbulence in a Boundary Layer With Zero Pressure Gradient," NASA TN 3178, July 1954.
25. Lewis, J. E., Gran, R. L., and Kubota, T., "An Experiment on the Adiabatic Compressible Turbulent Boundary Layer in Adverse and Favorable Pressure Gradients," *Journal of Fluid Mechanics*, Volume 51, 1992, pp. 657-672.
26. Liepmann, H. W. and Roshko, A., *Elements of Gasdynamics*, Galcit Aeronautical Series, John Wiley & Sons, Inc., New York, 1957.
27. Liou, W. W., and Shih, T. H., "On the Basic Equations for the Second-Order Modeling of Compressible Turbulence," NASA TM 105277, October 1991.
28. Lomas, C. G., *Fundamentals of Hot-Wire Anemometry*, Cambridge University Press, New York, 1986.
29. Luker, J. J., Hale, C. S., Bowersox, R. D. W., "Experimental Analysis of the Turbulent Shear Stresses for Distorted Supersonic Boundary Layers," AIAA-97-0426.
30. Luker, J. *Compressible Turbulence Measurements in a Supersonic Flow with Favorable Pressure Gradient*. MS Thesis. School of Engineering, Air Force Institute of Technology (AU), Wright-Patterson AFB OH, December 1995.

31. Miller, R. S. *Compressible Turbulence Measurements in a Supersonic Flow with Favorable Pressure Gradient*. MS Thesis. School of Engineering, Air Force Institute of Technology (AU), Wright-Patterson AFB OH, December 1994.
32. Morkovin, M. V., "Effects of Compressibility on Turbulent Flows," *The Mechanics of Turbulence*, New York, 1964, pp. 367-380.
33. *Nicolet Systems Operation*, Nicolet, Madison, WI, 1991.
34. Parrott, Tony L., Jones, Michael G., and Albertson, Cindy W., "Fluctuating Pressures Measured Beneath a High-Temperature, Turbulent Boundary Layer on a Flat Plate at a Mach Number of 5," NASA TP 2947, 1989.
35. Patel, V. C., and Richmond, M. C., "Pressure Gradient and Surface Curvature Effects in Turbulent Boundary Layers," AIAA-87-1301.
36. Pressman, AP report, August 3, 1996.
37. Reid, G. J., *Linear System Fundamentals: Continuous and Discrete, Classic and Modern*, New York: McGraw-Hill, 1983.
38. Robinson, S. K., Seegmiller, H. L., and Kussoy, M. I., "Hot-Wire and Laser Doppler Anemometry Measurements in a Supersonic Boundary Layer," AIAA-83-1723.
39. Settles, Gary S., and Dodson, Lori J., "Supersonic and Hypersonic Shock/Boundary-Layer Interaction Database," *AIAA Journal*, Vol. 32, No. 7, July 1994, pp. 1377 -1383.
40. Smith, D. R., and Smits, A. J., "The Effects of Streamline Curvature and Pressure Gradient on the Behavior of Turbulent Boundary Layers in Supersonic Flow," AIAA-94-2227.
41. Spina, E. F., *Organized Structures in a Supersonic Turbulent Boundary Layer*. PhD dissertation, Princeton University, Princeton, New Jersey, 1988.
42. Spina, E. F., Smits, A. J., and Robinson, S. K., "The Physics of Supersonic Turbulent Boundary Layers," *Annual Review of Fluid Mechanics*, Vol. 26, 1994, pp. 287-319.
43. *The Temperature Handbook*, Omega Engineering, 1992.
44. Van Driest, E. R., "Turbulent Boundary Layer in Compressible Flows," *Journal of the Aeronautical Sciences*, Vol. 18, March 1951, pp. 145-160.
45. White, F. M. *Viscous Fluid Flow (2nd ed. Edition)*. New York: McGraw-Hill, Inc., 1991.
46. Wilcox, David C. *Turbulence Modeling for CFD*. La Canada, California: DCW Industries, Inc., 1993.
47. Yao, C., Paschal, K., "PIV Measurements of Airfoil Wake-Flow Turbulence Statistics and Turbulent Structures," AIAA-94-0085, January 1994.

Vita

Capt Raymond C. Wier [REDACTED] He graduated from Elkton High School in 1987 and entered Rensselaer Polytechnic Institute in Troy, New York. He graduated with a Bachelor of Science degree in Aeronautical Engineering and received his commission in May 1996.

His first assignment was at Wright-Patterson AFB as an aircraft and missile performance engineer. His second assignment was also at Wright-Patterson AFB as the Lead F-15 aerodynamics and propulsion engineer. While at Wright-Patterson, he married the former Mary C. Lujan in [REDACTED]

Captain Wier entered the School of Engineering, Air Force Institute of Technology in May 1995. His follow-on assignment is at Wright Laboratories at Eglin AFB, Florida.

REPORT DOCUMENTATION PAGE

Form Approved
OMB No. 0704-0182

Public reporting burden for this collection of information is estimated to average 1 hour per response, including the time for reviewing instructions, searching existing data sources, gathering and maintaining the data needed, and completing and reviewing the collection of information. Send comments regarding this burden estimate or any other aspect of the collection of information, including suggested changes to the burden, to: Director, DOD Reporting and Analysis Division, Defense Acquisition University, 1000 Defense Highway, Suite 1204, Arlington, VA 22202-4302, and to the Office of Management and Budget, Paperwork Reduction Project (0704-0182), Washington, DC 20503.

1. AGENCY USE ONLY (Leave blank)		2. REPORT DATE	3. REPORT TYPE AND DATES COVERED	
		December 1996	Master's Thesis	
4. TITLE AND SUBTITLE		5. FUNDING SOURCE		
EXPERIMENTAL INVESTIGATION OF COMPRESSIBLE BOUNDARY LAYERS UNDER THE INFLUENCE OF PRESSURE GRADIENTS				
6. AUTHOR(S)				
Raymond C. Wier, Captain, USAF				
7. PERFORMING ORGANIZATION NAME(S) AND ADDRESS(ES)		8. PERFORMING ORGANIZATION REPORT NUMBER		
Air Force Institute of Technology 2750 P Street, WPAFB OH 45433-7765		AFIT/GAE/ENY/96D-04		
9. SPONSORING/MONITORING AGENCY NAME(S) AND ADDRESS(ES)		10. SECURED OR MONITORING AGENCY REPORT NUMBER		
Dr. James McMichael AFOSR/NA 110 Duncan Ave, Suite B115 Bolling AFB, Washington DC 20332-0001				
11. SUPPLEMENTARY NOTES				
12a. DISTRIBUTION / AVAILABILITY STATEMENT		12b. DISTRIBUTOR CODE		
Approved for public release; distribution unlimited		A		
13. ABSTRACT (Maximum 200 words)				
<p>This study examined the effect of mild pressure gradients on the mean and turbulent flow of high-speed boundary layers. Three Mach numbers (1.7, 3.0 and 5.0) were investigated. Three pressure gradients were examined; a zero pressure gradient (ZPG), a favorable pressure gradient (FPG), and a combined pressure gradient (CPG). The CPG consisted of an adverse pressure gradient followed by a favorable pressure gradient. Conventional pressure probes, hot-wire and particle image velocimetry (PIV) were used to examine the flow. Measurement included mean velocity, velocity turbulence intensity, mass flux turbulence intensity and energy spectra. Instantaneous (10 nsec) Mie scattering flow visualizations were acquired. Qualitatively, the flow visualizations indicated that the turbulent flow structures were strongly affected by the pressure gradients. For the Mach 2.8 case, the PIV contours and the hot-wire profiles both indicated that the boundary layer thickness increased by 40% and decreased by 100% relative to the ZPG for the favorable and adverse pressure gradients, respectively. Further, the PIV and hot-wire data indicated that the axial turbulence intensity levels increased by 22% for the CPG and decreased by 25% for the FPG. The energy spectra data indicated that once a pressure gradient was applied (favorable or adverse) the low frequency energy increased followed by a rapid decay. Lastly, it was found that nominally 20 to 30 PIV images were sufficient for mean flow boundary layer velocities, but 93 images (the maximum recorded in this study) were insufficient to adequately resolve Reynolds shear stresses.</p>				
14. SUBJECT TERMS		15. NUMBER OF PAGES		
Supersonic turbulent boundary layers, Particle Image Velocimetry (PIV) Adverse pressure gradient, Favorable pressure gradient, Compressible flow, Turbulence, Shock boundary layers		147		
16. PRICE CODE				
17. SECURITY CLASSIFICATION		18. SECURITY CLASSIFICATION	19. SECURITY CLASSIFICATION	20. LIMITATION OF ABSTRACT
Unclassified		Unclassified	Unclassified	UL